Chemie der Erde 77 (2017) 325–385

Contents lists available at ScienceDirect

Chemie der Erde

journal homepage: www.elsevier.de/chemer

INVITED REVIEW

Meteoritic minerals and their origins

Alan E. Rubin[a,b,*], Chi Ma[c,*]

[a] Department of Earth, Planetary, and Space Sciences, University of California, Los Angeles, CA 90095, USA
[b] Institute of Geophysics and Planetary Physics, University of California, Los Angeles, CA 90095, USA
[c] Division of Geological and Planetary Sciences, California Institute of Technology, Pasadena, CA 91125, USA

ARTICLE INFO

Article history:
Received 20 September 2016
Accepted 9 January 2017
Editorial handling - Dewashish Upadhyay

ABSTRACT

About 435 mineral species have been identified in meteorites including native elements, metals and metallic alloys, carbides, nitrides and oxynitrides, phosphides, silicides, sulfides and hydroxysulfides, tellurides, arsenides and sulfarsenides, halides, oxides, hydroxides, carbonates, sulfates, molybdates, tungstates, phosphates and silico phosphates, oxalates, and silicates from all six structural groups. The minerals in meteorites can be categorized as having formed by a myriad of processes that are not all mutually distinct: (1) condensation in gaseous envelopes around evolved stars (presolar grains), (2) condensation in the solar nebula, (3) crystallization in CAI and AOI melts, (4) crystallization in chondrule melts, (5) exsolution during the cooling of CAIs, (6) exsolution during the cooling of chondrules and opaque assemblages, (7) annealing of amorphous material, (8) thermal metamorphism and exsolution, (9) aqueous alteration, hydrothermal alteration and metasomatism, (10) shock metamorphism, (11) condensation within impact plumes, (12) crystallization from melts in differentiated or partially differentiated bodies, (13) condensation from late-stage vapors in differentiated bodies, (14) exsolution, inversion and subsolidus redox effects within cooling igneous materials, (15) solar heating near perihelion, (16) atmospheric passage, and (17) terrestrial weathering.

Contents

* Corresponding authors.
E-mail addresses: aerubin@ucla.edu (A.E. Rubin), chi@gps.caltech.edu (C. Ma).

http://dx.doi.org/10.1016/j.chemer.2017.01.005
0009-2819/

1. Introduction

Meteorites are derived from 100–150 asteroids (Burbine et al., 2002) as well as from the Moon and Mars (e.g., Shearer et al., 1998) and possibly from comets (Gounelle et al., 2006; Gounelle et al., 2008). Micrometeorites are derived mostly from asteroids (Kurat et al., 1994; Genge et al., 1997); a minority are from comets (Engrand and Maurette, 1998; Nakamura et al., 2005; Dartois et al., 2013). Because interplanetary dust particles (IDPs) (a.k.a. cosmic dust) are also meteoritic materials, the number of source bodies delivering extraterrestrial material to Earth may be several thousand (Taylor et al., 2016), including an unknown number of comets (e.g., Bradley, 2005).

Meteorites formed under a variety of conditions – primitive chondrites (e.g., L3.0 NWA 7731; LL3.0 Semarkona) are interpreted to be products of the processes that occurred in the solar nebula (modified by impact-induced compaction and minor alteration on their parent asteroids); many iron meteorites formed deep within the cores of differentiated asteroids (e.g., IIAB Negrillos; IIIAB Picacho); regolith breccias (e.g., H4 Fayetteville; LL6 St. Mesmin) formed near the surface of their parent bodies; olivine diogenites (e.g., NWA 6013; NWA 6232) likely formed at moderate depth within the mantle of the HED parent asteroid (probably Vesta); and martian and lunar meteorites formed as igneous rocks on substantially larger planetary and subplanetary bodies.

Meteorites exhibit diverse oxidation states, ranging from highly oxidized CI carbonaceous chondrites (which contain ~17 wt.% H_2O, mainly bound in fine-grained phyllosilicates; Jarosewich, 1990), to highly reduced enstatite chondrites (which contain graphite; Si-bearing metallic Fe-Ni; Ca-, Mg- Na-, K- and Ti-bearing sulfides; and enstatite with very low FeO; e.g., Keil, 1968; Wasson et al., 1994). The diversity in oxidation state is reflected in the set of meteoritic minerals: e.g., elemental C, carbides and carbonates; metallic Mo and molybdates; phosphides and phosphates; alloyed metallic Si, silicides and silicates; elemental S, sulfides and sulfates; and metallic Fe, wüstite (containing ferrous iron), magnetite (containing both ferrous and ferric iron), and hematite (containing ferric iron).

The list of meteoritic minerals (Table 1) has been updated in this paper from previous modern compilations (e.g., Krinov, 1960; Ramdohr, 1963, 1973; Mason, 1962, 1967, 1972; Miyashiro, 1966; Buchwald, 1975, 1984; El Goresy, 1976; Gomes and Keil, 1980; Olsen 1981a; Yudin and Kolomenskiy, 1987; Kerridge and Matthews, 1988; Ulyanov, 1991; Kimura, 1996, 2015; Rubin, 1997a; Rubin, 1997b; Weisberg and Kimura, 2012). We include a few mineraloids in the present list (e.g., opal and maskelynite) which are amorphous solids lacking long-range atomic order; nevertheless, they have short-range order and are naturally occurring extraterrestrial solids. We also include a couple of metallic-Al-rich quasicrystals (icosahedrite – $Al_{63}Cu_{24}Fe_{13}$ and decagonite – $Al_{71}Ni_{24}Fe_5$), whose validity as natural mineral species remains controversial (MacPherson et al., 2016). The structures of these phases are ordered but not periodic (i.e., they lack translational symmetry). A few minerals in the list (e.g., rhenium, niobium, molybdenum carbide and zirconium carbide) have not been officially approved, but have been positively identified. Their unofficial status is indicated. An alphabetical list of minerals and their corresponding formulae are in Table 2.

Over the past two decades, with such advanced analytical instrumentations as field-emission SEM and TEM, ~145 additional minerals were found in meteorites. Since 2007, a nanomineralogy investigation of meteorites, led by C. Ma at Caltech, has revealed more than 30 new minerals, approved by the IMA-CNMNC, including 17 from the Allende CV3 meteorite (Ma, 2015a) and high-pressure phases such as bridgmanite ($MgSiO_3$-perovskite; Tschauner et al., 2014; Ma et al., 2016c) and tissintite – $(Ca,Na,\square)AlSi_2O_6$-clinopyroxene (Ma et al., 2015b). As of this writing, a total of about 435 minerals has been identified or reported in meteorites (Table 1). These phases include native elements, metals and metallic alloys, carbides, nitrides and oxynitrides, phosphides, silicides, sulfides and hydroxysulfides, tellurides, arsenides and sulfarsenides, halides, oxides, hydroxides, carbonates, sulfates, molybdates, tungstates, phosphates and silico phosphates, oxalates, and silicates from all six structural groups. The Hadley Rille EH chondrite, recovered from an Apollo 15 soil sample (Haggerty, 1972), has an agglutinate-like rim containing silicate grains and fragments of lunar rocks (Rubin, 1997c). Other meteorites also contain voids, extraterrestrial abiogenic organic matter, fluid inclusions, amorphous materials and adsorbed noble gases. And, after landing on Earth, meteorites become contaminated with fungi and bacteria (e.g., Steele et al., 1999) as well as other organic and inorganic materials (e.g., Anders et al., 1964).

Meteoritic minerals formed by more than a dozen basic processes that are not all mutually distinct: (1) condensation in gaseous envelopes around evolved stars (presolar grains), (2) condensation in the solar nebula, (3) crystallization in CAI and AOI melts, (4) crystallization in chondrule melts, (5) exsolution during the cooling of CAIs, (6) exsolution during the cooling of chondrules and opaque assemblages, (7) annealing of amorphous material, (8) thermal metamorphism and exsolution, (9) aqueous alteration, hydrothermal alteration and metasomatism, (10) shock metamorphism, (11) condensation within impact plumes, (12) crystallization from melts in differentiated or partially differentiated bodies, (13) condensation from late- stage vapors in differentiated bodies, (14) exsolution, inversion and subsolidus redox effects within cooling igneous materials, (15) solar heating near perihelion, (16) atmospheric passage, and (17) terrestrial weathering.

Table 1
Minerals in meteorites.

Mineral	Synonyms and Varieties	Formula	Space Group	Selected References
native elements and metals				
aluminium		Al	Fm3m	Ma et al. (2017c)
antitaenite (not approved)		Fe_3Ni	unknown	Rancourt and Scorzelli (1995); Wojnarowska et al. (2008)
awaruite		Ni_3Fe	Pm3m	Buchwald (1977); Kimura and Ikeda (1995); McSween (1977); Rubin (1990)
chaoite		C	P6/mmm	Vdovykin (1969); Vdovykin (1972)
copper		Cu	Fm3m	Ramdohr (1963); Rubin (1994a)
cupalite		CuAl	unknown	Hollister et al. (2014)
decagonite		$Al_{71}Ni_{24}Fe_5$	~ $P10_5/mmc$	Bindi et al. (2015)
diamond		C	Fd3m	Anders and Zinner (1993); Buchwald (1975); Ksanda and Henderson (1939); Russell et al. (1992)
electrum (not approved)		Au-Ag	Fm3m	McCanta et al. (2008)
gold		Au	Fm3m	Rubin (2014)
gold-dominated alloys		(Au,Ag,Fe,Ni,Pt)	Fm3m	Bischoff et al. (1994); Geiger and Bischoff (1995); Schulze et al. (1994)
graphite-2H	cliftonite	C	$P6_3/mmc$	Anders and Zinner (1993); Buchwald (1975); Ramdohr (1963)
graphite-3R		C	R3m	Nakamuta and Aoki (2000)
hexaferrum		(Fe,Os,Ir,Mo)	$P6_3/mmc$	Ma (2012)
hexamolybdenum		(Mo,Ru,Fe)	$P6_3/mmc$	Ma et al. (2014a)
hollisterite	λ-(Al-Cu-Fe)	Al_3Fe	C2/m	Ma et al. (2017c)
icosahedrite		$Al_{63}Cu_{24}Fe_{13}$	$Fm\bar{3}\bar{5}$	Bindi et al. (2011)
iridium		Ir	Fm3m	McSween and Huss (2010)
iron	kamacite; ferrite	α-Fe	Im3m	Afiattalab and Wasson (1980); Ramdohr (1963); Rubin (1990)
khatyrkite		$CuAl_2$	I4/mcm	Hollister et al. (2014); Ma et al. (2016c)
kryachkoite	α-(Al-Cu-Fe)	$(Al,Cu)_6(Fe,Cu)$	$Cmc2_1$	Ma et al. (2017c)
lonsdaleite		C	$P6_3/mmc$	Buchwald (1975); Buchwald (1977); Frondel and Marvin (1967)
martensite (not approved)		α_2-(Fe,Ni)		Dodd (1981)
mercury		Hg	R3m	Caillet Komorowski et al. (2012)
molybdenum (not approved)		Mo		El Goresy et al. (1978)
nickel		Ni	$P6_3/mmc$	Nystrom and Wickman (1991)
niobium (not approved)		Nb		El Goresy et al. (1978)
osmium		Os	$P6_3/mmc$	Ma et al. (2014a)
platinum		Pt	Fm3m	El Goresy et al. (1978)
PGE-dominated alloys		(Pt,Os,Ir,Ru,Re,Rh,Mo,Nb, Ta,Ge,W,V,Pb,Cr,Fe,Ni,Co)	Fm3m	Armstrong et al. (1987); Bischoff and Palme (1987); El Goresy et al. (1978); Wark and Lovering (1978)
rhenium (not approved)		Re	$P6_3/mmc$	El Goresy et al. (1978)
rustenburgite		$(Pt,Pd)_3Sn$	Fm3m	Kimura (1996); Schulze et al. (1994)
ruthenium		Ru	$P6_3/mmc$	El Goresy et al. (1978)
ruthenosmiridim		RuOsIr	Fm3m	Bischoff et al. (2011); Rubin (2014)
selenium		Se	$P3_121$ or $P3_221$	Simpson (1938); Greenland (1965); Akaiwa (1966); www.mindat.org
steinhardtite		(Al,Ni,Fe)	Im3m	Bindi et al. (2014)
stolperite	β-(Al-Cu-Fe)	AlCu	Pm3m	Ma et al. (2017c)
sulfur		S	Fddd	Buchwald (1977)
taenite	austenite	γ-(Fe,Ni)	Fm3m	Ramdohr (1963)
tetrataenite		FeNi	P4/mmm	Clarke and Scott (1980)
wairauite		CoFe	Pm3m	Hua et al., 1995
zhanghengite		(Cu,Zn)	Im3m	Wang (1986)
carbides				
beta-moissanite		SiC	$P6_3/mc$	Alexander et al. (1991); Anders and Zinner (1993); Bernatowicz et al. (1991); Huss (1990)
cohenite		$(Fe,Ni)_3C$	Pbnm	Buchwald (1975); Ramdohr (1963)
haxonite		$(Fe,Ni)_{23}C_6$	Fm3m	Buchwald (1975); Scott and Agrell (1971)
iron carbide (not approved)		$Fe_{2.5}C$		Scott and Agrell (1971)
molybdenum carbide (not approved)		MoC		Bernatowicz et al. (1991)

khamrabaevite	titanium carbide	TiC	Fm3m	Ma and Rossman (2009a)
zirconium carbide (not approved)		ZrC		Bernatowicz et al. (1991); Ott (1996)
nitrides and oxynitrides				
carlsbergite		CrN	Fm3m	Buchwald (1975); Buchwald and Scott (1971)
nierite		a-Si_3N_4	$P3_1C$	Alexander et al. (1989); Alexander et al. (1994); Lee et al. (1995)
osbornite		TiN	Fm3m	Bischoff et al. (1993b); Ramdohr (1963)
roaldite		$(Fe,Ni)_4N$	$P\bar{4}3m$	Buchwald (1975); Nielsen and Buchwald (1981)
β-silicon nitride (not approved)		β-Si_3N_4		Lee et al. (1995)
sinoite		Si_2N_2O	$Cmc2_1$	Andersen et al. (1964)
phosphides				
allabogdanite		$(Fe,Ni)_2P$	Pnma	Britvin et al. (2002)
andreyivanovite		FeCrP	Pnma	Zolensky et al. (2008)
barringerite		$(Fe,Ni)_2P$	P62m	Buchwald (1977); Buseck (1977)
florenskyite		(Fe,Ni)TiP	Pnma	Ivanov et al. (2000)
melliniite		$(Ni,Fe)_4P$	$P2_13$	Pratesi et al. (2006)
monipite		MoNiP	$P\bar{6}2m$	Ma et al. (2014b)
nickelphosphide		Ni_3P	I4	Skála and Drábek (2003); Fisenko et al. (1990)
schreibersite	rhabdite	$(Fe,Ni)_3P$	I4	Ramdohr (1963)
silicides				
brownleeite		MnSi	$P2_13$	Nakamura-Messenger et al. (2010)
gupeiite		Fe_3Si	Fm3m	Yu (1984)
hapkeite		Fe_2Si	Pm3m	Anand et al. (2004)
linzhiite		$FeSi_2$	P4/mmm	Anand et al. (2004)
naquite		FeSi	$P2_13$	Ma et al. (2017c)
perryite		$(Ni,Fe)_5(Si,P)_2$	R3c	Wasson and Wai (1970)
suessite		Fe_3Si	Im3m	Keil et al. (1982)
xifengite		Fe_5Si_3	$P6_3/mcm$	Yu (1984); Ma et al. (2017c)
sulfides and hydroxysulfides				
alabandite		MnS	Fm3m	Mason and Jarosewich (1967)
bornite		Cu_5FeS_4	Pbca	El Goresy et al. (1988)
brezinaite		Cr_3S_4	I2/m	Satterwhite et al. (1993); Warren and Kallemeyn (1994)
browneite		MnS	F43m	Ma et al. (2012a)
buseckite		(Fe,Zn,Mn)S	$P6_3mc$	Ma et al. (2012b)
butianite		Ni_6SnS_2	$I\bar{4}/mmm$	Ma, 2017
caswellsilverite		$NaCrS_2$	R3m	Okada and Keil (1982)
chalcocite		Cu_2S	$P2_1C$	Yudin and Kolomenskiy (1987)
chalcopyrite		$CuFeS_2$	I42d	Geiger and Bischoff (1995); Ramdohr (1963)
cinnabar		HgS	$P3_121$, $P3_221$	Ulyanov (1991)
cooperite		PtS	$P4_{1/}mmc$	Geiger and Bischoff (1995)
covellite		CuS	$P6_3/mmc$	El Goresy et al. (1988)
cronusite		$Ca_{0.2}CrS_2{\cdot}2H_2O$	Rm, R3 m or R32	Britvin et al., 2001
cubanite		$CuFe_2S_3$	Pcmn	Dodd (1981); Zolensky and McSween (1988)
daubréelite		$FeCr_2S_4$	Fd3m	Keil (1968); Ramdohr (1963)
digenite		Cu_9S_5	R3m	Kimura (1996); Kimura et al. (1992)
djerfisherite		$K_6Na_9(Fe,Cu)_{24}S_{26}Cl$	Pm3m	Fuchs (1966a)
erlichmanite		OsS_2	Pa3	Geiger and Bischoff (1989, 1990, 1995)
ferroan alabandite		(Mn,Fe)S	Fm3m	Keil (1968)
galena		PbS	Fm3m	Nystrom and Wickman (1991)
gentnerite (not approved)	cuprian daubréelite	$Cu_8Fe_3Cr_{11}S_{18}$		Ulyanov (1991)
greigite		Fe_3S_4	Fd3m	El Goresy et al. (1988)
heazlewoodite		Ni_3S_2	R32	Buchwald (1977); McSween (1977)
heideite		$(Fe,Cr)_{1+x}(Ti,Fe)_2S_4$	I2/m	Keil and Brett (1974)
idaite		Cu_5FeS_6	$P6_3/mmc$	El Goresy et al. (1988)
isocubanite		$CuFe_2S_3$	Fm3m	Buchwald (1975)
joegoldsteinite		$MnCr_2S_4$	Fd3m	Isa et al. (2016)
keilite		(Fe,Mn,Mg,Ca,Cr)S	Fm3m	Shimizu et al. (2002); Keil (2007)
laurite		RuS_2	Pa3	Geiger and Bischoff (1989, 1990, 1995)

Table 1 (*Continued*)

Mineral	Synonyms and Varieties	Formula	Space Group	Selected References
mackinawite		FeS_{1-x}	P4/nmm	Buseck (1968)
marcasite		FeS_2	Pnnm	McSween (1994)
millerite		NiS	R3m	Geiger and Bischoff (1995)
molybdenite		MoS_2	$P6_3/mmc$	El Goresy et al. (1978)
murchisite		Cr_5S_6	$P\bar{3}1c$	Ma et al. (2011a)
niningerite		(Mg,Fe)S	Fm3m	Keil (1968); Keil and Snetsinger (1967)
nuwaite		Ni_6GeS_2	I4/mmm	Ma et al. (2015b)
oldhamite		CaS	Fm3m	Keil (1968)
pentlandite		$(Fe,Ni)_9S_8$	Fm3m	Ramdohr (1963); Buchwald (1977)
plagionite		$Pb_5Sb_8S_{17}$	C2/c	Watters and Prinz (1979); www.mindat.org
pyrite		FeS_2	Pa3	Ramdohr (1963); Nystrom and Wickman (1991)
pyrrhotite		$Fe_{1-x}S$	A2/a	Zolensky and McSween (1988); Berger et al. (2016)
rudashevskyite		(Fe,Zn)S	$F\bar{4}3m$	Britvin et al. (2008)
schöllhornite		$Na_{0.3}(H_2O)[CrS_2]$	R3m?	Okada et al. (1985)
smythite		Fe_9S_{11}	R3m	El Goresy et al. (1988)
sphalerite		(Zn,Fe)S	$F\bar{4}3m$	Dodd (1981); El Goresy et al. (1988)
tochilinite group				
tochilinite		2[(Fe,Mg,Cu,Ni)S].157-1.85[(Mg,Fe,Ni,Al,Ca)$(OH)_2$]	P2, Pm, or P2/m	Zolensky and McSween (1988); Ma et al. (2011a)
haapalaite		4(Fe,Ni)S·3(Mg,Fe^{2+})$(OH)_2$	R3m?	Buseck and Hua (1993)
valleriite		2[(Fe,Cu)S]·1.53[(Mg,Al)$(OH)_2$]	R3m	Ackermaand and Raase (1973)
troilite		FeS	$P6_3/mmc$	Ramdohr (1963)
tungstenite		WS_2	$P6_3/mmc$	El Goresy et al. (1978)
violarite		$FeNi_2S_4$	F d3m	Ulyanov (1991)
wassonite		TiS	R3m	Nakamura-Messenger et al. (2012)
wurtzite-2H		β-ZnS	$P6_3mc$	Yudin and Kolomenskiy (1987)
tellurides				
altaite		PbTe	Fm3m	Karwowski and Muszynski (2008)
chengbolite		$PtTe_2$	P3m1	El Goresy (1976)
moncheite		$Pt(Te,Bi)_2$	P3m1	Connolly et al. (2006); Grady et al. (2015); www.mindat.org
arsenides and sulfarsenides				
cobaltite		CoAsS	$Pca2_1$	Nystrom and Wickman (1991)
gersdorffite		NiAsS	$P2_13$	Nystrom and Wickman (1991)
irarsite		(Ir,Ru,Rh,Pt)AsS	Pa3	Kimura (1996); Schulze et al. (1994)
iridarsenite		$(Ir,Ru)As_2$	$P2_1/c$	El Goresy (1976)
löllingite		$FeAs_2$	Pnnm	El Goresy (1976)
maucherite		$Ni_{11}As_8$	$P4_12_12$, $P4_32_12$	Nystrom and Wickman (1991)
nickeline		NiAs	$P6_3/mmc$	Nystrom and Wickman (1991)
omeiite		$(Os,Ru)As_2$	Pnnm	El Goresy (1976)
orcelite		$Ni_{5-x}As_2$	$P6_3cm$	Nystrom and Wickman (1991)
rammelsbergite		$NiAs_2$	Pnnm	Nystrom and Wickman (1991)
safflorite		$CoAs_2$	Pnnm	Nystrom and Wickman (1991)
sperrylite		$PtAs_2$	Pa3	El Goresy (1976)
halides				
droninoite		$Ni_6Fe^{3+}{}_2Cl_2(OH)_{16}·4H_2O$	R3m	Chukanov et al. (2009)
halite		NaCl	Fm3m	Barber (1981); Berkley et al. (1980)
lawrencite		$(Fe^{2+},Ni)Cl_2$	R3m	Keil (1968)
sylvite		KCl	Fm3m	Barber (1981); Berkley et al. (1980)
oxides				
addibischoffite		$Ca_2Al_6Al_6O_{20}$	$P\bar{1}$	Ma and Krot (2015); Ma et al. (2016a,b)
akimotoite		$(Mg,Fe)SiO_3$	R3	Tomioka and Fujino (1999)
allendeite		$Sc_4Zr_3O_{12}$	R3	Ma et al. (2014a)
anatase		TiO_2	$I4_1/amd$	Wopenka and Swan (1985)
anosovite (not approved)		$(Ti^{4+},Ti^{3+},Mg,Sc,Al)_3O_5$	Bbmm	Zhang et al. (2015)
armalcolite		$(Mg,Fe)Ti_2O_5$	Bbmm	Lin and Kimura (1996)
baddeleyite		ZrO_2	$P2_1c$	Davis (1991); Delaney et al. (1984); Krot and Wasson (1994)

beckettite		$Ca_2V_6Al_6O_{20}$	$P\bar{1}$	Ma et al. (2016b)
bunsenite		NiO	Fm3m	Buchwald (1977)
Ca-armalcolite		$CaTi_2O_5$	Bbmm	Lin and Kimura (1996)
calcium oxide	lime	CaO	Fm3m	Greshake et al. (1996a); Greshake et al. (1996b); MacPherson et al. (1988)
chlormayenite	brearleyite	$Ca_{12}Al_{14}O_{32}Cl_2$	$I\bar{4}3d$	Ma et al. (2011c)
chromite		$FeCr_2O_4$	Fd3m	Ramdohr (1963); Zolensky and McSween (1988)
corundum		Al_2O_3	R3c	Greshake et al. (1996a); Greshake et al. (1996b); MacPherson et al. (1988)
coulsonite		FeV_2O_4	Fd3m	Armstrong et al. (1987); Ulyanov (1991)
cuprite		Cu_2O	Pn3m	Ulyanov (1991)
dmitryivanovite		$CaAl_2O_4$	$P2_1b$	Mikouchi et al. (2009)
eskolaite		Cr_2O_3	R3c	Greshake and Bischoff (1996)
ferropseudobrookite		$FeTi_2O_5$	Cmcm	Kimura (1996); Fujimaki et al. (1981)
geikielite		$MgTiO_3$	R3	Lin and Kimura (1996)
grossite		$CaAl_4O_7$	C2/c	Weber and Bischoff (1994a); Weber and Bischoff (1994b)
hematite		α-Fe_2O_3	$R\bar{3}c$	Buchwald (1977)
hercynite		$(Fe,Mg)Al_2O_4$	Fd3m	Treiman (1985); Zolensky and McSween (1988)
hibonite		$CaAl_{12}O_{19}$	$P6_3/mmc$	Dodd (1981); MacPherson et al. (1988)
hibonite-(Fe)		$(Fe,Mg)Al_{12}O_{19}$	$P6_3/mmc$	Ma (2010)
ilmenite		$FeTiO_3$	R3	Ramdohr (1963); Snetsinger and Keil (1969)
kamiokite		$Fe_2Mo_3O_8$	$P6_3mc$	Ma et al. (2014b)
kangite		$(Sc,Ti,Al,Zr,Mg,Ca,\square)_2O_3$	Ia3	Ma et al. (2013c)
krotite		$CaAl_2O_4$	$P2_1/n$	Ma et al. (2011d)
lakargiite		$CaZrO_3$	Pbnm	Ma (2011)
loveringite		$Ca(Ti,Fe,Cr,Mg)_{21}O_{38}$	R3	Ma et al. (2013a)
machiite	$Al_2Ti_3O_9$	$(Al,Sc)_2(Ti,Zr)_3O_9$	C2/c	Krot (2016)
maghemite		$Fe_{2.67}O_4$	$P2_13$	Buchwald (1977); Zolensky and McSween (1988)
Magnéli phases		Ti_5O_9 and Ti_8O_{15}	P1	Brearley (1993a, 1995)
magnesiochromite		$MgCr_2O_4$	Fd3m	Greshake and Bischoff (1996)
magnesioferrite		$MgFe_2O_4$	Fd3m	Yudin and Kolomenskiy (1987)
magnesiowüstite		(Mg,Fe)O	Fm3m	Chen et al. (1996)
magnetite		Fe_3O_4	Fd3m	Buchwald (1977); Kerridge et al. (1979); Ramdohr (1963); Zolensky and McSween (1988)
majindeite		$Mg_2Mo_3O_8$	$P6_3mc$	Ma and Beckett (2016b)
Nb-oxide		$(Nb,V,Fe)O_2$		Ma et al. (2014b)
olkhonskite		$Cr_2Ti_3O_9$	unknown	Schmitz et al. (2016)
panguite		$(Ti,Al,Sc,Mg,Zr,Ca)_{1.8}O_3$	Pbca	Ma et al. (2012c)
periclase		MgO	Fm3m	Greshake et al. (1996a); Greshake et al. (1996b); MacPherson et al. (1988)
perovskite		$CaTiO_3$	Pnma	Lin and Kimura (1996); MacPherson et al. (1988)
pleonaste		$(Mg,Fe)Al_2O_4$	Fd3m	MacPherson and Delaney (1985)
pseudobrookite		Fe_2TiO_5	Bbmm	Ramdohr (1967, 1973)
pyrophanite		$MnTiO_3$	R3	Krot et al. (1993)
rutile		TiO_2	P4/mnm	Greshake et al. (1996a); Greshake et al. (1996b); Lin and Kimura (1996); MacPherson et al. (1988)
spinel		$MgAl_2O_4$	Fd3m	MacPherson et al. (1988); Zolensky and McSween (1988)
tazheranite		$(Zr,Ti,Ca,Y)O_{1.75}$	Fm3m	Ma and Rossman (2008)
thorianite		ThO_2	Fm3m	MacPherson et al. (1988)
Ti-rich magnetite		$(Fe,Mg)(Fe,Ti)_2O_4$	Fd3m	Dodd (1981)
tistarite		Ti_2O_3	R3c	Ma and Rossman (2009a)
trevorite		$NiFe_2O_4$	Fd3m	Buchwald (1977)
tugarinovite		MoO_2	$P2_1/n$	Ma et al. (2014a)
ulvöspinel		Fe_2TiO_4	Fd3m	Papike et al. (1991)

Table 1 (*Continued*)

Mineral	Synonyms and Varieties	Formula	Space Group	Selected References
V-rich magnetite		$(Fe,Mg)(Fe,V)_2O_4$	Fd3m	Bischoff and Palme (1987); El Goresy (1976) Wark and Lovering (1978)
wangdaodeite		$FeTiO_3$	R3c	Xie et al. (2016)
warkite		$Ca_2Sc_6Al_6O_{20}$	$P\bar{1}$	Ma et al. (2015a)
wüstite		FeO	Fm3m	Buchwald (1977)
xieite		$FeCr_2O_4$	Bbmm	Chen et al. (2008)
zirconolite		$(Ca,Ce)Zr(Ti,Nb,Fe^{3+})_2O_7$		MacPherson et al. (1988); Ma and Rossman (2008)
zirkelite		$(Ca,Th,Ce)Zr(Ti,Nb)_2O_7$	Fm3m	Kimura (1996); MacPherson et al. (1988)
hydroxides				
akaganéite		β-FeO(OH,Cl)	I2/m	Buchwald (1977); Buchwald and Clarke (1988); Buchwald and Clarke (1989)
amakinite		$(Fe^{2+},Mg)(OH)_2$	P3m1	Zolensky and McSween (1988)
brucite		$Mg(OH)_2$	P3m1	Barber (1981)
chlormagmaluminite		$Mg_4Al_2(OH)_{12}Cl_2{\cdot}3H_2O$		Ivanova et al. (2016)
feroxyhyte		δ-FeO(OH)	unknown	Kimura (1996); Gooding (1981); Buseck and Hua (1993)
ferrihydrite		$Fe_{4\text{-}5}(OH,O)_{12}$		Tomeoka and Buseck (1988)
goethite		αFeO(OH)	Pbnm	Barber (1981); Buchwald (1977)
hibbingite		$\gamma\text{-}Fe_2(OH)_3Cl$	Pnam	Buchwald (1989); Saini-Eidukat et al. (1994)
hollandite		$(Fe_{15},Ni)(O_{12}(OH)_{20})Cl(OH)_2$	I2/m	Ulyanov (1991)
lepidocrocite		γ-FeO(OH)	Amam	Barber (1981); Buchwald (1977)
portlandite		$Ca(OH)_2$	P3m1	Okada et al. (1981)
pyrochlore		$(Na,Ca)_2Nb_2O_6(OH,F)$	Fd3m	Lovering et al. (1979)
zaratite		$Ni_3CO_3(OH)_4{\cdot}4H_2O$	unknown (in part amorphous)	Buddhue (1957)
carbonates				
ankerite		$Ca(Fe^{2+},Mg,Mn)(CO_3)_2$	R3	Zolensky and McSween (1988)
aragonite		$CaCO_3$	Pmcn	Endress and Bischoff (1996)
barringtonite		$MgCO_3{\cdot}2H_2O$	P1 or $P\bar{1}$	Ulyanov (1991)
breunnerite		$(Mg,Fe)CO_3$	R3c	Lee et al. (2014)
calcite		$CaCO_3$	R3c	Dodd (1981); Okada et al. (1981); Zolensky and Krot (1996)
chukanovite		$Fe_2(CO_3)(OH)_2$	$P2_1/a$	Pekov et al. (2007)
dolomite		$CaMg(CO_3)_2$	R3	Zolensky and McSween (1988)
hydromagnesite		$Mg_5(CO_3)_4(OH)_2{\cdot}4H_2O$	$P2_1/c$	Velbel (1988); Zolensky and Gooding (1986)
kutnohorite		$Ca(Mn,Mg,Fe^{2+})(CO_3)_2$	R3	Zolensky and McSween (1988)
magnesite		$(Mg,Fe)CO_3$	R3c	Zolensky and McSween (1988)
nesquehonite		$Mg(HCO_3)(OH){\cdot}2H_2O$	$P2_1/n$	Velbel (1988); Zolensky and Gooding (1986)
nyerereite		$Na_2Ca(CO_3)_2$	$Pmc2_1$	Ulyanov (1991)
reevesite		$Ni_6Fe_2(CO_3)(OH)_{14}{\cdot}4H_2O$	R3m	Buchwald (1977); White et al. (1967)
rhodochrosite		$MnCO_3$	R3c	Ulyanov (1991)
siderite		$FeCO_3$	R3c	Buchwald (1977)
vaterite		$CaCO_3$	$P6_3/mmc$	Okada et al. (1981)
zaratite		$Ni_3(CO_3)(OH)_4{\cdot}4H_2O$	unknown (in part amorphous)	Buchwald (1977)
sulfates				
anhydrite		$CaSO_4$	Amma	Brearley (1993a, 1995)
barite		$BaSO_4$	Pbnm	Nystrom and Wickman (1991)
bassanite		$CaSO_4{\cdot}½H_2O$	B2	Okada et al. (1981); Wentworth and Gooding (1994)
blödite		$Na_2Mg(SO_4)_2{\cdot}4H_2O$	$P2_1/a$	Zolensky and McSween (1988)
celestine		$SrSO_4$	Pnma	Ma (2015b)
copiapite		$Fe_5(SO_4)_6(OH)_2{\cdot}20H_2O$	P1	Ulyanov (1991)
coquimbite		$Fe_2(SO_4)_3{\cdot}9H_2O$	P3c	Kimura (1996); Gooding (1981)
epsomite		$MgSO_4{\cdot}7H_2O$	$P2_12_12_1$	Zolensky and McSween (1988)
gypsum		$CaSO_4{\cdot}2H_2O$	A2/a	Zolensky and McSween (1988)
hexahydrite		$MgSO_4{\cdot}6H_2O$	A2/a	Zolensky and McSween (1988)
honessite		$(Ni,Fe)_8SO_4(OH)_{16}{\cdot}nH_2O$	R3m	Buchwald (1977)
jarosite		$KFe_3(SO_4)_2(OH)_6$	R3	Buchwald (1977)
kieserite		$MgSO_4{\cdot}H_2O$	C2/c	Kimura (1996); Gooding et al. (1991)

melanterite		$FeSO_4{\cdot}7H_2O$	$P2_1/c$	Ulyanov (1991)
mendozite		$NaAl(SO_4)_2{\cdot}11H_2O$	C2/c	www.mindat.org
nickelblödite		$Na_2(Ni,Mg)(SO_4)_2{\cdot}4H_2O$	$P2_1/a$	Brearley (2006)
paraotwayite		$Ni(OH)_{2-x}(SO_4,CO_3)_{0.5x}$	Pm	Zubkova et al. (2008); Nickel and Graham (1987)
schwertmannite		$Fe^{3+}{}_{16}(OH,SO_4)_{12\text{-}13}O_{16}{\cdot}10H_2O$	P4/m	Pederson (1999)
slavikite		$NaMg_2Fe_5(SO_4)_7(OH)_6{\cdot}33H_2O$	R3	Kimura (1996); Gooding (1981)
starkeyite		$MgSO_4.4H_2O$	$P2_1/n$	Velbel (1988); Zolensky and Gooding (1986)
szomolnokite		$FeSO_4{\cdot}H_2O$	A2/a	Kimura (1996); Gooding (1981)
voltaite		$K_2Fe_8Al\,(SO_4)_{12}{\cdot}18H_2O$	Fd3c	Kimura (1996); Gooding (1981)
molybdates				
powellite		$CaMoO_4$	$I4_1/a$	Ulyanov (1991)
tungstates				
scheelite		$CaWO_4$	$I4_1/a$	MacPherson et al. (1988)
phosphates				
apatite		$Ca_5(PO_4)_3(F,OH,Cl)$	$P6_3/m$	MacPherson et al. (1988); Nystrom and Wickman (1991)
arupite		$Ni_3(PO_4)_2{\cdot}8H_2O$	I2/m	Buchwald (1977, 1990)
beusite		$(Mn,Fe,Ca,Mg)_3(PO_4)_2$	$P2_1/c$	Ulyanov (1991)
bobdownsite		$Ca_9Mg(PO_4)_6(PO_3F)$	R3c	Gnos et al. (2002); Tait et al. (2011)
brianite		$Na_2CaMg(PO_4)_2$	$P2_1/a$	Buchwald (1977); Bunch et al. (1970); Fuchs et al. (1967)
buchwaldite		$NaCaPO_4$	$Pmn2_1$	Buchwald (1977); Olsen et al. (1977)
carbonate-fluorapatite		$Ca_5(PO_4,CO_3)_3F$	$P6_3/m$	Nystrom and Wickman (1991)
cassidyite		$Ca_2(Ni,Mg)(PO_4)_2{\cdot}2H_2O$	P1	Buchwald (1977); White et al. (1967)
chlorapatite		$Ca_5(PO_4)_3Cl$	$P6_3/m$	Buchwald (1977); Fuchs and Olsen (1965)
chladniite		$Na_2CaMg_7(PO_4)_6$	R3	McCoy et al. (1994)
chopinite		$Mg_3(PO_4)_2$	$P2_1/b$	Grew et al. (2010)
collinsite		$Ca_2(Mg,Fe,Ni)(PO_4)_2{\cdot}2H_2O$	P1	Buchwald (1977)
farringtonite		$Mg_3(PO_4)_2$	$P2_1/a$	Buchwald (1977); Buseck (1977)
ferromerrillite		$Ca_9NaFe^{2+}(PO_4)_7$	R3c	Britvin et al. (2015)
fluorapatite		$Ca_5(PO_4)_3F$	$P6_3/m$	Kimura (1996); Kimura et al. (1992)
galileiite		$NaFe_4(PO_4)_3$	R3	Olsen and Steele (1997)
graftonite		$(Fe,Mn)_3(PO_4)_2$	$P2_1/c$	Buchwald (1977); Olsen and Fredriksson (1966)
hydroxylapatite		$Ca_5(PO_4)_3OH$	$P6_3/m$	Fuchs (1969)
johnsomervilleite		$Na_2Ca(Fe,Mg,Mn)_7(PO_4)_6$	R3	Olsen and Fredriksson (1966)
K-Na-Fe phosphate		$(K,Na)Fe_4(PO_4)_3$		Olsen and Steele (1997)
lipscombite		$(Fe,Mn)Fe_2(PO_4)_2(OH)_2$	$P4_12_12$	Buchwald (1977)
maricite		$NaFePO_4$	Pmnb	Clarke et al. (1990)
matyhite		$Ca_{18}(Ca,\square)_2Fe^{2+}{}_2(PO_4)_{14}$	R3c	Hwang et al. (2016a)
merrillite		$Ca_9MgNa(PO_4)_7$	R3c	Buchwald (1977); Buseck (1977)
monazite-(Ce)		$(Ce,La,Th)PO_4$	$P2_1/n$	Yagi et al. (1978)
moraskoite		$Na_2Mg(PO_4)F$	Pbcn	Karwowski et al. (2015)
panethite		$(Ca,Na)_2(Mg,Fe)_2(PO_4)_2$	$P2_1/n$	Buchwald (1977); Bunch et al. (1970); Fuchs et al. (1967)
sarcopside		$(Fe,Mn)_3(PO_4)_2$	$P2_1/a$	Buchwald (1977); Olsen and Fredriksson (1966)
stanfieldite		$Ca_4(Mg,Fe)_5(PO_4)_6$	P2/c	Buseck (1977)
tuite		γ-$Ca_3(PO_4)_2$	$R\bar{3}m$	Xie et al. (2003)
vivianite		$Fe_3(PO_4)_2{\cdot}8H_2O$	C2/m	Buchwald (1977)
xenophyllite		$Na_4Fe_7(PO_4)_6$	P1	www.mindat.org
xenotime		YPO_4	$I4_1/amd$	Liu et al. (2016)
silicates				
nesosilicates (independent SiO_4 tetrahedra)				
adrianite		$Ca_{12}(Al_4Mg_3Si_7)O_{32}Cl_6$	$I\bar{4}3d$	Ma and Krot (2014b)
ahrensite		Fe_2SiO_4	Fd3m	Ma et al. (2016c)
almandine		$Fe_3Al_2(SiO_4)_3$	Ia3d	Ulyanov (1991)
andradite		$Ca_3Fe_2(SiO_4)_3$	Ia3d	Kimura and Ikeda (1995)
bridgmanite	Mg-silicate perovskite	$(Mg,Fe)SiO_3$	Pnma	Tschauner et al. (2014)
britholite-(Ce)	beckelite	$(Ce,Y,Ca)_5(SiO_4,PO_4)_3(OH,F)$	$P6_3/m$	MacPherson et al. (1988)
eringaite		$Ca_3Sc_2Si_3O_{12}$	Ia3d	Ma (2012)
fayalite		Fe_2SiO_4	Pbnm	Krot et al. (1995)
forsterite		Mg_2SiO_4	Pbnm	Dodd (1981)

Table 1 (*Continued*)

Mineral	Synonyms and Varieties	Formula	Space Group	Selected References
goldmanite		$Ca_3V_2(SiO_4)_3$	Ia3d	Kimura (1996); Simon and Grossman (1992)
grossular		$Ca_3Al_2(SiO_4)_3$	Ia3d	Kimura and Ikeda (1995)
hutcheonite		$Ca_3Ti_2(SiAl_2)O_{12}$	Ia3d	Ma and Krot (2014a)
kirschsteinite		$CaFe(SiO_4)$	Pbmn	Kimura and Ikeda (1995); Krot et al. (1995)
larnite	felite; shannonite	Ca_2SiO_4		Krot (2016)
majorite		$Mg_3(SiMg)Si_3O_{12}$	Ia3d	Chen et al. (1996); Dodd (1981)
monticellite		$CaMgSiO_4$	Pnma	MacPherson et al. (1988); Ma and Krot (2014a)
mullite		$Al_6Si_2O_{13}$	Pbam	Ma and Rossman (2009a)
olivine	peridot; chrysolite	$(Mg,Fe)_2SiO_4$	Pbnm	Buchwald (1977); Dodd (1981); Rubin (1990)
pyrope		$Mg_3Al_{22}(SiO_4)_3$	Ia3d	Chen et al. (1996)
reidite		$ZrSiO_4$	$I4_1/a$	Glass et al. (2002)
ringwoodite		Mg_2SiO_4	Ia3d	Dodd (1981); Price et al. (1979)
rubinite		$Ca_3Ti_2Si_3O_{12}$	Ia3d	Ma et al. (2017a,d)
sapphirine		$(Mg,Al)_7(Mg,Al)O_2(Al,Si)_6O_{18}$		Ulyanov (1991)
sodium-bearing silicate		$(Na,K,Ca,Fe)_{0.973}(Al,Si)_{5.08}O_{10}$		El Goresy et al. (1997)
tetragonal almandine		$(Fe,Mg,Ca,Na)_3(Al,Si,Mg)_2Si_3O_{12}$	$I4_1/a$	Ma and Tschauner (2016)
tetragonal majorite		$Mg_3(SiMg)Si_3O_{12}$	$I4_1/a$	Tomioka et al. (2016)
titanite	sphene	$CaTiSiO_5$	$P2_1/a$	Delaney et al. (1984)
tranquillityite		$Fe^{2+}{}_8Ti_3Zr_2Si_3O_{24}$	unknown	Taylor et al. (2001)
wadalite		$Ca_6Al_5Si_2O_{16}Cl_3$	$I\bar{4}3d$	Ishii et al. (2010)
zircon		$ZrSiO_4$	$I4_1/amd$	Buchwald (1977); Ireland and Wlotzka (1992); Marvin and Klein (1964)
sorosilicates (two isolated SiO_4 tetrahedra sharing one O)				
åkermanite		$Ca_2MgSi_2O_7$	$P42_1m$	MacPherson et al. (1988)
chevkinite		$(Ce,La,Ca,Th)_4(Fe^{2+},Mg)_2(Ti,Fe^{3+})_3Si_4O_{22}$	C2/m	Liu et al. (2016)
paqueite		$Ca_3TiSi_2(Al,Ti,Si)_3O_{14}$	P321	Barber et al. (1994); Paque et al. (1994); Ma and Beckett (2016a)
perrierite		$(Ce,La,Ca)_4(Fe^{2+},Mg)_2(Ti,Fe^{3+})_3Si_4O_{22}$	C21/a	Liu et al. (2016)
gehlenite		$Ca_2Al(Si,Al)_2O_7$	$P42_1m$	MacPherson et al. (1988)
melilite		$(Ca,Na)_2(Al,Mg)(Si,Al)_2O_7$	$P42_1m$	MacPherson et al. (1988)
pumpellyite		$Ca_2(Mg,Fe^{2+})Al_2(SiO_4)(Si_2O_7)(OH)_2{\cdot}H_2O$	A2/m	Ulyanov (1991); Zolensky and McSween (1988)
thortveitite		$Sc_2Si_2O_7$	C2/m	Ma et al. (2011b)
wadsleyite		$(Mg,Fe)_2SiO_4$	I2/m	Ulyanov (1991)
cyclosilicates (closed rings of SiO_4 tetrahedra)				
cordierite		$Mg_2Al_4Si_5O_{18}$	Cccm	MacPherson et al. (1988); Petaev et al. (1993)
indialite		$Mg_2Al_3(AlSi_5O_{18})$	P6/mcc	Mikouchi et al. (2016)
merrihueite		$(K,Na)_2Fe_5Si_{12}O_{30}$	P6/mcc	Dodd et al. (1965); Dodd et al. (1966); Krot and Wasson (1994)
osumilite		$(K,Na)(Fe,Mg)_2(Al,Fe)_2[(Si,Al)_{12}O_{30}]$	P6/mcc	Ulyanov (1991)
roedderite		$(K,Na)_2Mg_5Si_{12}O_{30}$	P6/mmc	Buchwald (1977); Fuchs (1966b); Krot and Wasson (1994)
yagiite		$(K,Na)_2(Mg,Al)_5(Si,Al)_{12}O_{30}$	P6/mmc	Buchwald (1977)
inosilicates (continuous single or double chains of SiO_4 tetrahedra)				
aenigmatite		$Na_2Fe^{2+}{}_5TiSi_6O_{20}$	P1	
Al-Ti diopside	fassaite	$Ca(Mg,Ti,Al)(Si,Al)_2O_6$	C2/c	Dodd (1981); MacPherson et al. (1988)
akimotoite		$(Mg,Fe)SiO_3$	$R\bar{3}$	Tomioka and Fujino (1999)
anthophyllite		$(Mg,Fe)_7Si_8O_{22}(OH)_2$	Pnma	Brearley (1996)
augite		$Mg(Fe,Ca)Si_2O_6$	C2/c	Dodd (1981)
barroisite		$\square NaCa(Mg_3Al_2)(Si_7Al)O_{22}(OH)_2$	C2/m	Dobrică and Brearley (2014)
burnettite		$CaV^{3+}AlSiO_6$	C2/c	Ma and Beckett (2016a)
clinoenstatite		$Mg_2Si_2O_6$	$P2_1/c$	Lindstrom (1990); Britvin et al. (2008); Pekov (1998)
davisite	Sc-fassaite	$CaScAlSiO_6$	C2/c	Ma and Rossman (2009b); Ma et al. (2016a)
diopside		$CaMgSi_2O_6$	C2/c	Dodd (1981)
donpeacorite		$(Mn,Mg)Mg(SiO_3)_2$	Pbca	Kimura (1996); Kimura and El Goresy (1989)

enstatite		$Mg_2(SiO_3)_2$	Pbca	Dodd (1981); Keil (1968)
ferrosilite		$Fe_2(SiO_3)_2$	Pbca	Krot et al. (1997a)
fluor-richterite		$Na_2Ca(Mg,Fe)_5Si_8O_{22}F_2$	N/A	Bevan et al. (1977); Olsen et al. (1973)
grossmanite		$CaTi^{3+}AlSiO_6$	C2/c	Ma and Rossman (2009c); Ma et al. (2010)
hedenbergite		$CaFeSi_2O_6$	C2/c	Kimura and Ikeda (1995)
hemleyite		$FeSiO_3$	$R\bar{3}$	Bindi et al. (2017)
jadeite		$Na(Al,Fe)(Si_2O_6)$	C2/c	Ulyanov (1991)
jimthompsonite		$(Mg,Fe)_5Si_6O_{16}(OH)_2$	Pbca	Brearley (1996)
kaersutite		$Ca_2(Na,K)(Mg,Fe)_4Ti(Si_6Al_2)O_{22}(OH,F,Cl)_2$	C2/m	Treiman (1985)
kanoite		$(Mn,Mg)SiO_3$	$P2_1/c$	Kimura (1996); Kimura and El Goresy (1989)
kosmochlor	ureyite	$NaCrSi_2O_6$	C2/c	Buchwald (1977); Greshake and Bischoff (1996)
krinovite		$NaMg_2CrSi_3O_{10}$	P1	Buchwald (1977); Olsen and Fuchs (1968)
kuratite		$Ca_2(Fe^{2+}{}_5Ti)O_2[Si_4Al_2O_{18}]$	P1	Hwang et al. (2014)
kushiroite		$CaAlAlSiO_6$	C2/c	Kimura et al. (2009); Ma et al. (2009, 2010)
magnesio-arfvedsonite		$NaNa_2(Mg_4Fe^{3+})Si_8O_{22}(OH)_2$	C2/m	Ivanov et al. (2001)
magnesiohornblende		$Ca_2Mg_4Al_{0.75}Fe^{3+}{}_{0.25}(Si_7AlO_{22})(OH)_2$	C2/m	McCanta et al. (2008)
omphacite		$(Ca,Na)(Mg,Fe^{2+},Al)Si_2O_6$	P2/n	Kimura et al. (2013)
orthopyroxene		$(Mg,Fe)SiO_3$	Pbca	Buchwald (1977); Dodd (1981)
pigeonite		$(Fe,Mg,Ca)SiO_3$	$P2_1/c$	Dodd (1981)
potassic-chloro-hastingsite		$KCa_2(Fe^{2+}{}_4Fe^{3+})(Al_2Si_6O_{22})(Cl,OH)_2$	B2/m	McCubbin et al. (2009); Giesting and Filiberto (2016)
pyroxferroite		$(Fe,Mn,Ca)SiO_3$	P1	Papike et al. (1991)
rhodonite		$CaMn_4(Si_3O_{15})$	P1	Ulyanov (1991)
rhönite		$Ca_2(Mg,Al,Ti)_6(Si,Al)_6O_{20}$	P1	Fuchs (1971)
tissintite		$(Ca,Na,\square)AlSi_2O_6$	C2/c	Ma et al. (2015b)
wilkinsonite		$Na_2Fe^{2+}{}_4Fe^{3+}{}_2Si_6O_{20}$	P1	Ivanov et al. (2001)
winchite		$\square NaCa(Mg_4Al)Si_8O_{22}(OH)_2$	C2/m	Dobrică and Brearley (2014)
wollastonite		$CaSiO_3$	P1	Fuchs (1971)
phyllosilicates (continuous sheets of SiO_4 tetrahedra)				
aspidolite		$NaMg_3(Si_3Al)O_{10}(OH)_2$	B2/m	www.mindat.org
biotite		$K(Mg,Fe)_3(Si_3Al)O_{10}(OH,F)_2$	C2/m	Floran et al. (1978a); Johnson et al. (1991)
chlorite group				
chamosite		$(Fe^{2+},Mg,Fe^{3+})_5Al(Si_3Al)O_{10}(OH,O)_8$	C2/m	Barber (1981); Zolensky and McSween (1988)
clinochlore		$(Mg,Fe^{+2})_5Al(Si_3Al)O_{10}(OH)_8$	C2/m	Barber (1981)
clintonite		$Ca(Mg,Al)_3(Al,Si)_4O_{10}(OH,F)_2$	C2/m	Krot et al. (1995)
edenite		$NaCa_2Mg_5Si_7AlO_{22}(OH)_2$	C2/m	McCanta et al. (2008)
glauconite		$(K,Na)(Mg,Fe^{2+},Fe^{3+})(Fe^{3+},Al)(Si,Al)_4O_{10}(OH)_2$	B2/m	Kyte (1998)
illite		$(K,H_3O)Al_2(Si_3Al)O_{10}(H_2O,OH)_2$	C2/m	Gooding (1992)
margarite		$CaAl_2(Si_2Al_2)O_{10}(OH)_2$	C2/c	Krot et al. (1995)
mica		$(K,Na,Ca)(Al,Mg,Fe)_{2\text{-}3}(Si,Al,Fe)_4O_{10}(OH,F)_2$	C2/m	Velbel (1988); Zolensky and Gooding (1986)
muscovite		$KAl_2(AlSi_3O_{10})(OH)_2$	C2/m	Kurat et al. (1981)
oxyphlogopite		$K(Mg,Ti,Fe)_3[(Si,Al)_4O_{10}](O,F)_2$	C2/m	www.mindat.org
pecoraite		$Ni_3Si_2O_5(OH)_4$	C2/m	Faust et al. (1973)
phlogopite		$KMg_3(Si_3Al)O_{10}(F,OH)_2$	C2/m	Brearley (2006)
serpentine group				
amesite		$Mg_2Al(SiAl)O_5(OH)_4$	C1	Zolensky and McSween (1988)
antigorite		$Mg_3Si_2O_5(OH)_4$	Bm	Barber (1981)
berthierine		$(Fe^{2+},Fe^{3+},Mg)_{2\text{-}3}(Si,Al)_2O_5(OH)_4$	Cm	Barber (1981)

Table 1 (*Continued*)

Mineral	Synonyms and Varieties	Formula	Space Group	Selected References
chrysotile		$Mg_3Si_2O_5(OH)_4$	A2/m	Barber (1981)
cronstedtite		$Fe^{2+}{}_2Fe^{3+}(SiFe^{3+})O_5(OH)_4$	$P3_1m$	Zolensky and McSween (1988)
ferroan antigorite		$(Mg,Fe,Mn)_3(Si,Al)_2O_5(OH)_4$	Bm	Barber (1981)
greenalite		$(Fe^{2+},Fe^{3+})_{2-3}Si_2O_5(OH)_4$	unknown	Barber (1981)
lizardite		$Mg_3Si_2O_5(OH)_4$	P1	Barber (1981)
smectite group				
montmorillonite		$(Na,Ca)_{0.3}(Al,Mg)_2Si_4O_{10}(OH)_2{\cdot}nH_2O$	C2/m	Krot et al. (1995); Zolensky and McSween (1988)
nontronite		$Na_{0.3}Fe^{3+}{}_2(Si,Al)_4O_{10}(OH)_2.nH_2O$	C2/m	Zolensky and McSween (1988)
saponite		$(Ca,Na)_{0.3}(Mg,Fe^{2+})_3(Si,Al)_4O_{10}(OH)_2{\cdot}4H_2O$	C2/m	Brearley (1995); Krot et al. (1995)
sobotkite		$(K,Ca)_{0.3}(Mg_2Al)(Si_3Al)O_{10}(OH)_2{\cdot}5H_2O$	unknown	Barber (1981)
sodium-phlogopite	aspidolite	$(Na,K)Mg_3(Si_3Al)O_{10}(F,OH)_2$	B2/m	Krot et al. (1995)
talc		$Mg_3(Si_4O_{10})(OH)_2$	C2/c	Barber (1981); Brearley (1996)
vermiculite		$(Mg,Fe^{2+},Al)_3(Al,Si)_4O_{10}(OH)_2{\cdot}4H_2O$	C2/m	Ulyanov (1991); Zolensky and McSween (1988)
tectosilicates (continuous framework of SiO_4 tetrahedra)				
albite		$NaAlSi_3O_8$	C1	Keil (1968)
anorthite		$CaAl_2Si_2O_8$	P1, I1	MacPherson et al. (1988)
celsian		$BaAl_2Si_2O_8$	I2/c	Dodd (1981); MacPherson et al. (1988)
chabazite-Na		$(Na_3K)Al_4Si_8O_{24}{\cdot}11H_2O$	R3m	Zolensky and Ivanov (2003)
coesite		SiO_2	C2/c	Weisberg and Kimura (2010); Kimura et al. (2016)
cristobalite		SiO_2	$P4_12_12$	Marvin (1962); Dodd (1981)
dmisteinbergite		$CaAl_2Si_2O_8$	P6/mmm	Ma et al. (2013b)
feldspar group		$(K,Na,Ca)(Si,Al)_4O_8$		Buchwald (1977)
haüyne (tentative ID)		$Na_3Ca(Si_3Al_3)O_{12}(SO_4)$	$P\bar{4}3n$	Flight (1887)
liebermannite		$KAlSi_3O_8$	I4/m	Ma et al. (2015c)
lingunite		$NaAlSi_3O_8$	I4/m	Gillet et al. (2000)
marialite		$Na_4(Si,Al)_{12}O_{24}Cl$	I4/m	Kimura (1996); Alexander et al. (1987)
maskelynite		$(Na,Ca)(Si,Al)_4O_8$		Binns (1967); Rubin (2015c)
nepheline		$(Na,K)AlSiO_4$	$P6_3$	MacPherson et al. (1988)
opal		$SiO_2{\cdot}nH_2O$		Buchwald (1977)
orthoclase		$KAlSi_3O_8$	C2/m	Kerridge and Matthews (1988)
plagioclase		$(Na,Ca)(Si,Al)_3O_8$	C1	Dodd (1981)
quartz		SiO_2	$P3_121$, $P3_232$	Dodd (1981)
sanidine		$KAlSi_3O_8$	C2/m	Floran et al. (1978b); Johnson et al. (1991)
seifertite		SiO_2	Pbcn or Pb2n	El Goresy et al. (2008)
silica with α-PbO_2 structure (not approved)		SiO_2	unknown	Kimura et al. (2000); Sharp et al. (1997); Hu and Sharp (2016)
silica with ZrO_2-like structure (not approved)		SiO_2	unknown	Kimura et al. (2000); Sharp et al. (1997); Hu and Sharp (2016)
sodalite		$Na_4(Si_3Al_3)O_{12}Cl$	$P\bar{4}3n$	MacPherson et al. (1988)
sodium-calcium hexaluminosilicate (not approved)		$(Ca_xNa_{1-x})Al_{3+x}Si_{3-x}O_{11}$	unknown	Beck et al. (2004)
stilbite-Ca		$NaCa_4(Si_{27}Al_9)O_{72}{\cdot}30H_2O$	C2/m	Kimura (1996); Gooding (1981)
stishovite		SiO_2	P4/mnm	Chao et al. (1962)
tridymite		SiO_2	F1	Dodd (1981)
zagamiite		$CaAl_2Si_{3.5}O_{11}$	$P6_3/mmc$	Ma and Tschauner (2017); Ma et al. (2017b)
zeolite group		$(Na,K)_{0-2}(Ca,Mg)_{1-2}(Al,Si)_{5-10}O_{10-20}{\cdot}nH_2O$		MacPherson et al. (1988)
oxalate				
whewellite		$CaC_2O_4{\cdot}H_2O$	$P2_1/n$	Fuchs et al. (1973)
phosphate-silicate				
tsangpoite		$Ca_5(PO_4)_2(SiO_4)$	$P6_3/m$, $P6_3$, or $P6_322$	Hwang et al. (2016b)

Table 2
Alphabetical list of meteoritic minerals.

aluminium	Al
addibischoffite	$Ca_2Al_6Al_6O_{20}$
adrianite	$Ca_{12}(Al_4Mg_3Si_7)O_{32}Cl_6$
aenigmatite	$Na_2Fe^{2+}{}_5TiSi_6O_{20}$
ahrensite	Fe_2SiO_4
akaganéite	β-FeO(OH,Cl)
åkermanite	C
akimotoite	$(Mg,Fe)SiO_3$
alabandite	MnS
albite	$NaAlSi_3O_8$
allabogdanite	$(Fe,Ni)_2P$
allendeite	$Sc_4Zr_3O_{12}$
almandine	$Fe_3Al_2(SiO_4)_3$
altaite	PbTe
Al-Ti diopside	$Ca(Mg,Ti,Al)_2O_6$
amakinite	$(Fe^{2+},Mg)(OH)_2$
amesite	$Mg_2Al(SiAl)O_5(OH)_4$
anatase	TiO_2
andradite	$Ca_3Fe_2(SiO_4)_3$
andreyivanovite	FeCrP
anhydrite	$CaSO_4$
ankerite	$Ca(Fe^{2+},Mg,Mn)(CO_3)_2$
anorthite	$CaAl_2Si_2O_8$
anosovite (not approved)	$(Ti^{4+},Ti^{3+},Mg,Sc,Al)_3O_5$
anthophyllite	$(Mg,Fe)_7Si_8O_{22}(OH)_2$
antigorite	$Mg_3Si_2O_5(OH)_4$
antitaenite (not approved)	Fe_3Ni
apatite	$Ca_5(PO_4)_3(F,OH,Cl)$
aragonite	$CaCO_3$
armalcolite	$(Mg,Fe)Ti_2O_5$
arupite	$Ni_3(PO_4)_2{\cdot}8H_2O$
aspidolite	$NaMg_3(Si_3Al)O_{10}(OH)_2$
augite	$Mg(Fe,Ca)Si_2O_6$
awaruite	Ni_3Fe
baddeleyite	ZrO_2
barite	$BaSO_4$
barringerite	$(Fe,Ni)_2P$
barringtonite	$MgCO_3{\cdot}2H_2O$
barroisite	$□NaCa(Mg_3Al_2)(Si_7Al)O_{22}(OH)_2$
bassanite	$CaSO_4{\cdot}½H_2O$
beckettite	$Ca_2V_6Al_6O_{20}$
berthierine	$(Fe^{2+},Fe^{3+},Mg)_{2-3}(Si,Al)_2O_5(OH)_4$
beta-moissanite	SiC
beusite	$(Mn,Fe,Ca,Mg)_3(PO_4)_2$
biotite	$K(Mg,Fe)_3(Si_3Al)O_{10}(OH,F)_2$
blödite	$Na_2Mg(SO_4)_2{\cdot}4H_2O$
bobdownsite	$Ca_9Mg(PO_4)_6(PO_3F)$
bornite	Cu_5FeS_4
breunnerite	$(Mg,Fe)CO_3$
brezinaite	Cr_3S_4
brianite	$Na_2CaMg(PO_4)_2$
bridgmanite	$(Mg,Fe)SiO_3$
britholite-(Ce)	$(Ce,Y,Ca)_5(SiO_4,PO_4)_3(OH,F)$
browneite	MnS
brownleeite	MnSi
brucite	$Mg(OH)_2$
β-silicon nitride (not approved)	$β\text{-}Si_3N_4$
buchwaldite	$NaCaPO_4$
bunsenite	NiO
burnettite	$CaV^{3+}AlSiO_6$
buseckite	(Fe,Zn,Mn)S
butianite	Ni_6SnS_2
Ca-armalcolite	$CaTi_2O_5$
calcite	$CaCO_3$
calcium oxide	CaO
carbonate-fluorapatite	$Ca_5(PO_4,CO_3)_3F$
carlsbergite	CrN
cassidyite	$Ca_2(Ni,Mg)(PO_4)_2{\cdot}2H_2O$
caswellsilverite	$NaCrS_2$
celestine	SrSO4
celsian	$Ba(Al_2Si_2O_8)$
chabazite-Na	$(Na_3K)Al_4Si_8O_{24}{\cdot}11H_2O$
chalcocite	Cu_2S
chalcopyrite	$CuFeS_2$
chamosite	$(Fe^{2+},Mg,Fe^{3+})_5Al(Si_3Al)O_{10}(OH,O)_8$
chaoite	C
chengbolite	$PtTe_2$
chevkinite	$(Ce,La,Ca,Th)_4(Fe^{2+},Mg)_2(Ti,Fe^{3+})_3Si_4O_{22}$
chladniite	$Na_2CaMg_7(PO_4)_6$
chlorapatite	$Ca_5(PO_4)_3Cl$
chlormagmaluminite	$Mg_4Al_2(OH)_{12}Cl_2{\cdot}3H_2O$
chlormayenite	$Ca_{12}Al_{14}O_{32}Cl_2$
chopinite	$Mg_3(PO_4)_2$
chromite	$FeCr_2O_4$
chrysotile	$Mg_3Si_2O_5(OH)_4$
chukanovite	$Fe_2(CO_3)(OH)_2$
cinnabar	HgS
clinochlore	$(Mg,Fe^{2+})_5Al(Si_3Al)O_{10}(OH)_8$
clinoenstatite	$Mg_2Si_2O_6$
clintonite	$Ca(Mg,Al)_3(Al,Si)_4O_{10}(OH,F)_2$
cobaltite	CoAsS
coesite	SiO_2
cohenite	$(Fe,Ni)_3C$
collinsite	$Ca_2(Mg,Fe,Ni)(PO_4)_2{\cdot}2H_2O$
cooperite	PtS
copiapite	$Fe_5(SO_4)_6(OH)_2{\cdot}20H_2O$
copper	Cu
coquimbite	$Fe_2(SO_4)_3{\cdot}9H_2O$
cordierite	$Mg_2Al_4Si_5O_{18}$
corundum	Al_2O_3
coulsonite	FeV_2O_4
covellite	CuS
cristobalite	SiO_2
cronstedtite	$Fe^{2+}{}_2Fe^{3+}(SiFe^{3+})O_5(OH)_4$
cronusite	$Ca_{0.2}CrS_2{\cdot}2H_2O$
cubanite	$CuFe_2S_3$
cupalite	CuAl
cuprite	Cu_2O
daubréelite	$FeCr_2S_4$
davisite	$CaScAlSiO_6$
decagonite	$Al_{71}Ni_{24}Fe_5$
diamond	C
digenite	Cu_9S_5
diopside	$CaMgSi_2O_6$
djerfisherite	$K_6Na_9(Fe,Cu)_{24}S_{26}Cl$
dmisteinbergite	$CaAl_2Si_2O_8$
dmitryivanovite	$CaAl_2O_4$
dolomite	$CaMg(CO_3)_2$
donpeacorite	$(Mn,Mg)Mg(SiO_3)_2$
droninoite	$Ni_6Fe^{3+}{}_2Cl_2(OH)_{16}{\cdot}4H_2O$
edenite	$NaCa_2Mg_5Si_7AlO_{22}(OH)_2$
electrum (not approved)	Au-Ag
enstatite	$Mg_2(SiO_3)_2$
epsomite	$MgSO_4{\cdot}7H_2O$
eringaite	$Ca_3Sc_2Si_3O_{12}$
erlichmanite	OsS_2
eskolaite	Cr_2O_3
farringtonite	$Mg_3(PO_4)_2$
fayalite	Fe_2SiO_4
feldspar group	$(K,Na,Ca)(Si,Al)_4O_8$
feroxyhyte	δ-FeO(OH)
ferrihydrite	$Fe_{4-5}(OH,O)_{12}$
ferroan alabandite	(Mn,Fe)S
ferroan antigorite	$(Mg,Fe,Mn)_3(Si,Al)_2O_5(OH)_4$
ferromerrillite	$Ca_9NaFe^{2+}(PO_4)_7$
ferropseudobrookite	$FeTi_2O_5$
ferrosilite	$Fe_2(SiO_3)_2$
florenskyite	(Fe,Ni)TiP
fluorapatite	$Ca_5(PO_4)_3F$
fluor-richterite	$Na_2Ca(Mg,Fe)_5Si_8O_{22}F_2$
forsterite	Mg_2SiO_4
galena	PbS
galileiite	$NaFe_4(PO_4)_3$
gehlenite	$Ca_2Al(Si,Al)_2O_7$
geikielite	$MgTiO_3$
gentnerite (not approved)	$Cu_8Fe_3Cr_{11}S_{18}$
gersdorffite	NiAsS
glauconite	$(K,Na)(Mg,Fe^{2+},Fe^{3+})$ $(Fe^{3+},Al)(Si,Al)_4O_{10}(OH)_2$
goethite	α-FeO(OH)
gold	Au
gold-dominated alloys	(Au,Ag,Fe,Ni,Pt)

Table 2 (*Continued*)

goldmanite	$Ca_3V_2(SiO_4)_3$
graftonite	$(Fe,Mn)_3(PO_4)_2$
graphite-2H	C
graphite-3R	C
greenalite	$(Fe^{2+},Fe^{3+})_{2-3}Si_2O_5(OH)_4$
greigite	Fe_3S_4
grossite	$CaAl_4O_7$
grossmanite	$CaTi^{3+}AlSiO_6$
grossular	$Ca_3Al_2(SiO_4)_3$
gupeiite	Fe_3Si
gypsum	$CaSO_4{\cdot}2H_2O$
haapalaite	$4(Fe,Ni)S{\cdot}3(Mg,Fe^{2+})(OH)_2$
halite	NaCl
hapkeite	Fe_2Si
haüyne (tentative ID)	$Na_3Ca(Si_3Al_3)O_{12}(SO_4)$
haxonite	$(Fe,Ni)_{23}C_6$
heazlewoodite	Ni_3S_2
hedenbergite	$CaFeSi_2O_6$
heideite	$(Fe,Cr)_{1+x}(Ti,Fe)_2S_4$
hematite	α-Fe_2O_3
hemleyite	$FeSiO_3$
hercynite	$(Fe,Mg)Al_2O_4$
hexaferrum	(Fe,Os,Ir,Mo)
hexahydrite	$MgSO_4{\cdot}6H_2O$
hexamolybdenum	(Mo,Ru,Fe)
hibbingite	γ-$Fe_2(OH)_3Cl$
hibonite	$CaAl_{12}O_{19}$
hibonite-(Fe)	$(Fe,Mg)Al_{12}O_{19}$
hollandite	$(Fe_{15},Ni)(O_{12}(OH)_{20})Cl(OH)_2$
hollisterite	Al_3Fe
honessite	$(Ni,Fe)_8SO_4(OH)_{16}{\cdot}nH_2O$
hutcheonite	$Ca_3Ti_2(SiAl_2)O_{12}$
hydromagnesite	$Mg_5(CO_3)_4(OH)_2{\cdot}4H_2O$
hydroxylapatite	$Ca_5(PO_4)_3OH$
icosahedrite	$Al_{63}Cu_{24}Fe_{13}$
idaite	Cu_5FeS_6
illite	$(K,H_3O)Al_2(Si_3Al)O_{10}(H_2O,OH)_2$
ilmenite	$FeTiO_3$
indialite	$Mg_2Al_3(AlSi_5O_{18})$
irarsite	(Ir,Ru,Rh,Pt)AsS
iridarsenite	$(Ir,Ru)As_2$
iridium	Ir
iron	α-Fe
iron carbide (not approved)	$Fe_{2.5}C$
isocubanite	$CuFe_2S_3$
jadeite	$Na(Al,Fe)(Si_2O_6)$
jarosite	$KFe_3(SO_4)_2(OH)_6$
jimthompsonite	$(Mg,Fe)_5Si_6O_{16}(OH)_2$
joegoldsteinite	$MnCr_2S_4$
johnsomervilleite	$Na_2Ca(Fe,Mg,Mn)_7(PO_4)_6$
kaersutite	$Ca_2(Na,K)(Mg,Fe)_4Ti(Si_6Al_2)O_{22}(OH,F,Cl)_2$
kamiokite	$Fe_2Mo_3O_8$
kangite	$(Sc,Ti,Al,Zr,Mg,Ca,\square)_2O_3$
kanoite	$(Mn,Mg)SiO_3$
keilite	(Fe,Mn,Mg,Ca,Cr)S
khamrabaevite	TiC
khatyrkite	$CuAl_2$
kieserite	$MgSO_4{\cdot}H_2O$
kirschsteinite	$CaFe(SiO_4)$
K-Na-Fe phosphate	$(K,Na)Fe_4(PO_4)_3$
kosmochlor	$NaCrSi_2O_6$
krinovite	$NaMg_2CrSi_3O_{10}$
krotite	$CaAl_2O_4$
kryachkoite	$(Al,Cu)_6(Fe,Cu)$
kuratite	$Ca_2(Fe^{2+}{}_5Ti)O_2[Si_4Al_2O_{18}]$
kushiroite	$CaAlAlSiO_6$
kutnohorite	$Ca(Mn,Mg,Fe^{2+})(CO_3)_2$
lakargiite	$CaZrO_3$
larnite	Ca_2SiO_4
laurite	RuS_2
lawrencite	$(Fe^{2+},Ni)Cl_2$
lepidocrocite	γ-FeO(OH)
liebermannite	$KAlSi_3O_8$
lingunite	$NaAlSi_3O_8$
linzhiite	$FeSi_2$
lipscombite	$(Fe,Mn)Fe_2(PO_4)_2(OH)_2$
lizardite	$Mg_3Si_2O_5(OH)_4$

Table 2 (*Continued*)

löllingite	$FeAs_2$
lonsdaleite	C
loveringite	$Ca(Ti,Fe,Cr,Mg)_{21}O_{38}$
machiite	$Al_2Ti_3O_9$
mackinawite	FeS_{1-x}
maghemite	$Fe_{2.67}O_4$
Magnéli phases	Ti_5O_9 and Ti_8O_{15}
magnesio-arfvedsonite	$NaNa_2(Mg_4Fe^{3+})Si_8O_{22}(OH)_2$
magnesiochromite	$MgCr_2O_4$
magnesioferrite	$MgFe_2O_4$
magnesiohornblende	$Ca_2Mg_4Al_{0.75}Fe^{3+}{}_{0.25}(Si_7AlO_{22})(OH)_2$
magnesiowüstite	(Mg,Fe)O
magnesite	$(Mg,Fe)CO_3$
magnetite	Fe_3O_4
majindeite	$Mg_2Mo_3O_8$
majorite	$Mg_3(SiMg)Si_3O_{12}$
marcasite	FeS_2
margarite	$CaAl_2(Si_2Al_2)O_{10}(OH)_2$
marialite	$Na_4(Si,Al)_{12}O_{24}Cl$
maricite	$NaFePO_4$
martensite (not approved)	α_2-(Fe,Ni)
maskelynite	$(Na,Ca)(Si,Al)_4O_8$
matyhite	$Ca_{18}(Ca,\square)_2Fe^{2+}{}_2(PO_4)_{14}$
maucherite	$Ni_{11}As_8$
melanterite	$FeSO_4{\cdot}7H_2O$
melilite	$(Ca,Na)_2(Al,Mg)(Si,Al)_2O_7$
melliniite	$(Ni,Fe)_4P$
mendozite	$NaAl(SO_4)_2{\cdot}11H_2O$
mercury	Hg
merrihueite	$(K,Na)_2Fe_5Si_{12}O_{30}$
merrillite	$Ca_9MgNa(PO_4)_7$
mica	$(K,Na,Ca)(Al,Mg,Fe)_{2-3}(Si,Al,Fe)_4O_{10}(OH,F)_2$
millerite	NiS
molybdenite	MoS_2
molybdenum (not approved)	Mo
molybdenum carbide (not approved)	MoC
monazite-(Ce)	$(Ce,La,Th)PO_4$
moncheite	$Pt(Te,Bi)_2$
monipite	MoNiP
monticellite	$CaMgSiO_4$
montmorillonite	$(Na,Ca)_{0.3}(Al,Mg)_2Si_4O_{10}(OH)_2{\cdot}nH_2O$
moraskoite	$Na_2Mg(PO_4)F$
mullite	$Al_6Si_2O_{13}$
murchisite	Cr_5S_6
muscovite	$KAl_2(AlSi_3O_{10})(OH)_2$
naquite	FeSi
Nb-oxide	$(Nb,V,Fe)O_2$
nepheline	$(Na,K)AlSiO_4$
nesquehonite	$Mg(HCO_3)(OH){\cdot}2H_2O$
nickel	Ni
nickelblödite	$Na_2(Ni,Mg)(SO_4)_2{\cdot}4H_2O$
nickeline	NiAs
nickelphosphide	Ni_3P
nierite	a-Si_3N_4
niningerite	(Mg,Fe)S
niobium (not approved)	Nb
nontronite	$Na_{0.3}Fe^{3+}{}_2(Si,Al)_4O_{10}(OH)_2{\cdot}nH_2O$
nuwaite	Ni_6GeS_2
nyerereite	$Na_2Ca(CO_3)_2$
oldhamite	CaS
olivine	$(Mg,Fe)_2SiO_4$
olkhonskite	$Cr_2Ti_3O_9$
omeiite	$(Os,Ru)As_2$
omphacite	$(Ca,Na)(Mg,Fe^{2+},Al)Si_2O_6$
opal	$SiO_2{\cdot}nH_2O$
orcelite	$Ni_{5-x}As_2$
orthoclase	$KAlSi_3O_8$
orthopyroxene	$(Mg,Fe)SiO_3$
osbornite	TiN
osmium	Os
osumilite	$(K,Na)(Fe,Mg)_2(Al,Fe)_3[(Si,Al)_{12}O_{30}]$
oxyphlogopite	$K(Mg,Ti,Fe)_3[(Si,Al)_4O_{10}](O,F)_2$
panethite	$(Ca,Na)_2(Mg,Fe)_2(PO_4)_2$
panguite	$(Ti,Al,Sc,Mg,Zr,Ca)_{1.8}O_3$
paqueite	$Ca_3TiSi_2(Al,Ti,Si)_3O_{14}$
paraotwayite	$Ni(OH)_{2-x}(SO_4,CO_3)_{0.5x}$
pecoraite	$Ni_3Si_2O_5(OH)_4$

Table 2 (*Continued*)

pentlandite	$(Fe,Ni)_9S_8$
periclase	MgO
perovskite	$CaTiO_3$
perrierite	$(Ce,La,Ca)_4(Fe^{2+},Mg)_2(Ti,Fe^{3+})_3Si_4O_{22}$
perryite	$(Ni,Fe)_5(Si,P)_2$
PGE-dominated alloys	(Pt,Os,Ir,Ru,Re,Rh,Mo,Nb,Ta, Ge,W,V,Pb,Cr,Fe,Ni,Co)
phlogopite	$KMg_3(Si_3Al)O_{10}(F,OH)_2$
pigeonite	$(Fe,Mg,Ca)SiO_3$
plagioclase	$(Na,Ca)(Si,Al)_3O_8$
plagionite	$Pb_5Sb_8S_{17}$
platinum	Pt
pleonaste	$(Mg,Fe)Al_2O_4$
portlandite	$Ca(OH)_2$
potassic-chloro-hastingsite	$KCa_2(Fe^{2+}{}_4Fe^{3+})(Al_2Si_6O_{22})(Cl,OH)_2$
powellite	$CaMoO_4$
pseudobrookite	Fe_2TiO_5
pumpellyite	$Ca_2(Mg,Fe^{+2})Al_2(SiO_4)(Si_2O_7)(OH)_2{\cdot}H_2O$
pyrite	FeS_2
pyrochlore	$(Na,Ca)_2Nb_2O_6(OH,F)$
pyrope	$Mg_3Al_{22}(SiO_4)_3$
pyrophanite	$MnTiO_3$
pyroxferroite	$(Fe,Mn,Ca)SiO_3$
pyrrhotite	$Fe_{1-x}S$
quartz	SiO_2
rammelsbergite	$NiAs_2$
reevesite	$Ni_6Fe_2(CO_3)(OH)_{14}{\cdot}4H_2O$
reidite	$ZrSiO_4$
rhenium (not approved)	Re
rhodochrosite	$MnCO_3$
rhodonite	$CaMn_4(Si_3O_{15})$
rhönite	$Ca_2(Mg,Al,Ti)_6(Si,Al)_6O_{20}$
ringwoodite	Mg_2SiO_4
roaldite	$(Fe,Ni)_4N$
roedderite	$(K,Na)_2Mg_5Si_{12}O_{30}$
rubinite	$Ca_3Ti_2Si_3O_{12}$
rudashevskyite	(Fe,Zn)S
rustenburgite	$(Pt,Pd)_3Sn$
ruthenium	Ru
ruthenosmiridim	RuOsIr
rutile	TiO_2
safflorite	$CoAs_2$
sanidine	$KAlSi_3O_8$
saponite	$(Ca,Na)_{0.3}(Mg,Fe^{2+})_3(Si,Al)_4O_{10}(OH)_2{\cdot}4H_2O$
sapphirine	$(Mg,Al)_7(Mg,Al)O_2(Al,Si)_6O_{18}$
sarcopside	$(Fe,Mn)_3(PO_4)_2$
scheelite	$CaWO_4$
schöllhornite	$Na_{0.3}(H_2O)\,[CrS_2]$
schreibersite	$(Fe,Ni)_3P$
schwertmannite	$Fe^{3+}{}_{16}(OH,SO_4)_{12\text{-}13}O_{16}{\cdot}10H_2O$
seifertite	SiO_2
selenium	Se
siderite	$FeCO_3$
silica with α-PbO_2 structure (not approved)	SiO_2
silica with ZrO_2-like structure (not approved)	SiO_2
sinoite	Si_2N_2O
slavikite	$NaMg_2Fe_5(SO_4)_7(OH)_6{\cdot}33H_2O$
smythite	Fe_9S_{11}
sobotkite	$(K,Ca)_{0.3}(Mg_2Al)(Si_3Al)O_{10}(OH)_2{\cdot}5H_2O$
sodalite	$Na_4(Si_3Al_3)O_{12}Cl$
sodium-bearing silicate	$(Na,K,Ca,Fe)_{0.973}(Al,Si)_{5.08}O_{10}$
sodium-calcium hexaluminosilicate (not approved)	$(Ca_xNa_{1-x})Al_{3+x}Si_{3-x}O_{11}$
sodium-phlogopite	$(Na,K)Mg_3(Si_3Al)O_{10}(F,OH)_2$
sperrylite	$PtAs_2$
sphalerite	(Zn,Fe)S
spinel	$MgAl_2O_4$
stanfieldite	$Ca_4(Mg,Fe)_5(PO_4)_6$
starkeyite	$MgSO_4{\cdot}4H_2O$
steinhardtite	(Al,Ni,Fe)
stilbite-Ca	$NaCa_4(Si_{27}Al_9)O_{72}{\cdot}30H_2O$
stishovite	SiO_2
stolperite	AlCu
suessite	Fe_3Si

Table 2 (*Continued*)

sulfur	S
sylvite	KCl
szomolnokite	$FeSO_4{\cdot}H_2O$
taenite	γ-(Fe,Ni)
talc	$Mg_3(Si_4O_{10})(OH)_2$
tazheranite	$(Zr,Ti,Ca,Y)O_{1.75}$
tetragonal almandine	$(Fe,Mg,Ca,Na)_3(Al,Si,Mg)_2Si_3O_{12}$
tetragonal majorite	$Mg_3(SiMg)Si_3O_{12}$
tetrataenite	FeNi
thorianite	ThO_2
thortveitite	$Sc_2Si_2O_7$
Ti-rich magnetite	$(Fe,Mg)(Fe,Ti)_2O_4$
tissintite	$(Ca,Na,\square)AlSi_2O_6$
tistarite	Ti_2O_3
titanite	$CaTiSiO_5$
tochilinite	$2[(Fe,Mg,Cu,Ni)S]$ $\cdot 1.57\text{-}1.85[(Mg,Fe,Ni,Al,Ca)(OH)_2]$
tranquillityite	$Fe^{2+}{}_8Ti_3Zr_2Si_3O_{24}$
trevorite	$NiFe_2O_4$
tridymite	SiO_2
troilite	FeS
tsangpoite	$Ca_5(PO_4)_2(SiO_4)$
tugarinovite	MoO_2
tuite	γ-$Ca_3(PO_4)_2$
tungstenite	WS_2
ulvöspinel	Fe_2TiO_4
valleriite	$2[(Fe,Cu)S]{\cdot}1.53[(Mg,Al)(OH)_2]$
vaterite	$CaCO_3$
vermiculite	$(Mg,Fe^{2+},Al)_3(Al,Si)_4O_{10}(OH)_2{\cdot}4H_2O$
violarite	$FeNi_2S_4$
vivianite	$Fe_3(PO_4)_2{\cdot}8H_2O$
voltaite	$K_2Fe_8Al(SO_4)_{12}{\cdot}18H_2O$
V-rich magnetite	$(Fe,Mg)(Fe,V)_2O_4$
wadalite	$Ca_6Al_5Si_2O_{16}Cl_3$
wadsleyite	$(Mg,Fe)_2SiO_4$
wairauite	CoFe
wangdaodeite	$FeTiO_3$
warkite	$Ca_2Sc_6Al_6O_{20}$
wassonite	TiS
whewellite	$CaC_2O_4{\cdot}H_2O$
wilkinsonite	$Na_2Fe^{2+}{}_4Fe^{3+}{}_2Si_6O_{20}$
winchite	$\square NaCa(Mg_4Al)Si_8O_{22}(OH)_2$
wollastonite	$CaSiO_3$
wurtzite-2H	β-ZnS
wüstite	FeO
xenophyllite	$Na_4Fe_7(PO_4)_6$
xenotime	YPO_4
xieite	$FeCr_2O_4$
xifengite	Fe_5Si_3
yagiite	$(K,Na)_2(Mg,Al)_5(Si,Al)_{12}O_{30}$
zagamiite	$CaAl_2Si_{3.5}O_{11}$
zaratite	$Ni_3CO_3(OH)_4{\cdot}4H_2O$
zeolite group	$(Na,K)_{0\text{-}2}(Ca,Mg)_{1\text{-}2}$ $(Al,Si)_{5\text{-}10}O_{10\text{-}20}{\cdot}nH_2O$
zhanghengite	(Cu,Zn)
zircon	$ZrSiO_4$
zirconium carbide (not approved)	ZrC
zirconolite	$(Ca,Ce)Zr(Ti,Nb,Fe^{3+})_2O_7$
zirkelite	$(Ca,Th,Ce)Zr(Ti,Nb)_2O_7$

Some meteoritic minerals form by only a single mechanism (e.g., ringwoodite and ahrensite by high-pressure shock metamorphism of olivine); other minerals form by several mechanisms (e.g., olivine by condensation around red giant and AGB stars, condensation in the solar nebula, crystallization in CAI and AOI melts, crystallization in chondrule melts, thermal metamorphism, crystallization from impact melts, condensation within impact plumes, crystallization in magmatic bodies on differentiated asteroids, annealing of amorphous material, and aqueous alteration).

In this overview, no attempt has been made to describe every mode of formation of every meteoritic mineral. That monumental task would require a multi-volume book-length treatment. Even so, it should be recognized that meteoritic minerals represent only one small subset of planetary materials (e.g., Smith, 1979; Papike, 1998;

Davis, 2005; McSween and Huss, 2010; Lee and Leroux, 2015) and only ~8% of the total number of well-characterized mineral species.

2. Formation of meteoritic minerals

2.1. Condensation in gaseous envelopes around evolved stars

Presolar grains are the oldest meteoritic minerals. They range from 0.002–20 μm in size and formed in the outflows of old, evolved stars and as supernova ejecta. They may have drifted in and out of several interstellar clouds before being incorporated into the molecular cloud which spawned the Solar System (Zinner, 2005). Presolar phases include C polymorphs (diamond and graphite), Si-, Fe-, Ti-, Mo- and Zr-rich carbides, metallic Fe and metallic Fe-Ni, Si nitride, Mg-, Al- and Ti-rich oxides, and silicates (predominantly olivine, pyroxene and glass).

Although diamond is the most abundant presolar mineral species, its origin is enigmatic; this is due in large measure to the small average grain size (~2.6 nm) that has earned the phase the sobriquet "nanodiamond." Aggregates of presolar diamonds contain the noble-gas component Xe-HL, which is enriched in both heavy (H) and light (L) Xe isotopes; these enrichments probably reflect both r- and s-process neutron bombardment during supernova explosions. However, as pointed out by Zinner (2005), the concentration of Xe-HL is so low and the grains so small that only 0.0001% of diamond grains are likely to contain a single Xe atom. The individual diamonds that do contain the Xe-HL component (and, presumably, many of their Xe-free congeners) may have condensed from the expanding gas expelled by supernovae after temperatures dipped below ~1000 K (Anders and Zinner, 1993). However, it is possible that a significant fraction of the nanodiamonds in chondrites are not presolar at all, but originated within the Solar System (Dai et al., 2002).

Presolar silicon carbide grains range from 0.1–20 μm in size. Most of the grains probably condensed within the expanding envelopes around thermally pulsing, asymptotic giant branch (AGB) stars (Zinner, 2005). These late-type stars are highly luminous red giants that have exhausted the helium fuel in their cores. They have migrated on H-R diagrams along a track subparallel to the typical red giant track that they traversed at an earlier stage when they had exhausted their supply of hydrogen (e.g., Fig. 1 of Herwig, 2005). Many SiC grains have $^{13}C/^{12}C$, $^{15}N/^{14}N$ and $^{34}S/^{33}S$ isotopic ratios (e.g., Zinner et al., 1989; Hoppe et al., 1994; Hoppe et al., 1995; Hoppe et al., 2015; Nittler et al., 1995), consistent with those measured and modeled in AGB stars (e.g., Lambert et al., 1986; Huss et al., 1997).

Presolar graphite grains range from 1–20 μm. Many contain 20- to 500-nm-size grains of TiC; while some TiC-bearing graphite grains also contain Zr- and Mo- rich carbides (Bernatowicz et al., 1991, 1996), other TiC-bearing grains instead contain low-Ni metallic Fe (kamacite), cohenite and metallic Fe (Bernatowicz et al., 1999; Croat et al., 2003). The internal carbide and metallic-Fe- rich grains must have condensed before the graphite grains. One variety of graphite grain that is of low density ($\leq$2.05 g cm^{-3}) has numerous isotopic anomalies consistent with a supernova origin. Typically, such grains are enriched in ^{15}N, ^{26}Al, ^{13}C,^{18}O, ^{28}Si, and, in some cases, ^{29}Si and ^{30}Si; a few grains are enriched in ^{44}Ti, ^{49}Ti, ^{50}Ti, ^{41}K and ^{41}Ca (Zinner, 2005). Isotopic anomalies in Mo and Zr have also been reported. High- density graphite grains appear to have been derived from AGB stars and supernovae (e.g., Amari et al., 1995). Additional graphite grains may have originated in novae.

Presolar oxide grains include micrometer and submicrometer-size corundum (Al_2O_3), spinel ($MgAl_2O_4$), hibonite ($CaAl_{12}O_{19}$) and TiO_2 (Zinner, 2005; Bose et al., 2010). Isotopic anomalies in O, Al and Ti suggest derivation from red giant and AGB stars.

Rare presolar Si_3N_4 grains are enriched in ^{15}N, ^{28}Si and ^{26}Al and appear to have originated in supernovae. Silicon nitride grains have also been identified in the circumstellar shells of a few extreme carbon stars (Clément et al., 2005). These are AGB stars which achieved a high mass-loss rate (i.e., a superwind) and in which convection dredged up C produced in the He-burning shell (Volk et al., 1992; Messenger et al., 2013).

Presolar silicate grains have been identified in IDPs, micrometeorites, primitive carbonaceous chondrites, LL3 ordinary chondrites (OC) and EH3 enstatite chondrites mainly by their O-isotopic anomalies (e.g., Messenger et al., 2003; Mostefaoui et al., 2003; Nagashima et al., 2004; Nguyen and Zinner, 2004; Mostefaoui and Hoppe, 2004; Kobayashi et al., 2005; Ebata et al., 2006; Bose et al., 2010). The grains include olivine, pyroxene, Al-rich silicate and amorphous material; whereas most grains are magnesian, a few contain more FeO than MgO (Bose et al., 2010). Red giants and AGB stars are the likely sources of the presolar silicates.

2.2. Condensation in the solar nebula

There is broad consensus that at least some regions of the solar nebula were hot enough to evaporate preexisting dust and that a significant fraction of nebular materials spent time in such regions. As the entire nebula cooled or as the gas from hot regions passed into cooler zones, minerals began to condense as submicrometer-size grains. The phases that are predicted to condense can be modeled by assuming closed-system thermodynamic equilibrium, a fixed pressure (typically 10^{-2} to 10^{-6} atm), and an initial starting gas composition (usually solar). Such calculations were carried out by several workers including Urey (1955), Lord (1965), Larimer (1967), Grossman (1972), Yoneda and Grossman (1995) and Ebel (2006). Variants of the standard condensation models include those invoking significant dust enrichments (e.g., Wood and Hashimoto, 1993; Ebel and Grossman, 2000) and those involving the isolation of some fraction of the early condensates from the residual nebular gas (e.g., Petaev and Wood, 1998a; Petaev and Wood, 1998b).

Phases that appear in standard condensation calculations at temperatures between ~1770 K and 1100 K include spinel, anorthite, albite, Ca pyroxene (diopside), forsterite, enstatite, gehlenite ($Ca_2Al(Si,Al)_2O_7$), åkermanite ($Ca_2Al(Si,Al)_2O_7$), hibonite, corundum, perovskite ($CaTiO_3$) and metallic Fe-Ni (e.g., Fig. 2 of Davis and Richter, 2005). Most of these minerals are those most commonly found in Ca-Al inclusions (CAIs) as primary phases (e.g., Table 1 of MacPherson, 2005); corundum and albite, however, are rare in pristine CAIs. The presence of other refractory minerals (grossite – $CaAl_4O_7$; krotite – $CaAl_2O_4$; rhönite – $Ca_2(Mg,Al,Ti)_6(Si,Al)_6O_{20}$) in some CAIs suggests that, at least locally, there were minor variations in nebular conditions that allowed these phases to become stable. Common primary phases in CAIs also include submicrometer-size Pt-group metal nuggets (e.g., Wark and Lovering, 1978; Bischoff and Palme, 1987) that formed alloys via condensation of refractory siderophile elements at temperatures between ~1800 and 1300 K (e.g., Berg et al., 2009; Harries et al., 2012).

The newly-identified refractory mineral tistarite (Ti_2O_3) in Allende along with corundum and khamrabaevite (TiC) grains (Fig. 1), are likely condensates, sampling different environments in the solar nebula (Ma and Rossman, 2009a).

Brearley (1993a) reported rare 0.05-0.3-μm-size euhedral grains of Ti oxides (Ti_3O_5 and the nonstoichiometric Magnéli phases Ti_5O_9 and Ti_8O_{15}) in the matrices of Bells (CM2) and a CI-like carbonaceous-chondrite clast in the Nilpena polymict ureilite. Such phases were previously reported in some IDPs (e.g., Rietmeijer and MacKinnon, 1987; Rietmeijer and MacKinnon, 1990; Zolensky et al., 1989; Blake et al., 1989). It seems likely that these Ti oxides were

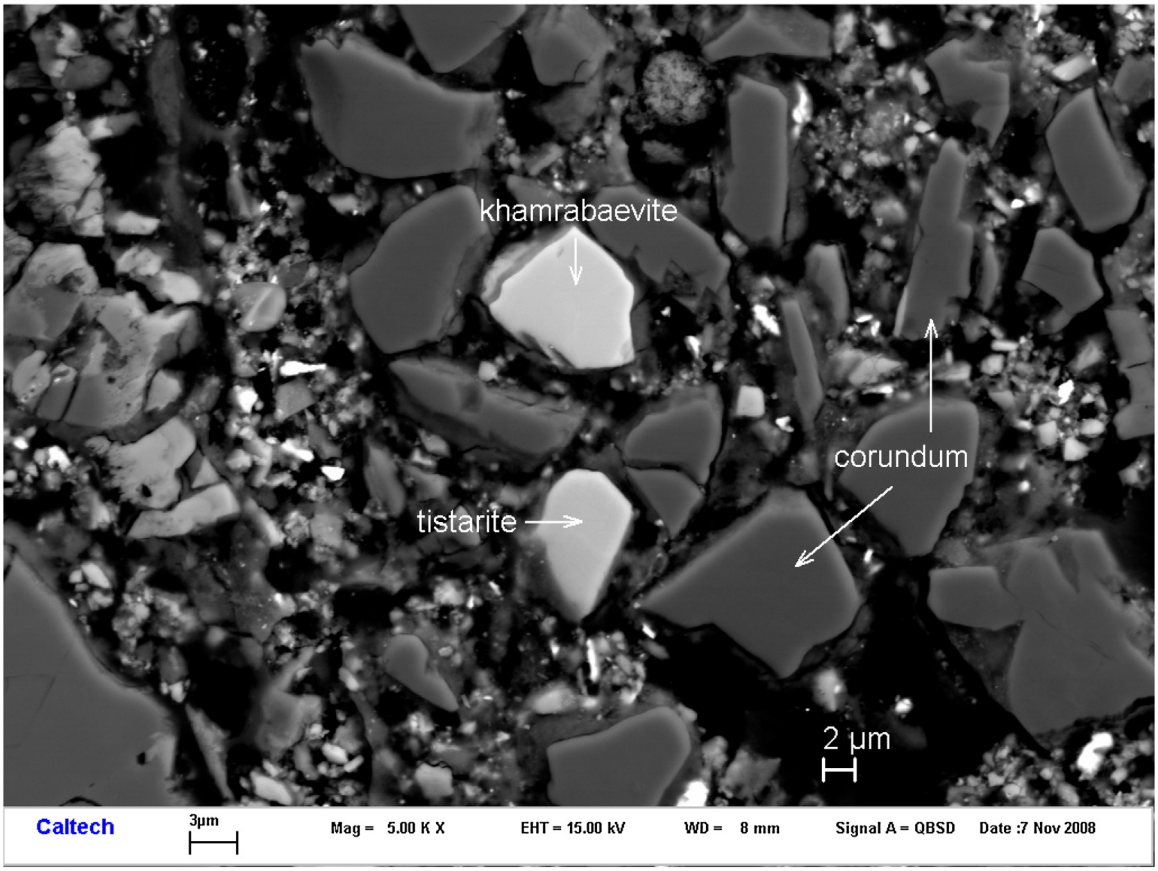

Fig. 1. New refractory mineral tistarite (Ti_2O_3) along with corundum (Al_2O_3) and khamrabaevite (TiC) grains in a chondrule from the Allende CV3 chondrite (Ma and Rossman, 2009a). BSE image.

formed by vapor-phase condensation, probably in the solar nebula. Nevertheless, a presolar environment cannot be ruled out.

The rare-earth elements (REE) provide additional evidence for condensation. CAIs can be categorized into different groups based on their bulk REE patterns. The so-called Group-II pattern (e.g., Fig. 17 of Mason and Taylor, 1982) is highly fractionated: light REEs (La through Sm) display a flat pattern, there is a negative Eu anomaly, the intermediate REEs (Gd through Er) are progressively depleted, there is a strong positive Tm anomaly, and Yb has an abundance similar to that of Eu. Boynton (1975) demonstrated that this fractionated pattern is a function of the volatility of the individual REE; the pattern can be accounted for if the REE-carrier phases within the CAIs (probably initially hibonite grains; Davis and Richter, 2005) are nebular condensates formed by equilibrium gas-solid fractionation.

As the nebular gas cooled, metallic Fe began to undergo oxidation, producing the fayalite component (Fa; Fe_2SiO_4) of olivine and the ferrosilite component (Fs; $FeSiO_3$) of low-Ca pyroxene. The very high olivine-Fa values in some FeO-rich chondrules in primitive CO3.0 chondrites (up to Fa_{77}; Wasson and Rubin, 2003) suggest gas temperatures <450 K (Wasson, 2008). Although solar-composition gas is too reducing to produce a substantial Fa component in condensate olivine grains (Fedkin and Grossman, 2006), evaporation of nebular fines during repeated episodes of chondrule formation at low nebular temperatures could have led to the incorporation of significant amounts of H_2O into the subsequently condensed fine-grained materials (Wasson, 2008). This in turn could have resulted in the local oxidation of metallic Fe and the subsequent condensation or crystallization of FeO-rich mafic silicates.

Rubin et al. (1999) inferred that some of the individual troilite grains within chondrules in LL3.0 Semarkona were probably primary phases (i.e., present among the chondrule precursors) if they fulfilled the following criteria: they were completely embedded in a mafic silicate phenocryst, located near the chondrule center, and were part of an opaque assemblage with an igneous texture. About 13% of Semarkona chondrules contain such troilite grains. If these grains are indeed primary, their submicrometer precursors must have condensed in the nebula after temperatures dipped below 650 K (the 50% condensation temperature of S; Table G-1 of Wasson, 1985).

Tiny grains of noble Pt-group metals, metallic alloys and Ge-rich phases found within R3 lithologies (e.g., Berlin et al., 2001) and CAIs in CV chondrites (e.g., Bischoff and Palme, 1987) have also been inferred to be condensates.

In the enstatite-chondrite-formation region of the nebula, the nebular gas may have had comparatively high C/O and/or high pH_2/pH_2O ratios. El Goresy et al. (2011) and Lin et al. (2011) described an EL3 clast in the Almahata Sitta breccia that contains metal nodules with fine-grained condensates including sinoite (Si_2N_2O), oldhamite (CaS), graphite, enstatite, diopside, sphalerite and troilite.

Rubin and Choi (2009) suggested that the most reactive halogens in the enstatite- chondrite region of the nebula condensed as halides that were incorporated into enstatite chondrites. Lawrencite ($(Fe^{+2},Ni)Cl_2$), a halide identified in enstatite chondrites, occurs as thin rims around silica grains, as inclusions within low-Ni metallic Fe and troilite, and as isolated grains associated with enstatite in the matrix of EH4 Indarch (Keil, 1968).

Although Buchwald and Clarke (1989) called lawrencite a "mineralogical chimera" and found that the Cl-bearing phase in iron meteorites and OC is akaganéite (β-FeO(OH,Cl) – a terrestrial alteration product), Rubin and Choi (2009) pointed out that the Fe- and Cl-bearing rims around the silica grains in Indarch (Fig. 3 of

Keil, 1968) are unlikely to have formed by alteration. Furthermore, Lin et al. (2011) measured excess ^{36}S in small grains of lawrencite within metal nodules in the aforementioned EL3 clast from Almahata Sitta; the excess ^{36}S formed from live ^{36}Cl by electron capture in the solar nebula.

Rubin (1983a) suggested that clasts in the Adhi Kot EH3 chondrite that are relatively rich in silica and niningerite ((Mg,Fe)S) and poor in enstatite could have formed under nebular conditions of high sulfur fugacity in which enstatite underwent sulfidation. The citing of the sulfidation was later attributed to the EH parent body during shock metamorphism (e.g., Rubin, 2015a). Lehner et al. (2013) proposed that the same basic mechanism of enstatite sulfidation also operated in the enstatite- chondrite region of the nebula around the time of chondrule formation; they invoked a gaseous reservoir with low H, high C and S and an oxygen fugacity 6 to 8 log units below the I-W buffer.

2.3. Crystallization in CAI and AOI melts

Many of the tiny oxide, silicate, metal and sulfide grains that formed during condensation in the nebula clumped together to form highly porous aggregates (dustballs) (e.g., Wright, 1987; Blum, 2004; Dominik et al., 2006), probably in the millimeter-to-centimeter size range (Rubin, 2011). Early dustballs were the progenitors of the CAIs and may have been concentrated in different regions of the nebula by aerodynamic forces (e.g., Weidenschilling, 1977; Nakagawa et al., 1986).

A significant proportion of the CAIs can be divided into different categories (A, B, C) (e.g., Grossman, 1975; Wark, 1987) that differ moderately in shape, size, mineralogy and mineral chemistry. The individual groups can themselves be subdivided. The largest CAIs are 2–3 cm in size and occur exclusively in CV3 chondrites; most CAIs outside the CV group are <1 mm (e.g., MacPherson et al., 2005).

Compact Type-A CAIs (CTAs) have spheroidal shapes and were apparently molded by surface tension during moderate melting (e.g., Beckett and Stolper, 1994; Simon et al., 1999). The heat source is unknown. CTAs consist mainly of zoned melilite enclosing spinel, hibonite, perovskite and noble-metal nuggets; some CTAs consist almost entirely of monomineralic melilite (Simon et al., 1999). Other CTA inclusions contain small amounts of Ti-Al-rich calcic pyroxene (fassaite) and relatively rare rhönite – $Ca_2(Mg,Al,Ti)_6(Si,Al)_6O_{20}$ (MacPherson, 2005); these grains crystallized from the melt, plausibly nucleating on relict condensates or relict phenocryst fragments from a previous generation of CTAs.

The CTAs are typically surrounded by Wark- Lovering (WL) rims. These rims are a few tens of micrometers thick and generally consist of a series of mono- or bi-mineralic layers of melilite, spinel and pyroxene along with some hibonite and perovskite (Wark and Lovering, 1977). The rims appear to have formed by a multi-stage process involving flash heating of the CAI surface (Wark and Boynton, 2001). This is consistent with the WL rims having ^{16}O enrichments similar to those of the underlying CAI (Wark and Boynton, 2001).

Fluffy Type-A CAIs (FTAs) have irregular shapes and appear not to have experienced significant melting as individual objects (MacPherson and Grossman, 1984; Beckett and Stolper, 1994). The FTAs in CV3 chondrites are ~0.3–3 cm in size (MacPherson and Grossman, 1984; MacPherson, 2005). Most of the centimeter-size FTAs are aggregates of numerous melilite-rich nodules; many nodules resemble individual CTAs with WL rims (MacPherson, 2005). Rubin (2012a) suggested that the individual nodules were independent CTAs (perhaps as well as a few other CAI types that contained hibonite) that collided with each other at low relative velocity and stuck together. The aggregated CTAs experienced minor remelting. The occurrence of ^{16}O-rich and ^{16}O-poor melilite in one FTA from CV3 Vigarano suggests that this particular inclusion experienced multiple melting events (Harazono and Yurimoto, 2003).

Type-B CAIs formed very early in Solar-System history – about 4.568 Ga ago (e.g., Amelin et al., 2002; Bouvier and Wadhwa, 2009; Bouvier et al., 2010). They occur exclusively in CV chondrites as multi- millimeter- to multi-centimeter-size coarse-grained spheroidal igneous objects that consist of melilite, Al- and Ti-rich calcic pyroxene, spinel and minor anorthite (Grossman, 1975).

There are three principal varieties of Type-B CAIs (Wark and Lovering, 1982; Wark et al., 1987): Type-B1 inclusions consist of a coarse-grained melilite mantle ($Åk_{\sim 10\text{-}72}$) surrounding a core of pyroxene, spinel, anorthite, metallic Fe-Ni, and noble metal nuggets (e.g., MacPherson, 2005). Type-B2 inclusions have no melilite mantle and are mineralogically similar to B1 cores. Type-B3 inclusions (the least-common variety) contain coarse forsterite grains along with pyroxene, spinel and melilite; they are also known as forsterite-bearing Type-B inclusions or FoB CAIs. Some FoBs also contain minor anorthite (e.g., Petaev and Jacobsen, 2009).

Rubin (2012a) suggested that Type-B CAIs formed via clumping of numerous CTAs (the same basic process invoked to form the centimeter-size FTAs), the incorporation of significant amounts of ^{16}O-rich mafic dust (mainly forsterite) into the assemblage, and extensive melting. Centimeter-size aggregates of CTAs that happened to incorporate greater amounts of forsterite prior to melting ultimately became centimeter-size B3 inclusions.

Because B2 inclusions are mineralogically similar to B1 cores, it seems plausible that the B2 s started out as normal B1 inclusions that acquired a melilite-rich mantle through inelastic collisions with CTAs (which are very rich in melilite; e.g., Simon et al., 1999). These compound objects were then extensively melted. As modeled by Rubin (2012a), the additional melilite made the B1 inclusions richer in bulk Ca and Al. Relatively slow cooling allowed the minerals to grow coarser in the B1 inclusions; non-equilibrium crystallization from the melt produced compositional zoning. Differences in cooling rate and the degree of melting among different B1 inclusions caused inclusion-to-inclusion variations in mineral composition.

Type-C CAIs are igneous objects that consist mainly of spinel, calcic pyroxene and anorthite exhibiting ophitic or poikilitic textures (e.g., MacPherson, 2005). They may have formed by flash melting finer-grained precursors consisting of nebular condensates (e.g., Beckett and Grossman, 1988).

Spinel-rich inclusions are fine-grained CAIs consisting primarily of spinel, melilite, anorthite, Al- and Ti-rich diopside with minor hibonite and perovskite and rare forsterite (Krot et al., 2004a). The spinel-rich inclusions in reduced CV3 chondrites have been little affected by parent-body aqueous alteration: (1) they contain only rare grains of secondary nepheline and sodalite (Krot et al., 2004a) and (2) all spinel and almost all Al-Ti-diopside grains are ^{16}O-rich (Aléon et al., 2005).

Hibonite-silicate spherules are small objects ($\lesssim$170 μm) of varying textures. Some inclusions consist of hibonite laths surrounded by glass that is enriched in an Al-pyroxene component, others of hibonite laths within Al- pyroxene crystals. Some of the spherules are texturally complex objects that contain hibonite, Al-pyroxene, melilite and grossite (MacPherson, 2005). The spheroidal shapes of all these objects attest to their origin as molten droplets formed from finer- grained precursors that may have contained condensates and/or fragments of collisionally disrupted pre-existing CAIs.

Rare grains of the refractory mineral osbornite (TiN) has been found in CAIs and fragments in the Isheyevo CB/CH-like carbonaceous chondrite (Grokhovsky, 2006; Ivanova et al., 2005, 2006; Krot et al., 2006) and in the ALH 85085 CH3 chondrite (Weisberg et al., 1988). The mineral was also identified amidst Stardust samples (presumably CAI fragments) collected from comet Wild 2 (Weisberg et al., 2006).

The irregularly shaped bodies known as amoeboid olivine inclusions (AOIs) or amoeboid olivine aggregates (AOAs) (Grossman and Steele, 1976) are the most abundant refractory objects in carbonaceous chondrites (e.g., Kornacki and Wood, 1984; Weber and Bischoff, 1997; Krot et al., 2002, 2004b). They consist of major olivine, major to minor calcic pyroxene, minor anorthite, accessory metallic Fe-Ni and perovskite, and in some minimally altered carbonaceous chondrites, accessory spinel ± low-Ca pyroxene ± melilite (Krot et al., 2004b). Many have porous interiors.

Weisberg et al. (2004) reported three AOIs attached to the forsterite-bearing WL rim around a CTA inclusion in CR2 EET 92105. This association of AOIs and CAIs is consistent with the Al-diopside, anorthite, spinel and melilite in the interiors of AOIs being components of fine-grained CAIs (Krot et al., 2004b). It thus seems plausible that AOIs formed from nebular condensates and fine-grained CAIs that acquired thick forsterite rims and were heated in the nebula by a flash-melting process analogous to the one thought responsible for producing igneous rims and secondary shells around chondrules (Rubin, 2013a). In some cases, coarse grains of forsterite and of plagioclase rimmed by calcic pyroxene crystallized near the rim forming a hypidiomorphic- granular-like texture. Although grains in the interior of many AOIs were not extensively melted (e.g., Komatsu et al., 2001; Ruzicka et al., 2012), the AOI ores were compressed during high- temperature processing. In a few AOIs, the surficial melt invaded the core, causing olivine crystallization adjacent to relict grains of plagioclase and calcic pyroxene (Rubin, 2013a). AOI olivine grains in primitive chondrites have variable CaO contents (Sugiura et al., 2009); this may have resulted from variations in the number and intensity of reheating episodes experienced by different AOIs.

2.4. Crystallization in chondrule melts

Chondrules are among the most abundant components of chondrites, constituting, for example, 55 vol.% of CR carbonaceous chondrites and 65-75 vol.% of type-3 OC (Table 1 of Rubin, 2000). Their average apparent diameters range from ~150 μm in CO3 chondrites to ~900 μm in CV3 chondrites (Table 5 of Rubin, 2010a; Table 7 of Friedrich et al., 2015); the overall range in diameter is 0.25 μm (Rubin et al., 1982) to ~5 cm (Prinz et al., 1988). The most abundant compositional variety (ferromagnesian chondrules) consists primarily of olivine and/or low-Ca pyroxene phenocrysts embedded in mesostasis consisting of feldspathic or silico-feldspathic glass (or devitrified glass) (e.g., Jones et al., 2005). Commonly present in the glass and/or along low-Ca-pyroxene grain boundaries are calcic-pyroxene crystallites (e.g., Fig. 2). Most low-FeO (Type I) chondrules contain small blebs of low-Ni metallic Fe (kamacite). Also present in some chondrules are primary grains of troilite (e.g., Rubin et al., 1999), small grains of chromite (e.g., Wasson and Rubin, 2003), tiny grains of merrillite – $Ca_9MgNa(PO_4)_7$ (Rubin et al., 2015a), and in rare cases, grains of silica (Brigham et al., 1986), merrihueite – $(K,Na)_2Fe_5Si_{12}O_{30}$ and roedderite – $(K,Na)_2Mg_5Si_{12}O_{30}$ (Krot and Wasson, 1994).

Enstatite-chondrite chondrules contain clinoenstatite ± forsterite embedded in halogen-bearing glass. Minor phases present in some chondrules include calcic pyroxene, anorthite, silica, low-Ni metallic Fe, troilite, niningerite ((Mg,Fe)S) or ferroan alabandite ((Mn,Fe)S), daubréelite ($FeCr_2S_4$), oldhamite (CaS), caswellsilverite ($NaCrS_2$) (and other Cr-rich sulfides), schreibersite and perryite ($(Ni,Fe)_5(Si,P)_2$) (e.g., Grossman et al., 1985). Kimura et al. (2005) suggested that tridymite and cristobalite in non-impact-melted EH3 and EL3 chondrites were the last phases to crystallize within chondrules during cooling.

The sulfide phases in enstatite-chondrite chondrules crystallized during chondrule formation: these include common phases such as troilite, niningerite, oldhamite and caswellsilverite (e.g., Grossman et al., 1985) and rare phases such as wassonite (TiS) (Nakamura-Messenger et al., 2012).

Aluminum-rich chondrules, which have been reported in both ordinary and carbonaceous chondrites, are defined as having >10 wt.% bulk Al_2O_3 (e.g., Bischoff and Keil, 1984; Huss et al., 2001; Krot et al., 2001, 2004c). Many contain crystals of anorthite, forsterite, calcic pyroxene and spinel embedded in aluminous glass. Some Al-rich chondrules consist almost entirely of glass (e.g., Krot and Rubin, 1994).

The spheroidal to ellipsoidal shapes of intact ferromagnesian and Al-rich chondrules were molded by surface tension; it is clear these objects formed from partially to completely molten silicate-rich droplets.

The igneous textures of chondrules also attest to their formation from melts. For example, the most common variety is the set of porphyritic chondrules (84% of OC chondrules; Nelson and Rubin, 2002). They consist of olivine and/or low-Ca pyroxene phenocrysts embedded in mesostasis. The phenocrysts in these chondrules nucleated on relict crystals (e.g., Lofgren, 1989, 1996; Lofgren and Russell, 1986; Connolly and Hewins, 1995) and grew from the residual melt. Granular olivine-pyroxene chondrules (3% of OC chondrules) are essentially finer-grained porphyritic chondrules that probably cooled at higher rates from droplets with numerous relict nuclei.

Many low-Ca-pyroxene-bearing FeO-rich (Type II) porphyritic pyroxene (PP) chondrules in type-3 ordinary chondrites contain pyroxene phenocrysts with a series of prominent overgrowth layers (e.g., Watanabe et al., 1986; Noguchi, 1989; Jones, 1996a; Wasson and Rubin, 2003; Wasson et al., 2014) that probably represent multiple melting/crystallization events (Wasson et al., 2014; Baecker et al., 2015). Although the phenocrysts have been characterized as exhibiting oscillatory zoning (Watanabe et al., 1986; Jones, 1996a), a phenomenon present in terrestrial, lunar and martian rocks, detailed analysis (e.g., Simonetti et al., 1996; Elardo and Shearer, 2014; Jambon et al., 2016), the cooling rates and length scales in these magmatic systems are many orders of magnitude greater than those in chondrules. Detailed analytical studies by Wasson et al. (2014) and Baecker et al. (2015) indicate that it is more likely that the compositional zoning in the pyroxene phenocrysts from chondrules result from multiple overgrowths during a series of melting/crystallization events.

Phosphorus X-ray maps of olivine phenocrysts in FeO-rich porphyritic olivine (PO) and porphyritic olivine-pyroxene (POP) chondrules in LL3.0 Semarkona and CO3.0 Y 81020 reveal multiple sets of thin dark/bright (P-poor/P-rich) layers (e.g., Fig. 3); these layers appear to be olivine overgrowths produced during a series of secondary low-intensity chondrule-heating events that typically melted only mesostasis (Rubin et al., 2015a). The relatively slow diffusion of P in olivine preserves the overgrowth layers even after several chondrule heating episodes. After each heating event, the chondrule cooled and underwent fractional crystallization; the P concentration increased in the liquid boundary layer, leading to the crystallization of a relatively P-rich olivine overgrowth layer. During a subsequent heating event, the mesostasis melted and mixed, reducing its overall P concentration and leading to crystallization of a P-poor olivine overgrowth layer.

Other evidence for multiple melting and crystallization in chondrules from different chondrite groups includes relict grains within chondrule phenocrysts (e.g., Nagahara, 1981; Rambaldi, 1981; Kracher et al., 1984; Jones, 1996b; Wasson and Rubin, 2003; Kunihiro et al., 2004, 2005), enveloping (i.e., nested) compound chondrules (e.g., Wasson et al., 1995; Rubin, 2013b), igneous rims around chondrules (e.g., Rubin, 1984a, 2010a; Rubin and Wasson, 1987; Krot and Wasson, 1995; Nagashima et al., 2013), the set of microchondrules formed by remelting low-Ca pyroxene grains at the surfaces of normal-size chondrules (e.g., Krot and Rubin,

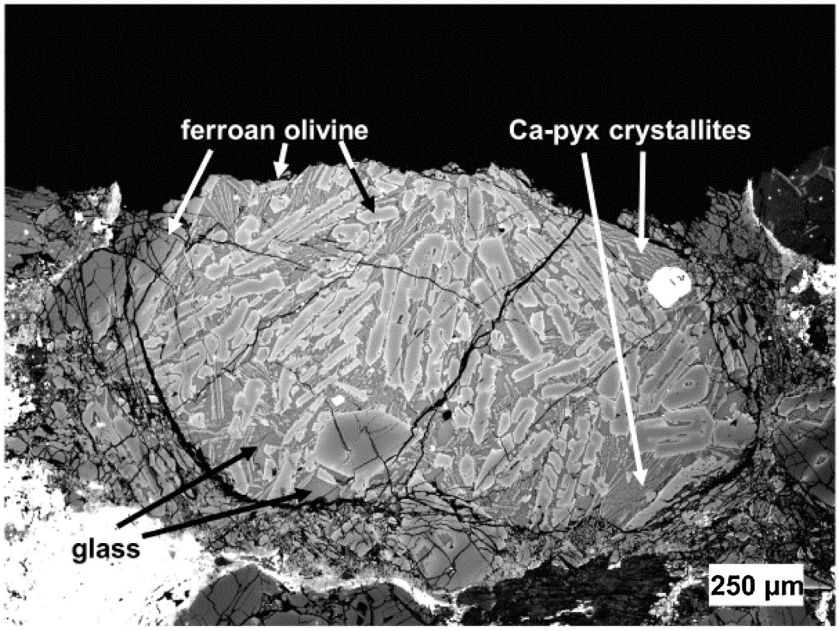

Fig. 2. Transitional barred-olivine-Type-IIA-porphyritic-olivine (BO-PO) chondrule in the Semarkona LL3.0 chondrite. The chondrule contains abundant ferroan olivine, an isotropic glassy mesostasis and Ca-pyroxene crystallites. pyx = pyroxene. BSE image.

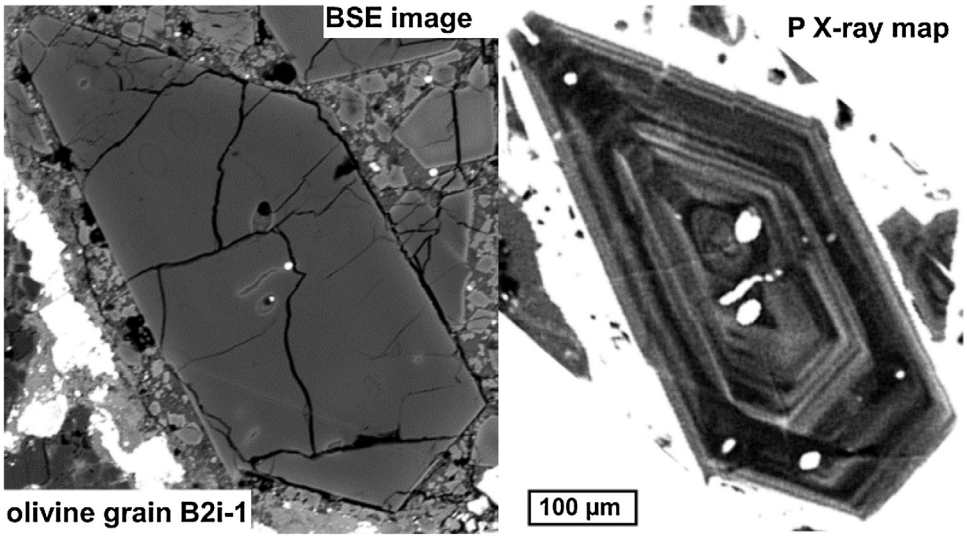

Fig. 3. BSE image and P X-ray map of olivine phenocryst B2i-1 from a 440 × 600-μm-size Type-IIA porphyritic- olivine chondrule fragment (labeled B2i) from the Semarkona LL3.0 chondrite. The P layers form a complicated pattern with numerous dark/bright (P-poor/P-rich) sets of overgrowths. The two oval-shaped melt inclusions contain relatively P- rich mesostasis and appear white in the P X-ray map. Both images are to the same scale.

1996; Krot et al., 1997a), and the presence of non-spherical, multilobate chondrules which, if fully molten, would have collapsed into spheres long before their phenocrysts could have grown to their present sizes (Rubin and Wasson, 2005).

Barred olivine (BO) chondrules occur in all chondrite groups save CI (which is chondrule free). These chondrules are rare in enstatite chondrites (e.g., Nakamura-Messenger et al., 2012), but constitute 6% of OC chondrules (Nelson and Rubin, 2002). Melting experiments indicate that these objects formed by essentially complete melting of olivine- rich precursors (Hewins, 1988; Hewins and Fox, 2004; Hewins et al., 2005). The olivine bars within these chondrules and the olivine rims around many of them tended to crystallize as optically continuous single crystals (or as adjacent sets of a few separate optically continuous crystals). Pyroxene is present in most BO chondrules in type-3 OC, averaging ~15–30 vol.% and, in rare cases, ranging up to 75 vol.%; feldspathic glass averages ~20–25 vol.% and ranges up to 55 vol.% (Weisberg, 1987). During crystallization of olivine, the concentrations of incompatible elements increase in the mesostasis, leading in some cases to the crystallization of opaque phases (metallic Fe-Ni and/or sulfide) between the olivine bars, e.g., in metal-rich chondrites such as NWA 5492 (Fig. 2j of Weisberg et al., 2012).

Radial pyroxene (RP) chondrules consist of fan-like arrays of low-Ca pyroxene laths that, in most cases, appear to radiate from a point on the chondrule surface. This may be the site of a collision between the molten droplet and a dust grain (e.g., Connolly and Hewins, 1995). Cryptocrystalline (C) chondrules are very-fine-grained ($\lesssim$2 μm), normative-pyroxene-rich objects consisting of numerous domains each of which appears to have crystallized from a quenched melt separate from its neighbors. Both RP and C chon-

drules occur in all chondrite groups except CI and CK; together they constitute 85% of CH3 chondrules, 18% of EH3 chondrules, 7% of H-L-LL3 chondrules, 3% of CO3 chondrules, 1.6% of CM2 and R3 chondrules, 0.7% of CR chondrules and 0.3% of CV chondrules (Rubin, 2010a).

2.5. Exsolution during the cooling of CAIs

Experimental studies and petrographic analysis by Blum et al. (1988, 1989) led these workers to propose that multi-phase opaque assemblages within CAIs in oxidized CV3 chondrites formed by crystallization of metallic droplets within molten CAIs. The compositionally homogeneous metal grains later underwent exsolution, oxidation and sulfidation. Although the oxidation and sulfidation was probably caused by aqueous alteration on the parent body (see Section 2.9), the work of Simon and Grossman (1992) suggests that the exsolution probably occurred during subsolidus cooling of the CAIs. Simon and Grossman examined two opaque assemblages in Leoville ($CV3_{red}$) and reported that one of them contains sets of regularly spaced, parallel, ≤1 -μm-thick lamellae of εRu-Fe with sharp boundaries within a larger grain of taenite. They concluded that these lamellae were crystallographically controlled and formed by exsolution. These workers also determined that partitioning of Ir and Pt between the lamellae and host in the other Leoville opaque assemblage was consistent with equilibration at ~600 °C. Because the Leoville whole rock appears to have experienced a much lower equilibration temperature (i.e., ~250 °C; Huss et al., 2006), it seems probable that the exsolution lamellae in these opaque assemblages formed during sub-solidus cooling of the CAIs, prior to agglomeration.

2.6. Exsolution during the cooling of chondrules and opaque assemblages

At high temperatures, minerals that exhibit solid solution have more extensive compositional fields than they have at lower temperatures. Exsolution typically occurs when, at a particular subsolidus temperature, a parental mineral's crystal structure can no longer accommodate substantial amounts of a particular cation (in most cases due to that cation's size) and lamellae of a new mineral phase (enriched in that particular cation) nucleate and grow from the parental phase.

Some minerals formed by exsolution in chondrules during cooling: (1) Pigeonite and calcic pyroxene (augite) in clinoenstatite in several type-3 OC (Weinbruch et al., 2001). These authors inferred cooling rates of 0.1–60 °C/hr at temperatures between 1350 and 1200 °C for FeO-poor chondrules and between 1100 and 900 °C for FeO-rich chondrules. However, these slow rates must be viewed with caution; they are based on experiments on monotonically cooled synthetic chondrule analogs and do not examine the possibility of multiple heating events (including subsolidus heating) (e.g., Wasson et al., 2014; Baecker et al., 2015; Rubin et al., 2015a). (2) Pentlandite in pyrrhotite in LL3.0 Semarkona (Schrader et al., 2016). Sulfide compositions are most consistent with an equilibration temperature of ~230 °C; this is above the estimated peak metamorphic temperature of the Semarkona whole rock (<220 °C; Busemann et al., 2007), suggesting that pentlandite exsolution occurred during an earlier higher-temperature event such as chondrule cooling (Schrader et al., 2016).

Opaque assemblages, rich in metallic Fe-Ni in type-3 ordinary and enstatite chondrites, were probably also melted during the epoch of chondrule formation. Such assemblages include the "metallic chondrules" in unequilibrated OC described by Gooding and Keil (1981) and subrounded metal- and sulfide-rich nodules in type-3 enstatite chondrites (e.g., Figs. 2j and k of Weisberg and Kimura, 2012). During the cooling of opaque assemblages in EH and EL chondrites from ≥700 °C, it is likely that schreibersite and graphite exsolved from taenite due to the limited solubility of P and C in low- Ni metallic Fe (kamacite) (e.g., Scott, 1971). In many sulfide-rich assemblages, daubréelite exsolved from troilite.

2.7. Annealing of amorphous material

Amorphous meteoritic materials include the glassy mesostases of chondrules in unequilibrated chondrites, clumps within the matrices of unequilibrated chondrites, portions of IDPs, and shock-produced glasses including shock veins and maskelynite in chondrites and achondrites.

Because presolar dust grains typically spent 10^8-10^9 years in the interstellar medium (Seab, 1987; Mathis, 1993), long exposure to stellar ionizing radiation is expected to have transformed the vast majority of the grains into amorphous materials (Li and Draine, 2001). Grains with such an origin include some GEMS; these are submicrometer-sized spheroidal patches of magnesian silicate Glass with Embedded Metal and Sulfides (e.g., Fig. 8 of Bradley, 2005). The metal and sulfide grains in the interiors of GEMS are relict crystals; other relicts include embayed forsterite and enstatite grains (Zolensky et al., 2003; Bradley, 2005). Many GEMS in IDPs are surrounded by amorphous carbonaceous material that probably contains both organic and inorganic C (Bradley, 2005). A presolar origin for a minority of GEMS (perhaps 1-6%) is indicated by their anomalous O-isotopic compositions (e.g., Messenger et al., 2003; Keller and Messenger, 2011). However, because most GEMS have heterogeneous elemental abundances and normal solar-system O- isotopic compositions, they may instead be late-stage nebular condensates (Keller and Messenger, 2011).

Many GEMS appear to have undergone moderate annealing. These include those containing compositionally distinct subdomains and those with chemically distinct subparallel layers (Keller and Messenger, 2011). Some of the nanophase inclusions in GEMS (e.g., low-Ni metallic Fe, taenite, sulfide, and possibly chromite) may have formed from the amorphous material by annealing and sulfidation in the solar nebula (e.g., Lauretta et al., 1997). The heat source responsible for the annealing could be associated with chondrule formation.

The matrices of primitive chondrites contain compacted nanometer-to-micrometer-sized patches of amorphous material that include tiny grains of magnesian olivine and low-Ca pyroxene, including some that are enriched in Mn (e.g., Klöck et al., 1989; Nuth et al., 2005 Nuth et al., 2005). Annealing of amorphous material in circumstellar outflows or in the early solar nebula could have produced some of the magnesian silicate grains within GEMS (e.g., Hallenbeck et al., 1998, 2000). Heating associated with chondrule-formation events or with passage through hot regions of the solar nebula could have annealed some clumps of amorphous material and formed the Mg-Fe silicate grains that were later incorporated into chondrite matrices (Nuth et al., 2005). Alternatively, much of the amorphous material in chondrite matrices may have formed during chondrule formation, as volatiles condensed on nearby dust grains (Nuth et al., 2005); the associated crystalline grains may have formed later, at the earliest stages of thermal metamorphism on chondrite parent asteroids.

During these early stages, primary feldspathic chondrule glass in primitive chondrites begins to devitrify to form fine-grained crystalline feldspar (e.g., Guimon et al., 1986; Grossman and Brearley, 2005 Grossman and Brearley, 2005). This results in a significant increase in the thermoluminescence (TL) sensitivity of the whole rock (Sears et al., 1980). In some cases, the reaction leading to the crystallization of feldspar may have been catalyzed by water (Guimon et al., 1986), consistent with the evidence for aqueous alteration in the most primitive ordinary and carbonaceous chondrites (Section 2.9).

2.8. Thermal metamorphism and exsolution

2.8.1. Heat sources

There are two heat sources plausibly responsible for the bulk of meteorite metamorphism and melting: (1) the decay of short-lived radionuclides such as ^{26}Al ($t_{½}$ = 730,000 years) (e.g., Urey, 1955; Fish et al., 1960; Reeves and Audouze, 1968; Lee et al., 1976; Wasserburg and Papanastassiou, 1982; Grimm and McSween, 1993; McSween et al., 2002; Nyquist et al., 2003; McSween and Huss, 2010; Schiller et al., 2010) and (2) collisional heating (e.g., Rubin, 1995a, 2002a, 2003, 2004; Rubin and Wasson, 2011; Rubin et al., 2001). It is possible that both mechanisms were important heat sources (e.g., Friedrich et al., 2014). Rubin (2015a) summarized arguments against radiogenic heating being the principal cause of chondrite metamorphism; Wasson (2016) presented arguments against radiogenic heating being mainly responsible for melting the parent asteroids of differentiated meteorites. [Other proposed asteroidal heating mechanisms (e.g., exothermic chemical reactions, adiabatic compression of nebular gas, an early superluminous Sun, FU Orionis-type events, explosive reconnection events in the nebula, electromagnetic induction in a fierce protosolar wind) have few current adherents.]

2.8.2. Ordinary chondrites

Every ordinary chondrite (OC) of petrologic type >3.00 (i.e., 99.99% of OC) has experienced some degree of parent-body thermal metamorphism. In many cases, the early stages of thermal metamorphism include reactions with an aqueous fluid (in some instances, also CO_2-rich) fluid, so the pedagogical separation between thermal metamorphism, aqueous alteration and hydrothermal alteration is somewhat arbitrary.

Textural effects of thermal metamorphism include devitrification of chondrule glass, textural integration, mineral recrystallization, homogenization of mineral compositions, loss of some primary mineral phases, loss of presolar grains, growth of secondary minerals, transformation of low-Ca Fe-Mg pyroxene to orthopyroxene, and loss of bulk C, H_2O, noble gases and volatile siderophile elements (e.g., Huss et al., 2006). Grain coarsening occurs as large grains of a phase grow at the expense of small grains; this leads to a reduction in internal energy as the total area of grain boundaries of that phase are reduced. For example, the mean sizes of opaque grains in H chondrites increase with increasing metamorphic grade (troilite: ~30 μm in H3, 80 μm in H6; metallic Fe-Ni: ~65 μm in H3, 120 μm in H6; Table 2 of Rubin et al., 2001).

Whole-rock physical effects include changes in thermoluminescence (TL) properties due to the order/disorder transition of feldspar between 500 and 600 °C (Guimon et al., 1985; Sears et al., 1991) and changes in cathodoluminescence (CL) due to the destruction of chondrule glass in low-FeO chondrules, the growth of albite, and the FeO-enrichment of mafic phases during equilibration (DeHart et al., 1992; Sears et al., 1995; Grossman and Brearley, 2005). Table 1 of Huss et al. (2006) summarizes the myriad changes experienced by OC during thermal metamorphism.

Olivine grains in FeO-rich chondrules in type 3.00 chondrites tend to be normally zoned in Cr, with higher Cr concentrations near the grain edge, consistent with fractional crystallization (e.g., Jones, 1990). At the earliest stages of thermal metamorphism, in type 3.1-3.2 OC, thin streaks of a Cr-rich phase (probably chromite) form by exsolution in the olivine along crystallographic axes (Grossman and Brearley, 2005). By type 3.3, the olivine grains in these chondrules have developed uniformly low Cr concentrations except for scattered equant internal chromite grains (Grossman and Brearley, 2005).

Appreciable numbers of metallic Fe-Ni grains within low-FeO chondrules in type-3.00 OC contain P, Si and Cr alloyed with metallic Fe in solid solution; in some cases, the metal grains contain small inclusions of phosphide and silicide (Zanda et al., 1994). At slightly higher metamorphic grades (type 3.15), the reduced P, Si and Cr species have reacted with O, Ca, Fe, Na and Cl from other regions of the meteorite (most likely chondrule mesostases and small matrix grains) to produce Na, Fe, and Ca phosphate, silica and chromite (Huss et al., 2006). Many of these newly formed grains occur in opaque assemblages consisting of troilite-merrillite ± metal, troilite-chlorapatite and metal- chlorapatite (Rubin and Grossman, 1985). Chlorapatite appears to partly replace merrillite during metasomatic reactions (Jones et al., 2014). With increasing metamorphism to type-4-6 levels, chromite and phosphate grains continue to grow.

Metallic Fe-Ni grains inside chondrules in LL3.0 Semarkona tends to consist of plessitic intergrowths with submicrometer- size patches of low-Ni metallic Fe (kamacite) surrounded by Ni-rich regions (Kimura et al., 2008). The metal grains in type-3 chondrites of higher metamorphic grade consist of coarser low-Ni metallic Fe (kamacite) and Ni-rich metal.

Coarse grains of plagioclase are absent in type-3 OC (outside rare Al-rich chondrules), but the compositional components of plagioclase reside in the feldspathic mesostases of ferromagnesian chondrules. In low-FeO chondrules, albite crystallizes within the mesostases by type ~3.4 (Grossman and Brearley, 2005); in high-FeO chondrules, the abundance of albite increases progressively from type 3.00 to higher petrologic types (Huss et al., 2006). The sizes of albite (or oligoclase) grains increase from <1 μm in type-3 to ~2 μm in type-4 to 2–10 μm in type-5 to ≥50 μm in type-6 OC (Van Schmus and Wood, 1967; Huss et al., 2006).

Many chondrule feldspathic mesostases also have a normative pyroxene component (e.g., Snellenburg, 1978; Gooding, 1979; Jones, 1990, 1996a). The concentration of this component increases in metamorphosed OC after plagioclase crystallizes, leading in a few barred-olivine (BO) chondrules to the growth of optically continuous coarse pyroxene grains between the olivine bars.

The principal pyroxene phase in type-3 and some type-4 OC is low-Ca clinopyroxene exhibiting polysynthetic twinning and inclined extinction; it occurs as phenocrysts in pyroxene-rich chondrules and chondrule fragments. This phase transforms into orthopyroxene at ~630 °C (Boyd and England, 1965); this is above the maximum metamorphic temperature of some type-4 OC (~600–700 °C), but below those of type-5 and type-6 OC (~700–750 °C and ~820–930 °C, respectively) (Dodd, 1981; Olsen and Bunch, 1984). That accounts for the absence of low-Ca clinopyroxene in unshocked type-5 and -6 chondrites. [Nevertheless, low-Ca clinopyroxene exhibiting polysynthetic twinning can form by shock heating and quenching of pyroxene grains in any rock, irrespective of metamorphic grade, at shock stage ≥S3 (Stöffler et al., 1991; Rubin et al., 1997).]

Type-3 OC have heterogeneous olivine and low-Ca pyroxene compositional distributions (e.g., Dodd et al., 1967). During thermal metamorphism, diffusion causes the grains to approach equilibrium, diminishing grain-to-grain variations in mineral chemistry. The mean olivine/low-Ca-pyroxene modal ratio co-varies with oxidation state among the three OC groups: 1.4 in H, 2.0 in L and 3.6 in LL (Table 5.1 of Hutchison, 2004). As more metallic Fe is transformed into FeO during oxidation, the divalent- cation/Si ratio increases, facilitating the formation of $(Mg,Fe)_2SiO_4$ olivine (which has a 2:1 ratio) at the expense of $(Mg,Fe)SiO_3$ low-Ca pyroxene (which has a 1:1 ratio).

Rubin (2005) modeled OC as having acquired water with relatively high $\Delta^{17}O$, perhaps contained within phyllosilicates, at the time of agglomeration. (Wasson (2008) suggested that phyllosilicates could have condensed in the nebula during episodes of chondrule formation after evaporated fines reacted with H_2O in ambient nebular gas.) The water acted as an oxidizing agent during whole-rock thermal metamorphism as phyllosilicates were

dehydrated. The liberated water oxidized metallic Fe-Ni, causing correlated changes with increasing petrologic type in all three OC groups; these include decreasing modal abundances of metallic Fe-Ni, increasing FeO/(FeO + MgO) in olivine, low-Ca pyroxene, chromite, and possibly ilmenite, increasing olivine/low-Ca-pyroxene ratios, increasing Co and Ni concentrations in the remaining kamacite, and decreasing bulk (whole-rock) values of $\delta^{18}O$ and $\delta^{17}O$ (Bunch et al., 1967; Snetsinger and Keil, 1969; Scott et al., 1986; Rubin, 1990, 2005; Clayton et al., 1991; McSween and Labotka, 1993).

Minerals in OC that formed by exsolution during metamorphism include chromite in olivine (Ramdohr, 1973; Ashworth, 1979; Grossman and Brearley, 2005), chromite and rutile in ilmenite (Buseck and Keil, 1966), calcic pyroxene in orthopyroxene (e.g., Yagi et al., 1978), alkali feldspar in albite (Lewis and Jones, 2014, 2015, 2016; Lewis et al., 2016), and mackinawite (FeS_{1-x}) in pentlandite ($(Fe,Ni)_9S_8$) (Koeberl et al., 1990).

Wasson et al. (1993) found that three type-3 OC (Willaroy, Suwahib (Buwah) and Moorabie) and one type-4 OC (Cerro los Calvos) experienced reduction during thermal metamorphism. Although their bulk siderophile element abundances and mean chondrule sizes indicate that they are members of the H (Willaroy and Cerro los Calvos) and L (Suwahib (Buwah) and Moorabie) groups, their olivine Fa values are appreciably below those of equilibrated members of these groups. The reducing agents may have been similar to the C-rich clasts observed in other OC (e.g., Scott et al., 1988).

2.8.3. Carbonaceous chondrites

About half of the CI chondrites have undergone some thermal metamorphism; ~25% of CM chondrites were metamorphosed as well. In some cases, the secondary heating of CM chondrites (e.g., Kimura et al., 2011) is probably attributable to impacts (e.g., Kimura and Ikeda, 1992; Nakato et al., 2008) and is discussed in Section 2.10. The other major carbonaceous chondrite groups that experienced significant thermal metamorphism are CO and CV-CK. In addition, the Coolidge-Loongana 001 subgroup is partly equilibrated (Kallemeyn and Rubin, 1995).

2.8.4. CI chondrites

A typical metamorphosed CI chondrite is Yamato 86029. Phyllosilicates are absent; the crystalline material that is present in the rock consists of olivine, magnetite and troilite (Tonui et al., 2014). Metamorphism caused Mg-Fe- rich carbonates to break down into Ca-Mg-Fe-Mn oxides, and sulfide to break down into elongated magnetite grains with sulfide inclusions (Tonui et al., 2014).

2.8.5. CM chondrites

One of the most-metamorphosed CM chondrites is Belgica 7904 (e.g., Skirius et al., 1986; Tomeoka, 1990 Kimura and Ikeda, 1992; Ikeda and Prinz, 1993). It contains low bulk H_2O and C (Shimoyama and Harada, 1984). There are abundant desiccated phyllosilicates (with high analytical totals) consisting of Fe-rich serpentine, normal serpentine and clinochlore ($(Mg,Fe^{+2})_5Al(Si_3Al)O_{10}$ $(OH)_8$) (Tonui et al., 2014). Secondary phases in the matrix include olivine, low-Ca pyroxene, troilite, taenite and low-Ni metallic Fe (kamacite). Tochilinite (2[(Fe,Mg,Cu,Ni[]) S·1.57–1.85[(Mg,Fe,Ni,Al,Ca)$(OH)_2$]) is absent. Similar metamorphic effects are evident in Yamato 86720 and Yamato 86789 (Tonui et al., 2014). Some CM chondrites that were aqueously altered and subsequently metamorphosed contained highly strained fayalite grains with voids (Akai, 1988).

2.8.6. CO chondrites

Metamorphic effects in CO3 chondrites, first noted by McSween (1977) and summarized by Huss et al. (2006), are inextricably linked to aqueous alteration (Rubin, 1998; Chizmadia et al., 2002). The CO3 chondrites can be divided into petrologic subtypes ranging from 3.0 to 3.8 (Chizmadia et al., 2002). Progressive mineralogical changes with increasing subtype include annealing of an amorphous silicate component of the matrix, destruction of tiny forsterite and enstatite grains in the matrix and the growth of fine-grained ferroan olivine (Brearley, 1995), destruction of presolar grains (Huss, 1990; Huss et al., 2003), alteration of chondrule mesostases and replacement by nepheline ((Na,K) $AlSiO_4$) (e.g., Scott and Jones, 1990), replacement of melilite in CAIs with feldspathoids, pyroxene and Fe-rich spinel (Russell et al., 1998), gradual replacement of forsterite with more-ferroan olivine in AOIs (Chizmadia et al., 2002), removal of alloyed Cr, P and Si from low-Ni metallic Fe (kamacite) (McSween, 1977; Scott and Jones, 1990) and the growth of troilite-merrillite ± schreibersite assemblages (Rubin and Grossman, 1985).

As in ordinary chondrites, the early stages of metamorphism appear to cause chromite to exsolve from ferroan olivine grains and albite to crystallize within chondrule mesostases (Grossman and Brearley, 2005).

The Acfer 094 primitive ungrouped carbonaceous chondrite contains martensitic metal (Kimura et al., 2008). Metal within CO3.03–3.1 chondrites resembles that in 3.05–3.10 OC in consisting of coarser grains of low- Ni metallic Fe (kamacite) with small patches of Ni-rich metal. Such grains formed during incipient parent-body thermal metamorphism.

2.8.7. CV-CK chondrites

The CV3 and CK3.8–CK6 chondrites may constitute a single metamorphic sequence (Scott and Taylor, 1985; Greenwood et al., 2010; Wasson et al., 2013). Magnetite-bearing carbonaceous chondrites with large chondrules and minor to negligible amounts of metallic Fe-Ni are routinely assigned either to the CV3 group (if they are relatively unequilibrated and have low mean olivine Fa contents) or to the CK group (if they are more equilibrated with olivine compositions near Fa_{30} and possess more-recrystallized textures). CK chondrites appear to differ from CV chondrites in their lower proportions of CAIs, AOIs, and chondrules with igneous rims; however, detailed observations by Wasson et al. (2013) have shown that these differences are probably due solely to metamorphic recrystallization of the CK chondrites. Two meteorites listed in the Meteoritical Bulletin Database suggest that there may be a single CV-CK sequence: Camel Donga 040 is a genomict breccia that appears to contain separate CV and CK lithologies; NWA 10588 appears to be intermediate between typical CV3 and CK4 chondrites.

Dunn et al. (2016) found that magnetite grains in CK3, CK4 and CV3 chondrites differ in their concentrations of Cr_2O_3, NiO and TiO_2. The differences between CK3 and CK4 magnetite is mainly in TiO_2 and is apparently attributable to thermal metamorphism. However, CV3 magnetite is closer in composition to CK4 than to CK3 magnetite, casting doubt on whether there is a single CV-CK metamorphic sequence. Yin et al. (2017) found that bulk CV and CK chondrites differ in $\varepsilon^{54}Cr$, consistent with derivation of these samples from different parent bodies.

Geiger and Bischoff (1995) proposed that thermal metamorphism caused (1) metallic Fe-Ni in CK chondrites to transform into magnetite at oxygen fugacities near that of the Ni-NiO buffer, (2) spinel and ilmenite to exsolve from the magnetite during cooling, and (3) noble-metal-rich sulfides, arsenides and tellurides to form (either from the oxidizing metallic Fe-Ni or from monosulfide solid solution (MSS)).

CV3 chondrites are divided into three subgroups: an Allende-like oxidized subgroup ($CV3_{OxA}$), a Bali-like oxidized subgroup ($CV3_{OxB}$), and a reduced subgroup ($CV3_{red}$) that includes Arch, Efremovka and Leoville (Weisberg et al., 1997). These subgroups

have experienced different degrees of alteration (discussed in Section 2.9) and thermal metamorphism. Metamorphic effects in CV3 chondrites include: (1) a diminishment in grain-to-grain compositional variation among olivines in the two oxidized subgroups (Krot et al., 1995), (2) progressive destruction of presolar grains in $CV3_{OxA}$ and $CV3_{red}$ (Huss and Lewis, 1995; Huss et al., 2003), and (3) systematic changes in the Raman spectroscopic characteristics of organic material (Bonal et al., 2004). Efremovka ($CV3_{red}$) contains dark inclusions with dehydrated phyllosilicates and strained fayalite grains with voids, indicative of aqueous alteration followed by mild thermal metamorphism (Krot et al., 1999).

2.8.8. CR chondrites

The edges of metallic Fe-Ni grains located at the margins of some chondrules in CR chondrites have low concentrations of Co and Ni, reflecting the addition of Fe produced during the reduction of FeO from mafic silicates during mild thermal metamorphism (Lee et al., 1992). Briani et al. (2013) found that the matrices of GRA 06100 and GRO 03116 have undergone extensive dehydration; the organic matter in these samples differs from that in other CR and (CM) chondrites, and that a significant proportion of low-Ni metallic Fe grains contain Ni-rich plessite regions. They attributed these features to thermal metamorphism and suggested that the heating was triggered by impact events. Although two chondrites are currently listed in the Meteoritical Bulletin Database (MBD) as CR6 (NWA 6921 and NWA 7317) and one is listed as CR7 (NWA 7531), the petrographic descriptions of these rocks in the MBD resemble those of some OC impact-melt rocks (e.g., PAT 91501; Mittlefehldt and Lindstrom, 2001), suggesting that the CR6 and CR7 chondrites are also probably impact melts.

2.8.9. Coolidge-Loongana 001

These two carbonaceous chondrites constitute a grouplet and have been metamorphosed to subtype 3.8-4 levels; both meteorites are moderately recrystallized and have fairly narrow olivine compositional distributions (Kallemeyn and Rubin, 1995).

2.8.10. R chondrites

About 55% of R chondrites are moderately metamorphosed rocks (mainly type 3.6–4); ~25% are more-extensively metamorphosed (type 5–6); and ~20% are breccias with clasts displaying a range of petrologic types (including some highly unequilibrated type-3 clasts). Equilibrated R chondrites are highly oxidized rocks with mean olivine Fa contents of $Fa_{39\pm2}$ (e.g., Bischoff et al., 2011). Partially equilibrated samples (e.g., PCA 91002) contain Type-I chondrules containing olivine grains with forsteritic cores and ferroan rims (e.g., Fig. 4a of Rubin and Kallemeyn, 1994) caused by diffusion during moderate thermal metamorphism.

The modal abundance of low-Ca pyroxene is highly variable: it is abundant in unequilibrated R3 clasts (e.g., Bischoff, 2000; Greenwood et al., 2000), R3.6 chondrites (e.g., ALH 85151; Rubin and Kallemeyn, 1989), and some R3.8-3.9 chondrites (Fig. 2 of Kallemeyn et al., 1996). However, it is rare to absent in other R3.8 chondrites (Kallemeyn et al., 1996) and in many R5 and R6 lithologies (e.g., Imae and Zolensky, 2003; Berlin and Stöffler, 2004; Gross et al., 2013). This suggests that oxidation associated with progressive thermal metamorphism could be responsible for destroying low-Ca pyroxene.

The restriction of tiny grains of Pt-group metals to R3 lithologies and the restriction of Pt-rich arsenides and tellurides to R6 lithologies strongly suggest that the latter phases formed during parent- body metamorphism (Berlin et al., 2001). The occurrence of troilite in several R chondrites (Bischoff et al., 2011) suggests that this was the principal sulfide phase prior to oxidation. As troilite or MSS was transformed into pyrrhotite ($Fe_{1-x}S$) during the oxidation that accompanied metamorphism, it seems likely that some As and Te were removed from the sulfide and formed the noble-metal-bearing arsenides and tellurides.

Mineral phases formed during exsolution in R chondrites include flame-like lamellae of pentlandite in pyrrhotite and thin lamellae of ilmenite in pentlandite (Schulze et al., 1994; Rubin and Kallemeyn, 1994; Kallemeyn et al., 1996).

The amphibole and mica in a few R6 chondrites were produced by hydrothermal alteration and will be discussed in Section 2.9.

2.8.11. Enstatite chondrites

The enstatite chondrites comprise two major groups, EH and EL, that differ in degree of oxidation, abundance of siderophiles and halogens, sulfide mineralogy, mineral chemistry, and mean chondrule size. Each group comprises a complete metamorphic sequence from type 3 to type 6 (although Rubin and Wasson, 2011; suggested that the known EH6 chondrites were actually impact-melt breccias).

There are several mineralogical changes that occur in enstatite chondrites during parent-body thermal metamorphism:

(1) Additional albite forms at the expense of the feldspathic component in chondrule glass. For example, although type-3 enstatite chondrites contain little crystalline albite (e.g., <1 wt.% in EH3 ALH A77156; McKinley et al., 1984), type-6 enstatite chondrites contain appreciably more (e.g., 9 wt.% in EL6 Atlanta; Rubin, 1983b). Additional enstatite crystallizes from the mafic-silicate component of the glass.
(2) Forsterite disappears via reaction with silica (which constitutes ~1–2 vol.% of E3 chondrites) to produce additional enstatite:

$$Mg_2SiO_4 + SiO_2 = 2MgSiO_3$$

forsterite + silica = 2enstatite

The modal abundance of forsterite in EH3 and EL3 chondrites is 4.4 and 2.4 vol.%, respectively (Table 3 of Weisberg and Kimura, 2012); it is rare to absent in EH4 and EL4 chondrites and absent in type-5 and −6 EH and EL chondrites (e.g., Keil, 1968).

(3) Diopside is present in type-3 enstatite chondrites (0.1-0.3 vol.%: Weisberg and Kimura, 2012), but is extremely rare in more-equilibrated enstatite chondrites. We speculate that diopside may have been destroyed through sulfidation by a reaction such as:

$$CaMgSi_2O_6 + H_2S = MgSiO_3 + CaS + SiO_2 + H_2O$$

diopside + hydrogensulfide = enstatite + oldhamite + silica + water

(4) The unusual (unique?) occurrence of diopside in EL6 EET 90102 (Fogel, 1997) may have resulted from the reverse reaction under peculiar metamorphic conditions (Floss et al., 2003).
(5) Clinoenstatite in EH3 and EL3 chondrite chondrules is transformed into orthoenstatite at a temperature of ~630 °C (Boyd and England, 1965), accounting for its absence in type-5 and −6 enstatite chondrites (which, by analogy to OC, were heated to ≥700 °C).
(6) The cathodoluminescence (CL) properties of pyroxene change with increasing degrees of metamorphism. For example, EL3 pyroxene grains emit mainly violet-blue CL, whereas EL5 and EL6 pyroxene grains emit a magenta CL (Dehart and Lofgren,

1995). This may be related to the incorporation of minor-element red activators such as Cr^{+3} and Mn^{+2} into pyroxene during metamorphism.

(7) The presence of quartz in some EH5 chondrites was attributed by Kimura et al. (2005) to transformation from tridymite or cristobalite (primary phases formed in chondrules) during long-duration, low-temperature metamorphism.

(8) Perryite constitutes 0.8 and 0.1 vol.% of EH3 and EL3 chondrites (Weisberg and Kimura, 2012), but is absent in more-equilibrated enstatite chondrites. It probably breaks down into schreibersite and Si-bearing low-Ni metallic Fe (kamacite). Perryite is a Ni- rich mineral, containing an average of 78.8 wt.% Ni in EH3 chondrites (Prinz et al., 1984); its breakdown during thermal metamorphism is reflected in the increase in the mean Ni content of low-Ni metallic Fe (kamacite) (3.0 wt.% in EH3 Qingzhen, ALH A77156 and Kota-Kota vs. 7.1 wt.% in EH4 Indarch; McKinley et al., 1984; Keil, 1968).

(9) Some grains of troilite in the matrix of type-3 enstatite chondrites contain daubréelite exsolution lamellae (e.g., Rubin et al., 2009), probably formed during cooling after minor metamorphic heating.

(10) Sulfide undergoes changes in the EH group (El Goresy et al., 1988). (a) Djerfisherite in EH3 chondrites breaks down to form troilite, covellite (CuS), idaite (Cu_5FeS_6), bornite (Cu_5FeS_4) and other phases, (b) Fe diffuses from troilite to niningerite, causing the latter phase to become reversely zoned, and (c) sphalerite forms (in Y 691) due to Zn mobilization.

(11) Presolar silicate and carbonaceous grains (identified in EH3 chondrites; Ebata et al., 2006, 2007, 2008; Ebata and Yurimoto, 2008) were destroyed during metamorphism.

(12) Within type-3 enstatite chondrites, low levels of thermal metamorphism also caused an increase in the structural order of organic matter (Quirico et al., 2011) and partial loss of noble gases.

2.8.12. Eucrites

As of this writing, the Meteoritical Bulletin Database lists ~1070 eucrites, probably representing 500-600 separate falls, widely conjectured to have been derived from Vesta (e.g., Consolmagno and Drake, 1977; Burbine et al., 2001; Russell et al., 2012). Non-cumulate eucrites are basalts that crystallized with ophitic or sub-ophitic textures. Takeda and Graham (1991) divided the eucrites into six types (1–6) based on their degree of metamorphic recrystallization. Type-1 eucrites are the most pristine; they retain their primary textures, contain moderately heterogeneous pyroxenes (including some grains with ferroan compositions), have compositionally zoned pyroxene grains, do not possess microscopically identifiable exsolution lamellae in the pyroxene, and contain primary glassy mesostases. With increasing metamorphic grade, the following processes occur: (1) pyroxenes become compositionally more homogeneous, (2) pigeonite exsolves in type-5 and -6 eucrites, (3) augite exsolution lamellae coarsen, (4) the low-Ca pyroxene host flanking coarse augite exsolution lamellae in type-6 eucrites partly inverts to orthopyroxene, (5) pyroxene becomes "cloudy" due to the precipitation of small chromite grains (type 4–6), and (6) mesostasis glass disappears or recrystallizes.

Metamorphic temperatures for eucrites appear mostly to have been in the range of 800–900 °C (Yamaguchi et al., 1996). The mechanism that caused thermal metamorphism has been suggested to be impact heating (Takeda and Graham, 1991; Yamaguchi et al., 2001), the decay of ^{26}Al (e.g., Hutchison, 2004), or burial by subsequent lava flows (Yamaguchi et al., 1996) (which presumably were created after solid rock was melted either by impacts or ^{26}Al decay).

2.8.13. Ureilites, aubrites and irons

The petrographic features indicative of annealing observed in some ureilites (e.g., ALH 81101, LEW 86216; Rubin, 2006) and aubrites (e.g., Bishopville, LAP 03719; Rubin, 2015b) were attributed to shock-induced heating and will be discussed in Section 2.10. The recrystallization evident in some iron meteorites (e.g., IIIAB Roebourne, IVA Social Circle; Buchwald, 1975) was probably also caused by shock (see Section 2.10). Nevertheless, it is possible that recrystallization in a few irons was partly caused by solar heating during "repeated orbital passages near the Sun" (Buchwald, 1975); this topic is explored in Section 2.15.

2.9. Aqueous alteration, hydrothermal alteration and metasomatism

The proposed identification of hydrous phyllosilicates on the surfaces of asteroids of the C, D, G, F and B classes (e.g., Vilas and Gaffey, 1989; Vilas et al., 1993; Vilas et al., 1994) indicates that aqueous alteration processes are likely to have affected the meteorites (i.e., the carbonaceous chondrites) thought to have derived from those bodies. Although some workers have postulated that alteration took place in the nebula (e.g., Cyr et al., 1998), most studies have concluded that alteration occurred principally on asteroids (e.g., Kerridge and Bunch, 1979; McSween, 1979; Fredriksson and Kerridge, 1988; Hanowski and Brearley, 2001; Rubin et al., 2007). As summarized by Brearley (2006), inferred alteration temperatures for CI and CM chondrites are 0–150 °C and 20–80 °C, respectively; those for type-3 OC are <260 °C.

2.9.1. CI chondrites

CI chondrites contain appreciable amounts of bulk water (e.g., ~11 wt.% H_2O^+ (indigenous water) in the Orgueil fall; Jarosewich, 1990), mainly occurring as hydroxyl in Fe-Mg serpentines and as water of hydration in the interlayered saponite. These phases constitute the matrix of CI chondrites and account for ~95 vol.% of these rocks (Scott and Krot, 2005). Other water-bearing minerals include sulfate [gypsum ($CaSO_4{\cdot}2H_2O$) with minor blödite ($Na_2Mg(SO_4)_2{\cdot}4H_2O$) and nickelblödite ($Na_2(Ni,Mg)(SO_4)_2{\cdot}4H_2O$)] and ferrihydrite ($Fe_{4\text{-}5}(OH,O)_{12}$) (Brearley, 2006). Anhydrous minerals formed in CI chondrites by aqueous alteration (e.g., Kerridge et al., 1979) include magnetite (which occurs in three distinct morphologies – framboids, platelets and plaquettes), several sulfides (pyrrhotite with minor pentlandite and cubanite) and several carbonates (calcite – $CaCO_3$, dolomite – $CaMg(CO_3)_2$, breunnerite – $(Mg,Fe)CO_3$ and minor siderite – $FeCO_3$). [By analogy to the mechanism most likely responsible for producing pyrite framboids in terrestrial sediments and low-temperature ore deposits (Butler and Rickard, 2000), the magnetite framboids in CI chondrites may have formed by rapid nucleation from fluids supersaturated with oxidized iron. The fact that many magnetite framboids appear to have formed around dissolving sulfide grains, suggests that the source of the oxidized iron is the associated sulfide.]

CI chondrites contain compositionally heterogeneous iron–nickel sulfide grains (pyrrhotite and pentlandite) formed during late-stage aqueous alteration; sulfide compositions vary among the members of the group. Berger et al. (2016) concluded that Orgueil and Alais experienced different equilibration temperatures (~25 and 100–135 °C, respectively). They concluded that the aqueous alteration conditions (e.g., temperature, pH, oxygen fugacity, duration) varied on the scale of millimeters.

The relatively rare coarse isolated olivine and pyroxene grains (probably dislodged chondrule phenocrysts) (e.g., Leshin et al., 1997), refractory minerals (probably CAI fragments) (Huss et al., 1995) and altered intact CAIs (Frank et al., 2011) indicate that CI

chondrites have the same set of major components as other carbonaceous chondrites, albeit in different proportions.

2.9.2. CM chondrites

Although generally not as altered as CI chondrites, CM chondrites still contain a significant amount of bulk water (e.g., ~9 wt.% H_2O^+; Jarosewich, 1990). The CM group exhibits large variations in degree of aqueous alteration (e.g., Zolensky et al., 1997). Many individual CM meteorites (e.g., Murray, Cold Bokkeveld) are breccias that contain millimeter-to-centimeter-size clasts that have been altered to a different extent than the host (e.g., Rubin and Wasson, 1986; Metzler et al., 1992). Several schemes have been devised to classify CM chondrites by their degree of aqueous alteration (e.g., McSween, 1979; Browning et al., 1996; Howard et al., 2009); the most successful scheme (and the one most widely adopted) is that of Rubin et al. (2007). It takes into account the modal abundance of metallic Fe-Ni, the degree of alteration of mafic silicate phenocrysts in chondrules, the abundance of large clumpy intergrowths of tochilinite-cronstedtite, the bulk composition of these intergrowths, carbonate composition, and the distribution of sulfide phases.

In going from the least-altered CM chondrites (ideally type 3.0) to the most altered (type 2.0; called CM1 in other schemes), the following mineralogical changes occur: (1) glassy chondrule mesostases transform into phyllosilicate (beginning at about type 2.9), (2) tiny mafic silicate grains and amorphous material in the matrix also transform into phyllosilicate (beginning at about type 2.9), (3) melilite in CAIs transforms into phyllosilicates at about type 2.8, (4) the modal abundance of metallic Fe- Ni systematically decreases throughout the sequence due to oxidation, (5) thin magnetite rinds surround some of the metal grains, (6) mafic silicate phenocrysts in chondrules transform into phyllosilicates (beginning at type 2.3), (7) the modal abundance of large clumpy tochilinite-cronstedtite intergrowths decreases (beginning at about type 2.1), (8) the "FeO"/SiO_2 ratio of tochilinite-cronstedtite intergrowths [2[(Fe,Mg,Cu,Ni[])S·1.57-1.85[(Mg,Fe,Ni,Al,Ca)$(OH)_2$] – $Fe_2^{+2}Fe^{+3}(SiFe^{+3})O_5(OH)_4$] decreases (beginning at about type 2.4) (wherein "FeO" refers to FeO in phyllosilicates, Fe^{+3} in cronstedtite and Fe^{+2} in sulfide), (9) the S/SiO_2 ratio of tochilinite-cronstedtite intergrowths decreases (beginning at about type 2.4) as S leaves the intergrowths to help form relatively coarse Fe,Ni-sulfide grains, (10) the modal abundance of sulfides with "intermediate" compositions (those with atomic Ni/(Fe + Ni) ratios of 0.10-0.40) increases (beginning at about type 2.4), (11) the modal abundance of pyrrhotite decreases appreciably by type 2.2, and (12) Ca carbonate (mainly calcite) forms at about type 2.8 or 2.9 and is partly replaced by more complex carbonates (with significant amounts of Ca, Mg, Fe and Mn) beginning at about 2.1.

In some cases, different aqueous-alteration products are intergrown. Maribo (CM2) contains bands of tochilinite transecting calcite (Fig. 4) and magnetite of different morphologies (quasi-equant grains, spherulites and framboids) occurring together with spherules of hydroxylapatite within serpentine (Fig. 5). [Magnetite spherulites can be distinguished from spherules: spherulites have internal radial structures that spherules lack (Hyman et al., 1985).]

The least-altered CM chondrite appears to be Paris, type 2.7, but the rock is a breccia with regions as little altered as type 2.9 (Hewins et al., 2014; Marrocchi et al., 2014; Rubin, 2015c). A few chondrules contain unaltered glassy mesostases, rare CAIs contain melilite, and some amorphous material occur in the matrix. In contrast, the most altered samples, i.e., the CM2.0 chondrites(a.k.a. CM1), contain chondrule pseudomorphs made up of phyllosilicates. A few of these meteorites (e.g., MET 01070) also possess tochilinite-cronstedtite lenses more than a centimeter in length (Rubin et al., 2007). In some cases, the lenses cut across one another; they probably formed within sheer-induced fractures in the rocks.

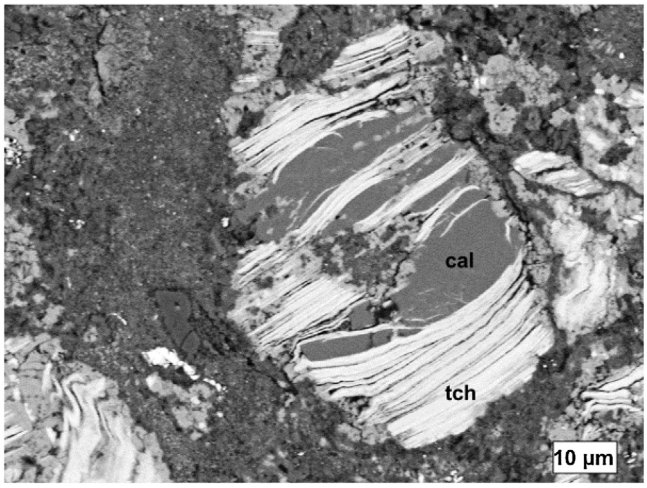

Fig. 4. Bands of tochilinite (tch) in calcite (cal) in the Maribo CM2 chondrite. BSE image courtesy of M. E. Zolensky, NASA – JSC.

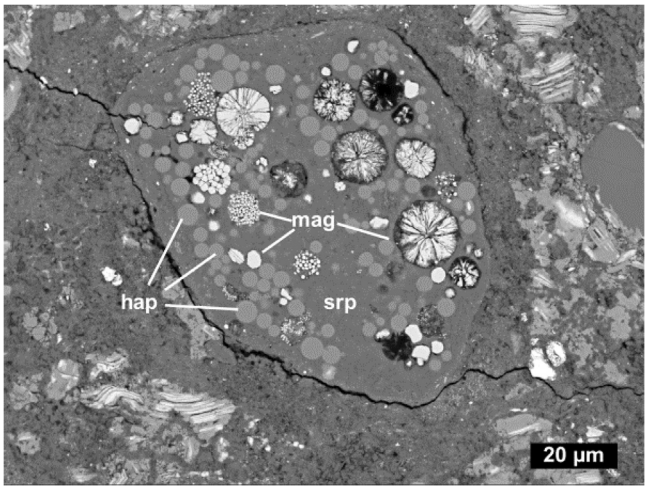

Fig. 5. Magnetite (mag) framboids, spherulites and quasi-equant crystals (white to light gray) occurring along with hydroxylapatite (hap) (gray spherules) inside a clast of serpentine (srp) (medium gray) in the Maribo CM2 chondrite. BSE image courtesy of M. E. Zolensky, NASA – JSC.

Rubin (2012b) found a strong positive correlation between the degree of alteration of a CM chondrite and the extent of particle alignment (i.e., the strength of the petrofabric) within it. He suggested that random collisions on the parent body created fractures and produced petrofabrics in some rocks. When water was later mobilized (presumably due to impact-heating of accreted ice and/or water-bearing phases), the more-fractured regions were preferentially altered.

Anomalous CM chondrites that have been aqueously altered include Belgica-7904, WIS 91600 and GRO 95566 (Choe et al., 2010).

2.9.3. CR chondrites

The CR chondrites vary in their degree of alteration. Some rocks contain chondrules with glassy mesostases (e.g., Weisberg et al., 1993; Abreu and Brearley, 2010), have abundant metallic Fe-Ni (up to ~17 wt.%) and lack magnetite. In others, the metallic Fe-Ni has been largely transformed into oxide (e.g., Weisberg and Huber, 2007).

A recent scheme that attempts to categorize CR chondrites by their degree of aqueous alteration is that of Harju et al. (2014).

In going from the least- altered samples (ideally type 3.0) to the most altered (type 2.0, a.k.a. CR1), the following mineralogical changes occur: (1) glassy chondrule mesostases transform into phyllosilicate (beginning at type 2.8), (2) tiny mafic silicate grains and amorphous material in the matrix transform into phyllosilicate, mainly serpentine intergrown with saponite (beginning at type 2.9), (3) magnetite grows at the expense of metallic Fe-Ni (beginning at type 2.7), forming rinds on coarse metal grains and framboids in the matrix, (4) mafic silicate phenocrysts in chondrules alter to phyllosilicate (beginning at type 2.5), (5) Ca carbonate forms (beginning at type 2.5), and (6) siderite and ferrous sulfate form in type 2.0 rocks. Abreu (2016) recently used TEM studies of CR matrices to refine the alteration classification scheme.

Some of the least-altered samples have chondrules surrounded by phyllosilicate rims containing silica and moderately ferroan low-Ca pyroxene. The association of the silica with phyllosilicate suggests that the silica is also an alteration product, but it is possible that it pre-dates alteration and formed as part of an igneous chondrule rim. It is not clear if the silica phase is amorphous or crystalline, but because it contains minor amounts of FeO, MgO and Al_2O_3, it is unlikely to be quartz (Harju et al., 2014).

Some CR chondrites are breccias containing dark inclusions (e.g., Weisberg et al., 1993; Bischoff et al., 1993a; Endress et al., 1994). These inclusions have sharp boundaries with their hosts and appear to be clasts of CR-chondrite matrices that have experienced more-extensive aqueous alteration than their hosts (Bischoff et al., 1993a; Brearley, 2006). They contain microchondrules, small (<200 μm) polycrystalline fragments, sulfide laths (pentlandite and pyrrhotite), magnetite (framboids, platelets and spherules) and accessory phases (Cr-spinel, metallic Fe-Ni, schreibersite, ilmenite, Ca-phosphate and breunnerite) embedded in fine-grained serpentine- smectite intergrowths. Endress et al. (1994) also reported two Os,Mo,Ir-rich particles within dark inclusions in CR2 Acfer 059 and its paired specimens.

2.9.4. CO chondrites

The CO chondrites were affected by fluid- assisted thermal metamorphism (e.g., McSween, 1977; Rubin, 1998; Chizmadia et al., 2002). Unlike the case for CM and CR chondrites (which range in subtype from least-altered 3.0 to most-altered 2.0 and have experienced little thermal metamorphism), the CO chondrites range from least-altered, least-metamorphosed type 3.0 to most-altered, most-metamorphosed type 3.8.

In addition to the metamorphic and metasomatic effects described in Section 2.8, CO chondrites exhibit an apparent correlation between subtype and mean chondrule size, i.e., the most-altered CO chondrites (e.g., type 3.8) tend to have the largest chondrules (Rubin, 1998). This is probably an artifact due to the recrystallization and alteration of chondrule margins, preferentially making the smallest chondrules in the most-metamorphosed CO chondrites unrecognizable as intact objects.

Another effect of aqueous alteration in CO chondrites involves the dissolution of primitive melilite in refractory inclusions (grains with $\Delta^{17}O$ values ≤-20‰) and the reprecipitation of new melilite in the presence of H_2O with a high $\Delta^{17}O$ value (Wasson et al., 2001).

The presence of phyllosilicate in the matrices of some CO3.0 to CO3.4 chondrites (Brearley, 1993b, 2006) indicates that mafic silicates and amorphous material were being destroyed at the beginning of the alteration sequence.

2.9.5. CV chondrites

The Allende-like oxidized subgroup ($CV3_{OxA}$) contains such secondary phases as nepheline, sodalite, grossular, hedenbergite, anorthite, monticellite, wadalite, hutcheonite and adrianite, consistent with alkali-halogen-Fe metasomatism (e.g., Fuchs, 1971; Krot et al., 1995; Ma and Krot, 2014a,b). Hutcheonite ($Ca_3Ti_2(SiAl_2)O_{12}$) is a new garnet mineral occurring in alteration areas of an Allende CAI (Fig. 6) (Ma and Krot, 2014a). A. Krot (pers. commun., 2016) found larnite (Ca_2SiO_4) replacing melilite in an Allende CAI. Another phase present in many Allende chondrules is awaruite (e.g., Rubin, 1991). The Bali-like oxidized subgroup ($CV3_{OxB}$) has undergone aqueous alteration that produced phyllosilicate, pentlandite, tetrataenite (FeNi) and awaruite (Ni_3Fe) grains in the matrix (Krot et al., 1995, 1998a). Members of the reduced subgroup ($CV3_{red}$) contain moderate amounts of metallic Fe-Ni and troilite, little magnetite, and small to negligible amounts of secondary phases (Krot et al., 1995, 1998b). Thermodynamic calculations indicate that the hydrothermal-alteration/metasomatism experienced by the CV chondrites occurred at temperatures in the range of 200–300 °C (Krot et al., 1998b, 2000).

Many CAIs in oxidized CV3 chondrites contain multi-phase opaque assemblages that were dubbed “Fremdlinge” (German for “foreigners”) by El Goresy et al. (1977, 1978). Typically, the assemblages consist of refractory metal nuggets, varying in diameter from 1 to 1000 μm, surrounded by metallic Fe-Ni, V- rich magnetite and Fe-Ni sulfides; these phases are associated with molybdenite (MoS_2), molybdates, tungstate and phosphate (e.g., El Goresy et al., 1978; Armstrong et al., 1985a; Armstrong et al., 1985b; Bischoff and Palme, 1987). These opaque assemblages were initially thought to be possible presolar grains (El Goresy et al., 1978), but were later interpreted as products of secondary alteration and sulfidation of metallic Fe- Ni on the CV parent body (e.g., MacPherson, 2005).

The presence of ^{26}Mg excesses in some primary phases (e.g., anorthite, diopside) in many non-FUN CAIs is due to the in situ decay of ^{26}Al (a short-lived radionuclide; $t_{½}$ = 730,000 years). The absence of ^{26}Mg excesses in secondary phases (e.g., nepheline, grossular) in CAIs in oxidized CV chondrites implies that these minerals formed much later, after ^{26}Al had decayed away.

The reduced CV3 chondrites have experienced the least amount of alteration. Nevertheless, there are a number of indicators of alteration: (1) ferrihydrite

($Fe_{4-5}(OH,O)_{12}$) and saponite ($(Ca,Na)_{0.3}(Mg,Fe^{+2})_3(Si,Al)_4O_{10}(OH)_2{\cdot}4H_2O$) replace some ferroan olivine grains in the matrix of Vigarano (Lee et al., 1996), (2) the matrix contains minor magnetite (Krot et al., 1995) and such secondary phases as hedenbergite ($CaFeSi_2O_6$), andradite ($Ca_3Fe_2(SiO_4)_3$) and kirschteinite ($CaFe(SiO_4)$) (MacPherson and Krot, 2002), (3) these same phases also occur at the surfaces of Wark-Lovering rims, accretionary rims and CAIs (MacPherson and Krot, 2002), (4) some chondrules have fine-grained phyllosilicate-bearing rims (Tomeoka and Tanimura, 2000), (5) minor carbonate is present (Mao et al., 1990; Davis et al., 1991; Abreu and Brearley, 2005), and (6) some regions of the Vigarano matrix show correlations among elements (Ca, S, Na, K) associated with water-soluble phases (e.g., $CaSO_4$, KCl, NaCl) (Hurt et al., 2012).

As discussed by Brearley (2006), members of the Allende-like oxidized subgroup ($CV3_{OxA}$) contain small amounts of phyllosilicates in the matrix (phlogopite – $KMg_3(Si_3Al)O_{10}(F,OH)_2$, montmorillonite – $(Na,Ca)_{0.3}(Al,Mg)_2Si_4O_{10}(OH)_2{\cdot}nH_2O$, clintonite – $Ca(Mg,Al)_3(Al,Si)_4O_{10}(OH,F)_2$, margarite – $CaAl_2(Si_2Al_2)O_{10}(OH)_2$, saponite – $(Ca,Na)_{0.3}(Mg,Fe^{+2})_3(Si,Al)_4O_{10}(OH)_2{\cdot}4H_2O$ and chlorite- group minerals). Some low-Ca-pyroxene-rich chondrules have small amounts of talc, amphibole and disordered biopyriboles (Brearley, 1997). Igneous rims around many chondrules in Allende also contain secondary nepheline ($(Na,K)AlSiO_4$) and sodalite ($Na_4(Si_3Al_3)O_{12}Cl$) (e.g., Rubin, 1984a). Many Allende low-FeO porphyritic chondrules have awaruite- and magnetite-bearing nodules which also contain pentlandite and merrillite (Fig. 7); these nodules probably formed from metallic-Fe-Ni and troilite assemblages during parent-body alteration. As in the CO3 chondrites, the low $\Delta^{17}O$ values of melilite in Allende (−4 ± 2‰) is consistent with the dissolution of primitive melilite and the repre-

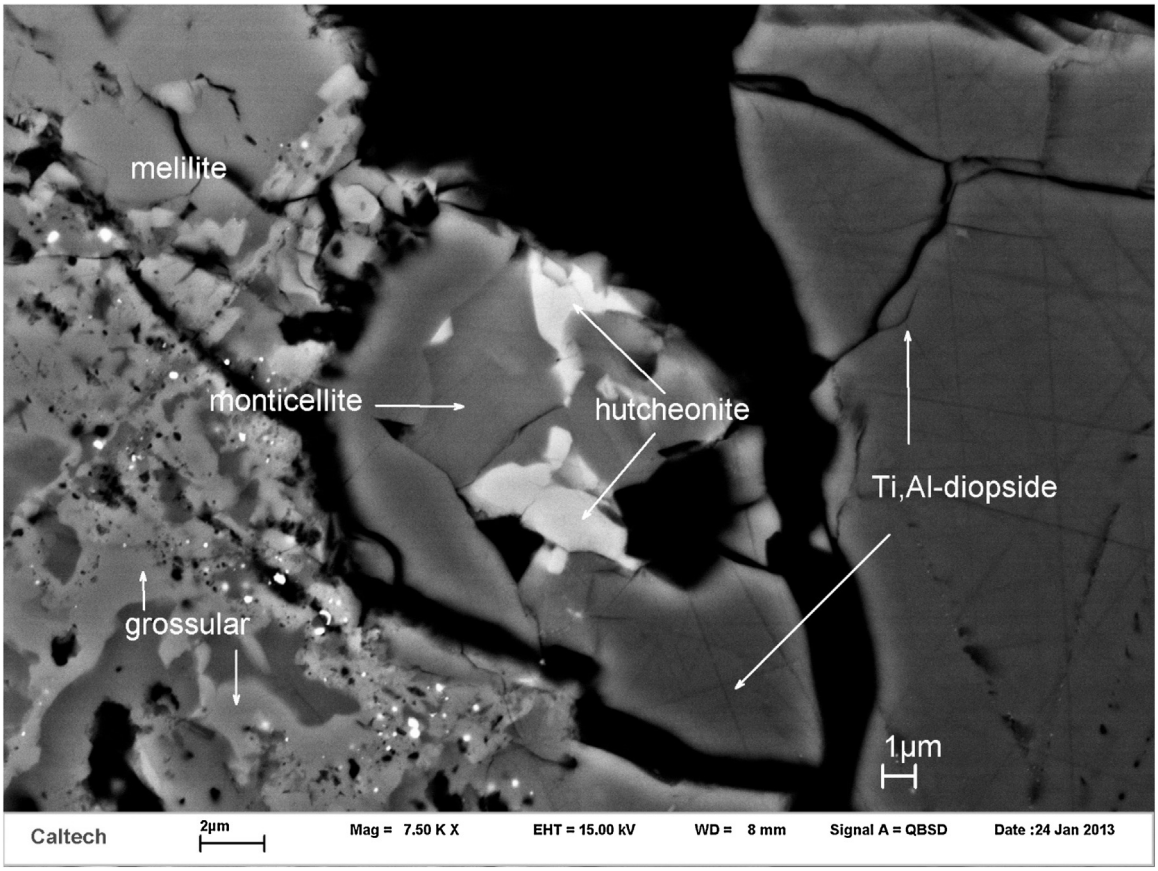

Fig. 6. New alteration mineral hutcheonite, $Ca_3Ti_2(SiAl_2)\,O_{12}$, in CAI Egg-3 from the Allende CV3 chondrite, along with secondary monticellite ($CaMgSiO_4$) and grossular $Ca_3Al_2(SiO_4)_3$ in an alteration area between primary melilite and Ti,Al-diopside (Ma and Krot, 2014a). BSE image.

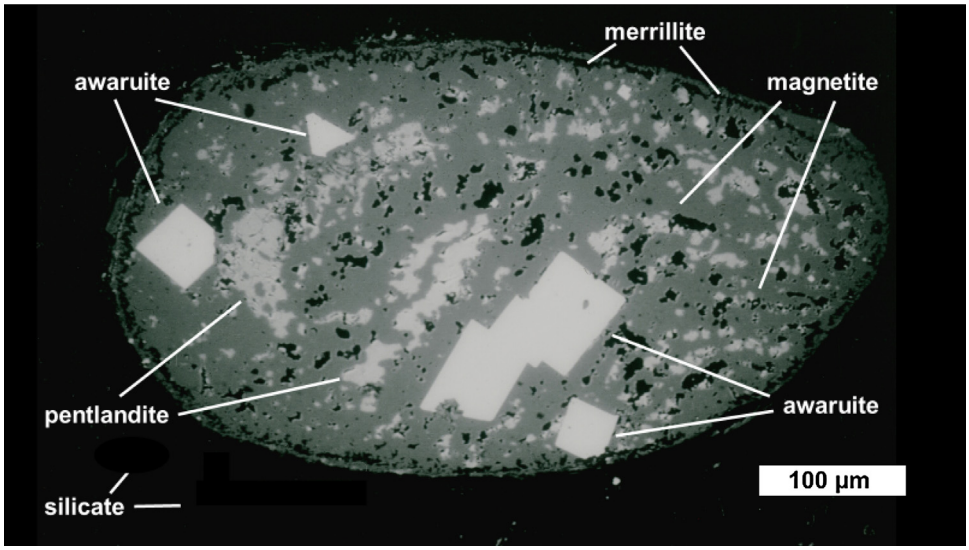

Fig. 7. Opaque nodule in a low-FeO (Type-IA) porphyritic-olivine chondrule from the Allende CV3 chondrite. The nodule is composed mainly of magnetite (dark gray). Embedded in the magnetite are euhedral grains of awaruite (white) and blebby pentlandite (light gray). A somewhat irregular ring of merrillite is present at the inside margin of the nodule. Black regions outside the nodule are silicate. After Rubin (1991). BSE image.

cipitation of new melilite in the presence of H_2O with high $\Delta^{17}O$ (Wasson et al., 2001).

Brearley (2006) pointed out that members of the Bali-like oxidized subgroup ($CV3_{OxB}$) contain chondrules and CAIs in which several phyllosilicates occur: Fe-bearing saponite, Na phlogopite, Al-rich serpentine, and Na-K mica. Saponite is also abundant in the matrix of these meteorites. Secondary phases in the subgroup include magnetite, carbonates, secondary phosphates, Ni-rich sulfides, fayalite, Ca-Fe-rich pyroxene, and andradite ($Ca_3Fe_2(SiO_4)_3$) (Brearley, 2006).

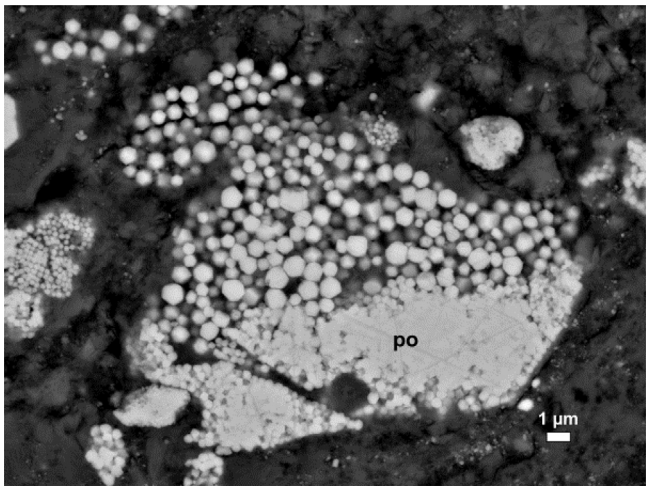

Fig. 8. Framboidal magnetite spherules forming from pyrrhotite (po) during aqueous alteration in the Kaidun polymict-brecciated ungrouped carbonaceous chondrite. BSE image courtesy of M. E. Zolensky, NASA – JSC.

MacPherson and Krot (2002, 2014) suggested that the alteration of CV3 chondrites was caused by mobilized water seeping into voids. Rubin (2012b) pointed out that oxidized CV chondrites have much higher porosities (typically 20-28%) than reduced CVs (0.6 -8%) and that many $CV3_{OxB}$ chondrites are shocked and have strong petrofabrics. When water was later mobilized (presumably by impact heating), the more-fractured, more-porous rocks facilitated greater degrees of alteration. Although $CV3_{red}$ chondrites were also shocked and also have strong petrofabrics (Rubin, 2012b), they formed from low-porosity materials which inhibited subsequent aqueous alteration.

CV3 chondrites contain dark inclusions (Johnson et al., 1990; Krot et al., 1995; Grossman and Brearley, 2005), many of which have been aqueously altered: they are enriched in heavy O isotopes (Clayton and Mayeda, 1999), a few contain phyllosilicates, and many contain chondrule pseudomorphs (e.g., Kojima et al., 1993; Kojima and Tomeoka, 1996; Krot et al., 1997b), veins of Ca-rich pyroxenes (Brearley, 2006) and veins with pseudomorphs after phyllosilicates. Some dark inclusions in Efremovka ($CV3_{red}$) were thermally metamorphosed after being aqueously altered (Krot et al., 1999).

2.9.6. Ungrouped carbonaceous chondrites

Several ungrouped carbonaceous chondrites show evidence of aqueous alteration – Tagish Lake, MAC 88107, Kaidun, LEW 85332, GRA 98025 and QUE 99038 (e.g., Brearley, 2006; Choe et al., 2010). All of the samples contain phyllosilicates in their matrices; some have chondrules that have been partly altered to phyllosilicate; some contain magnetite, carbonates, fayalite, hedenbergite and Fe,Ni sulfides. Kaidun contains grains of pyrrhotite that were oxidized to form magnetite framboids (Fig. 8); the S was apparently leached away by aqueous fluids. This meteorite also contains enstatite-chondrite clasts that have been aqueously altered; secondary phases include a poorly crystalline Si-Fe phase, serpentine, plagioclase, and calcite (Zolensky et al., 2014a). [Although listed in the Meteoritical Bulletin Database as a carbonaceous chondrite, Kaidun is actually a breccia composed mainly of sub- equal amounts of carbonaceous-chondrite and enstatite-chondrite materials and lesser amounts of ordinary-chondrite, R-chondrite and achondrite clasts (e.g., Zolensky and Ivanov, 2003).]

These ungrouped carbonaceous chondrites are likely derived from otherwise-unsampled asteroids, attesting to the commonality of parent-body aqueous alteration.

2.9.7. Ordinary chondrites

Aqueous alteration has affected the type-3 OC. This is consistent with the presence of 1.2 wt.% H_2O^+ (indigenous water) in the Semarkona LL3.0 fall (Jarosewich, 1990). The aqueous alteration of these rocks cannot be cleanly separated from the changes induced during the earliest stages of thermal metamorphism (e.g., Grossman and Brearley, 2005) – see Section 2.8.

The fine-grained silicate matrix of Semarkona contains Fe-rich smectite (Hutchison et al., 1987) as well as opaque phases (magnetite, pentlandite, cohenite, haxonite, Ni-rich metal) that formed from low-Ni metallic Fe and troilite (Taylor et al., 1981; Krot et al., 1997c; Keller, 1998). Portions of the glassy mesostases of some Semarkona chondrules have been hydrated and leached; the sharp lobate boundaries between hydrated altered glass and unaltered isotropic glass is readily discerned (e.g., Fig. 6 of Rubin, 2013b). Some Semarkona chondrules contain FeO-rich smectite (Grossman et al., 2002).

Semarkona and all other type-3 OC contain "bleached" radial pyroxene and cryptocrystalline chondrules characterized by having porous outer regions in which mesostasis was broken down and alkalis, Ca and Al were lost (Grossman et al., 2000). A few bleached chondrules have also been identified in type-4 to −6 OC despite the metamorphic recrystallization of these rocks. Trains of calcite crystals occur in the vicinity of some chondrules (Hutchison et al., 1987).

The composition of the fluid that caused alteration of OC may have varied with time as additional phases were altered. Apatite formed from a fluid that was dry, acidic and halogen rich (with a high Cl/F ratio) (Jones et al., 2014). Secondary phosphates, carbides and magnetite formed from a fluid that was P- and CO_2-bearing. Smectite (which contains water of hydration) must have formed from an H_2O-rich fluid. Albitization of metamorphic plagioclase required an alkali-rich fluid that presumably contained some K (e.g., Lewis et al., 2016). During cooling from peak metamorphic temperatures, K-feldspar lamellae exsolved from the albite grains.

Tieschitz (H/L3.6) contains geode-like voids and veins filled with sodic-calcic amphiboles (winchite – $\square NaCa(Mg_4Al)\ Si_8O_{22}(OH)_2$ and barroisite – $\square NaCa(Mg_3Al_2)\ (Si_7Al)O_{22}(OH)_2$) emplaced during hydrothermal alteration (Dobrică and Brearley, 2014). The same fluid that produced the amphiboles also gave rise to the so-called "white matrix" of this meteorite (Christophe Michel-Levy, 1976).

The occurrence of millimeter-size aggregates of halite with inclusions of sylvite in two H-chondrite regolith breccias (Zolensky et al., 1999) led Rubin et al. (2002) to suggest that they formed from mobilized brines on the H-chondrite asteroid. However, Zolensky et al. (1999, 2013, 2015) and Fries et al. (2013) concluded that the salt crystals are exogenous, formed by cryovolcanic activity, possibly on Ceres. This conjecture is consistent with the subsequent report of an extrusive cryovolcanic dome on Ceres (Russell et al., 2016).

2.9.8. R chondrites

R chondrites contain abundant matrix material (an average of 42 vol.%; Rubin and Kallemeyn, 1993), far higher than in OC (12 vol.%; Huss et al., 1981). Equilibrated R chondrites have the highest mean olivine Fa values (37-42 mol%) among chondrite groups. R chondrites also have high bulk $\Delta^{17}O$ values ($+2.72 \pm 0.31$‰; Bischoff et al., 2011). These three properties are probably related; it seems plausible that R chondrites accreted a large amount of matrix material laden with ^{17}O-rich water (either occurring as ice or bound within phyllosilicates). During parent-body metamorphism (Section 2.8), the water was mobilized, the rocks were oxidized, and the bulk samples reflected the high $\Delta^{17}O$ values. This is consistent with the presence of magnetite within sulfide-bearing intergrowths in an unequilibrated clast in the R-chondrite genomict breccia PCA 91241 (Rubin and Kallemeyn, 1994; Greenwood et al., 2000);

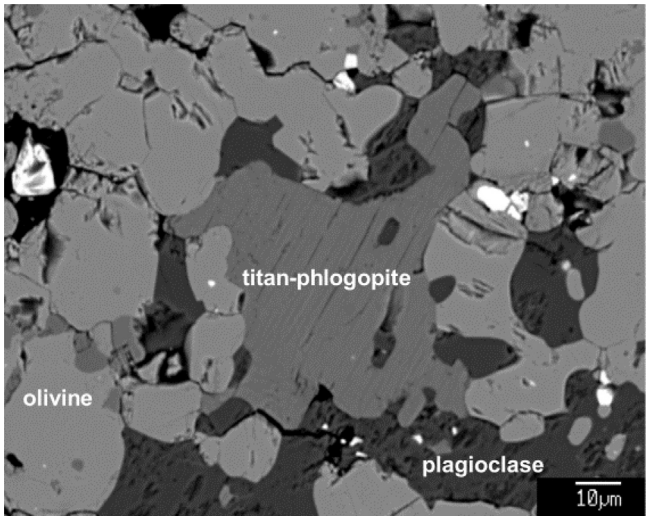

Fig. 9. Titan-phlogopite flanked by olivine and plagioclase in the matrix of the MIL 07440 R6 chondrite. After Rubin (2014). BSE image.

magnetite attests to parent-body aqueous alteration of metallic Fe-Ni (e.g., Choi et al., 1998a; Choi et al., 1998b). LAP 04840, R6 also contains magnetite (Mikouchi et al., 2007; McCanta et al., 2008). Metasomatic alteration of rare CAIs produced nepheline and sodalite in R chondrites.

The strongest evidence for parent-body hydrothermal alteration is the occurrence of 10-15 vol.% amphibole (ferri- magnesio-hornblende – $Ca_2Mg_4Al_{0.75}Fe^{+3}{}_{0.25}$ $(Si_7AlO_{22})(OH)_2$ or edenite – $NaCa_2Mg_5Si_7AlO_{22}(OH)_2$) and accessory phlogopite in R6 MIL 11207 and R6 LAP 04840 and accessory (0.01 vol.%) titan-phlogopite (Fig. 9) in R6 MIL 07440 (McCanta et al., 2008; Ota et al., 2009; Gross et al., 2013; Rubin, 2014). Another water-bearing phase present in several R chondrites is hydroxylapatite – $Ca_5(PO_4)_3OH$.

As discussed by McCanta et al. (2008) and Rubin (2014), the amphibole- and mica-bearing R chondrites underwent hydrothermal alteration. The rocks were probably heated to maximum temperatures of 700–900 °C under conditions of moderately high PH_2O (perhaps 250-500 bars), presumably at a depth of a few tens of kilometers. Patches within some of the hornblende grains in MIL 11207 and LAP 04840 were dehydrated during annealing, producing 2-20-μm-long subparallel pyroxene blades flanked by pore spaces. The $^{40}Ar/^{39}Ar$ plateau ages of 4340-4380 Ma for hornblende separates of LAP 04840 likely date this annealing event (Righter et al., 2016). A subsequent giant impact would have been necessary to excavate the samples.

2.9.9. Enstatite chondrites

Minor aqueous alteration has affected enstatite chondrites: (1) El Goresy et al. (1988) identified hydrated NaCr sulfides in troilite-daubréelite clasts and in NaCr sulfide clasts in the Qingzhen EH3 fall. (2) Chondrule glass within Qingzhen chondrules is halogen rich, containing up to 4.4 wt.% Cl (Grossman et al., 1985; El Goresy et al., 1988). Although Qingzhen chondrules contain several primary sulfide minerals (troilite, niningerite, daubréelite, oldhamite, caswellsilverite, and two Cr-sulfides – minerals A and B of Ramdohr, 1963), djerfisherite – $K_6Na_9(Fe,Cu)_{24}S_{26}Cl$ (which contains ~1.5 wt.% Cl and ~8 wt.% K; El Goresy et al., 1988; Lin and El Goresy, 2002) is virtually absent from chondrules (Grossman et al., 1985; El Goresy et al., 1988). It seems likely that djerfisherite formed in the Qingzhen matrix after Cl and K were scavenged from chondrule mesostases, possibly by an aqueous fluid. This is consistent with the occurrence of djerfisherite inside veins throughout Qingzhen. (It is also present in millimeter-size clasts in Qingzhen as well as in other EH3 and EL3 chondrites; e.g., Lin et al., 1991.)

During subsequent low-level thermal metamorphism, djerfisherite in Qingzhen and other EH3 chondrites broke down to form troilite, covellite, idaite, bornite and additional phases (El Goresy et al., 1988).

2.9.10. Eucrites

Eucrites contain little water (e.g., Jarosewich, 1990) and there is no evidence that these basalts were subjected to low-temperature aqueous alteration on their parent asteroid. Nevertheless, Warren et al. (2014) described higher-temperature alteration in the NWA 5738 eucrite driven by a mainly non-aqueous fluid. The rock contains microscopic fluid- metasomatic vein deposits including microveins filled with major Ca-plagioclase and Fe^{+3}-bearing Cr-spinel (indicative of relatively high fO_2). Also present are veins of essentially Ni-free metallic Fe that may have formed from a fluid with appreciably lower fO_2. The cause of the apparent decrease in the fO_2 of the fluid is unknown. However, Warren et al. (2014) speculated that foreign volatile-rich carbonaceous material buried within that region of the asteroid was displaced by an impact into a region with higher temperature and/or lower pressure where lower fluid fO_2 was caused by carbon-fueled smelting. The occurrence of buried carbonaceous-chondrite material is consistent with the presence on Vesta (the likely eucrite parent body; e.g., Burbine et al., 2001; Russell et al., 2013) of dark material that seems to have been derived from carbonaceous-chondrite projectiles (e.g., McCord et al., 2012; Nathues et al., 2014).

The secondary alteration of the NWA 5738 eucrite may constitute a link between metasomatism and shock metamorphism (Section 2.10).

2.9.11. Mesosiderites

Lorenz et al. (2010) suggested that an anhydrous, gaseous fluid, rich in S_2, CO and CO_2, penetrated fractures within olivine grains in the Budulan mesosiderites. This process caused the adjacent olivine to become more reduced; it also facilitated the production of secondary mineral assemblages within the fractures including aggregates of troilite-low-Ca-pyroxene and metallic-Fe-Ni- pyroxene. A few olivine grains were replaced by aggregates of troilite, pyroxene and silica.

It is not clear if the fluid was produced on the parent asteroid during differentiation or was ultimately derived from a projectile containing organic matter and sulfides.

2.9.12. Ureilites

The polymict ureilite EET 83309 contains bands of opal (hydrated amorphous silica) more than 300 μm long, in some cases associated with schreibersite, olivine or suessite (Beard et al., 2009, 2011). Although the O-isotopic composition of the opal is close to the terrestrial fractionation line (Downes et al., 2016), this could reflect exchange of water in the Antarctic environment. If the opal is indeed pre-terrestrial, this indicates the presence of water during the late stages of ureilite formation.

Small grains of halite (NaCl) and sylvite (KCl) are common accessory constituents of ureilites (Berkley et al., 1978). Although Berkley et al. suggested that the halides formed from a late-stage residual magmatic fluid, given the probable presence of indigenous opal (Beard et al., 2009, 2011), it seems plausible that they precipitated from a brine. Alternatively, they could have been derived from carbonaceous-chondrite projectiles, clasts of which occur in polymict ureilites (e.g., Brearley and Prinz, 1992).

2.9.13. Martian meteorites

In view of the abundant evidence for the presence of water on Mars in the past (e.g., McSween, 2006), it is not surprising that mar-

tian meteorites show evidence of aqueous alteration (e.g., Gooding, 1986a; Gooding, 1986b; Gooding and Muenow, 1986; Treiman et al., 1993; Wentworth and Gooding, 1993, 1994; Meyer, 1996; Bridges et al., 2001; Treiman, 2005; Fisk et al., 2006; McSween, 2008). Aqueous fluids in the Gale Crater region of Mars appear to have been enriched in Na, K and Si and depleted in Mg, Fe and Al relative to modeled martian fluids (Schwenzer et al., 2016).

The numerous multi-millimeter-size spheroids of hematite (dubbed "blueberries") in Meridiani Planum (Squyres et al., 2004) appear to be concretions similar to those in the Navajo Sandstone in southern Utah, USA (Chan et al., 2005). These are diagenetic products formed by the precipitation of aqueous fluids in pores within sediments. Although hematite blueberries have not been reported in martian meteorites, grains of hematite do occur. Some occurrences of hematite in association with jarosite may have been produced by higher-temperature magmatic-hydrothermal fluids (McCubbin et al., 2009).

The topic of aqueous alteration in martian meteorites was reviewed by Velbel (2012); the following list is derived mainly from that paper. Hydrous phases include amphibole, biotite, apatite and opal (e.g., Watson et al., 1994; Lee et al., 2015). Nakhlites contain phyllosilicates – smectite (saponite), serpentine, and so-called iddingsite (apparently a smectite-hydroxide assemblage). Halite is also present. According to Treiman (2005), nakhlites were invaded by water ~620 Ma ago; the water altered olivine and mesostasis glass and produced "iddingsite" and halite.

Giesting and Filiberto (2016) reported potassic-chlorohastingsite within melt inclusions in two nakhlites (MIL 03346 and NWA 5790) that formed after trapped chloride-rich fluids reacted with adjacent silicate. Glass within some melt inclusions in Nakhla were replaced by berthierine (Lee and Chatzitheodoridis, 2016).

All varieties of martian meteorites contain carbonate – calcite, aragonite ($CaCO_3$), siderite-magnesite ($FeCO_3$-$(Mg,Fe)CO_3$) solid solution and dolomite-ankerite solid solution. Some carbonates occur in veins; some fill fractures and voids (e.g., Harvey and McSween, 1996). Sulfates include gypsum ($CaSO_4{\cdot}2H_2O$), anhydrite ($CaSO_4$), bassanite ($CaSO_4{\cdot}½H_2O$) and jarosite ($KFe_3(SO_4)_2(OH)_6$) (in association with hematite).

The ALH 84001 orthopyroxenite experienced aqueous alteration and collisions. Aqueous alteration was responsible for forming carbonates. Subsequent decomposition of the carbonate appears to have produced magnetite and periclase.

Some REE minerals (monazite – $(Ce,La,Th)PO_4$, xenotime – $YbPO_4$ and chevkinite-perrierite – $(Ce,La,Ca,Th)_4(Fe^{+2},Mg)_2(Ti,Fe^{+3})_3Si_4O_{22}$) in the martian meteorite breccias NWA 7034 and 7533 most likely formed by fluid-rock interaction in the martian crust (Liu et al., 2016).

2.9.14. Lunar rocks

Apollo samples exhibit evidence of metasomatism. (1) Fluorapatite is present in lunar granulite breccia 79215; Treiman et al. (2014) proposed that vapor-phase metasomatism added P and halogens to a typical granulite via a process similar to terrestrial rock alteration by fumaroles. (2) Primary igneous olivine in Mg-Suite lithologies of subsamples of 69715 have been pseudomorphically replaced by secondary silicate, sulfide and oxide (e.g., Haskin and Warren, 1991; Colson, 1992; Norman et al., 1995; Shearer et al., 2012). Bell et al. (2015) suggested that this was caused by a metasomatic fluid consisting predominantly of H_2 and CH_4 with minor H_2O, CO and H_2S; the fluid composition is consistent with late-stage degassing of a shallow intrusive magma. Although these features have not yet been reported in lunar meteorites, it seems likely that additional study will reveal their presence.

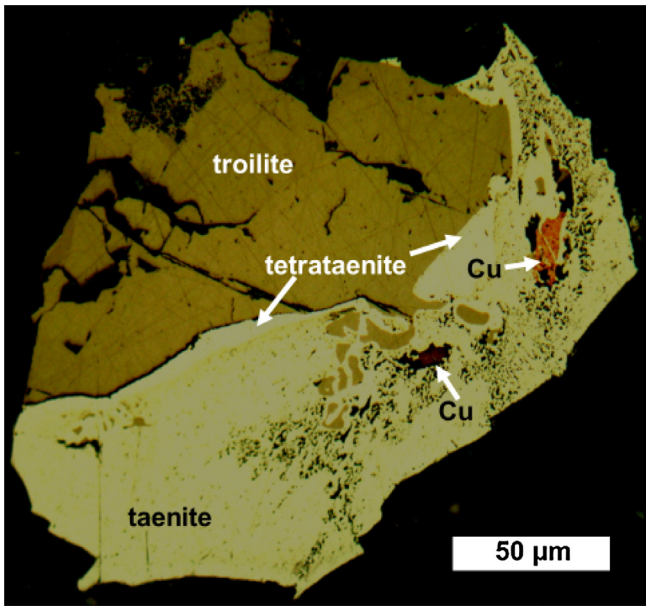

Fig. 10. Metallic Cu grains adjacent to small irregular grains of troilite embedded in taenite in the Stratford L6 chondrite. Between the taenite and more-massive troilite is a thin layer of tetrataenite. The black area surrounding the opaque grain is silicate. The section has been etched with Nital. Reflected light.

2.10. Shock metamorphism

There is a myriad of features produced in meteorites as a result of shock metamorphism (e.g., Stöffler et al., 1988; Bischoff and Stöffler, 1992). Those involved in forming new phases are listed below.

2.10.1. Ordinary chondrites

The shock effects in OC have been summarized and reviewed by Bischoff and Stöffler (1992), Rubin (1985, 2004) and Sharp and DeCarli (2006). Several minerals were formed by impact processes in OC at different shock stages:

(1) Chromite was melted along with plagioclase and crystallized in chromite veinlets and chromite-plagioclase assemblages. Temperatures probably reached ≥1100 °C.
(2) Metallic Cu grains (e.g., Fig. 10) formed after localized shock melting of metal-troilite assemblages reached or exceeded the Fe-Ni-FeS eutectic (~960 °C); this was followed by crystallization of taenite, supersaturation of Cu in the residual sulfide-rich melt, and nucleation of small metallic Cu grains at high-surface- energy sites (e.g., Rubin, 1994a; Tomkins, 2009).
(3) Small irregular grains of troilite crystallized within larger masses of metallic Fe-Ni after metal-sulfide assemblages were melted and quenched.
(4) Rapidly crystallized metal-sulfide melts crystallized finely-intergrown globular assemblages of metal and sulfide (dubbed "fizzed troilite" by Scott, 1982).
(5) Quenched metallic Fe-Ni melts produced martensite, that, in some cases, annealed to form patches of plessite.
(6) Shock-melted metal and sulfide was injected into fractures within silicate grains to form opaque veins upon quenching.
(7) Curvilinear trails of small metallic Fe-Ni ± troilite blebs entered narrow fractures in the silicate grains causing the whole rocks to become darker; this phenomenon, known as "shock darkening" or "silicate darkening," forms so-called "black chondrites." It results from the shock melting of metal

and sulfide (which melt at a lower temperature than silicates, i.e., ~960° vs. ~1100 °C).
(8) Molten silicate formed at ≥1100 °C and was also injected into fractures in silicate grains. Within some fractures the melt quenched into glassy (pseudotachylite-like) veins; in other fractures, fine-grained mafic silicate phases crystallized.
(9) (9) Melt pockets containing silicate glass and small grains of chromite, olivine, pyroxene and plagioclase formed by localized shock melting at temperatures ≥1100 °C.
(10) Orthopyroxene grains were impact heated to between 950 and 1230 °C (or above) and entered the proto-enstatite field; upon quenching, it transformed into clinoenstatite with polysynthetic twinning parallel to (100).
(11) Impact-melt rock clasts formed in many OC; these clasts typically contain major olivine and low-Ca clinopyroxene and minor diopside with interstitial K-rich feldspathic glass.
(12) A few agglutinates (vesicular, glassy objects containing chunks of rock, glass and mineral fragments) formed in some OC regolith breccias (e.g., Rubin, 1982).
(13) Some regions in OC breccias contain crushed silicate grains surrounded by fine-grained troilite; the troilite/metallic-Fe-Ni modal ratios range up to ~500:1, suggesting deposition from a shock-generated vapor (Rubin, 2002b).
(14) Many shocked OC have millimeter-to-centimeter-size vugs that contain some euhedral mineral crystals (metallic Fe-Ni, troilite, low-Ca pyroxene, albite, fayalitic olivine, merrillite and possibly chromite) that appear to have been deposited by an impact-generated vapor (Olsen, 1981b). These occurrences are similar to euhedral mineral crystals (metallic Fe-Ni, troilite, ilmenite, pyroxene, plagioclase, merrillite and apatite) inside vugs in lunar breccias that were previously interpreted to have formed through vapor deposition during shock (McKay et al., 1972).
(15) A euhedral tetrataenite grain within an impact-melt-rock clast in LL6 Jelica formed after impact melting, crystallization of euhedral taenite, and after cooling to 320 °C underwent an ordering reaction and formed tetrataenite (Rubin, 1994b).
(16) Pyrophanite ($MnTiO_3$) in a Mg-Al-chromite fragment in H3.8 Raguli most likely formed from an impact melt of a chromite-rich assemblage containing Mn-rich ilmenite (Krot et al., 1993).
(17) Plagioclase transforms into a diaplectic glass – maskelynite – during compression at high shock pressures.
(18) High-pressure phases, reviewed by Sharp and DeCarli (2006), formed in the vicinity of silicate melt veins in many highly shocked OC. These phases include ringwoodite (a polymorph of olivine with the spinel structure), wadsleyite (the β-spinel polymorph of olivine), majorite (a polymorph of orthopyroxene with the garnet structure), magnesiowüstite, lingunite ($NaAlSi_3O_8$-hollandite), akimotoite (a polymorph of enstatite with the ilmenite structure), bridgmanite ($MgSiO_3$-perovskite; Tschauner et al., 2014), coesite (a monoclinic polymorph of silica), stishovite (a tetragonal polymorph of silica), two post-stishovite polymorphs of silica (one with an orthorhombic α-PbO_2 structure and one with a monoclinic ZrO_2-like structure), and tuite (a trigonal polymorph of whitlockite; Xie et al., 2002, 2003). Such phases have been reported in all three OC groups – H (e.g., Kimura et al., 2000), L (e.g., Sharp et al., 1997) and LL (e.g., Hu and Sharp, 2016).

Some OC were totally (or nearly totally) impact melted; these rocks include PAT 91501 (Mittlefehldt and Lindstrom, 2001), Y-74160 (Takeda et al., 1984), and the vesicular sample LAR 06299 (Rubin and Moore, 2011). The principal phases in these rocks (olivine, low-Ca pyroxene, Ca-pyroxene, Cr- rich spinels, metallic Fe-Ni and troilite with minor sodic plagioclase and silico-feldspathic interstitial melt) crystallized from the impact-generated melt.

There are also a number of impact-melt breccias which contain shocked, but largely unmelted chondritic clasts surrounded by impact-generated melt. These samples include H chondrites (e.g., Rose City, Yanzhuang), L chondrites (e.g., Cat Mountain, Chico, Orvinio, Shaw) and LL chondrites (e.g., Bison, Y-790143, Y-790964) (Table 1 of Rubin, 1995b).

Some large metal nodules and elongated metal veins in OC formed by a complicated processes involving impact vaporization of bulk metal-sulfide assemblages, oxidation of W and Mo to form volatile oxides, partial oxidation of Re and Os, separation of the oxidized siderophiles from the refractory siderophiles, rapid fractional condensation of refractory siderophiles, transport of the residual vapor, condensation of Cu, S and Se into vugs and fractures to form sulfide, and condensation of the remaining siderophiles to form metal nodules and veins (e.g., Widom et al., 1986; Rubin, 1995b, 1999). During vapor cooling and condensation, the residual W, Mo, Re and Os oxides were reduced. One 4×9×12-mm metal nodule in the Rose City impact-melt breccia is divided into three compositionally distinct zones – the "top" is enriched in refractory Os and Ir by 30-40% relative to bulk H-chondrite metal, the middle is depleted in Os and Ir by 31-35%, and the "bottom" is depleted by 75% (Rubin, 1995b). This one heterogeneous metal nodule shows that the vapor transport distance was on the order of 0.5 cm.

2.10.2. Carbonaceous chondrites

Mineral phases formed by shock-metamorphic processes are relatively rare in carbonaceous chondrites.

2.10.3. CI chondrites

The Orgueil CI chondrite contains an agglutinate with desiccated phyllosilicates and impact-melted matrix glass that has partially devitrified to olivine (Zolensky et al., 2015). Also present in this meteorite are vesicular glass beads that were interpreted as impact products.

2.10.4. CM chondrites

Zolensky et al. (2015, 2016) reported vesicular glass beads that have been altered from glass to serpentine in CM2 Nogoya, melted sulfides in Jbilet Winselwan (CM2), and shock melt veins in CM2 lithologies in the Kaidun polymict breccia.

As pointed out by Kimura et al. (2011), a few CM chondrites experienced secondary heating after having been aqueously altered. Dehydration reactions in these rocks produced olivine and metallic Fe-Ni as secondary anhydrous phases (e.g., Akai, 1988; Tomeoka et al., 1989; Tonui et al., 2002). Although he did not identify the heat source, Nakamura (2005) divided the CM chondrites into five heating stages based on their abundances of phyllosilicate and secondary anhydrous phases: Unheated, I, II, III, and I Kimura et al. (2011) classified CM chondrites into three categories based on the inferred degree of secondary heating: Category A (corresponding mainly to the Unheated samples of Nakamura) is characterized by low-Ni metallic Fe (kamacite) and/or martensite; Category B (corresponding to Stage II and III samples) is characterized by pyrrhotite containing blebs or lamellae of pentlandite; and Category C (corresponding to Stage III and IV samples) is characterized by opaque assemblages consisting of low-Ni metallic Fe (kamacite), Ni-Co-rich metal and pyrrhotite. The absence of coarse-grained assemblages of low-Ni metallic Fe, plessite and Ni-rich metal in CM chondrites led Kimura and Ikeda (1992) to suggest that the opaque assemblages in CM Category C formed by rapid cooling following impact heating, a view consistent with the heating experiments on Belgica-7904 (Nakato et al., 2008).

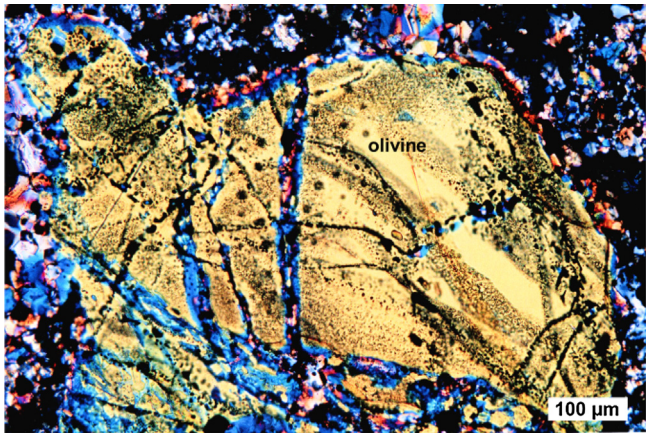

Fig. 11. Olivine grain transected by numerous, intersecting, curvilinear trails of small blebs of metallic Fe-Ni and troilite in the MIL 99301 LL6 chondrite. The olivine exhibits sharp optical extinction because it underwent post-shock annealing. After Rubin (2002a). Transmitted light, crossed polarizers.

2.10.5. CO chondrites

Scott et al. (1992) reported shock melting at the interface between metal and sulfide in CO3 Lancé; at this location, there are micrometer-size intergrowths of the two phases, indicative of melting and rapid crystallization (Scott, 1982). Although most olivine grains in this chondrite exhibit sharp optical extinction (shock-stage S1), localized areas experienced impact melting where temperatures apparently exceeded the Fe- Ni-FeS eutectic.

2.10.6. CV-CK chondrites

Efremovka ($CV3_{red}$) contains impact-melted cellular metal-troilite assemblages, opaque veins and melt pockets (Scott et al., 1992). Many CK chondrites exhibit silicate darkening caused by curvilinear trails of abundant tiny grains of magnetite and pentlandite within silicate grains (Rubin, 1992). By analogy to silicate darkening in OC (caused by trails of small blebs of metal and sulfide) (e.g., Fig. 11), it seems plausible that darkening in CK chondrites was due to impact melting and dispersion of metal and sulfide followed by oxidation to form magnetite and pentlandite. Also present in some CK5 and CK6 chondrites are black glassy to microcrystalline shock veins several millimeters in length (Kallemeyn et al., 1991). These veins formed from impact-melted silicate and contain submicrometer-size grains of magnetite and pentlandite (which are probably post-impact oxidation products of metal and troilite).

EET 83311 (CK5; shock-stage S4) has undergone extensive in situ melting (Scott et al., 1992). Some regions of this meteorite contain tiny olivine grains surrounded by a feldspathic melt; also present in the melt are relict, shocked- but-unmelted olivine grains.

Lunning et al. (2016) identified carbonaceous-chondrite impact-melt clasts in two CV3 chondrites – $CV3_{red}$ RBT 04143 and $CV3_{oxA}$ LAR 06317. The clasts contain no evidence for water and have zoned olivine microphenocrysts embedded in vesicular glass; these features show that these objects have been melted, devolatilized and quenched.

2.10.7. CR chondrites

Kimura et al. (2013) described eclogitic clasts containing omphacite (Ca,Na) ($Mg,Fe^{+2},Al)Si_2O_6$) and pyrope-rich garnet ($Mg_3Al_{22}(SiO_4)_3$) in CR2 NWA 801. The clasts appear to have formed at moderately high temperatures and pressures (940–1080 °C and 2.8-4.2 GPa) and are either achondrites derived from a large parent body or impact-melt rocks presumably formed on the CR parent asteroid. In light of the existence of CR impact-melt rocks (see below), it seems likely that these eclogitic clasts are also impact products.

The Meteoritical Bulletin Database currently lists NWA 6921 as a CR6 chondrite and suggests that it is paired with several specimens (NWA 2994, 3250, 6901 and 7317); two of these samples (NWA 3250 and 6901) are individually listed as primitive achondrites. These rocks are generally described as having poikiloblastic to porphyroblastic textures and containing some relict chondrules (particularly BO types) and chondrule fragments. These descriptions resemble those of OC impact-melt rocks such as PAT 91501 (Mittlefehldt and Lindstrom, 2001). It thus seems likely that NWA 6921 and its paired specimens are CR-related impact-melt rocks.

The Meteoritical Bulletin Database currently lists NWA 7531 as a CR7 polymict breccia. It is described as a chondrule-free rock with a poikiloblastic texture; it resembles some essentially chondrule-free OC impact-melt rocks such as Y-74160 (Takeda et al., 1984) and is probably a CR-related impact-melt rock, very similar to NWA 6921.

2.10.8. CH chondrites

Dmitryivanovite is a high-pressure polymorph of $CaAl_2O_4$ found in a CAI in the NWA 470 CH3 chondrite (Mikouchi et al., 2009). These authors proposed that $CaAl_2O_4$ condensed in the solar nebula under local conditions that included a high dust/gas ratio and became incorporated into the CAI; after agglomeration, an impact on the CH3 parent asteroid transformed the phase into dmitryivanovite.

2.10.9. CB chondrites

Patches of impact melt occur between the coarser components (chondrule-like objects and metal nodules) in several Bencubbin-like carbonaceous chondrites (CB chondrites) (Newsom and Drake, 1979; Weisberg and Kimura, 2010). Also present within the matrix and chondrule-like fragments of CB Gujba are high-pressure phases (majorite, possibly majorite-$pyrope_{ss}$, wadsleyite and coesite). Weisberg and Kimura (2010) pointed out that the occurrence of a majorite-wadsleyite assemblage suggests pressures of $\gtrsim$19 GPa and temperatures of $\gtrsim$2000 °C were reached during the shock event.

2.10.10. Enstatite chondrites

Shock effects in enstatite chondrites were recently reviewed by Rubin (2015a). References not listed here can be found in that paper.

1. *Progressive deformation of the crystal structures of olivine, low-Ca pyroxene and plagioclase* are reflected in the shock-stage classification of Stöffler et al. (1991) and Rubin et al. (1997). Shock stage ranges from S1 (unshocked) to S6 (very strongly shocked) and orders meteoritic samples by. In unshocked S1 materials, olivine, low-Ca pyroxene and plagioclase have no fractures or irregular fractures and exhibit sharp optical extinction when viewed microscopically in transmitted light using crossed polarizers. With increasing levels of shock, olivine develops undulose extinction, planar fractures and mosaic extinction; low-Ca pyroxene develops undulose extinction, planar fractures, clinoenstatite lamellae on (100) and mosaic extinction; plagioclase develops undulose extinction, becomes partially isotropic, transforms into maskelynite, and undergoes extensive melting.
2. *Brecciation* is evident in several EH (e.g., Abee, Adhi Kot, Parsa) and EL (e.g., Hvittis, Atlanta, Blithfield) chondrites. These samples contain a variety of clast types including impact-melt rocks, some with high sulfide/metal ratios, some with high silica/enstatite ratios and a few with chondritic textures. The mineral phases in all of these clast types (save the chondritic clasts) crystallized from impact melts.
3. *Petrofabrics* are evident in several EH3 (e.g., ALH 81189, Y-691) and EL3 (e.g., PCA 91020, MAC 02635, EET 90992) chondrites and one EL6 chondrite (LEW 87119), reflecting shearing dur-

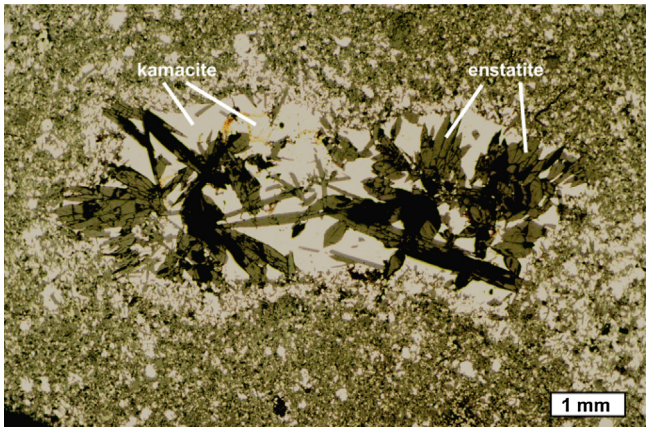

Fig. 12. A 3 × 7-mm nodule rich in low-Ni metallic Fe in the Abee EH impact-melt breccia containing clusters and isolated grains of coarse euhedral enstatite. The clast has a rim, readily visible at the top center and bottom left of the clast, that consists mainly of low-Ni metallic Fe (kamacite) and fine-grained euhedral enstatite. After Rubin and Scott (1997). Reflected light.

ing impact events. In general, no new mineral phases were produced as the rocks developed foliations.

4. *Opaque veins* were formed by impact melting enstatite chondrite materials. Vein types include those rich only in metallic Fe-Ni, those containing metallic Fe-Ni, sulfide and silicate, and a 16-mm-long oldhamite vein in EL6 Jajh deh Kot Lalu.
5. *High-pressure phases* were produced during impacts. In enstatite chondrites, only coesite has been identified (Kimura et al., 2014, 2016). It was found in a shock vein in EH3 Asuka 10164.
6. *Silicate darkening* involves the in situ melting and mobilization of metallic Fe-Ni and troilite, their dispersion through fractures in neighboring silicate grains, and quenching.
7. *Silicate-rich melt veins* (formed by impacts) occur in several enstatite chondrites: EH3 Y-791790 contains a vein similar in composition to the whole rock, reflecting total melting of the host; EH5 RKP A80259 contains veins of feldspathic glass, reflecting preferential melting of phases with low impedances to shock compression; and EH3 Asuka 10164 contains a vein enriched in fine-grained silicate including coesite, reflecting high transient shock pressures.
8. *Silicate-rich melt pockets* in EH5 RKP A80259 are rich in feldspathic glass flanking coarse enstatite grains. The feldspathic glass formed by the impact melting of plagioclase due to its high compressibility during shock loading (Schaal et al., 1979).
9. *Diamonds* that formed from graphite at high shock pressures occur in the Abee EH chondrite impact melt breccia.
10. *Euhedral enstatite grains* in many enstatite chondrites, including Abee (Fig. 12), Adhi Kot and RKP A80259, crystallized from local pyroxene-normative impact melts.
11. *Nucleation of enstatite on relict chondrules* occurred in the cooling impact melt in several enstatite chondrites, most particularly Abee.
12. *Low-MnO enstatite, high-Mn troilite, and high-Mn oldhamite* occur in Abee, Adhi Kot and Saint-Sauveur. Rubin (2008) suggested that when MnO-bearing enstatite was impact-melted under highly reducing conditions, Mn was preferentially partitioned into crystallizing sulfide phases at the expense of crystallizing enstatite. Crystallizing troilite and oldhamite acquired relatively high Mn contents due in part to enrichment of Mn in the melt from the enstatite and by the melting of pre-existing Mn-bearing niningerite.
13. *Keilite* – (Fe,Mn,Mg,Ca,Cr)S occurs only in enstatite chondrites such as Abee, Adhi Kot, Saint-Sauveur and RKP A80259 that appear to have been impact melted (Keil, 2007). Quenching is required for the retention of keilite; if these rocks had cooled slowly or been subsequently annealed, the keilite would have exsolved into troilite and niningerite (Keil, 2007).
14. *Relatively abundant silica* is present in Abee; some Abee clasts contain up to 16 wt.% silica (Rubin and Keil, 1983). In Adhi Kot there are 3–5-mm-size chondrule-free clasts (presumably impact products) that contain up to twice as much silica (18–28 wt. %) as enstatite (12–14 wt.%). (This is in contrast to most enstatite chondrites which contain very little free silica.) As a result of impact melting, reduced Si derived from kamacite may have reacted with FeO from melted enstatite to produce silica and metallic Fe during crystallization; some silica may also have been produced (along with niningerite) by sulfidation of enstatite (Rubin, 1983a; Lehner et al., 2013) during crystallization from the impact melt.
15. *Euhedral graphite* occurs as euhedral lath-like grains with pyramidal terminations in enstatite-chondrite impact-melt breccias (Rubin, 1997d). These grains most likely crystallized from the impact melt; their precursors probably occurred as graphite aggregates within low-Ni metallic Fe (kamacite).
16. *Euhedral sinoite* grains are present in many EL6 chondrites as well as in impact-melted portions of the EL4 chondrites QUE 94368 and Grein 002 (that also contain euhedral grains of enstatite and graphite). As discussed by Rubin (1997e, 2015a), it seems likely that sinoite in EL4 chondrites crystallized from a shock melt. (Nevertheless, it is likely that some sinoite grains in primitive EL3 materials are nebular condensates; Lin et al., 2011.)
17. *Fluor-richterite and fluorphlogopite* – $(Na_2Ca(Mg,Fe)_5Si_8O_{22}F_2$ and $KMg_3(Si_3Al)O_{10}F_2)$ occur in impact-melted enstatite chondrites: Abee contains rare 3.5-mm-long radiating acicular grains of fluor- richterite; Saint-Sauveur contains ~40 × 100-μm-size subhedral grains of fluor- richterite occurs; Y-82189 contains rare subhedral, 10-30-μm-size grains of fluorphlogopite. These two phases probably crystallized from the impact melts – it is plausible that after impact melting, most of the F in Abee, Saint-Sauveur and Y-82189 that had not been driven off during heating was scavenged by the crystallizing grains of fluor- richterite and fluorphlogopite.
18. *Melt globules and spherules* are present in several enstatite chondrite impact melt breccias: Abee contains 0.1-1-mm-diameter globules of low-Ni metallic Fe (kamacite) as well as kamacite-rich nodules up to 11 mm in maximum dimension; Blithfield contains coarse, irregularly shaped nodules of low-Ni metallic Fe; Adhi Kot contains a 110-μm-diameter stoichiometric plagioclase glass spherule that is enriched in K_2O. These objects have been interpreted as having crystallized from the impact melt (see Rubin, 2015a and references therein).
19. *A metal nodule depleted in refractory siderophiles, but not depleted in common or volatile siderophiles* in Abee was reported by Sears et al. (1983). It seems likely that the nodule is analogous to those formed by vaporization and fractional condensation in OC (Widom et al., 1986; Rubin 1995b; 1999). However, the Abee nodule formed under more-reduced conditions that did not allow W to form volatile oxides and separate from the rest of the vaporized metal (Rubin and Scott, 1997).
20. *A vesicular impact-melt rock* known as Al Haggounia 001 was described by Rubin (2016). The sample is an incompletely melted, EL-chondrite impact melt rock with a mass of ~3 metric tons that fell ~23,000 years ago. The meteorite exhibits numerous shock effects including (1) development of undulose to weak mosaic extinction in low-Ca pyroxene, (2) dispersion of metal-sulfide blebs within silicates causing "darkening", (3) incomplete impact melting wherein some relict chondrules survived, (4) vaporization of troilite, resulting in S_2 bubbles that

infused the melt, (5) formation of immiscible silicate and metal-sulfide melts, (6) shock-induced transportation of the metal-sulfide melt to distances >10 cm, (7) partial resorption of relict chondrules and coarse silicate grains by the surrounding silicate melt, (8) crystallization of enstatite in the matrix and as overgrowths on relict silicate grains and relict chondrules, (9) crystallization of plagioclase from the melt, and (10) quenching of the vesicular silicate melt.

During cooling of enstatite chondrites that were impact melted, daubréelite exsolved from troilite (e.g., in EL Blithfield; Rubin, 1984b) and thin pearlitic lamellae of cohenite exsolved from low-Ni metallic Fe (e.g., in EH Abee; Herndon and Rudee, 1978).

2.10.11. Enstatite-rich impact-melt rocks

Table 3 of Rubin (2015a) lists various enstatite-rich impact-melt rocks of EH (e.g., QUE 94204; Y-82189; Y-8414), EL (e.g., Ilafegh (009); MIL 090807; NWA 6258) and ungrouped (e.g., NWA 4301; Zaklodzie) parentage. These rocks typically contain grains of plagioclase, enstatite, and sulfide that crystallized from the impact melt.

2.10.12. Aubrites

As discussed in Rubin (2015a,b), Keil (1989, 2010) and references therein, approximately half of the aubrites are monomict fragmental breccias, most of which are moderately shocked (shock-stage S4). The commonality of brecciation among aubrites and their moderate degree of shock indicate an extensive collisional history.

Several aubrites (e.g., LAP 03719, Bishopville, Khor Temiki, ALH 83015) contain orthopyroxene grains that exhibit more-pronounced shock effects than associated olivine grains, suggesting that these rocks were shocked and buried within warm ejecta blankets or beneath fallback debris under the crater floor (Rubin, 2015b). Entombed olivine crystal lattices healed (and became unstrained, reaching shock-stage S1), but orthopyroxene lattices retained their S4-level shock-damaged features.

Three aubrites have experienced at least minor amounts of impact melting. Norton County has an impact-comminuted matrix and a few clasts that appear to be impact melt breccias (Okada et al., 1988). Cumberland Falls is a polymict breccia that contains OC clasts as well as a few clasts that are impact-melt breccias containing shocked OC material (Rubin, 2010b). These clasts may all be part of an OC projectile that impacted the aubrite parent asteroid. Mayo Belwa is an impact-melt breccia; its enstatite grains are surrounded by a melt matrix composed of 3-15-μm-size euhedral and subhedral enstatite grains embedded in sodic plagioclase; numerous vugs are present in the melt matrix. Fluor- richterite occurs as bundles of acicular grains in vugs (Bevan et al., 1977; Graham et al., 1977). Also present in some vugs are bundles of 4-10-μm-thick laths of sodic plagioclase (Rubin, 2010b).

Keil et al. (1989) suggested that the unbrecciated aubrite Shallowater underwent a complex multi-stage history involving disruption of its progenitor (molten, enstatite-rich) asteroid, followed by rapid cooling and gravitational reassembly of that body, and annealing, excavation and quenching of the Shallowater material. They concluded that Shallowater formed on a different asteroid than most aubrites. Rubin (2015a) later modeled Shallowater as having formed by (1) impact-melting of enstatite-chondrite material and concomitant partial loss of a metal-sulfide melt, (2) admixing of cold xenoliths (causing rapid cooling of the assemblage from high temperatures), (3) burial beneath warm ejecta with low thermal diffusivity (causing annealing), and (4) subsequent collisional excavation (causing rapid cooling to low temperatures).

2.10.13. Howardite-Eucrite-Diogenite samples (HEDs)

The O-isotopic compositions of these igneous rocks are similar, indicative of a genetic relationship. Most workers believe these samples come from 4 Vesta – the second largest asteroid (e.g., Consolmagno and Drake, 1977; Burbine et al., 2001; Russell et al., 2012). As discussed by Hutchison (2004), most eucrites are monomict breccias, consisting of clasts of a single, basaltic lithology; a few eucrites are polymict breccias, containing mineralogically diverse eucritic clasts and relatively few (or no) diogenitic clasts. Many diogenites are monomict breccias, consisting of clasts with major orthopyroxene and minor to accessory plagioclase. Howardites are polymict regolith breccias containing both eucritic and diogenitic materials. Some polymict eucrites, diogenites and howardites also contain exogenous carbonaceous-chondrite clasts, mainly with CM2, CR2 and thermally processed CI lithologies (e.g., Zolensky et al., 1992, 1996; Buchanan et al., 1993; Gounelle et al., 2003). The brecciated nature of most HEDs indicates that these rocks were pummeled by projectiles. It is to be expected that shock metamorphism would have caused the production of mineral phases in these rocks.

About 5% of eucrites contain maskelynite, the diaplectic glass formed on the parent body from crystalline plagioclase at shock pressures $\gtrsim$20 GPa (Rubin, 2015d). One of the most shocked eucrites is Padvarninkai; it is unusual in containing maskelynite in the unbrecciated host of the rock (Yamaguchi et al., 1993).

Glassy and crystalline impact-melt-breccia clasts constitute 30 ± 10% of the lithic clasts in howardites (Fuhrman and Papike, 1981) and a few percent of those in polymict eucrites (Metzler, 1985). Lunning et al. (2016) reported a CM-chondrite impact-melted clast in the GRO 95574 howardite. Pseudotachylite-like glassy shock-melt veins occur in some eucrites (e.g., Bischoff and Stöffler, 1992). The veins in Cachari are vesicular and vary from pure glass to partly crystalline (Bogard et al., 1985). The latter veins contain pyroxene grains that crystallized from the melt; these are surrounded by feldspathic glass. Small clasts of chromite and blebs of metallic Fe-Ni also crystallized from the shock melt. Takeda and Mori (1985) described a few brecciated diogenites (Y-75032, Y-791199, Y- 791200) with shock-melted matrices containing mineral fragments.

Also present in howardites are chondrule- like impact-melt spherules (e.g., Brownlee and Rajan, 1973; Olsen et al., 1990), similar to those from the Moon (e.g., Chao et al., 1972; Warner, 1972; King et al., 1972a; King et al., 1972b; Symes et al., 1998). Some of the spherules in the Kapoeta howardite have submicrometer-diameter micrometeorite impact craters at their surfaces (Brownlee and Rajan, 1973).

2.10.14. Ureilites

Ureilites are brecciated rocks; both monomict and polymict varieties occur. The heavily shocked samples contain mosaicized olivine grains. The myriad shock effects in ureilites include some in which mineral phases were formed (e.g., Rubin, 1988, 2006): (1) silicate darkening (which involved melting of metallic Fe-Ni and accessory sulfide and crystallization of small blebs of these phases within curvilinear trails in coarse olivine grains), (2) the presence of the C polymorphs diamond, lonsdaleite and chaoite (Lipschutz, 1964; Vdovykin, 1972) (which formed from indigenous graphite at high shock pressures), (3) the common occurrence of fine-grained interstitial silicates consisting of low-Ca pyroxene, augite and Si-Al-alkali-rich glass (Goodrich, 1992) (which appear to be plagiophile-rich shock products injected into the rocks; Rubin, 2006), (4) the presence of the silicide suessite – Fe_3Si (which probably formed by shock-heating of low-Ni metallic Fe and silicate; Keil et al., 1982), (5) the occurrence of Ca-, Al- and alkali-rich shock melts located at olivine grain boundaries in LEW 86216 and ALH 81101 (Saito and Takeda, 1990), (6) the presence of orthopyrox-

ene in MET 78008 (Goodrich, 1992), which probably formed from pigeonite during impact-induced annealing (Rubin, 2006) and (7) the occurrence of chondrule-like crystalline spherules (which are probably impact-melt droplets). Some of the diverse inclusions in ureilites (e.g., enstatite-granular olivine clasts, basaltic clasts, feldspathic melt rocks) could also have been produced during impact melting. If ureilites are impact-melt products as Rubin (1988, 2006) suggested, then the principal phases – olivine, low-Ca pyroxene (mainly pigeonite), euhedral graphite and metallic Fe-Ni – crystallized from the shock-generated melt.

In three ureilites (LAR 04315, LAP 03587, Almahata Sitta) pyroxene was reduced (and in some cases melted) by impact- induced smelting, resulting in porous grains with small blebs of metallic Fe-Ni, silica and felsic glass (Warren and Rubin, 2010).

2.10.15. Acapulcoites and lodranites

Many workers consider acapulcoites and lodranites (which have been dubbed "primitive achondrites") to have formed by incomplete melting of chondritic material (e.g., Palme et al., 1981; Nagahara, 1992; Zipfel et al., 1995; McCoy et al., 1996, 1997; Mittlefehldt et al., 1996; Patzer et al., 2004). If this view is correct then the mineral phases in these rocks may be (a) relict chondritic grains, (b) igneous grains that crystallized from a relatively large-scale melt, (c) phases that exsolved during cooling from igneous temperatures, or (d) grains formed during annealing.

Some workers have taken a different view (Kallemeyn and Wasson, 1985; Rubin, 2007). Rubin modeled acapulcoites and lodranites as having formed by shock-melting CR-carbonaceous-chondrite-like precursors. If this view is correct, then some of the phases crystallized from impact melts. In acapulcoites, such phases would include metallic Fe-Ni and troilite within opaque veins, fine-grained rapidly cooled assemblages, and in assemblages consisting of small irregular troilite grains within metallic Fe-Ni (some of which also contain metallic Cu). Lodranites were modeled as having formed in a similar manner to acapulcoites, but experienced more extensive heating, loss of plagioclase and loss of an Fe-Ni-S melt. Orthopyroxene in acapulcoites and lodranites could have formed from low-Ca clinopyroxene (produced during impact melting and quenching) when the rocks were annealed to temperatures $\geq$630 °C (Boyd and England, 1965; Grover, 1972).

2.10.16. Mesosiderites

Rubin and Mittlefehldt (1993) compiled available data on mesosiderite mineralogy, petrology, geochemistry and chronology and proposed a six-stage petrogenetic history: (1) accretion of the parent asteroid 4.56 Ga ago, (2) initial melting ~4.56 Ga ago, (3) crustal remelting of the body $\geq$4.47 Ga ago, (4) localized impact melting 4.5–3.9 Ga ago, (5) collisional disruption and gravitational reassembly ~3.9 Ga ago, and (6) impact excavation and ejection of buried breccias «3.9 Ga ago. Minerals produced in Stage 2 formed by igneous processes; those formed during stages 3 and 4 involved shock metamorphism. There is no petrographic evidence for mineral species being formed during Stages 5 and 6.

Mesosiderites contain large clasts, 39% of which are coarse-grained gabbros that are highly depleted in incompatible elements relative to chondrites (Rubin and Mittlefehldt, 1992). These clasts have the most extreme positive Eu anomalies known among Solar-System rocks (Rubin and Mittlefehldt, 1992; Mittlefehldt et al., 1992). It seems likely that these abundant clasts formed during a crustal remelting event (Stage 3), plausibly caused by the impact of an iron-core projectile (with some adhering silicate mantle) from a disrupted differentiated asteroid (Mittlefehldt et al., 1992; Rubin and Mittlefehldt, 1993). The phases in the gabbro clasts (major pyroxene, plagioclase and silica, and minor-to-accessory troilite, metallic Fe-Ni, ilmenite, merrillite and chromite) thus appear to be impact-melt products.

The most significant effect of impact melting during Stage 4 is the creation of the four basic mesosiderite petrologic types, classified by the degree of recrystallization of their fine-grained silicate matrices. The Type-3/4 and Type-4 rocks are impact-melt breccias with igneous matrices (Powell, 1971; Floran, 1978; Floran et al., 1978a; Hewins, 1984). Impact melting at this time produced spheroidal nodules of metallic Fe-Ni and troilite in Bondoc and Estherville that range up to 10 cm in diameter (e.g., Wilson, 1972). Many mesosiderites contain pebble-size clasts with quench textures that also formed by impact melting basaltic material during Stage 4; their mineralogy is the same as that in the gabbro clasts. Annealing associated with these impact events is probably responsible for the orthopyroxene-chromite-merrillite coronas on millimeter-size olivine grains in the Emery and Morristown mesosiderites (Delaney et al., 1981; Ruzicka et al., 1994); the coronas formed by the reaction of olivine with silica in the matrix (e.g., Powell, 1971; Floran, 1978; Nehru et al., 1980).

Much of the metallic Fe-Ni in relatively unshocked Type-I mesosiderites (e.g., Crab Orchard, Vaca Muerta) occurs as small grains, homogeneously distributed among the silicates. It seems likely that the large metallic clasts (up to 3 cm in diameter; Powell, 1969) in some Type-1 mesosiderites (e.g., those in Barea) are shock products. They probably formed by impact melting of fine-grained mesosiderite material and segregation of the molten metal. These metallic clasts somewhat resemble the large metal nodules in ordinary chondrites, which are also shock products (e.g., Widom et al., 1986; Rubin, 1999).

2.10.17. Irons

Many iron meteorites have experienced shock metamorphism, typically involving the production of Neumann bands in low-Ni metallic Fe (kamacite), recrystallization of low-Ni metallic Fe, mosaicism and twinning of troilite, shock-melting and quenching of metallic Fe-Ni and sulfide (and in some cases daubréelite, cohenite and schreibersite), development of martensite and/or plessite from taenite during cooling, and the development of the ε structure (a high-density hexagonal close-packed structure) from low-Ni metallic Fe at ~13 GPa (and reversion to the α structure upon pressure release) (e.g., Buchwald, 1975). In rare cases (e.g., Canyon Diablo and ALH A77283), high shock pressure transformed graphite into diamond (e.g., Clarke et al., 1981). For illustrative purposes, we discuss shock-induced formation of mineral phases in iron meteorites from the IAB Complex, Group IIE, Group IIIE, IIIAB Haig, IVA Social Circle, and the ungrouped irons Guin, Sombrerete, Tucson and Willamette.

2.10.18. IAB Complex and winonaites

Wasson and Kallemeyn (2002) reevaluated analytical data on IAB and related iron meteorites and defined a IAB Complex in which these meteorites occupy six distinct clusters on element-Au diagrams. In contrast to magmatic iron-meteorite groups (i.e., IIAB, IIIAB, IVA) that formed by fractional crystallization in slowly cooling, well mixed magmas, the IAB Complex is designated non-magmatic; these samples likely formed from impact-generated melts of chondritic material (e.g., Wasson et al., 1980; Choi et al., 1995; Wasson and Kallemeyn, 2002). Nevertheless, this view is not universally accepted (cf. Kelly and Larimer, 1977; Kracher, 1982, 1985; McCoy et al., 1993).

Most silicate inclusions in IAB irons have basic chondritic mineralogy and bulk chemical composition (e.g., Ruzicka, 2014). The major mineral phases are olivine, low-Ca pyroxene, plagioclase, Ca-pyroxene, troilite, graphite, phosphates, metallic Fe-Ni; minor phases include daubréelite and chromite (Mittlefehldt et al., 1998). These phases were probably inherited from chondritic precursors; they probably either crystallized from the shock melt (along with

the surrounding metallic Fe-Ni) or underwent extensive metamorphic recrystallization.

Some of the sulfide nodules in IAB irons contain graphite. It is likely that both the graphite and troilite crystallized from the residual S- and C-rich shock melt.

Winonaites are stony meteorites that were probably derived from the same parent body as the IAB irons – their silicates have similar mineralogy and near-identical bulk O-isotopic compositions (McCoy et al., 1993; Yugami et al., 1997; Benedix et al., 1998; Clayton and Mayeda, 1996). Whatever process produced the IAB silicate inclusions (presumed here to be shock related), also produced the winonaites. Most workers (e.g., Bild, 1977; Bevan and Grady, 1988; Benedix et al., 1998; Benedix et al., 2000; Choi et al., 1995) have concluded that both sets of objects were derived from the same parent body. In fact, winonaites might be large IAB silicate inclusions dislodged from their metallic hosts – Winona (24 kg) was recovered from the same Arizona county as IAB Canyon Diablo (30 MT); the winonaite Mount Morris (Wisconsin) (676 g) was recovered from the same Wisconsin county as IAB Pine River (3.6 kg) (Grady, 2000).

Some workers have considered winonaites and IAB silicate inclusions to be "primitive achondrites." However, several features of winonaites suggest that, instead of having formed in a partially differentiated asteroid, these rocks formed by incomplete impact melting. Such features include (1) chondritic proportions of metallic Fe-Ni, sulfide and silicate (Table 3 of Benedix et al., 1998), (2) the chondritic bulk compositions of many samples (Hidaka et al., 2012; Hunt et al., 2012), (3) a component containing planetary-type rare gases (e.g., Benedix et al., 1998), (4) several winonaites (Pontlyfni; Mount Morris (Wisconsin); NWA 1463; Y 74063) containing relict chondrules (Benedix et al., 1998, 2003; Patzer et al., 2004; Yanai and Kojima, 1991) and (5) the preservation of relict shock features including metallic Cu, chromite veinlets, chromite-plagioclase assemblages, and curvilinear metal veins. The variable Ar-Ar and Hf-W ages of winonaites (Vogel and Renne, 2008; Schultz et al., 2010) seem most consistent with discrete impact-heating events. IAB silicate inclusions also have chondritic mineralogy, chondritic bulk compositions and contain planetary-type rare gases (e.g., Bunch et al., 1970; Bild, 1977; Choi et al., 1995).

It is difficult to reconcile the thermal histories of winonaites and IAB irons with an internal heating model as favored by many workers (e.g., Kracher, 1985; Benedix et al., 2000; Takeda et al., 2000). For example, Benedix et al. (1998) invoked "extensive heating" that caused metamorphism and partial melting, followed by "impact brecciation during cooling," followed by a second episode of "metamorphism (that) produced recrystallization, grain growth, and reduction of mafic silicates." However, this hypothesis seems untenable because models invoking the decay of short-lived radionuclides cannot readily accommodate two separate episodes of heating. Prolonged heating would also be expected to drive off planetary gases.

A couple of IAB irons (Caddo County and Ocotillo) have non-chondritic (basaltic and troctolitic) silicate inclusions. The origin of these chemically evolved inclusions is unclear, but it seems plausible that they were produced from larger scale impact-generated magmas.

2.10.19. IIE

Although Netschaëvo contains recrystallized chondrule-bearing chondritic inclusions (e.g., Olsen and Jarosewich, 1971), many IIE silicate inclusions are not chondritic in composition; they are enriched in plagiophile elements (Si, Al, Na, K) (e.g., Bunch and Olsen, 1968; Olsen and Jarosewich, 1970). Although there are numerous phases that occur in one or more inclusions (orthopyroxene, clinopyroxene, olivine, albite with K-feldspar exsolution lamellae (antiperthite), sanidine ($KAlSi_3O_8$), yagiite – $(K,Na)_2(Mg,Al)_5(Si,Al)_{12}O_{30}$, silico-feldspathic glass, tridymite, phosphate), plagioclase and feldspathic glass are dominant in many of the inclusions (Mittlefehldt et al., 1998).

The inclusions appear to have been shock melted (Bunch et al., 1970; Scott and Wasson, 1976). Many inclusions are globular, consistent with their shapes having been molded by surface tension. Plagioclase has a low impedance to shock compression and is readily compressible (Schaal et al., 1979); during shock heating, plagioclase is preferentially melted relative to mafic silicates. Ruzicka et al. (1999) identified glass-rich inclusions in IIE Weekeroo Station that formed by remelting pre-existing plagioclase and orthopyroxene, presumably as the result of collisions. As pointed out by Rubin et al. (1986), IIE inclusions have similar bulk compositions to melt- pocket glasses in ordinary chondrites that were impact melted in situ (Dodd and Jarosewich, 1979, 1982). It thus seems likely that the alkali-rich IIE silicate inclusions also formed by the preferential shock melting of pre-existing broadly chondritic inclusions such as those present in some IAB irons. In addition to the shock-melting of silicates, the opaque phases were affected by impact heating. For example, Bevan et al. (1979) described metal-phosphide globules with dendritic textures in Verkhne Dnieprovsk.

2.10.20. IIIE

A comprehensive study of impact effects in Group IIIE irons was completed by Breen et al. (2016). Members of this C-rich magmatic group can be ordered into four categories based on their degree of shock. Then weakly shocked samples in Category 1 (Armanty, Colonia Obrera, Coopertown, Porto Alegre, Rhine Villa, Staunton, Tanokami Mountain) contain haxonite within plessite, unrecrystallized low-Ni metallic Fe (kamacite) grains with Neumann bands or possessing the ε structure, and sulfide inclusions consisting of polycrystalline troilite with daubréelite exsolution lamellae. Mineral transformations begin in the sole moderately shocked Category 2 sample (NWA 4704) wherein the haxonite is partially decomposed to graphite and the sulfide inclusions are partly melted. In the strongly shocked samples of Category 3 (Cachiyuyal, Kokstad, Paloduro) haxonite has fully decomposed to graphite, troilite has melted and quenched and the low-Ni metallic Fe has been extensively recrystallized. In the severely shocked samples of Category 4 (Aliskerovo, Willow Creek), haxonite has fully decomposed to graphite. These meteorites contain sulfide assemblages that have been crushed; the troilite within these assemblages has largely vaporized, residual troilite has crystallized as spidery filaments (e.g., Fig. 13), and low-Ni, high-Co taenite grains crystallized from the melt and transformed into low-Ni metallic Fe at sub-solvus temperatures. Breen et al. invoked one or more major collisions as being responsible for these effects.

2.10.21. Haig (IIIAB)

Haig, a member of the magmatic IIIAB group, has a spectacular regmaglypt pattern (Plate 10 of McCall, 1973). Bevan et al. (1981) reported a small troilite- daubréelite-cohenite nodule that was sheared by an impact in Haig. Finely dendritic globular masses consisting of troilite, metallic Fe-Ni, daubréelite and cohenite associated with the nodule formed by impact melting and very rapid quenching.

2.10.22. Social Circle (IVA)

As discussed in Isa et al. (2016), a late-stage shock event caused wide-spread heating of Social Circle, recrystallizing the low-Ni metallic Fe (kamacite), partially obliterating previously formed Neumann lines, partly decomposing taenite and plessite fields, and forming troilite-metal eutectic shock melts. These workers suggested that impact melting of the sulfide assemblages (possibly involving Mn-bearing daubréelite, $FeCr_2S_4$) could have increased the Mn concentration in portions of the S-rich melts, leading to

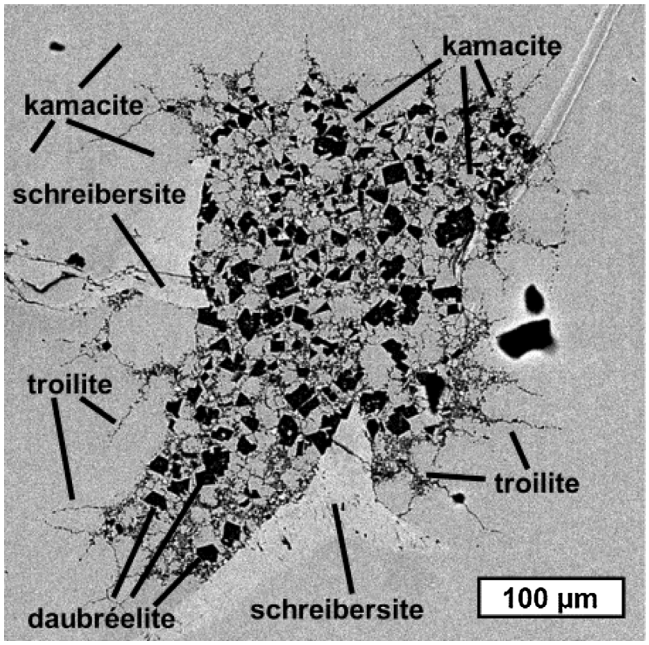

Fig. 13. Sulfide-rich inclusion in the severely shocked Aliskerovo IIIE iron. The inclusion consists of euhedral, subhedral and fragmental grains of daubréelite (black), semi-equant grains of low-Ni metallic Fe (medium gray), rare tiny grains of tetrataenite (white specks) and spidery, filamentary troilite (dark gray), partially surrounded by schreibersite (light gray). The metallic host is composed mainly of low-Ni metallic Fe (kamacite). BSE image.

crystallization of the rare (and newly described) phase joegoldsteinite ($MnCr_2S_4$). The shock event that affected Social Circle is unrelated to the major impact-melting event inferred to have formed the IVA magma initially from pre-existing L-LL- chondritic materials (Wasson et al., 2006).

2.10.23. Guin

Rubin et al. (1986) described the Guin ungrouped iron as a coarse octahedrite containing an unusually high bulk Ni content (92.5 mg/g). The meteorite contains ~6 vol.% silicate inclusions petrologically and compositionally similar to those in many IIE irons. The largest inclusion (2 × 4 cm) is an ovoid mass consisting mainly of a shock-melted-and-quenched fine-grained plagioclase matrix surrounding coarse partly melted augite grains. The bulk chemical composition of this inclusion is similar to that of some melt pocket glasses in OC (Dodd and Jarosewich, 1982) that were produced by the in situ preferential shock-melting of plagioclase. Shock veins within the inclusion consist of fine-grained-to-glassy silicate mesostasis containing small blebs of troilite.

2.10.24. Sombrerete

This ungrouped iron (Malvin et al., 1984) contains ~7 vol.% silicate inclusions similar to those in the Weekeroo Station and Miles IIE irons (Prinz et al., 1982). The Sombrerete inclusions consist primarily of sodic-plagioclase glass containing acicular chlorapatite and orthopyroxene; also present are accessory kaersutite, tridymite, chromite, ilmenite and rutile. These phases formed by impact melting and quenching a pre-existing silicate-rich assemblage.

2.10.25. Tucson

The metal phase of this ungrouped iron is very reduced; it contains 0.8 wt.% Si (Nehru et al., 1982a; Nehru et al., 1982b). Troilite, daubréelite, chromite, graphite and carbides appear to be absent. The meteorite contains ~8 vol.% millimeter- and submillimeter-size elongated silicate inclusions arrayed in curvy subparallel rows (Buchwald, 1975); the inclusions consist of major forsterite and enstatite, minor Al-rich diopside and calcic plagioclase (or plagioclase-composition glass) and accessory spinel and brezinaite (Cr_3S_4). They appear to have formed by impact melting and quenching of pre-existing silicate inclusions and impact-induced shearing of the host. The presence of brezinaite rather than troilite was ascribed by Buchwald (1975) to the relatively high concentration of Cr in solid solution in the metal. Nehru et al. suggested that the silicate was derived from the projectile, but survival of such material after a major impact is unlikely; it is more plausible that all these phases were derived from the target.

2.10.26. Willamette

Although Willamette was previously designated IIIAB (Scott et al., 1973), new data show it is compositionally anomalous and should be considered an ungrouped iron (Rubin et al., 2015b). Shock effects in Willamette were described by Rubin et al. (2015b). Willamette contains elongated troilite nodules that were crushed and penetrated by wedges of crushed metal during a collisional event. The troilite nodules formed during initial crystallization of the iron core magma from trapped melt. A major impact caused melting of metal-sulfide assemblages to form lobate taenite masses. Ensuing mechanical damage included impact crushing of the nodules, the jamming of metal wedges into the nodules, and the crushing of metal grains adjacent to sulfide throughout the meteorite. This was followed by post-shock annealing and late-stage shock production of Neumann bands in low-Ni metallic Fe.

2.10.27. Lunar meteorites

Shock effects in lunar meteorites were reviewed by Bischoff and Stöffler (1992) . Phases formed by shock processes include chondrule-like glassy-to- microcrystalline spherules, agglutinate glasses, irregularly shaped glassy clumps, maskelynite formed at high shock pressure from crystalline plagioclase (probably during launch off the Moon; Rubin, 2015d), and polysynthetically twinned low-Ca clinopyroxene formed from orthopyroxene.

As discussed by Taylor et al. (1991), lunar crystalline melt breccias formed as impact melts that acquired cold clastic debris (older igneously formed mineral grains and rocks) and cooled quickly. During cooling, fine-grained minerals (mainly plagioclase and Ca-pyroxene) crystallized to form the groundmass. Minor phases include low-Ca pyroxene, olivine, silica, ilmenite, spinel, ulvöspinel (Fe_2TiO_4), metallic Fe-Ni, troilite, phosphate and glass. Clast-poor melt breccias crystallized from impact-generated silicate liquids that had been heated above the liquidus (~1200–1300 °C) (Taylor et al., 1991). The major minerals in these breccias that crystallized from the shock melt are plagioclase and Ca- pyroxene; minor phases include low-Ca pyroxene, olivine, silica, ilmenite, spinel, ulvöspinel, metallic Fe-Ni, troilite, phosphate and glass; accessory phases include schreibersite, armalcolite ((Mg,Fe) Ti_2O_5), tranquillitite ($Fe^{+2}{}_8Ti_3Zr_2Si_3O_{24}$), K-Ba feldspar and akaganéite. The occurrence of these phases in Apollo samples suggests that they are also probably present in lunar meteorites.

2.10.28. Martian meteorites

Shock effects in martian meteorites are confined largely to shergottites (as reviewed by Stöffler et al., 1986; Bischoff and Stöffler, 1992; and McSween and Treiman, 1998). The principal phase produced by shock metamorphism is maskelynite, generated during launch off Mars (e.g., Rubin, 2015d). Rubin found that ~93% of martian basaltic meteorites contain maskelynite; among the five individual shergottites in his compilation that lacked maskelynite, four of them instead have vesicular plagioclase glass, produced at shock pressures *higher* than that required to form maskelynite (i.e., >45 GPa; Stöffler et al., 1986). The fifth maskelynite-free shergottite in Rubin's compilation is NWA 7034 and its paired specimens,

dubbed "Black Beauty" by collectors. This rock is a monomict brecciated porphyritic basalt, probably a volcanic breccia that contains crystalline plagioclase (Agee et al., 2013). Rubin (2015d) suggested that this sample experienced relatively low shock pressure (<29 GPa) during launch off Mars, perhaps as the result of a rare oblique impact. [Shock pressures decrease with decreasing impact angle (e.g., Pierazzo and Melosh, 2000).]

Shock melts in EET A79001 consist of vesicular glass containing relict grains as well as skeletal olivine and pyroxene grains that crystallized from the melt (McSween and Treiman, 1998). Some lherzolitic shergottites (e.g., ALH A77005) contain melt pockets consisting of impact- produced glass with small skeletal olivine crystals and dendritic or clustered chromite grains (McSween and Treiman, 1998).

Basu Sarbadhikari et al. (2016) described P-rich recrystallization rims on olivine grains in the Tissint shergottite that formed during impact melting and deformation of host materials.

High-pressure minerals identified in Tissint include ahrensite (the high-pressure polymorph of ferroan olivine; Ma et al., 2016c; Fig. 14), ringwoodite (the high-pressure polymorph of magnesian olivine), bridgmanite ($MgSiO_3$-perovskite) (Fig. 14), wüstite – FeO, tissintite – (Ca,Na,□) $AlSi_2O_6$, and xieite – $FeCr_2O_4$ (Ma et al., 2015b; Ma et al., 2016c). Tissintite is a new shock-induced clinopyroxene with a plagioclase composition (Fig. 15); it is the most vacancy-rich pyroxene known (Ma et al., 2015b). Three high-pressure polymorphs of silica are present in many shergottites: stishovite (tetragonal), seifertite (orthorhombic) and an unnamed monoclinic phase with the β-ZrO_2-type structure (El Goresy et al., 2013). Ringwoodite (the high-pressure polymorph of magnesian olivine) occurs in Dar al Gani 670. Zagami contains black shock veins with a high-pressure assemblage consisting of omphacite, a new (Na,Ca)- hexaluminosilicate phase (Beck et al., 2004), stishovite and liebermannite ($KAlSi_3O_8$- hollandite) surrounded by silicate glass (Langenhorst and Poirier, 2000; Ma et al., 2015c). Steele and Smith (1982) tentatively identified ringwoodite and majorite (the high-pressure polymorph of orthopyroxene) inside shock veins in EET A79001.

2.11. Condensation within impact plumes

The Bencubbin-like carbonaceous chondrites (CB chondrites) have been divided into two groups: CB_a chondrites such as Bencubbin, Gujba and Weatherford contain 40–60 vol.% metal and have barred olivine (BO) and cryptocrystalline (C) chondrule-like spherules and large metallic-Fe-Ni-rich globules (and deformed globules); CB_b chondrites such as Hammadah al Hamra 237 and QUE 94411 contain ~70 vol.% metal, smaller BO and C chondrules and a few CAIs (Weisberg et al., 1990; Krot et al., 2002).

Rubin et al. (2003) found that the large metal globules in Gujba exhibit metal- troilite quench textures and vary in their modal abundances of troilite and concentrations of volatile siderophile elements. Campbell et al. (2002) analyzed metal nodules in Gujba, Bencubbin and Weatherford and found that the less-refractory siderophile elements were fractionated from refractory siderophiles. Rubin et al. (2003) modeled the metal globules as having formed as liquid droplets either via condensation in an impact-generated vapor plume on an asteroid or by evaporation of pre-existing metal particles in such a plume. They also suggested that the large silicate chondrule-like objects formed in the plume at high temperatures, leading to a significant loss in volatile elements. Campbell et al. (2002) proposed that a large impact event involving a metal-rich body generated a high-density metal-enriched gas from which the CB metal nodules condensed.

Krot et al. (2005) reported ^{207}Pb- ^{206}Pb ages of the chondrule-like objects in Gujba and Hammadah al Hamra 237; all the measured objects have the same, relatively young age of ~4563 Ma, inconsistent with formation in the solar nebula. They pointed out that these ages are similar to those of the ^{182}Hf–^{182}W ages of the fractionation between metal and silicates recorded by metal condensates in CB_a and CB_b chondrites (Kleine et al., 2005). However, Weisberg and Kimura (2010) cautioned that CB chondrites may have been shocked to ~19 GPa and experienced shock temperatures of ~2000 °C; this may have reset the chondrule ages due to Pb loss.

Krot et al. (2005) concluded that the chondrule-like objects and the metallic Fe-Ni grains in CB meteorites formed in a vapor-melt plume created by a giant impact event involving planetary embryos. Similar scenarios were offered by Kallemeyn et al. (1978), Campbell et al. (2002) and Rubin et al. (2003). If these scenarios are correct, then the principal minerals in these rocks – low-Ni metallic Fe, troilite, olivine, low-Ca pyroxene – formed by condensation in a vapor plume.

2.12. Crystallization from melts in differentiated or partially differentiated bodies

The minerals in asteroidal achondrites (HED samples, angrites, aubrites), magmatic iron meteorites, most martian meteorites and large portions of lunar meteorites crystallized from magmas inside differentiated bodies. Many workers maintain that acapulcoites, lodranites, brachinites and ureilites formed in partially differentiated bodies and should not be considered shock products (cf. Section 2.10).

2.12.1. Eucrites

Eucrites typically contain major orthopyroxene or pigeonite and calcic plagioclase and minor to accessory silica, chromite, phosphate, ilmenite, low-Ni metallic Fe and troilite. Olivine is rare. Most eucrites are monomict breccias; most of the clasts that compose them have ophitic, subophitic, variolitic or intersertal textures, consistent with igneous crystallization. Plagioclase crystals tend to be normally zoned wit calcic cores and more sodic rims. Pyroxene exhibits a variety of compositions and textures. Temperatures of the parent basaltic melt probably exceeded 1100 °C (Stolper, 1977).

When eucrites are plotted on a diagram of bulk Ti vs. bulk Mg/(Mg + Fe) ratio (e.g., Fig. 1.2.8.7 of BVSP, 1981; Fig. 1 of Warren and Jerde, 1987), two compositional trends are evident – the Neuvo Laredo Trend (rocks such as Nuevo Laredo and Lakangaon that underwent fractional crystallization, most likely as partial cumulates) and the Stannern Trend (rocks such as Stannern and Bouvante that formed by partial melting) (Warren and Jerde, 1987). The main-group eucrites probably belong to the Neuvo Laredo Trend. Cumulate eucrites are coarse-grained gabbros; their crystals grew slowly and settled to the bottom of a magma chamber on the eucrite parent body. They do not plot along the trends of the non- cumulate eucrites.

2.12.2. Diogenites

The diogenites are coarse-grained rocks consisting mainly of orthopyroxene; minor phases include olivine, chromite, Ca- pyroxene, plagioclase, silica, low-Ni metallic Fe and troilite. Phosphates are rare. Most diogenites are monomict breccias; some appear unbrecciated. These rocks crystallized from a Ca-poor, pyroxene-normative melt, leading to a more- feldspathic (more-basaltic) residual liquid that gave rise to the eucrites.

2.12.3. Howardites

Howardites are polymict breccias that are mechanical mixtures mainly of eucritic (cumulate and non-cumulate) and diogenitic materials (e.g., Duke and Silver, 1967). The minerals in the howardites formed in the same way as those in eucrites and diogenites. In addition to these components, some diogenites contain melt rocks and glass particles formed by impact-melting of eucritic and

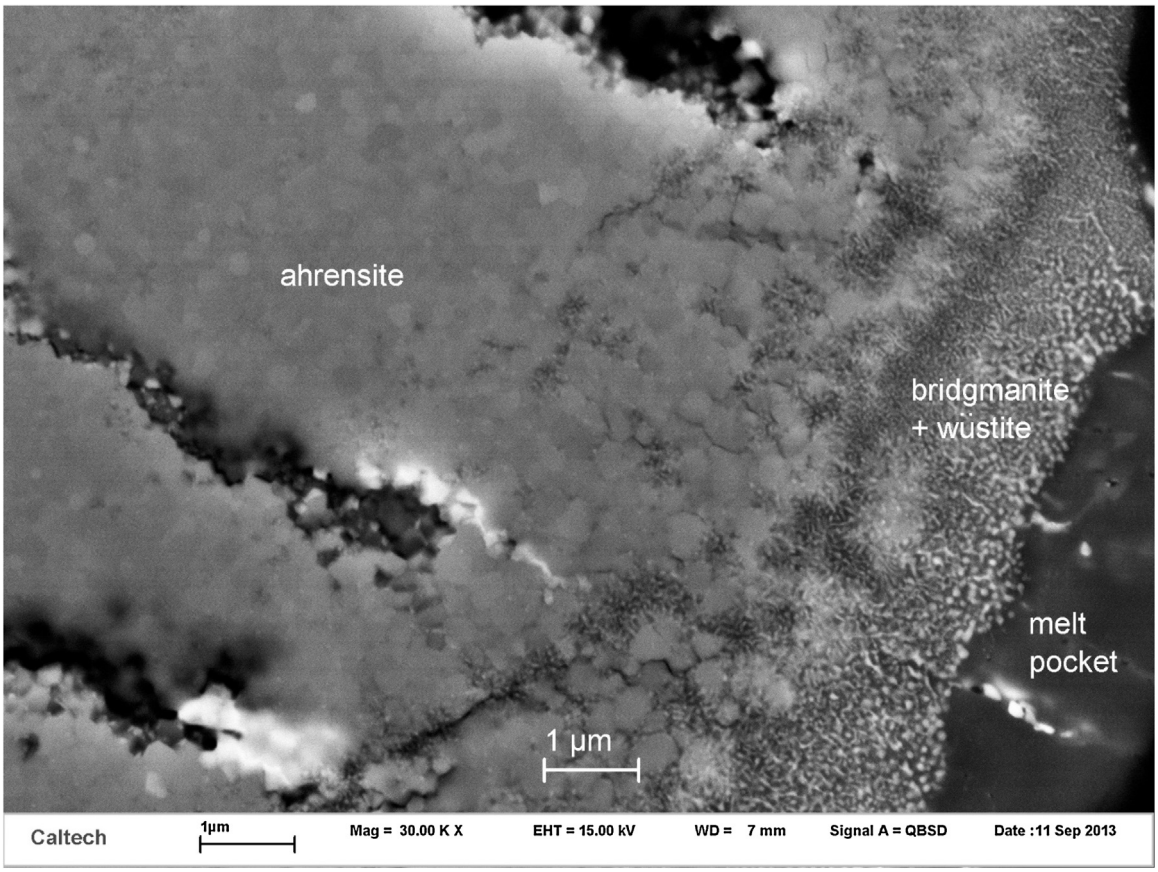

Fig. 14. Ahrensite (γ-Fe_2SiO_4), bridgmanite ($MgSiO_3$-perovskite) and wüstite next to a shock melt pocket from the Tissint martian meteorite (Ma et al., 2016c). BSE image.

diogenitic precursors. Although some howardites contain carbonaceous chondrite clasts (Zolensky et al., 1996), these are fragments of projectiles that impacted the surface of the HED parent body at low relative velocity.

2.12.4. Angrites

Mittlefehldt et al. (1998) described the prototypical angrite, Angra dos Reis, as a medium-to-coarse grained igneous rock composed mainly of Al-Ti-diopside with minor olivine, spinel and troilite and accessory magnesian kirschsteinite, celsian. merrillite, titanomagnetite, baddeleyite and metallic Fe-Ni. Other angrites have hypidiomorphic-granular or porphyritic textures and, in addition to the phases in Angra dos Reis, some contain plagioclase, hercynite – $(Fe,Mg)Al_2O_4$, ulvöspinel, Ca phosphate and silicophosphate (Mittlefehldt et al., 1998, 2002; Keil, 2012).

The angrites are basically basaltic in bulk composition and it is clear that they formed as igneous rocks. LEW 86010 formed by partial melting of a carbonaceous-chondrite-like precursor at an oxygen fugacity of about 1 log unit above the iron-wüstite buffer (Jurewicz et al., 1993). Asuka 881371 and LEW 87051 could be either contaminated partial melts (Mittlefehldt and Lindstrom, 1990) or impact melts of pre-existing igneous rocks (Jurewicz et al., 1993). Angra dos Reis could have formed as a cumulate with substantial trapped melt (Jones, 1982). The magmas from which D'Orbigny and Sahara 99555 crystallized could have been contaminated with batches of more-primitive melt (Mittlefehldt et al., 2002).

2.12.5. Aubrites

The aubrites (enstatite achondrites) are highly reduced igneous rocks related to the enstatite chondrites. They are composed principally of enstatite with minor-to-accessory forsterite, diopside, albite, Si-bearing low-Ni metallic Fe, troilite and schreibersite, with trace amounts of sulfide (oldhamite, alabandite, niningerite, daubréelite, caswellsilverite, heideite – $(Fe,Cr)_{1+x}(Ti,Fe)_2S_4$, djerfisherite, brezinaite – Cr_3S_4), perryite, osbornite – TiN, graphite, roedderite – $(K,Na)_2Mg_5Si_{12}O_{30}$, metallic Cu, perovskite and geikielite – $MgTiO_3$ (Hutchison, 2004; Keil, 2010).

Most of the clasts in Norton County are plutonic orthopyroxenites; also present are dunites, plutonic pyroxenites and plagioclase-silica rocks (Okada et al., 1988). Keil (2010) modeled the aubrites as having formed from enstatite-chondrite-like material by melting and crystallization, possibly from a magma ocean. Separation of a metal-sulfide melt from the silicate melt would account for the low modal abundances of metallic Fe-Ni (averaging ~0.2 vol.%) and sulfide (averaging ~0.5 vol.%) in the aubrites. The negative Eu anomalies of most aubrites (Keil, 2010) may reflect separation and loss of oldhamite grains with positive Eu anomalies (Rubin, 2015b).

The unusual unbrecciated Shallowater and Mount Egerton aubrites were modeled by Rubin (2015a), not as primary igneous rocks, but as impact-melt rocks derived from large cratering events on the same porous enstatite-chondrite-like asteroid.

2.12.6. Magmatic iron meteorites

The magmatic iron meteorite groups IC, IIAB, IIC, IID, IIF, IIIAB, IIIE, IIIF, IVA and IVB formed by fractional crystallization in the molten metallic cores of differentiated asteroids. Each group formed within a different asteroid inside cores of different bulk chemical and isotopic compositions.

During initial cooling, taenite (fcc – face-centered cubic γ-iron) crystallized from the melt in these cores at high temperatures.

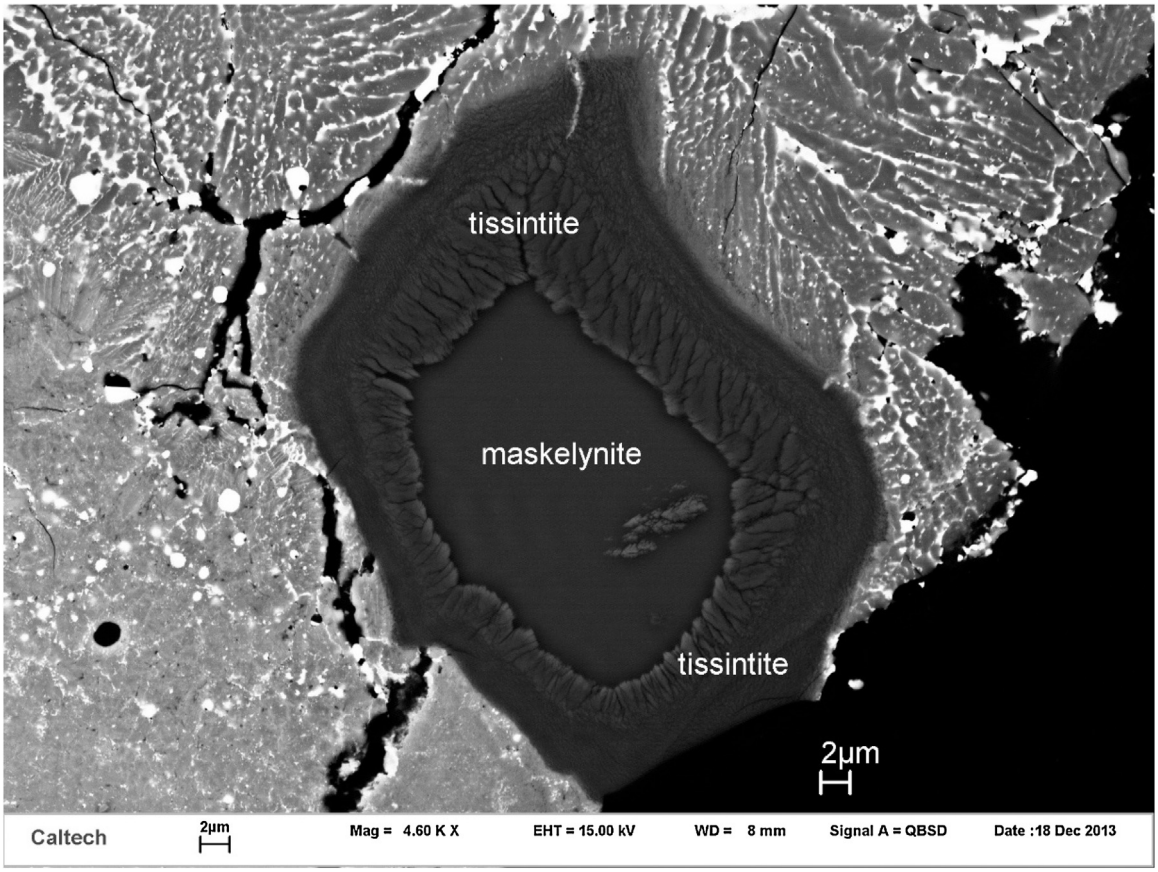

Fig. 15. Tissintite, (Ca,Na,□)$AlSi_2O_6$, formed from maskelynite in a melt pocket within the Tissint martian meteorite (Ma et al., 2015b). BSE image.

Eventually the two-phase field was reached and low-Ni metallic Fe (kamacite, bcc – body-centered cubic α-iron) nucleated and began to crystallize (Section 2.14).

The sulfide nodules within several magmatic groups probably formed from trapped S-rich liquid. As discussed by Olsen et al. (1999), non-siderophile trace elements (e.g., O, Na, K, Ca, Mg, Mn, Pb) in the crystallizing metallic core of the parent asteroid were concentrated in the late-stage residual S-rich liquids. As the partial pressure of O increased, P and Fe from the metal host was oxidized and phosphate precipitated from the residual S-rich melt. The principal phosphate phase that crystallized directly from the residual liquid in many of the IIIAB irons was sarcopside. In IIIAB Cape York (Figs. 189 and 511 of Buchwald, 1975), there are five distinct phosphates including buchwaldite, maricite and three incompletely characterized phases – phase I – $Na_4Ca_3Fe(PO_4)_4$; phase III – $Na_4(Mn,Fe)(PO_4)_2$; and phase IV – $Na_4CaCr(PO_4)_3$.

2.12.7. Mesosiderites

Mesosiderites are fragmental breccias composed of roughly 50 vol.% silicate clasts (mainly basalts, gabbros, orthopyroxenites, dunites, quench-textured impact-melt rocks and breccias) and roughly 50 vol.% metallic Fe-Ni. As discussed in Section 2.10 and in Rubin and Mittlefehldt (1992), 76% of the silicate clasts (gabbros, polygenic basalts and quench-textured rocks) appear to have formed by impact-melting processes.

On the other hand, about 11% of the large silicate clasts are monogenic basalts (Rubin and Mittlefehldt, 1992) that are nearly indistinguishable from eucrites in texture, mineralogy, mineral chemistry and bulk composition. These rocks may be fragments of basalt flows on the mesosiderite parent body (MPB), their major phases (pyroxene and plagioclase) having crystallized from the cooling melt. They plot along the eucrites' Neuvo Laredo Trend and thus probably formed by fractional crystallization (Rubin and Mittlefehldt, 1992).

Ultramafic rocks constitute 13% of the silicate clasts. There are two varieties – (1) dunites (exemplified by 10-cm olivine crystals in Mount Padbury; McCall, 1966) are igneous cumulates formed either in the mantle of the MPB or the projectile that brought metal to the MPB surface, and (2) orthopyroxenites which resemble diogenites and probably crystallized within the lower crust or mantle of the MPB (Rubin and Mittlefehldt, 1992).

The metallic Fe-Ni in the Type-1 mesosiderites (the rocks least affected by later-stage impact melting) was likely derived from the impacting metal-rich projectile (see Section 2.10). Hassanzadeh et al. (1990) found that large metallic clasts from mesosiderites have a narrow range of compositions (with near-chondritic siderophile element ratios), suggesting that the impacting core was ≥95% molten. This is consistent with the electrical interconnectedness of the metal (indicating that it flowed through pre-existing fractures; Powell, 1971). If this scenario is correct, the metal grains in the mesosiderites should be considered shock products rather than minerals formed by crystallization within a differentiated body.

2.12.8. Pallasites

The main-group pallasites are mixtures of 65 ± 20 vol.% silicate (mostly olivine with minor-to-accessory low-Ca pyroxene), 35 ± 20 vol.% metallic Fe-Ni, and 0.3–1.0 vol.% each of schreibersite, chromite, troilite and phosphate (mainly farringtonite – $Mg_3(PO_4)_2$, stanfieldite – $Ca_4(Mg,Fe)_5(PO_4)_6$ and merrillite – $Ca_9MgNa(PO_4)_7$) (Ulff-Møller et al., 1998; Mittlefehldt et al., 1998). These phases all crystallized deep within a differentiated aster-

oid. Ulff-Møller et al. (1998) proposed that main-group pallasites formed by the following process: (1) Olivine grains crystallized from the molten silicate mantle at ~1680 °C and settled to the bottom, atop the molten metal core. At lower temperatures, rare pyroxene grains also crystallized and settled. (2) The metal core crystallized from its center toward its edge. (3) After temperatures had cooled to ~1480 °C, the late-stage, moderately low- viscosity, metallic magma invaded the silicate mantle, crystallized around large olivine-rich mantle fragments and penetrated some individual olivine grains. Chromite and troilite probably crystallized very late from residual S-rich liquids.

A few pallasites contain phosphoran olivine (with ~4–5 wt.% P_2O_5) (Buseck, 1977); Brenham olivines range up to 7.4 wt.% P_2O_5 (Wasson et al., 1999). In the olivine crystal structure, P^{+5} substitutes for Si^{+4} in the tetrahedral sites; charge balance is maintained by the presence of some vacant octahedral sites. Dynamic crystallization and isothermal experiments show that the phosphoran olivine was likely produced as a metastable phase from a P- enriched melt (Boesenberg and Hewins, 2010).

Some olivine grains from pallasites are of gemstone quality (e.g., Sinkankas et al., 1992) and can be faceted to make jewelry; they have been labeled as peridot (Kunz, 1890) and chrysolite (Brown et al., 1953). A few display chatoyancy (cat's eye), apparently caused by light reflected at right angles to subparallel, tube-like hollow inclusions in the grains (Overlin, 2008).

2.12.9. Lunar meteorites

The major types of primary rocks returned from the Moon are mare basalts and three varieties of pristine highland rocks – ferroan anorthosites, Mg-rich rocks and KREEP rocks (e.g., Taylor et al., 1991). The latter samples are rich in incompatible elements including K, REE and P. Additional rock types identified among returned lunar samples are polymict breccias (formed by impact mixing and melting of the primary rocks) and lunar soil (containing fragments of primary rocks and impact-melted materials). As discussed by Korotev (2005), lunar meteorites include unbrecciated basalts, olivine cumulates, and various types of breccias (basaltic, feldspathic, and mixed basaltic-feldspathic). One impact-melt breccia (Sayh al Uhaymir 169) contains a KREEP component. Also present among lunar meteorites are regolith breccias containing glass spherules (produced by impacts or by pyroclastic processes), agglutinates, and fragments of common rock types.

Lunar meteorites do not contain unmelted lunar soil samples; there are few or no clasts of ferroan anorthosites and Mg- rich rocks. It appears that KREEP samples and mafic, magnesium-suite rocks (which are abundant among Apollo samples) formed only in restricted locales on the Moon (Korotev, 2005). Because lunar meteorites were derived from the entire lunar globe, the rarity of geographically limited samples is to be expected.

The principal minerals in lunar meteorites are anorthitic plagioclase, pyroxene, olivine and minor ilmenite (e.g., Frondel, 1975). Also abundant is impact- generated glass derived from melting the principal mineral phases. Mare basalts formed from cooling lava flows; their constituent mineral phases crystallized from the melt. The feldspathic lunar meteorite breccias have clasts of noritic anorthosites, troctolitic anorthosites, anorthitic norites and anorthitic troctolites (Korotev, 2005); their label is a function of their normative mineral abundances. These rock fragments are likely derived from the lunar highlands; their constituent phases crystallized from the melt during cooling of the anorthositic crust. The high plagioclase contents of these rocks suggest that the rocks are cumulates, wherein newly formed plagioclase crystals separated from the residual melt.

2.12.10. Martian meteorites

Martian meteorites are all igneous rocks; the principal types include nakhlites (olivine clinopyroxenites), chassignites (dunites), the ALH 84001 orthopyroxenite, and basaltic shergottites and related rocks (including those classified as lherzolites, basaltic breccias, gabbros, microgabbros, diabases, olivine-phyric shergottites, and augite basalt).

As discussed by Treiman (2005), nakhlites are igneous augite-rich cumulate rocks formed in thick lava flows or shallow intrusions, plausibly near the large volcanoes in the Tharsis, Elysium or Syrtis Major regions. Augite and olivine crystallized from the magma and settled to the bottom of the magma chamber. Later-stage igneous processes included crystallization of the residual magma, flow of the melt relative to the crystals, and elemental diffusion and chemical reactions among the minerals and the magma.

Chassignites are igneous olivine-chromite cumulate rocks. Major olivine and minor pyroxene crystals formed within a magma, in some cases enveloping previously crystallized chromite grains. The crystals settled to the bottom of the magma chamber and continued to grow; grains impinged on one another, squeezing out most of the intercumulus liquid (Hutchison, 2004). The last phases to crystallize were alkali feldspars – plagioclase (ranging from albite to andesine) and K-feldspar.

A simplified petrogenetic history of the ALH 84001 orthopyroxenite would include the rock's formation within a magma chamber in which orthopyroxene and euhedral chromite grains crystallized and settled.

The major original phases in the basaltic shergottites were pyroxene, plagioclase and, in some cases, olivine. (Plagioclase was later transformed into maskelynite during launch off Mars.) The major phase in the lherzolitic shergottites is olivine, accompanied by minor Ca-poor pyroxene. Minerals in the basaltic shergottites crystallized within lava flows; the lherzolitic shergottites formed as olivine cumulates at the base of a magma chamber. In each case, minor phases crystallized from the residual melt: titanomagnetite, ilmenite, ulvöspinel, magnetite, chromite and hercynite in the basaltic shergottites; pyroxene, plagioclase and chromite in the lherzolitic shergottites.

2.12.11. Acapulcoites and lodranites

Many workers consider acapulcoites and lodranites to be "primitive achondrites" and have modeled them as having formed by different degrees of partial melting of primary chondritic rocks (e.g., Palme et al., 1981; Nagahara, 1992; Zipfel et al., 1995; McCoy et al., 1996, 1997; Mittlefehldt et al., 1996; Patzer et al., 2004). If these models are correct, then the phases in acapulcoites and lodranites that are not chondritic relicts would have crystallized from the endogenic melt; this would include some of the olivine, pyroxene, plagioclase, metal and sulfide grains.

The alternative view of the origin of these meteorites is that they are impact melt products, as discussed in Section 2.10.

2.12.12. Ureilites

Ureilites are C-rich ultramafic rocks whose origins remain poorly understood. In Section 2.10, we present the arguments of Rubin (1988, 2006) who suggested that the major phases in ureilites crystallized from shock-generated melts. However, some workers have considered ureilites to be "primitive achondrites." Among the more-popular alternative models are those that have ureilites forming as: (1) partial melt residues that were infused with carbon (e.g., Boynton et al., 1976; Wasson et al., 1976), (2) intrusive igneous cumulates formed from C-rich magmas (e.g., Berkley et al., 1976, 1980; Berkley and Jones, 1982; Berkley, 1986; Goodrich et al., 1987) and (3) paracumulates derived from disrupted partially molten asteroids (Warren and Kallemeyn, 1988).

The shortcomings of these models were discussed by Rubin (1988). Nevertheless, if any of them are correct, then the principal primary phases in ureilites (olivine, pyroxene, graphite, metallic Fe-Ni, sulfide) and, perhaps, the minor to accessory phases in related rocks (e.g., plagioclase and chlorapatite; e.g., Goodrich et al., 2006) crystallized from endogenic melts on the parent asteroid(s).

2.12.13. Brachinites

As discussed by Mittlefehldt et al. (1998), brachinites are dunitic wehrlites, consisting dominantly (roughly 80–95%) of olivine with minor augite, chromite, sulfide, phosphate, metallic Fe-Ni, and, in some cases, plagioclase and orthopyroxene. They have been labeled "primitive achondrites" by Nehru et al. (1983, 1992, 1996) and considered to be either highly metamorphosed chondritic rocks or chondrites that have undergone very low degrees of partial melting. If these scenarios are correct, then the constituent minerals of brachinites are mainly chondritic relicts. Keil (2014) modeled them as partial melt residues from an FeO-rich asteroid. Alternatively, Warren and Kallemeyn (1989) compared their textures to those of ureilites and modeled the brachinites as cumulates. If that model is correct, then the minerals in brachinites formed igneously; some phases accumulated at the bottom of a magma chamber, others crystallized from the residual liquid.

2.13. Condensation from late-stage vapors in differentiated bodies

Tabular grains of tridymite, up to ~1 cm in maximum dimension and containing very low concentrations of Al and Ti, occur in the IVA irons Gibeon (e.g., Berwerth, 1902; Schaudy et al., 1972; Ulff-Møller et al., 1995) and Bishop Canyon (Scott et al., 1996). Wasson et al. (2006) suggested that these tridymite occurrences formed by late-stage condensation from a cooling SiO-rich vapor within fissures in solid metal in the IVA core. The SiO(g) itself may have formed by reduction of SiO_2 or $FeSiO_3$ from the asteroid mantle; the reducing agent could have been C dissolved in the metallic magma. Alternatively, SiO(g) could have formed by oxidation of minute amounts of Si dissolved in the metallic melt; the oxidizing agent could have been O dissolved in the melt or CO, CO_2 or H_2O vapors derived from the mantle (Ulff-Møller et al., 1995). The fissures containing the tridymite platelets may have been thinner initially, but widened after the cooling metal contracted. The platelet morphology may then have arisen as tridymite minimized its surface energy (Wasson et al., 2006).

2.14. Exsolution, inversion and subsolidus redox effects within cooling igneous materials

Minerals in all the igneous meteorites cooled from high temperatures to below the solidus and were subject to exsolution. In some cases, particularly, in pyroxene, cooling causes the inversion of a high-temperature crystal structure to a low-temperature structure; this inversion is commonly attended by exsolution.

2.14.1. Eucrites

Basaltic eucrites originally contained pigeonite, which, upon cooling below the solidus, exsolved lamellae of augite. In cumulate eucrites, primary pigeonite also underwent subsolidus exsolution of augite; in some rocks, the pigeonite inverted to orthopyroxene and subsequently exsolved augite. Studies illustrating more-complicated exsolution in eucritic pyroxenes are discussed by Mittlefehldt et al. (1998).

2.14.2. Diogenites

Diogenites contain minor-to-accessory amounts of diopside (0–2 vol.%) mainly as ~3-μm-thick exsolution lamellae within orthopyroxene or low-Ca pigeonite. Mori and Takeda (1981) identified much thinner augite exsolution lamellae in Ibbenbüren (0.077 μm) and Johnstown (0.006 μm).

2.14.3. Angrites

Millimeter-size olivine grains in the LEW 86010 angrite contain kirschsteinite exsolution lamellae up to 20 μm thick (e.g., Delaney and Sutton, 1988; Goodrich, 1988; McKay et al., 1988; Mikouchi et al., 1995).

2.14.4. Aubrites

Diopside in aubrites is present as primary grains that crystallized from the melt as well as exsolution lamellae within enstatite (Reid and Cohen, 1967; Watters and Prinz, 1979; Okada et al., 1988). Schreibersite exsolved from metallic Fe-Ni during cooling when the P concentration within the metal became oversaturated.

2.14.5. Magmatic irons

After taenite crystallized in the cores of the differentiated asteroids that produced the magmatic irons, the cores continued to cool until the two-phase Fe-Ni field was reached; the temperature of this boundary (between 800° and 500 °C) depends upon the bulk Ni content of the taenite. Low-Ni metallic Fe nucleated and began to crystallize along the {111} planes of the taenite. Upon further cooling, both low-Ni metallic Fe and taenite grains grew richer in Ni as the low-Ni metallic Fe formed at the expense of taenite (see Figs. IV-2 and IV-4 of Wasson, 1985). The intergrowth of low-Ni metallic Fe lamellae and Ni-rich lamellae forms the Widmanstätten pattern in most iron meteorites; because the low-Ni metallic Fe lamellae are oriented along the planes of an octahedron, the meteorites with this pattern are known as octahedrites. [The general thermal history may actually be more complicated than this. Yang et al. (1997a,b) suggested that taenite undergoes decomposition <400 °C, producing tetrataenite, martensite and awaruite.]

In many irons, schreibersite (in many cases occurring in the prismatic form of rhabdite) exsolved from the cooling taenite when the face-centered-cubic crystal structure could no longer accommodate appreciable amounts of P. In IIIE irons, the carbide haxonite exsolved from taenite as C became oversaturated; in some members of groups IIAB and IIIAB, cohenite formed in a similar fashion. Cliftonite is a form of graphite that displays a cubic morphology; it exsolved from the metallic Fe-Ni during cooling. In some iron groups, oriented platelets of 1–5 μm-thick chromite lamellae flanked by secondary troilite (collectively known as Reichenbach lamellae) also exsolved from taenite during cooling (Buchwald, 1975). Daubréelite commonly occurs as exsolution lamellae within troilite in magmatic groups IIAB, IIIAB and IVA.

In troilite nodules in IIIAB irons, the phosphate johnsomervilleite ($Na_2Ca(Fe,Mg,Mn)_7(PO_4)_6$) occurs inside sarcopside ($(Fe,Mn)_3(PO_4)_2$) and probably exsolved from it during cooling (Olsen et al., 1999). Some occurrences of galileiite ($NaFe_4(PO_4)_3$) also seem to have exsolved from primary graftonite ($(Fe,Mn)_3(PO_4)_2$) or sarcopside during cooling.

2.14.6. Mesosiderites

The ultramafic and mafic silicate clasts in mesosiderites contain pyroxene grains that have undergone exsolution and inversion, i.e., orthopyroxene inverting from pigeonite and pigeonite exsolving augite lamellae. Perryite within metallic Fe-Ni in some mesosiderites apparently exsolved from taenite during cooling from high temperatures.

2.14.7. Pallasites

Schreibersite is an accessory phase occurring within the metal of pallasites. It formed by exsolution from taenite at high subsolidus temperatures when the P concentration in the γ-iron exceeded the

accommodation capacity of the face-centered-cubic crystal structure.

2.14.8. Lunar meteorites

Some pyroxene grains in Apollo samples have undergone exsolution, producing thin pigeonite lamellae within augite and augite lamellae within pigeonite. Subsolidus reduction reactions (Papike et al., 1998) include ulvöspinel breaking down into different products – (a) ilmenite and metallic Fe, (b) rutile and metallic Fe, or (c) chromite, rutile and metallic Fe. In some samples, Ti-rich ulvöspinel has broken down into Ti-poor spinel, titanian chromite, ilmenite and metallic Fe. Although not all these features have been observed in lunar meteorites, they are likely to be present.

2.14.9. Martian meteorites

As reviewed by McSween and Treiman (1998), two sets of augite lamellae exsolved from pigeonite in the shergottites – one set parallel to (001), the other parallel to (100). Primary ulvöspinel grains in QUE 94201 underwent exsolution and oxidation to produce titanomagnetite and ilmenite. In the nakhlites, kirschsteinite lamellae within olivine appear to have undergone oxidation to produce augite and magnetite (Yamada et al., 1997a; Yamada et al., 1997b). Symplectic intergrowths of augite and magnetite formed by exsolution in olivine from two nakhlites (Nakhla and Governador Valadares) under oxidizing conditions at temperatures >900 °C during cooling (Mikouchi et al., 2000). Titanomagnetite has exsolution lamellae of ilmenite and (perhaps) ulvöspinel. The chassignites contain orthopyroxene with thin augite exsolution lamellae that were inferred to have formed from primary pigeonite (Wadhwa and Crozaz, 1995). Chassigny also contains symplectic intergrowths of augite and magnetite within olivine grains that are similar to those in nakhlites (Greshake et al., 1998). The orthopyroxene grains in the ALH 84001 orthopyroxenite appear to be free of augite exsolution lamellae (McSween and Treiman, 1998).

2.14.10. Ureilites

Although most pyroxene grains in ureilites lack exsolution lamellae, there are a few exceptions: (a) LEW 85440 contains very thin (~0.01 μm) orthopyroxene and clinopyroxene lamellae within orthopyroxene parallel to (100) (Takeda et al., 1992). (b) ALH 82130 contains pigeonite with irregular augite lamellae. (c) LEW 88774 contains pyroxene crystals consisting of ~50-μm-thick lamellae of orthopyroxene and augite in similar proportions (Warren and Kallemeyn, 1994; Chikami et al., 1997).

2.15. Solar heating near perihelion

Buchwald (1975) pointed out that asteroids or meteoroids with elliptical orbits and small perihelion distances can be periodically heated by solar radiation. Many near-Earth objects (NEOs) undergo orbital evolution that bring them close to the Sun, leading to appreciable heating (e.g., Marchi et al., 2009). For example, asteroid 1566 Icarus (with a perihelion distance of 0.187 AU) can experience temperatures up to ~365 °C every 409 days. [Mercury's perihelion is at 0.313 AU.] Although meteorites that strike the Earth spent time in NEO-like orbits, they are likely to have experienced less Sun-driven heating than the NEOs themselves. This is due to the meteorites' generally shorter collisional lifetimes, much smaller sizes, and greater perihelion distances; furthermore, it is likely that the regions of the meteoroids that were most strongly heated by the Sun (i.e., those regions close to the subsolar point of the parent NEO) are ablated and lost during atmospheric entry (Marchi et al., 2009). Nevertheless, solar heating of meteorites remains a viable, albeit minor, mechanism.

The IVA iron Social Circle is a fine octahedrite containing recrystallized low-Ni metallic Fe grains that partially overprint lamellae with Neumann lines (Buchwald, 1975). Buchwald suggested that prolonged temperatures of ~500 °C could have produced the recrystallization of low-Ni metallic Fe. He also described "rhythmic growth lines" throughout the meteorite and concluded that Social Circle was "reheated several times" to about the same temperature. He suggested that the meteorite could have been heat-treated by periodic close approaches to the Sun (an idea first proposed by Henderson and Furcron, 1957).

The IIAB Indian Valley hexahedrite contains recrystallized low-Ni metallic Fe grains with concentric growth rings, possibly consistent with cyclic reheating (Buchwald, 1975). Buchwald described graphite plumes associated with rhabdite plates within certain regions of the low-Ni metallic Fe in this meteorite. He suggested that these plumes formed from cohenite that had nucleated on rhabdite and subsequently decomposed; the cause was ascribed to the same cyclic reheating events that caused the low-Ni metallic Fe to recrystallize. If these features actually formed during cyclic heating events as Buchwald (1975) suggested, then it is plausible they were caused by close passages to the Sun.

Some CM carbonaceous chondrites may also have experienced minor thermal metamorphism caused by solar heating. For example, Sutter's Mill is a regolith breccia containing some components that have been heated sufficiently to destroy carbonates, transform phyllosilicates into fine-grained olivine, break down tochilinite to form troilite, and eliminate indigenous amino acids (Zolensky et al., 2014b; Burton et al., 2014). The meteorite contains solar-cosmic-ray-produced nuclides produced when the meteoroid's orbit was <1 AU from the Sun (Nishiizumi et al., 2014). It seems possible that solar heating of some CM chondrites could be partly responsible for low-temperature thermal metamorphism in these rocks. Alternatively, most or all of the heating could be due to impacts, the effects of which are evident in the petrofabrics of CM chondrites (e.g., Rubin, 2012b; Lindgren et al., 2015).

2.16. Atmospheric passage

A typical meteoroid enters the Earth's atmosphere at ~18 km s^{-1} (Shoemaker et al., 1990). During the traverse, the surface of a chondritic meteoroid reaches temperatures of 1180–1410 °C (Wood, 1963; Ivanova et al., 1968) and melts to depths of ~0.3–1.0 mm due to friction with the surrounding air (Ramdohr, 1967). The surface of the meteoroid ablates, exposing a new surface that also melts and ablates; this process can be repeated several times.

Most meteoroids break into fragments as aerodynamic stresses increase during their descent. For objects travelling at 20 km s^{-1}, stresses rise from 10 MPa at an altitude of 30 km to 100 MPa at 15 km (Melosh, 1989). This exceeds the crushing strengths of many stony meteorites (which range from ~6 to ~500 MPa and average ~200 MPa; Petrovic, 2001). The crushing strengths of carbonaceous chondrites are on the order of 1 MPa (Melosh, 1989), consistent with the small median size of carbonaceous chondrites listed in the Meteoritical Bulletin Database (~34 g). The median size of CM chondrites (which are matrix-rich friable samples) is ~10 g.

An individual stony meteoroid that does not break into fragments, could lose >95% of its original mass by the time it reaches the Earth's surface. Its final fusion crust would typically consist of three zones: an outer zone consisting of vesicular black opaque glass and containing submicrometer magnetite, an intermediate zone containing partly melted silicate grains, and an inner zone containing unmelted silicate and rapidly solidified metal-troilite intergrowths (Sears, 1978). The zones in the fusion crusts of enstatite chondrites are less developed (Genge and Grady, 1999).

As pointed out by Rubin (1997a), minerals that form in the fusion crusts of chondritic meteorites include eskolaite (formed by the reduction and breakdown of chromite), pseudobrookite – Fe_2TiO_5 (formed by the breakdown of ilmenite), magnetite and

wüstite (formed by the oxidation of metallic Fe; Ramdohr, 1967, 1973), and intergrowths of metallic Fe-Ni and troilite (formed by the melting and quenching of these phases). In some cases, phases produced during atmospheric passage flow a few hundred micrometers toward the meteorite interior through fractures: e.g., wüstite in CO3 DOM 03238 (Kim et al., 2009) and metal-sulfide veins in EL6 DOM 10088 (Rubin, 2015a).

Heating caused by atmospheric passage can produce back transformations of high-pressure phases to low-pressure ones. The fusion crust of the H6 chondrite Y-75267 transects a shock vein containing ringwoodite, majorite-pyrope$_{ss}$ and $NaAlSi_3O_8$ hollandite (Kimura et al., 2003). However, portions of the vein near the fusion crust (where temperatures of ~1400 °C were reached) contain no high-pressure phases – only olivine, low-Ca pyroxene and plagioclase glass.

Because achondrites and oxidized carbonaceous chondrites have little metallic Fe, their fusion crusts are less likely to contain rapidly cooled metal-sulfide intergrowths. Achondritic minerals melt over a relatively narrow temperature range and are likely to form a smooth glossy fusion crust (Sears, 1978).

Iron meteorite fusion crusts typically contain magnetite and wüstite (Buchwald, 1977; Sears, 1978). Veins of wüstite can penetrate the interior of the meteorite (e.g., Breen et al., 2016).

Micrometeorites (10–2000 μm in size) and interplanetary dust particles (<10–100 μm) are also heated and partly melted during atmospheric passage. Secondary minerals formed within these small objects include magnetite, maghemite, poorly characterized Fe oxides, laihunite and skeletal olivine grains surrounded by silicate glass (e.g., Keller et al., 1996; Rietmeijer, 1996; Genge and Grady, 1998).

2.17. Terrestrial weathering

The phenomenon of meteorites "rusting" in museum cabinets (at least those cabinets not filled with inert gas) is well known to curators (e.g., Bagnall, 1991). In many cases, slabs of fresh falls develop thin red coatings (possibly goethite – αFeO(OH)) due to oxidation of metallic Fe from atmospheric water.

Meteorite finds are more extensively altered; numerous color images of weathered finds appear in Yanai (1981), Yanai and Kojima (1987), Killgore and Killgore (2002) and Stinchcomb (2011). Metallic Fe-Ni and sulfide, in particular, show progressive alteration with time; this is reflected by the weathering index for ordinary chondrites devised by Wlotzka (1993) and refined by Zurfluh et al. (2016). Rubin and Huber (2005) proposed a weathering index for CK and R chondrites (oxidized meteorites that contain little metallic Fe-Ni). The index is based on the percentage of brown-stained silicates, reflecting the degree of mobilization of oxidized iron produced by terrestrial weathering of Ni-bearing sulfide (mainly pentlandite and pyrrhotite).

Although Buddhue (1957) found that the most important minerals formed in meteorites by terrestrial weathering are goethite and magnetite, there are more than 60 such species (Table 7 of Rubin, 1997a; Rubin, 2016 and references therein).

As discussed by Rubin (1997a), minerals produced by weathering in iron meteorites include: (1) oxides and hydroxides formed directly from metallic Fe-Ni by oxidation and the incorporation of H_2O, Cl^{-1} and $CO_3{}^{-2}$ (Cl-bearing akaganéite, bunsenite, goethite, ferrihydrite, hematite, hibbingite, lepidocrocite, maghemite, magnetite, trevorite, and possibly zaratite), (2) graphite and low-Ni metallic Fe formed by the decomposition of iron carbide, (3) phosphates formed by the oxidation of schreibersite (apatite, arupite, cassidyite, collinsite, lipscombite, vivianite) and (4) sulfates formed from troilite (honessite, jarosite). Additional phases formed in irons by terrestrial weathering include metallic Cu, opal, various sulfides (pentlandite, bornite, chalcopyrite, heazlewoodite, isocubanite), carbonates (reevesite, siderite), phyllosilicate (pecoraite) and elemental S (White et al., 1967; Buchwald, 1975, 1977, 1989, 1990; Faust et al., 1973; Buchwald and Clarke, 1988, 1989; Saini-Eidukat et al., 1994; Rubin, 1997a).

In enstatite meteorites, the unusual sulfides rich in cations that are found only in silicate or oxide minerals under less-reducing conditions (e.g., Na, Mg, K, Ca, Ti, Cr, Mn) are unstable at the Earth's surface. They break down to produce an assortment of weathering products: (a) Schöllhornite forms from caswell-silverite (Okada et al., 1981). (b) Bassanite, vaterite, calcite and portlandite form from oldhamite (CaS) (Okada et al., 1981). (c) Nakamura-Messenger et al. (2012) examined a small BO chondrule in the Y-691 EH3 chondrite and found a tiny grain of an unknown Ti-rich layer phase associated with wassonite (TiS); they also found a few small patches of an unknown S-rich layer phase associated with schöllhornite. These two new uncharacterized phases are probably terrestrial weathering products of wassonite or of additional as-yet-undescribed titanium-sulfide phases that Nakamura-Messenger et al. (2012) also found in the chondrule.

The ≥3-metric-ton fossil EL chondrite impact-melt rock Al Haggounia 001 (Rubin, 2016) contains a plethora of terrestrial alteration phases including calcite, barite, jarosite, gypsum, halite, sylvite, melanterite, native S and clay (Kuehner et al., 2006; Irving et al., 2010; Bunch et al., 2014). Al Haggounia 001 has a ^{14}C age of 23,000 ± 2000 years (Chennaoui-Aoudjehane et al., 2009) and has been called a fossil meteorite. Some specimens are cemented together with terrestrial limestone clasts and rhyolite pebbles within conglomerates (Kuehner et al., 2006; Chennaoui-Aoudjehane et al., 2007; Chennaoui-Aoudjehane et al., 2009).

Evaporite deposits on the surfaces of Antarctic meteorites include carbonates (nesquehonite, hydromagnesite, amorphous Mg-carbonate) and sulfates (epsomite, starkeyite, gypsum, hydronium jarosite, poorly characterized K-Fe sulfate) (e.g., Zolensky and Gooding, 1986; Velbel, 1988). The fusion crusts of Antarctic meteorites contain poorly ordered clay minerals similar in composition to smectite and mica formed by terrestrial weathering (Gooding, 1986a).

Sulfate veins within CI chondrites and sulfate patches at the surfaces of these meteorites include epsomite, bloedite, gypsum, and poorly characterized Fe-, Mg-, Na- and Ca-sulfates (some containing Ni). These veins are not indigenous to the meteorites, but instead formed on Earth in museum cabinets via reactions with atmospheric water (Zolensky, 1999; Gounelle and Zolensky, 2001). The terrestrial sulfates in these rocks formed mainly by the dissolution and remobilization of indigenous sulfate grains (Gounelle and Zolensky, 2001) as well as by weathering of indigenous pyrrhotite (Bass, 1970).

A major impact appears to have disrupted the L-chondrite parent body 470 ± 6 Ma ago and sent fragments to Earth (e.g., Heymann, 1967; Bogard, 1995; Bogard et al., 1976, 1995; McConville et al., 1988; Turner, 1988; Britt and Pieters, 1994; Keil et al., 1994; Haack et al., 1996; Schmitz et al., 2003; Korochantseva et al., 2007; Nesvorný et al., 2007; Swindle et al., 2013). The Lockne-Målingen (7.5 km, 0.7 km) doublet crater in Central Sweden formed 458 Ma ago (Ormö et al., 2014) and may be a product of the L-chondrite break-up event (Schmitz et al., 2001).

Dozens of highly altered L chondrites from this event have been recovered as fossil meteorites in a quarry of Ordovician limestone in Sweden (e.g., Schmitz et al., 2001). One of these fossil meteorites is Brunflo (Thorslund and Wickman, 1981; Thorslund et al., 1984). Except for relict chromite grains, all the primary minerals in this meteorite have been replaced. The secondary phases, formed by extensive terrestrial alteration, include carbonate (major calcite), sulfate (barite), a disordered illite-type phyllosilicate, rare grains of elemental Ni, sulfarsenides (cobaltite, gersdorffite), arsenides (rammelsbergite, safflorite, nickeline, maucherite, orcelite), sul-

fides (chalcopyrite, sphalerite, galena, pyrite, and several poorly characterized Cu sulfides), TiO_2 (probably anatase or brookite), quartz, and carbonate-fluorapatite (francolite). Alteration phases in a different fossil L chondrite found in this limestone (Österplana) include calcite, Cr-bearing layered silicate, barite, apatite and TiO_2 (Nyström et al., 1988). Numerous additional highly altered fossil L chondrites have been found in the last few decades; the list of secondary phases will undoubtedly increase.

Kyte (1998) reported a ~2.5-mm-size fossil carbonaceous chondrite from a deep-sea drill core at the Cretaceous-Paleogene (K-Pg) boundary (formerly the Cretaceous/Tertiary, KT boundary). The object is probably a fragment of the asteroid that produced the Chicxulub impact structure in the Yucatán 65.5 Ma ago and triggered a mass extinction (e.g., Alvarez, 1997). Terrestrial alteration phases in this fossil meteorite include hematite, clay (saponite and interlayered glauconite and smectite), Ni-Fe sulfide, and a Ni-rich metal grain ($Ni_{87}Fe_{13}$). Also present are ≤50-μm-size phosphate grains probably derived from fish scales and fish bones (Kyte, 1998).

3. Conclusions

Meteorites are delivered to Earth from at least 100 different asteroids as well as from the Moon and Mars. Some of the meteorite parent bodies melted and differentiated; they developed metal cores and basaltic crusts. Other bodies never melted, preserving materials formed in the solar nebula. Some unmelted bodies were thermally metamorphosed; many were aqueously altered. Meteorites suffered shock damage on their parent bodies, ranging from fracturing and brecciation to impact melting and devolatilization. After their formation, many samples experienced thermal metamorphism, aqueous alteration and shock metamorphism to different extents; some were altered or shocked more than once.

Martian meteorites were subjected to high shock pressures when they were launched off Mars; in contrast, meteorites ejected from small asteroids typically experienced little shock during launch. Some samples were probably in highly elliptical orbits and had relatively small perihelion distances; they may have been subject to periodic heating from solar radiation.

All the meteorites in our collections (except for a couple of small meteorite specimens brought back from the Moon along with Apollo samples) traversed the Earth's atmosphere and developed fusion crusts. The meteorites that were not immediately collected after falling experienced some degree of terrestrial weathering. All meteoritic samples, even witnessed falls stored in museum cabinets, have reacted with atmospheric water.

About 435 minerals have been identified in meteorites, about 8% of the total number of well-characterized mineral phases. Meteorite mineral species include native elements, metals and metallic alloys, carbides, nitrides and oxynitrides, phosphides, silicides, sulfides and hydroxysulfides, tellurides, arsenides and sulfarsenides, halides, oxides, hydroxides, carbonates, sulfates, molybdates, tungstates, phosphates and silico phosphates, oxalates, and silicates from all six structural groups.

The minerals in meteorites formed by numerous processes that are not all mutually distinct: (1) condensation in gaseous envelopes around evolved stars, (2) condensation in the solar nebula, (3) crystallization in CAI and AOI melts, (4) crystallization in chondrule melts, (5) exsolution during the cooling of CAIs, (6) exsolution during the cooling of chondrules and opaque assemblages, (7) annealing of amorphous material, (8) thermal metamorphism and exsolution, (9) aqueous alteration, hydrothermal alteration and metasomatism, (10) shock metamorphism, (11) condensation within impact plumes, (12) crystallization from melts in differentiated or partially differentiated bodies, (13) condensation from late- stage vapors in differentiated bodies, (14) exsolution, inversion and subsolidus redox effects within cooling igneous materials, (15) solar heating near perihelion, (16) atmospheric passage, and (17) terrestrial weathering.

Acknowledgments

We thank M. Kimura, M. E. Zolensky, M. K. Weisberg and Associate Editor K. Keil for very helpful and incisive comments. We are also grateful to M. E. Zolensky for providing some images and to S. Chow for her assistance in compiling the references. This work was supported in part by NASA grant NNX14AF39G (AER). The nanomineralogy investigations of meteorites by C. Ma were carried out at the Geological and Planetary Science Division Analytical Facility, Caltech, which is supported in part by NSF grants EAR- 0318518 and DMR-0080065. CM thanks his collaborators O. Tshauner, J. R. Beckett, G. R. Rossman, A. N. Krot, H. C. Connolly, Jr, A. R. Kampf, T. J. Zega, Y. Liu, C. Lin, L. Bindi and P. J. Steinhardt on new mineral studies. This review was solicited and handled by Associate Editor Klaus Keil.

References

Abreu, N.M., 2016. Why is it so difficult to classify Renazzo-type (CR) carbonaceous chondrites? – implications from TEM observations of matrices for the sequences of aqueous alteration. Geochim. Cosmochim. Acta 194, 91–122.
Abreu, N.M., Brearley, A.J., 2005. Carbonates in Vigarano: terrestrial, preterrestrial, or both? Meteorit. Planet. Sci. 40, 609–625.
Abreu, N.M., Brearley, A.J., 2010. Early solar system processes recorded in the matrices of two highly pristine CR3 carbonaceous chondrites, MET 00426 and QUE 99177. Geochim. Cosmochim. Acta 74, 1146–1171.
Ackermaand, D., Raase, P., 1973. Die mineralogische Zusammensetzung des Meteoriten von Kiel. Contrib. Mineral. Petrol. 39, 289–300.
Afiattalab, F., Wasson, J.T., 1980. Composition of the metal phases in ordinary chondrites: implications regarding classification and metamorphism. Geochim. Cosmochim. Acta 44, 431–446.
Agee, C.B., Wilson, N.V., McCubbin, F.M., Ziegler, K., Polyak, V.J., Sharp, Z.D., Asmerom, Y., Nunn, M.H., Shaheen, R., Thiemens, M.H., 2013. Unique meteorite from early Amazonian Mars: water-rich basaltic breccia Northwest Africa 7034. Science 339, 780–785.
Akai, J., 1988. Incompletely transformed serpentine-type phyllosilicates in the matrix of Antarctic CM chondrites. Geochim. Cosmochim. Acta 52, 1593–1599.
Akaiwa, H., 1966. Abundances of selenium, tellurium, and indium in meteorites. J. Geophys. Res. 71, 1919–1923.
Aléon, J., Krot, A.N., McKeegan, K.D., MacPherson, G.J., Ulyanov, A.A., 2005. Fine-grained, spinel-rich inclusions from the reduced CV chondrite Efremovka: II. Oxygen isotopic compositions. Meteorit. Planet. Sci. 40, 1043–1058.
Alexander, C.M.O., Hutchison, R.H., Graham, A.L., Yabuki, H., 1987. Discovery of scapolite in the Bishunpur (LL3) chondritic meteorite. Mineral. Mag. 51, 733–735.
Alexander, C.M.O., Barber, D.J., Hutchison, R.H., 1989. The microstructure of Semarkona and Bishunpur. Geochim. Cosmochim. Acta 53, 3045–3057.
Alexander, C.M.O.D., Prombo, C.A., Swan, P.D., Walker, R.M., 1991. SiC and Si3N4 in Qingzhen (EH3) (abstract). Lunar Planet. Sci. 22, 5–6.
Alexander, C.M.O.D., Swan, P., Prombo, C.A., 1994. Occurrence and implications of silicon nitride in enstatite chondrites. Meteoritics 29, 79–85.
Alvarez, W., 1997. T. rex and the Crater of Doom. Vintage Books, New York, pp. 185.
Amari, S., Lewis, R.S., Anders, E., 1995. Interstellar grains in meteorites: III. Graphite and its noble gases. Geochim. Cosmochim. Acta 59, 1411–1426.
Amelin, Y., Krot, A.N., Hutcheon, I.D., Ulyanov, A.A., 2002. Lead isotopic ages of chondrules and calcium-aluminum-rich inclusions. Science 297, 1678–1683.
Anand, M., Taylor, L.A., Nazarov, M.A., Shu, J., Mao, H.-K., Hemley, R.J., 2004. Space weathering on airless planetary bodies: clues from the lunar mineral hapkeite. PNAS 101, 6847–6851.
Anders, A., Zinner, E., 1993. Interstellar grains in primitive meteorites: Diamond, silicon carbide, and graphite. Meteoritics 28, 490–514.
Anders, E., DuFresne, E.R., Hayatsu, R., Cavaille, A., DuFresne, A., Fitch, F.W., 1964. Contaminated meteorite. Science 146, 1157–1161.
Andersen, C.A., Keil, K., Mason, B., 1964. Silicon oxynitride: a meteoritic mineral. Science 146, 256–257.
Armstrong, J.T., El Goresy, A., Wasserburg, G.J., 1985a. Willy: a prize noble Ur-Fremdling— its history and implications for the formation of Fremdlinge and CAI. Geochim. Cosmochim. Acta 49, 1001–1022.
Armstrong, J.T., Hutcheon, I.D., Wasserburg, G.I., 1985b. Ni-Pt-Ge-rich fremdlinge: indicators of a turbulent early solar nebula (abstract). Meteoritics 20, 603–604.
Armstrong, J.T., Hutcheon, I.D., Wasserburg, G.J., 1987. Zelda and company: petrogenesis of sulfide-rich Fremdlinge and constraints on solar nebula processes. Geochim. Cosmochim. Acta 51, 3155–3173.
Ashworth, J.R., 1979. Two kinds of exsolution in chondritic olivine. Mineral. Mag. 43, 535–538.

Baecker, B., Rubin, A.E., Wasson, J.T., 2015. Overgrowth layers on pyroxene in an FeO-rich porphyritic chondrule in CO3.0 Y-81020. Meteorit. Planet. Sci. 50, abstract#5082.

Bagnall, P.M., 1991. The Meteorite and Tektite Collector's Handbook. A Practical Guide to their Acquisition, Preservation and Display. Willmann-Bell, Richmond, VA (USA).

Barber, D.J., 1981. Matrix phyllosilicates and associated minerals in C2M carbonaceous chondrites. Geochim. Cosmochim. Acta 45, 945–970.

Barber, D.J., Beckett, J.R., Paque, J.M., Stolper, E., 1994. A new titanium-bearing calcium aluminosilicate phase: II. Crystallography and crystal chemistry of grains formed in slowly cooled melts with bulk compositions of calcium-aluminum-rich inclusions. Meteoritics 29, 682–690.

Basaltic Volcanism Study Project (BVSP), 1981. Basaltic Volcanism on the Terrestrial Planets. Pergamon Press, New York, pp. 1286.

Bass, M.N., 1970. Textural relations of sulfide, sulfate and sulfur in Orgueil meteorite. Meteoritics 5, 180–181.

Basu Sarbadhikari, A., Babu, E.V.S.S.K., Vijaya Kumar, T., Chennaoui Aoudjehane, H., 2016. Martian meteorite Tissint records unique petrogenesis among the depleted shergottites. Meteorit. Planet. Sci., 1–23.

Beard, A., Downes, H., Howard, K.T., 2009. Hydrated silica (opal) in a polymict ureilite, EET 83309. Meteorit. Planet. Sci. 72, 5027.pdf.

Beard, A., Downes, H., Howard, K.T., 2011. Significance of opal in ureilites- delivery of H2O to the inner solar system? Meteorit. Planet. Sci. 74, 5088.pdf.

Beck, P., Gillet, P., Gautron, L., Daniel, I., El Goresy, A., 2004. A new natural high-pressure (Na,Ca)-hexaluminosilicate [(CaxNa1-x)Al3 + xSi3-xO11] in shocked Martian meteorites. Earth Planet. Sci. Lett. 219, 1–12.

Beckett, J.R., Grossman, L., 1988. The origin of type C inclusions from carbonaceous chondrites. Earth Planet. Sci. Lett. 89, 1–14.

Beckett, J.R., Stolper, E., 1994. The stability of hibonite, melilite, and other aluminous phases in silicate melts: implications for the origin of hibonite-bearing inclusion from carbonaceous chondrites. Meteoritics 29, 41–65.

Bell, A.S., Shearer, C.K., Maarten deMoor, J., Provencio, P., 2015. Using the sulfide replacement petrology in lunar breccia 67915 to construct a thermodynamic model of S-bearing fluid in the lunar crust. Geochim. Cosmochim. Acta 171, 50–60.

Benedix, G.K., McCoy, T.J., Keil, K., Bogard, D.D., Garrison, D.H., 1998. A petrologic and isotopic study of winonaites: evidence for early partial melting, brecciation, and metamorphism. Geochim. Cosmochim. Acta 62, 2535–2553.

Benedix, G.K., McCoy, T.J., Keil, K., Love, G.1, 2000. A petrologic study of the IAB iron meteorites: constraints on the formation of the IAB-Winonaite parent body. Meteorit. Planet. Sci. 35, 1127–1141.

Benedix, G.K., McCoy, T.J., Lauretta, D.S., 2003. Is NWA 1463 the most primitive winonaite? Meteorit. Planet. Sci. 38, abstract#5125.

Berg, T., Maul, J., Schönhense, G., Marosits, E., Hoppe, P., Ott, U., Palme, H., 2009. Direct evidence for condensation in the early solar system and implications for nebular cooling rates. Astrophys. J. 702, L172.

Berger, E., Lauretta, D.S., Zega, T.J., Keller, L.P., 2016. Heterogeneous histories of Ni-bearing pyrrhotite and pentlandite grains in the CI chondrites Orgueil and Alais. Meteorit. Planet. Sci. 51, 1813–1829.

Berkley, J.L., 1986. Four antarctic ureilites: petrology and observations on ureilite petrogenesis. Meteoritics 21, 169–187.

Berkley, J.L., Jones, J.H., 1982. Primary igneous carbon in ureilites: petrological implications. Proc. Lunar Planet. Sci. Conf. 13, A353–A364.

Berkley, J.L., Brown, H.G., Keil, K., Carter, N.L., Mercier, J.C.C., Huss, G., 1976. The Kenna ureilite: an ultramafic rock with evidence for igneous, metamorphic, and shock origin. Geochim. Cosmochim. Acta 40, 1429–1437.

Berkley, J.L., Taylor, G.J., Keil, K., Healey, J.T., 1978. Fluorescent accessory phases in the carbonaceous matrix of ureilites. Geophys. Res. Lett. 5, 1075–1078.

Berkley, J.L., Taylor, G.J., Keil, K., Harlow, G.E., Prinz, M., 1980. The nature and origin of ureilites. Geochim. Cosmochim. Acta 44, 1579–1597.

Berlin, J., Stöffler, D., 2004. Modification of the Van Schmus and Wood petrologic classification for lithic fragments in the chondritic breccia Rumuruti. Lunar Planet. Sci. Conf., 35.

Berlin, J., Lingemann, C.M., Stöffler, D., 2001. Occurrence of noble metal phases in fragments of different petrologic type in the Rumuruti chondrite. Meteorit. Planet. Sci. 36.

Bernatowicz, T.J., Amari, S., Zinner, E.K., Lewis, R.S., 1991. Interstellar grains within interstellar grains. Astrophys. J. 373, L73–L76.

Bernatowicz, T.J., Cowsik, R., Gibbons, P.C., Lodders, K., Fegley, B., Amari, S., Lewis, R.S., 1996. Constraints on stellar grain formation from presolar graphite in the Murchison meteorite. Astrophys. J. 472, 760.

Bernatowicz, T., Bradley, J.P., Amari, S., Messenger, S., Lewis, R.S., 1999. New kinds of massive star condensates in a presolar graphite from Murchison. Lunar Planet. Sci. 30, 1392.pdf.

Berwerth, F., 1902. Der Meteoreisenzwilling von Mukerop, Bezirk Gibeon, Deutsch-Südwest- Afrika. Sitzungsber. Akad. Wiss. 11, 646–667.

Bevan, A.W.R., Grady, M.M., 1988. Mount Morris (Wisconsin): a fragment of the IAB iron Pine River? Meteoritics 23, 349–352.

Bevan, A.W.R., Bevan, J.C., Francis, J.G., 1977. Amphibole in the Mayo Belwa meteorite: First occurrence in an enstatite achondrite. Mineral. Mag. 41, 531–534.

Bevan, A.W.R., Kinder, J., Axon, H.J., 1979. A metallographic study of the iron meteorite Verkhne Dnieprovsk (BM 51183). Mineral. Mag. 43, 149–154.

Bevan, A.W.R., Kinder, J., Axon, H.J., 1981. Complex shock-induced Fe-Ni-S-Cr-C melts in The Haig (IIIA) iron meteorite. Meteoritics 16, 261–267.

Bild, R.W., 1977. Silicate inclusions in group IAB irons and a relation to the anomalous stones Winona and Mt. Morris (Wis.). Geochim. Cosmochim. Acta 41, 1439–1456.

Bindi, L., Steinhardt, P.J., Yao, N., Lu, P.J., 2011. Icosahedrite, Al63Cu24Fe13, the first natural quasicrystal. Am. Mineral. 96, 928–931.

Bindi, L., Yao, N., Lin, C., Hollister, L.S., MacPherson, G.J., Poirier, G.R., Andronicos, C.L., Distler, V.V., Eddy, M.P., Kostin, A., 2014. Steinhardtite, a new body-centered-cubic allotropic form of aluminum from the Khatyrka CV3 carbonaceous chondrite. Am. Mineral. 99, 2433–2436.

Bindi, L., Yao, N., Lin, C., Hollister, L.S., Andronicos, C.L., Distler, V.V., Eddy, M.P., Kostin, A., Kryachko, V., MacPherson, G.J., 2015. Decagonite, Al71Ni24Fe5, a quasicrystal with decagonal symmetry from the Khatyrka CV3 carbonaceous chondrite. Am. Mineral. 100, 2340–2343.

Bindi, L., Chen, M., Xie, X., 2017. Discovery of the Fe-analogue of akimotoite in the shocked Suizhou L6 chondrite. Sci. Rep. 7, Article number 42674.

Binns, R., 1967. Stony meteorites bearing maskelynite. Nature 213, 1111–1112.

Bischoff, A., 2000. Mineralogical characterization of primitive, type-3 lithologies in Rumuruti chondrites. Meteorit. Planet. Sci. 35, 699–706.

Bischoff, A., Keil, K., 1984. Al-rich objects in ordinary chondrites: related origin of carbonaceous and ordinary chondrites and their constituents. Geochim. Cosmochim. Acta 48, 693–709.

Bischoff, A., Palme, H., 1987. Composition and mineralogy of refractory metal-rich assemblages from a Ca,Al-rich inclusion in the Allende meteorite. Geochim. Cosmochim. Acta 51, 2733–2748.

Bischoff, A., Stöffler, D., 1992. Shock metamorphism as a fundamental process in the evolution of planetary bodies: information from meteorites. Eur. J. Mineral. 4, 707–756.

Bischoff, A., Palme, H., Ash, R.D., Clayton, R.N., Schultz, L., Herpers, U., Stoffler, D., Grady, M.M., Pillinger, C.T., Spettel, B., Weber, H., Grund, T., Endress, M., Weber, D., 1993a. Paired Renazzo-type (CR) carbonaceous chondrites from the Sahara. Geochim. Cosmochim. Acta 57, 1587–1603.

Bischoff, A., Palme, H., Schultz, L., Weber, D., Weber, H.W., Spettel, B., 1993b. Acfer 182 and paired samples, an iron-rich carbonaceous chondrite: Similarities with ALH 85085 and relationship to CR chondrites. Geochim. Cosmochim. Acta 57, 2631–2648.

Bischoff, A., Geiger, T., Palme, H., Spettel, B., Schultz, L., Scherer, P., Loeken, T., Bland, P., Clayton, R.N., Mayeda, T.K., Herpers, U., Meltzow, B., Michel, R., Dittrich-Hannen, B., 1994. Acfer 217-A new member of the Rumuruti chondrite group (R). Meteoritics 29, 264–274.

Bischoff, A., Vogel, N., Roszjar, J., 2011. The Rumuruti chondrite group. Chem. Erde 71, 101–133.

Blake, D., Fleming, R.H., Bunch, T.E., 1989. Identification and characterization of a carbonaceous titanium containing interplanetary dust particle (abstract). Lunar. Planet. Sci. Conf. 20, 84–85.

Blum, J., 2004. Grain growth and coagulation. Astron. Soc. Pacific Conf. Ser. 309, 369–391.

Blum, J.D., Wasserburg, G.J., Hutcheon, I.D., Beckett, J.R., Stolper, E.M., 1988. 'Domestic' origin of opaque assemblages in refractory inclusions in meteorites. Nature 331, 405–409.

Blum, J.D., Wasserburg, G.J., Hutcheon, I.D., Beckett, J.R., Stolper, E.M., 1989. Origin of opaque assemblages in CV3 meteorites: implications for nebular and planetary processes. Geochim. Cosmochim. Acta 53, 543–556.

Boesenberg, J.S., Hewins, R.H., 2010. An experimental investigation into the metastable formation of phosphoran olivine and pyroxene. Geochim. Cosmochim. Acta 74, 1923–1941.

Bogard, D.D., 1995. Impact ages of meteorites: a synthesis. Meteoritics 30, 244–268.

Bogard, D.D., Husain, L., Wright, R.J., 1976. 40Ar-39Ar dating of collisional events in chondritic parent bodies. J. Geophys. Res. 81, 5664–5678.

Bogard, D.D., Taylor, G.J., Keil, K., Smith, M.R., Schmitt, R.A., 1985. Impact melting of the Cachari eucrite 3.0 Gy ago. Geochim. Cosmochim. Acta 49, 941–946.

Bogard, D.D., Garrison, D.H., Norman, M., Scott, E.R.D., Keil, K., 1995. 39Ar-40Ar age and petrology of Chico: large-scale impact melting on the L-chondrite parent body. Geochim. Cosmochim. Acta 59, 1383–1400.

Bonal, L., Quirico, E., Bourot-Denise, M., 2004. Petrologic type of CV3 chondrites as revealed by Raman spectroscopy of organic matter. Lunar Planet. Sci., 1562.

Bose, M., Floss, C., Stadermann, F.J., 2010. An investigation into the origin of Fe-rich presolar silicates in Acfer 094. Astrophys J. 714, 1624–1630.

Bouvier, A., Wadhwa, M., 2009. Synchronizing the absolute and relative clocks: Pb-Pb and Al-Mg systematics in CAIs from the Allende and NWA 2364 CV3 chondrites. Lunar Planet. Sci. Conf., 40, abstracct#2184.

Bouvier, A., Wadhwa, M., Bullock, E.S., MacPherson, G.J., 2010. Pb-Pb dating of a CAI from the reduced CV3 chondrite Vigarano. Meteorit. Planet. Sci. 73, 5400.

Boyd, F.R., England, J.L., 1965. The rhombic enstatite- clinoenstatite inversion. Carnegie Inst. Washington, Ann. Rpt. Dir. Geophys. Lab. 1964–65, 117–120.

Boynton, W.V., 1975. Fractionation in the solar nebula: condensation of yttrium and the rare earth elements. Geochim. Cosmochim. Acta 39, 569–584.

Boynton, W.V., Starzyk, P., Schmitt, R., 1976. Chemical evidence for the genesis of the ureilites, the achondrite Chassigny and the nakhlites. Geochim. Cosmochim. Acta 40, 1439–1447.

Bradley, J.P., 2005. Interplanetary Dust Particles. In: Davis, A.M. (Ed.), Meteorites, Comets, and Planets: Treatise on Geochemistry. Elsevier B. V., Amsterdam, The Netherlands, p. 689.

Brearley, A.J., 1993a. Matrix and fine- grained rims in the unequilibrated CO3 chondrite, ALHA77307: Origins and evidence for diverse, primitive nebular dust components. Geochim. Cosmochim. Acta 57, 1521–1550.

Brearley, A.J., 1993b. Occurrence and possible significance of rare Ti oxides (Magneli phases) in carbonaceous chondrite matrices. Meteoritics 28, 590–595.
Brearley, A.J., 1995. Aqueous alteration and brecciation in Bells, an unusual, saponite-bearing, CM chondrite. Geochim. Cosmochim. Acta 59, 2291–2317.
Brearley, A.J., 1996. Disordered biopyriboles in the Allende meteorite: first extraterrestrial occurrence (abstract). Geol. Soc. Am. Abst. with Prog. 28, A103.
Brearley, A.J., 1997. Disordered biopyriboles, amphibole, and talc in the Allende meteorite: products of nebular or parent body aqueous alteration? Science 276, 1103–1105.
Brearley, A.J., 2006. The action of water. Meteorites and the early solar system II. In: Lauretta, D.S., McSween, H.Y. (Eds.). Univ. Arizona Press, Tucson, pp. 587–624.
Brearley, A.J., Prinz, M., 1992. CI chondrite-like clasts in the Nilpena polymict ureilite: Implications for aqueous alteration processes in CI chondrites. Geochim. Cosmochim. Acta 56, 1373–1386.
Breen, J.P., Rubin, A.E., Wasson, J.T., 2016. Variations in impact effects among IIIE iron meteorites. Meteorit. Planet. Sci. 51, 1611–1631.
Briani, G., Quirico, E., Gounelle, M., Paulhiac-Pison, M., Montagnac, G., Beck, P., Orthous- Daunay, F.-R., Bonal, L., Jacquet, E., Kearsley, A., 2013. Short duration thermal metamorphism in CR chondrites. Geochim. Cosmochim. Acta 122, 267–279.
Bridges, J.C., Catling, D.C., Saxton, J.M., Swindle, T.D., Lyon, I.C., Grady, M.M., 2001. Alteration assemblages in Martian meteorites: Implications for near-surface processes. In: Chronology and evolution of Mars. Springer, Springer, pp. 365–392.
Brigham, C.A., Yabuki, H., Ouyang, Z., Murrell, M.T., El Goresy, A., Burnett, D.S., 1986. Silica-bearing chondrules and clasts in ordinary chondrites. Geochim. Cosmochim. Acta 50, 1655–1666.
Britt, D.T., Pieters, C.M., 1994. Darkening in black and gas- rich ordinary chondrites: the spectral effects of opaque morphology and distribution. Geochim. Cosmochim. Acta 58, 3905–3919.
Britvin, S.N., Guo, X.Y., Kolomensky, V.D., Boldyreva, M.M., Kretser, Y.L., Yagovkina, M.A., 2001. Cronusite, Ca0. 2(H2O)2CrS2, a new mineral from the Norton County enstatite achondrite. Zap. Vseross. Mineral. Obshch. 130, 29–36.
Britvin, S.N., Rudashevsky, N.S., Krivovichev, S.V., Burns, P.C., Polekhovsky, Y.S., 2002. Allabogdanite,(Fe, Ni)2P, a new mineral from the Onello meteorite: the occurrence and crystal structure. Am. Mineral. 87, 1245–1249.
Britvin, S.N., Bogdanova, A.N., Boldyreva, M.M., Aksenova, G.Y., 2008. Rudashevskyite, the Fe-dominant analogue of sphalerite, a new mineral: description and crystal structure. Am. Mineral. 93, 902–909.
Britvin, S.N., Krivovichev, S.V., Armbruster, T., 2015. Ferromerrillite, Ca9NaFe2+ (PO4) 7, a new mineral from the Martian meteorites, and some insights into merrillite-tuite transformation in shergottites. Eur. J. Mineral. 28, ejm2508_pap_gsw.
Brown, H., Kullerud, G., Nichiporuk, W., 1953. A Bibliography on Meteorites. University of Chicago Press, Chicago.
Browning, L., McSween, H., Zolensky, M., 1996. Correlated alteration effects in CM carbonaceous chondrites. Geochim. Cosmochim. Acta 60, 2621–2633.
Brownlee, A.J., Rajan, R.S., 1973. Micrometeorite craters discovered on chondrule-like objects from Kapoeta meteorite. Science 182, 1341–1344.
Buchanan, P.C., Zolensky, M.E., Reid, A.M., 1993. Carbonaceous chondrite clasts in the howardites Bholghati and EET 87513. Meteoritics 28, 659–682.
Buchwald, V.F., 1975. Handbook of Iron Meteorites. Univ. California Press.
Buchwald, V.F., 1977. The mineralogy of iron meteorites. Philos. Trans. R. Soc. Lond. A 286, 453–491.
Buchwald, V.F., 1984. Phosphate minerals in meteorites and lunar rocks. In: Nriagu, J.O., Moore, P.B. (Eds.), Phosphate Minerals. Springer-Verlag, Heidelberg, pp. 199–214.
Buchwald, V.F., 1989. Mineralogi og Reaktionsmodeller ved Korrosion of Jordfundne Jergenstande (Meteoritter og Oldsager) , Lyngby Denmark.
Buchwald, V.F., 1990. A new Danish iron meteorite, Felsted, and a new Danish law, involving meteorites (abstract). Meteoritics 25, 351–352.
Buchwald, V.F., Clarke, R.S., 1988. Akaganeite, not lawrencite, corrodes Antarctic iron meteorites (abstract). Meteoritics 23, 261.
Buchwald, V.F., Clarke, R.S., 1989. Corrosion of Fe-Ni alloys by Cl-containing akaganeite (beta- FeOOH): the Antarctic meteorite case. Am. Mineral. 74, 656–667.
Buchwald, V.F., Scott, E.R.D., 1971. First nitride (CrN) in iron meteorites. Nature 233, 113–114.
Buddhue, J.D., 1957. The Oxidation and Weathering of Meteorites. University of New Mexico, Albuquerque, pp. 161.
Bunch, T.E., Keil, K., Snetsinger, K.G., 1967. Chromite composition in relation to chemistry and texture of ordinary chondrites. Geochim. Cosmochim. Acta 31, 1569–1582.
Bunch, T.E., Olsen, E., 1968. Potassium feldspar in Weekeroo Station, Kodaikanal, and Colomera iron meteorites. Science 160, 1223–1225.
Bunch, T.E., Keil, K., Olsen, E., 1970. Mineralogy and petrology of silicate inclusions in iron meteorites. Contrib. Mineral. Petrol. 25, 297–340.
Bunch, T.E., Wittke, J.H., Irving, A.J., 2014. The Al Haggounia fossil or paleo meteorite problem, Accessed December 15, 2015 http://www.cefns.nau.edu/geology/naml/Meteorite/Al_Haggouni a.html.
Burbine, T.H., Buchanan, P.C., Binzel, R.P., Bus, S.J., Hiroi, T., Hinrichs, J.L., Meibom, A., Mccoy, T.J., 2001. Vesta, Vestoids, and the howardite, eucrite, diogenite group: relationships and the origin of spectral differences. Meteorit. Planet. Sci. 36, 761–781.
Burbine, T.H., McCoy, T.J., Meibom, A., Gladman, B., Keil, K., 2002. Meteoritic Parent Bodies: Their Number and Identification. In: Bottke Cellino, J.W.F.A., Paolicchi, P., Binzel, R.P. (Eds.), Asteroids III. The University of Arizona Press, Tucson, pp. 653–667.
Burton, A.S., Glavin, D.P., Elsila, J.E., Dworkin, J.P., Jenniskens, P., Yin, Q.-Z., 2014. The amino acid composition of the Sutter's Mill CM2 carbonaceous chondrite. Meteorit. Planet. Sci. 49, 2074–2086.
Buseck, P.R., 1968. Mackinawite, pentlandite and native copper from the Newport pallasite. Mineral. Mag. 36, 717–725.
Buseck, P.R., 1977. Pallasite meteorites-mineralogy, petrology and geochemistry. Geochim. Cosmochim. Acta 41, 711–740.
Buseck, P.R., Hua, X., 1993. Matrices of carbonaceous chondrite meteeorites. Annu. Rev. Earth Planet. Sci. 21, 255–305.
Buseck, P.R., Keil, K., 1966. Meteoritic rutile. Am. Mineral. 51, 1506–1515.
Busemann, H., Alexander, M.D., Nittler, L.R., 2007. Characterization of insoluble organic matter in primitive meteorites by microRaman spectroscopy. Meteorit. Planet. Sci. 42, 1387–1416.
Butler, I.B., Rickard, D., 2000. Framboidal pyrite formation via the oxidation of iron (II) monosulfide by hydrogen sulphide. Geochim. Cosmochim. Acta 64, 2665–2672.
Caillet Komorowski, C., El Goresy, A., Miyahara, M., Boudouma, O., Ma, C., 2012. Discovery of Hg–Cu-bearing metal-sulfide assemblages in a primitive H-3 chondrite: towards a new insight in early solar system processes. Earth Planet. Sci. Lett. 349, 261–271.
Campbell, A.J., Humayun, M., Weisberg, M.K., 2002. Siderophile element constraints on the formation of metal in the metal-rich chondrites Bencubbin, Weatherford, and Gujba. Geochim. Cosmochim. Acta 66, 647–660.
Chan, M.A., Bowen, B.B., Parry, W.T., Ormö, J., Komatsu, G., 2005. Red rock and red planet diagenesis: comparisons of Earth and Mars concretions. GSA Today 15, 4–10.
Chao, E.C.T., Fahey, J.J., Littler, J., Milton, D.J., 1962. Stishovite, SiO2, a very high pressure new mineral from Meteor Crater, Arizona. J. Geophys. Res. 67, 419–421.
Chao, E.C.T., Best, J.B., Minkin, J.A., 1972. Apollo 14 glasses of impact origin and their parent rock types. Lunar Planet. Sci. Conf. Proc., 907.
Chen, M., Sharp, T.G., El Goresy, A., Wopenka, B., Xie, X., 1996. The majorite-pyrope-magnesiowustite assemblage: constraints on the history of shock veins in chondrites. Science 271, 1570–1573.
Chen, M., Shu, J., Mao, H.K., 2008. Xieite, a new mineral of high-pressure $FeCr_2O_4$ polymorph. Chin. Sci. Bull. 53, 3341–3345.
Chennaoui-Aoudjehane, H., Jambon, A., Rjimati, E., 2007. Al Haggounia (Morocco) strewn field. Meteorit. Planet. Sci. 42, A30.
Chennaoui-Aoudjehane, H., Jambon, A., Rjimati, E., Jull, A.J.T., Leclerc- Giscard, M.D., 2009. The Late Quaternary fall at Al Haggounia (Morocco): the 14C evidence. Meteorit. Planet. Sci. 44, A100.
Chikami, J., Mikouchi, T., Takeda, H., Miyamoto, M., 1997. Mineralogy and cooling history of the calcium-aluminum-chromium enriched ureilite, Lewis Cliff 88774. Meteorit. Planet. Sci. 32, 343–348.
Chizmadia, L.J., Rubin, A.E., Wasson, J.T., 2002. Mineralogy and petrology of amoeboid olivine inclusions in CO3 chondrites: relationship to parent-body aqueous alteration. Meteorit. Planet. Sci. 37, 1781–1796.
Choe, W.H., Huber, H., Rubin, A.E., Kallemeyn, G.W., Wasson, J.T., 2010. Compositions and taxonomy of 15 unusual carbonaceous chondrites. Meteorit. Planet. Sci. 45, 531–554.
Choi, B., Ouyang, X., Wasson, J.T., 1995. Classification and origin of IAB and IIICD iron meteorites. Geochim. Cosmochim. Acta 59, 593–612.
Choi, B.-G., Huss, G.R., Wasserburg, G.J., Gallino, R., 1998a. Presolar corundum and spinel in ordinary chondrites: origins from AGB stars and a supernova. Science 282, 1284–1289.
Choi, B.-G., McKeegan, K.D., Krot, A.N., Wasson, J.T., 1998b. Extreme oxygen-isotope compositions in magnetite from unequilibrated ordinary chondrites. Nature 392, 577–579.
Christophe Michel-Levy, M., 1976. La matrice noire et blanche de la chondrite de Tieschitz (H3). Earth Planet. Sci. Lett. 30, 143–150.
Chukanov, N., Pekov, I., Levitskaya, L., Zadov, A., 2009. Droninoite, $Ni_3Fe^{3+}{}_2Cl(OH)8\bullet 2H2O$, a new hydrotalcite-group mineral species from the weathered Dronino meteorite. Geology of Ore Deposits 51, 767–773.
Clarke, R.S., Scott, E.R.D., 1980. Tetrataenite–ordered FeNi, a new mineral in meteorites. Am. Mineral. 65, 624–630.
Clarke Jr., R.S., Appleman, D.E., Ross, D.R., 1981. An Antarctic iron meteorite contains preterrestrial impact- produced diamond and lonsdaleite. Nature 291, 396–398.
Clarke, R.S., Buchwald, V.F., Olsen, E., 1990. Anomalous ataxite from Mount Howe, Antarctica. Meteoritics 25, 354.
Clayton, R.N., Mayeda, T.K., 1996. Oxygen isotope studies of achondrites. Geochim. Cosmochim. Acta 60, 1999–2017.
Clayton, R.N., Mayeda, T.K., 1999. Oxygen isotope studies of carbonaceous chondrites. Geochim. Cosmochim. Acta 63, 2089–2104.
Clayton, R.N., Mayeda, T.K., Goswami, J.N., Olsen, E.J., 1991. Oxygen isotope studies of ordinary chondrites. Geochim. Cosmochim. Acta 55, 2317–2337.
Clément, D., Mutschike, H., Klein, R., Jäger, C., Dorschner, J., Sturm, E., Henning, T., 2005. Detection of silicon nitride particles in extreme carbon stars. Astrophys. J. 621, 985–990.
Colson, R.O., 1992. Mineralization on the moon? Theoretical considerations of Apollo 16 'rusty rocks', sulfide replacement in 67016, and surface-correlated volatiles on lunar volcanic glass. Lunar Planet. Sci., 427–436.

Connolly, H.C., Hewins, R.H., 1995. Chondrules as products of dust collisions with totally molten droplets within a dust-rich nebular environment: an experimental investigation. Geochim. Cosmochim. Acta 59, 3231–3246.
Connolly, H.C., Zipfel, J., Grossman, J.N., Folco, L., Smith, C., Jones, R.H., Righter, K., Zolensky, M., Russell, S.S., Benedix, G.K., 2006. The Meteoritical Bulletin, no. 90, 2006 September. Meteorit. Planet. Sci. 41, 1383–1418.
Consolmagno, G.J., Drake, M.J., 1977. Composition and evolution of the eucrite parent body: evidence from rare earth elements. Geochim. Cosmochim. Acta 41, 1271–1282.
Croat, T., Bernatowicz, T., Amari, S., Messenger, S., Stadermann, F.J., 2003. Structural, chemical, and isotopic microanalytical investigations of graphite from supernovae. Geochem. Cosmochim. Acta 67, 4705–4725.
Cyr, K.E., Sears, W.D., Lunine, J.I., 1998. Distribution and evolution of water ice in the solar nebula: implications for solar system body formation. Icarus 135, 537–548.
Dai, Z.R., Bradley, J.P., Joswiak, D.J., Brownlee, D.E., Hill, H.G.M., Genge, M.J., 2002. Possible in situ formation of meteoritic nanodiamonds in the early Solar System. Nature 418, 157–159.
Dartois, E., Engrand, C., Brunetto, R., Duprat, J., Pino, T., Quirico, E., Remusat, L., Bardin, N., Briani, G., Mostefaoui, S., Morinaud, G., Crane, B., Szwec, N., Delauche, L., Jamme, F., Sandt, Ch., Dumas, P., 2013. Ultracarbonaceous Antarctic micrometeorites, probing the Solar Ssytem beyond the nitrogen snow- line. Icarus 224, 243–252.
Davis, A.M., 1991. Ultrarefractory inclusions and the nature of the group II REE fractionation (abstract). Meteoritics 26, 330.
Davis, A.M., 2005. Meteorites, Comets, and Planets. Elsevier, Amsterdam, The Netherlands, pp. 737.
Davis, A.M., Richter, F.M., 2005. Condensation and evaporation of solar system material. In: Davis, A.M. (Ed.), Meteorites, Comets, and Planets. Elsevier, Oxford, pp. 407–430.
Davis, A.M., MacPherson, G.J., Clayton, R.N., Mayeda, T.K., Sylvester, P.J., Grossman, L., Hinton, R.W., Laughlin, J.R., 1991. Melt solidification and late-stage evaporation of a FUN inclusion from the Vigarano C3 V chondrite. Geochim. Cosmochim. Acta 55, 621–637.
Dehart, J.M., Lofgren, G.E., 1995. Formation and metamorphism in enstatite chondrites. Lunar Planet. Sci. 26, 325–326.
DeHart, J.M., Lofgren, G.E., Lu, J., Benoit, P.H., Sears, D.W.G., 1992. Chemical and physical studies of chondrules X: cathodoluminescence and phase composition studies of metamorphism and nebular processes in chondrules of type 3 ordinary chondrites. Geochim. Cosmochim. Acta 56, 3791–3807.
Delaney, J.S., Sutton, S.R., 1988. Lewis Cliff 86010, an ADORable Antarctican (abstract). Lunar Planet. Sci. 19, 265–266.
Delaney, J.S., Nehru, C.E., Prinz, M., Harlow, G.E., 1981. Metamorphism in mesosiderites. Proc. Lunar Planet. Sci. Conf. 12B, 1315–1342.
Delaney, J.S., Prinz, M., Takeda, H., 1984. The polymict eucrites. Proc. Lunar Planet. Sci. Conf. 15, C251–C288.
Dobrică, E., Brearley, A.J., 2014. Widespread hydrothermal alteration minerals in the fine-grained matrices of the Tieschitz unequilibrated ordinary chondrite. Meteorit. Planet. Sci. 49, 1323–1349.
Dodd, R.T., 1981. Meteorites – A Petrologic-Chemical Synthesis. Cambridge, New York, pp. 368.
Dodd, R.T., Jarosewich, E., 1979. Incipient melting and shock classification of L-group chondrites. Earth Planet. Sci. Lett. 44, 335–340.
Dodd, R.T., Jarosewich, E., 1982. The compositions of incipient shock melts in L6 chondrites. Earth Planet. Sci. Lett. 59, 355–363.
Dodd, R.T., Van Schmus, W.R., Marvin, U.B., 1965. Merrihueite, a new alkali-ferromagnesian silicate from the Mezö-Madaras chondrite. Science 149, 972–974.
Dodd, R.T., Van Schmus, W.R., Marvin, U.B., 1966. Significance of iron-rich silicate in the Mezö-Madaras chondrite. Am. Mineral. 51, 1177–1191.
Dodd, R.T., Van Schmus, W.R., Koffman, D.M., 1967. A survey of the unequilibrated ordinary chondrites. Geochim. Cosmochim. Acta 31, 921–951.
Dominik, C., Blum, J., Cuzzi, J., Wurm, G., 2006. Growth of dust as th. In: tial step toward planet formation in: Reipurth, B., Jewitt, D., Keil, K. (Eds.), Protostars and Planets V. University of Arizona Press, Tucson, pp. 783–800.
Downes, H., Beard, A.D., Franchi, I.A., Greenwood, R.C., 2016. Origin of opal (hydrated silica) in polymict ureilites. Lunar Planet. Sci. 47, abstract#1443.
Duke, M.B., Silver, L.T., 1967. Petrology of eucrites, howardites and mesosiderites. Geochim. Cosmochim. Acta 31, 1637–1665.
Dunn, T.L., Gross, J., Ivanova, M.A., Runyon, S.E., Bruck, A.M., 2016. Magnetite in the unequilibrated CK chondrites: implications for metamorphism and new insights into the relationship between the CV and CK chondrites. Meteorit. Planet. Sci.
Ebata, S., Yurimoto, H., 2008. Identification of silicate and carbonaceous presolar grains in the type 3 enstatite chondrites. In: AIP Conference Proceeding, American Institute of Physics, pp. 412–414.
Ebata, S., Nagashima, K., Itoh, S., Kobayashi, S., Sakamoto, N., Fagan, T.J., Yurimoto, H., 2006. Presolar silicate grains in enstatite chondrites. Lunar Planet. Sci. 37, abstract#1619.
Ebata, S., Fagan, T.J., Yurimoto, H., 2007. Identification of silicate and carbonaceous presolar grains in the Type 3 enstatite chondrite ALHA81189. Meteorit. Planet. Sci. 42, 5150.
Ebata, S., Fagan, T.J., Yurimoto, H., 2008. Identification of silicate and carbonaceous presolar grains by SIMS in the type-3 enstatite chondrite ALHA81189. Appl. Surf. Sci. 255, 1468–1471.
Ebel, D.S., 2006. Condensation of rocky material in astrophysical environments. Meteorites and the early solar system II. In: Lauretta, D.S., McSween, H.Y. (Eds.). Univ. Arizona Press, Tucson, pp. 253–277.
Ebel, D.S., Grossman, L., 2000. Condensation in dust-enriched systems. Geochim. Cosmochim. Acta 64, 339–366.
Elardo, S.M., Shearer, C.K., 2014. Magma chamber dynamics recorded by oscillatory zoning in pyroxene and olivine phenocrysts in basaltic lunar meteorite Northwest Africa 032. Am. Mineral. 99, 355–368.
El Goresy, A., 1976. Opaque oxide minerls in meteorites. In: Rumble, D. (Ed.), Oxide Minerals. Mineralogical Society of America, Southern Printing Company, Blacksburg, Virginia, pp. EG47–EG72.
El Goresy, A., Nagel, K., Dominik, B., Ramdohr, P., 1977. Fremdlinge: potential presolar material in Ca-Al-rich inclusions of Allende. Meteoritics 12, 215–216.
El Goresy, A., Nagel, K., Ramdohr, P., 1978. Fremdlinge and their noble relatives. Proc. Lunar Planet. Sci. Conf. 9, 1279–1303.
El Goresy, A., Wopenka, B., Chen, M., Weinbruch, S., Sharp, T., 1997. Evidence for two different shock induced high-pressure events and alkali-vapor metasomatism in Peace River and Tenham (L6) chondrites. Lunar Planet. Sci. 28, abstract#1044.
El Goresy, A., Yabuki, H., Ehlers, K., Woolum, D., Pernicka, E., 1988. Qingzhen and Yamato-691: a tentative alphabet for the EH chondrites. Proc. NIPR Symp. Antarct. Meteorites 1, 65–101.
El Goresy, A., Dera, P., Sharp, T.G., Prewitt, C.T., Chen, M., Dubrovinsky, L., Wopenka, B., Boctor, N.Z., Hemley, R.J., 2008. Seifertite, a dense orthorhombic polymorph of silica from the Martian meteorites Shergotty and Zagami. Eur. J. Mineral. 20, 523–528.
El Goresy, A., Boyer, M., Miyahara, M., 2011. Almahata Sitta MS-17 EL-3 chondrite fragment: contrasting oldhamite assemblages in chondrules and matrix and significant oldhamite REE- patterns. Meteorit. Planet. Sci. 46, abstract#5079.
El Goresy, A., Gillet, P., Miyahara, M., Ohtani, E., Ozawa, S., Beck, P., Montagnac, G., 2013. Shock-induced deformation of Shergottites: shock-pressures and perturbations of magmatic ages on Mars. Geochim. Cosmochim. Acta 101, 233–262.
Endress, M., Bischoff, A., 1996. Carbonates in CI chondrites: Clues to parent body evolution. Geochim. Cosmochim. Acta 60, 489–507.
Endress, M., Keil, K., Bischoff, A., Spettel, B., Clayton, R.N., Mayeda, T.K., 1994. Origin of dark clasts in the Acfer/El Djouf 001 CR2 chondrite. Meteoritics 29, 26–40.
Engrand, C., Maurette, M., 1998. Carbonaceous micrometeorites from Antarctica. Meteorit. Planet. Sci. 33, 565–580.
Faust, G.T., Fahey, J.J., Mason, B.H., Dwornik, E.J., 1973. The disintegration of the Wolf Creek meteorite and the formation of pecoraite, the nickel analog of clinochrysotile. U.S. Geol. Survey Prof. Pap. 384-C, 107–135.
Fedkin, A.V., Grossman, L., 2006. The fayalite content of chondritic olivine: Obstacle to understanding the condensatioon of rocky material. Meteorites and the early solar system II. In: Lauretta, D.S., McSween, H.Y. (Eds.). Univ. Arizona Press, Tucson, pp. 279–294.
Fisenko, A.V., Ignatenko, K.I., Lavrukhina, A.K., 1990. Heterogeneity of metallic particle enriched in refractory elements in CAI chondrite Efremovka CV. Geokhimiya 3, 264–356.
Fish, R.A., Goles, G.G., Anders, E., 1960. The record in the meteorites: III. On the development of meteorites in asteroidal bodies. Astrophys. J. 132, 243–258.
Fisk, M.R., Popa, R., Mason, O.U., Storrie-Lombardi, M.C., Vicenzi, E.P., 2006. Iron-magnesium silicate bioweathering on Earth (and Mars?). Astrobiology 6, 48–68.
Flight, W., 1887. A Chapter in the History of Meteorites. Dulau and Co., London.
Floran, R.J., 1978. Silicate petrography, classification, and origin of the mesosiderites: Review and new observations. Proceedings Lunar and Planetary Science Conference 9th, 1053–1081.
Floran, R.J., Caulfield, J.B.D., Harlow, G.E., Prinz, M., 1978a. Impact-melt origin for the Simondium, Pinnaroo, and Hainholz mesosiderites: Implications for impact processes beyond the earth-moon system. Proc. Lunar Planet. Sci. Conf. 9th, 1083–1114.
Floran, R.J., Prinz, M., Hlava, P.F., Keil, K., Nehru, C.E., Hinthorne, J.R., 1978b. The Chassigny meteorite: a cumulate dunite with hydrous amphibole-bearing melt inclusions. Geochim. Cosmochim. Acta 42, 1213–1229.
Floss, C., Fogel, R.A., Lin, Y.T., Kimura, M., 2003. Diopside-bearing EL6 EET 90102: insights from rare earth element distributions. Geochim. Cosmochim. Acta 67, 543–555.
Fogel, R., 1997. On the significance of diopside and oldhamite in enstatite chondrites and aubrites. Meteorit. Planet. Sci. 32, 577–591.
Frank, D.R., Zolensky, M.E., Martinez, J., Mikouchi, T., Ohsumi, K., Hagiya, K., Satake, W., Le, L., Ross, D., Peslier, A., 2011. A CAI in the Ivuna CI1 chondrite.
Fredriksson, K., Kerridge, J.F., 1988. Carbonates and sulfates in CI chondrites: formation by aqueous activity on the parent body. Meteoritics 23, 35–44.
Friedrich, J.M., Rubin, A.E., Beard, S.P., Swindle, T.D., Isachsen, C.E., Rivers, M.L., Macke, R.J., 2014. Ancient porosity preserved in ordinary chondrites: shock, compaction, and thermal metamorphism. Meteorit. Planet. Sci. 49, 1214–1231.
Friedrich, J.M., Weisberg, M.K., Ebel, D.S., Biltz, A.E., Corbett, B.M., Iotzov, I.V., Khan, W.S., Wolman, M.D., 2015. Chondrule size and related physical properties: a compilation and evaluation of current data across all meteorite groups. Chem. Erde 75, 419–443.
Fries, M., Messenger, S., Steele, A., Zolensky, M., 2013. Do we already have samples of Ceres? H chondrite halites and the Ceres-Hebe link. Meteorit. Planet. Sci.
Frondel, C., Marvin, U.B., 1967. Lonsdaleite, a hexagonal polymorph of diamond. Nature 214, 587–589.
Frondel, J.W., 1975. Lunar Mineralogy. Wiley, New York.

Fuchs, L.H., 1966a. Djerfisherite, alkali copper-iron sulfide: a new mineral from enstatite chondrites. Science 153, 166–167.
Fuchs, L.H., 1966b. Roedderite, a new mineral from the Indarch meteorite. Am. Mineral. 51, 949–955.
Fuchs, L.H., 1969. The Phosphate Mineralogy of Meteorites. Reidel, Dordrecht, The Netherlands.
Fuchs, L.H., 1971. Occurrence of wollastonite, rhonite, and andradite in the Allende meteorite. Am. Mineral. 56, 2053–2068.
Fuchs, L.H., Olsen, E., 1965. The occurrence of chlorapatite in the Mount Stirling octahedrite (abstract). Trans. Ame. Geophys. Unio. 46, 122.
Fuchs, L.H., Olsen, E., Henderson, E.P., 1967. On the occurrence of brianite and panethite, two new phosphate minerals from the Dayton meteorite. Geochim. Cosmochim. Acta 31, 1711–1719.
Fuchs, L.H., Olsen, E., Jensen, K.J., 1973. Mineralogy, mineral-chemistry, and composition of the Murchsion (C2) meteorite. Smithsonian Contrib. Earth Sci. 10, 1–39.
Fuhrman, M., Papike, J.J., 1981. Howardites and polymict eucrites: Regolith samples from the eucrite parent body: Petrology of Bholgati, Bununu, Kapoeta, and ALHA76005. Proc. Lunar Planet. Sci. Conf. 12th, 1257–1279.
Fujimaki, H., Matsu-ura, M., Sunagawa, I., Aoki, K., 1981. Chemical compositions of chondrules and matrices in the ALH- 77015 chondrite (L3). Proc. Symp. Antarct. Meteorites 6, 161–174.
Geiger, T., Bischoff, A., 1989. Mineralogy of metamorphosed carbonaceous chondrites (abstract). Meteoritics 24, 269–270.
Geiger, T., Bischoff, A., 1990. Exsolution of spinel and ilmenite in magnetites from type 4-5 carbonaceous chondrites–indications for metamorphic processes (abstract). Lunar Planet. Sci. 21, 409–410.
Geiger, T., Bischoff, A., 1995. Formation of opaque minerals in CK chondrites. Planet. Space Sci. 43, 485–498.
Genge, M.J., Grady, M.M., 1998. Melted micrometeorites from Antarctic ice with evidence for the separation of immiscible Fe-Ni-S liquids during entry heating. Meteorit. Planet. Sci. 33.
Genge, M.J., Grady, M.M., 1999. The fusion crusts of stony meteorites: implications for the atmospheric reprocessing of extraterrestrial materials. Meteorit. Planet. Sci. 34, 341–356.
Genge, M.J., Grady, M.M., Hutchison, R., 1997. The textures and compositions of fine-grained Antarctic micrometeorites – Implications for comparisons with meteorites. Geochim. Cosmochim. Acta 61, 5149–5162.
Giesting, P.A., Filiberto, J., 2016. The formation environment of potassic-chloro-hastingsite in the nakhlites MIL 03346 and pairs and NWA 5790: insights from terrestrial chloro-amphibole. Meteorit. Planet. Sci. 51, 2127–2153.
Gillet, P., Chen, M., Dubrovinsky, L., El Goresy, A., 2000. Natural NaAlSi3O8-hollandite in the shocked Sixiangkou meteorite. Science 287, 1633–1636.
Glass, B.P., Liu, S., Leavens, P.B., 2002. Reidite: an impact-produced high-pressure polymorph of zircon found in marine sediments. Am. Mineral. 87, 562–565.
Gnos, E., Hofmann, B.A., Franchi, I.A., Al-Kathiri, A., Huser, M., Moser, L., 2002. Sayh al Uhaymir 094: a new martian meteorite from the Oman desert. Meteorit. Planet. Sci. 37, 835–854.
Gomes, C.B., Keil, K., 1980. Brazilian Stone Meteorites. Univ. New Mexico Press, Albuquerque, New Mexico, pp. 161.
Gooding, J.L., 1979. Petrogenetic properties of chondrules in unequilibrated H-, L-, and LL-group chondritic meteorites. In: Ph.D. thesis. Univ. New Mexico, pp. 392.
Gooding, J.L., 1981. Mineralogical aspects of terrestrial weathering effects in chondrites from Allan Hills, Antarctica. Proc. Lunar Planet. Sci. 12, 1105–1122.
Gooding, J.L., 1986a. Clay-mineraloid weathering products in Antarctic meteorites. Geochim. Cosmochim. Acta 50, 2215–2223.
Gooding, J.L., 1986b. Planetary surface weathering. In: Kivelson, M.G. (Ed.), The Solar System: Observations and Interpretations. Prentice Hall, Englewood Cliffs, New Jersey.
Gooding, J.L., 1992. Soil mineralogy and chemistry on Mars: possible clues from salts and clays in SNC meteorites. Icarus 99, 28–41.
Gooding, J.L., Keil, K., 1981. Relative abundances of chondrule primary textural types in ordinary chondrites and their bearing on conditions of chondrule formation. Meteoritics 16, 17–43.
Gooding, J.L., Muenow, D.W., 1986. Martian volatiles in shergottite EETA 79001: new evidence from oxidized sulfur and sulfur-rich aluminosilicates. Geochim. Cosmochim. Acta 50, 1049–1059.
Gooding, J.L., Wentworth, S.J., Zolensky, M.E., 1991. Aqueous alteration of the Nakhla meteorite. Meteorit. Planet. Sci. 26, 135–143.
Goodrich, C.A., 1988. Petrology of the unique achondrite LEW 86010. Lunar Planet. Sci. XIX, 399–400.
Goodrich, C.A., 1992. Ureilites: a critical review. Meteoritics 27, 327–352.
Goodrich, C.A., Jones, J.H., Berkley, J.L., 1987. Origin and evolution of the ureilite parent magmas: multi-stage igneous activity on a large parent body. Geochim. Cosmochim. Acta 51, 2255–2273.
Goodrich, C.A., Wlotzka, F., Ross, D.K., Bartoschewitz, R., 2006. Northwest Africa 1500: plagioclase-bearing monomict ureilite or ungrouped achondrite? Meteorit. Planet. Sci. 41, 925–952.
Gounelle, M., Zolensky, M.E., 2001. A terrestrial origin for sulfate veins in CI1 chondrites. Meteorit. Planet. Sci. 36, 1321–1329.
Gounelle, M., Zolensky, M.E., Liou, J.-C., Bland, P.A., Alard, O., 2003. Mineralogy of cabonaceous chondritic microclasts in howardites: identification of C2 fossil micrometeorites. Geochim. Cosmochim. Acta 67, 507–527.
Gounelle, M., Spurný, P., Bland, P.A., 2006. The orbit and atmospheric trajectory of the Orgueil meteorite from historical records. Meteorit. Planet. Sci. 41, 135–150.
Gounelle, M., Morbidelli, A., Bland, P.A., Spurný, P., Young, E.D., Septhon, M., 2008. Meteorites from the outer solar system? In The Solar System Beyond Neptune. In: Barucci, M.A., Boehnhardt, H., Cruikshank, D.P., Morbidelli, A. (Eds.). Univeristy of Arizona Press, Tucson, pp. 525–541.
Grady, M.M., 2000. Catalogue of Meteorites, 5th ed. Cambridge Univ. Press, pp. 689.
Grady, M.M., Pratesi, G., Moggi- Cecchi, V., 2015. Atlas of Meteorites. Cambridge Unversity Press, Cambridge, United Kingdom, pp. 373.
Graham, A.L., Easton, A.J., Hutchison, R., 1977. The Mayo Belwa meteorite: a new enstatite achondrite fall. Mineralogical Magazine 41, 487–492.
Greenland, L., 1965. The abundances of selenium, tellurium, silver, palladiumm, cadmium, and zinc in chondritic meteorites. Geochim. Cosmochim. Acta 31, 849–860.
Greenwood, J., Rubin, A.E., Kallemeyn, G.W., Wasson, J.T., 2000. Oxygen-isotopes in R-chondrite magnetite and olivine: links between R chondrites and ordinary chondrites. Geochim. Cosmochim. Acta 64, 3897–3911.
Greenwood, R.C., Franchi, I.A., Kearsley, A.T., Alard, O., 2010. The relationship between CK and CV chondrites. Geochim. Cosmochim. Acta 74, 1684–1705.
Greshake, A., Bischoff, A., 1996. Chromium-bearing phases in Orgueil (CI): Discovery of magnesiochromite ($MgCr_2O_4$), ureyite ($NaCrSi_2O_6$), and chromium-oxide (Cr_2O_3) (abstract). Lunar Planet. Sci. 27, 461–462.
Greshake, A., Bischoff, A., Putnis, A., 1996a. Pure CaO, MgO (periclase), TiO_2 (rutile), and Al_2O_3 (corundum) in Ca,Al-rich inclusions from carbonaceous chondrites (abstract). Lunar Planet. Sci. 27, 463–464.
Greshake, A., Bischoff, A., Putnis, A., Palme, H., 1996b. Corundum, rutile, periclase, and CaO in Ca,Al-rich inclusions from carbonaceous chondrites. Science 272, 1316–1318.
Greshake, A., Stephen, T., Rost, D., 1998. Symplectic exsolutions in olivine from the martian meteorite Chassigny: Evidence for slow cooling under highly oxidizing conditions (abstract). Lunar. Planet. Sci. Conf. 29, abstract #1069.
Grew, E.S., Yates, M.G., Beane, R.J., Floss, C., Gerbi, C., 2010. Chopinite- sarcopside solid solution,$[(Mg, Fe)_3\square](PO_4)_2$, in GRA95209, a transitional acapulcoite: implications for phosphate genesis in meteorites. Am. Mineral. 95, 260–272.
Grimm, R.E., McSween, H., 1993. Heliocentric zoning of the asteroid belt by aluminum-26 heating. Science 259, 653–655.
Grokhovsky, V.I., 2006. Osbornite in CB/CH-like carbonaceous chondrite Isheyevo. Meteorit. Planet. Sci. 41, A68, abstract#5231.
Gross, J., Treiman, A.H., Connolly, H.C., 2013. A new subgroup of amphibole-bearing R chondrites: evidence from the wew R-Chondrite MIL 11207. Lunar Planet. Sci. 44, abstract#2212.
Grossman, J.N., Brearley, A.J., 2005. The onset of metamorphism in ordinary and carbonaceous chondrites. Meteorit. Planet. Sci. 40, 87–122.
Grossman, J.N., Rubin, A.E., Rambaldi, E.R., Rajan, R.S., Wasson, J.T., 1985. Chondrules in the Qingzhen type-3 enstatite chondrite: possible precursor components and comparison to ordinary chondrite chondrites. Geochim. Cosmochim. Acta 49, 1781–1795.
Grossman, J.N., Alesander, C.M.O.D., Brearley, A.J., 2000. Bleached chondrules: evidence for widespread aqueous processes on the parent asteroids of ordinary chondrites. Meteorit. Planet. Sci. 35, 467–486.
Grossman, J.N., Alexanders, C.M.O.D., Wang, J., Brearley, A.J., 2002. Zoned chondrules in Semarkona: evidence for high-and low-temperature processing. Meteoritics & Planetary Science 37, 49–73.
Grossman, L., 1972. Condensation in the primitive solar nebula. Geochim. Cosmochim. Acta 36, 597–619.
Grossman, L., 1975. Petrography and mineral chemistry of Ca-rich inclusions in the Allende meteorite. Geochim. Cosmochim Acta 39, 433–454.
Grossman, L., Steele, I.M., 1976. Amoeboid olivine aggregates in the Allende meteorite. Geochim. Cosmochim. Acta 40, 149–155.
Grover, J.E., 1972. The stability of low-clinoenstatite in the system Mg2Si2O6-CaMgSi2O6 (abstract). Trans. Am. Geophys. Union 53, 539.
Guimon, R.K., Keck, D.B., Weeks, S.K., Dehart, J., Sears, G., 1985. Chemical and physical studies of type 3 chondrites-IV: annealing studies of a type 3, 4 ordinary chondrite and the metamorphic history of meteorites. Geochim. Cosmochim. Acta 49, 1515–1524.
Haack, H., Farinella, P., Scott, E.R.D., Keil, K., 1996. Meteoritic, asteroidal, and theoretical constraints on the 500 Ma disruption of the L chondrite parent body. Icarus 119, 182–191.
Haggerty, S.E., 1972. An enstatite chondrite from Hadley Rille (abstract). In: Chamberlain, J.W., Watkins, C. (Eds.), The Apollo 15 Lunar Samples. Lunar Science Institute, Houston, pp. 85–87.
Hallenbeck, S.L., Nuth, J.A., Daukantas, P.L., 1998. Mid-infrared spectral evolution of amorphous magnesium silicate smokes annealed in vacuum: Comparison to cometary spectra. Icarus 131, 198–209.
Hallenbeck, S.L., Nuth III, J.A., Nelson, R.N., 2000. Evolving optical properties of annealing silicate grains: from amorphous condensate to crystalline mineral. Astrophys. J. 535, 247.
Hanowski, N.P., Brearley, A.J., 2001. Aqueous alteration of chondrules in the CM carbonaceous chondrite, Allan Hills 81002: implications for parent body alteration. Geochim. Cosmochim. Acta 65, 495–518.
Harazono, K., Yurimoto, H., 2003. Oxygen isotopic variations in a fluffy Type A CAI from the Vigarano meteorite. Lunar and Planetary Science Conference, 1540.
Harju, E.R., Rubin, A.E., Ahn, I., Choi, B., Ziegler, K., Wasson, J.T., 2014. Progressive aqueous alteration of CR carbonaceous chondrites. Geochim. Cosmochim. Acta 139, 267–292.

Harries, D., Berg, T., Langenhorst, F., Palme, H., 2012. Structural clues to the origin of refractory metal alloys as condensates of the solar nebula. Meteorit. Planet. Sci. 47, 2148–2159.
Harvey, R.P., McSween, H.Y., 1996. A possible high-temperature origin for the carbonates in the Martian meteorite ALH84001. Nature 382, 49–51.
Haskin, L., Warren, P., 1991. Lunar chemistr. In: Heiken, G.H., Vaniman, D.T., French, B.M. (Eds.), Lunar Sourcebook: A User's Guide to the Moon. Cambridge University Press, Cambridge, pp. 357–474.
Hassanzadeh, J., Rubin, A.E., Wasson, J.T., 1990. Compositions of large metal nodules in mesosiderites: links to iron meteorite group IIIAB and the origin of mesosidertie subgroups. Geochim. Cosmochim. Acta 54, 3197–3208.
Henderson, E.P., Furcron, A.S., 1957. Meteorites in Georgia, Part 2: description of falls. Georgia Min. Newslett. 10, 113–142.
Herndon, J.M., Rudee, M.L., 1978. Thermal history of the Abee enstatite chondrite. Earth Planet. Sci. Lett. 41, 101–106.
Herwig, F., 2005. Evolution of asymptotic giant branch stars. Annu. Rev. Astron. 43, 435–479.
Hewins, R.H., 1984. The case for a melt matrix in plagioclase-POIK mesosiderites. Proceedings Lunar and Planetary Science Conference 15th, C289–C297.
Hewins, R.H., 1988. Experimental studies of chondrule. In: Kerridge, J.F., Matthews, M.S. (Eds.), Meteorites and the Early Solar System. Univ. of Arizona Press, Tucson, pp. 660–679.
Hewins, R., Fox, G., 2004. Chondrule textures and precursor grain size: an experimental study. Geochim. Cosmochim. Acta 68, 917–926.
Hewins, R.H., Connolly, H.C., Lofgren, G.E., Libourel, G., 2005. Experimental constraints on chondrule formation. In: Krot, A.N., Scott, E.R.D., Reipurth, B. (Eds.), Chondrules and the Protoplanetary Disk. ASP Conference Series, San Francisco, pp. 286–316.
Hewins, R.H., Bourot-Denise, M., Zanda, B., Leroux, H., Barrat, J.-A., Humayun, M., Göpel, C., Greenwood, R.C., Franchi, I.A., Pont, S., 2014. The Paris meteorite, the least altered CM chondrite so far. Geochim. Cosmochim. Acta 124, 190–222.
Heymann, D., 1967. On the origin of hypersthene chondrites: ages and shock effects of black chondrites. Icarus 6, 189–221.
Hidaka, Y., Yamaguchi, A., Shirai, N., Sekimoto, S., Ebihara, M., 2012. Lithophile element characteristics of Acapulcoite-Lodranite and Winonaites: Implications for the chemical composition of their precursor materials. Lunar Planet Sci. Conf. 1785.
Hollister, L.S., Bindi, L., Yao, N., Poirier, G.R., Andronicos, C.L., MacPherson, G.J., Lin, C., Distler, V.V., Eddy, M.P., Kostin, A., 2014. Impact-induced shock and the formation of natural quasicrystals in the early solar system. Nat. Commun. 5, 1–8.
Hoppe, P., Amari, S., Zinner, E., Ireland, T., Lewis, R.S., 1994. Carbon, nitrogen, magnesium, silicon, and titanium isotopic compositions of single interstellar silicon carbide grains from the Murchison carbonaceous chondrite. Astrophys. J. 430, 870–890.
Hoppe, P., Amari, S., Zinner, E., Lewis, R.S., 1995. Isotopic compositions of C, N, O, Mg, and Si, trace element abundances, and morphologies of single circumstellar graphite grains in four density fractions from the Murchison meteorite. Geochim. Cosmochim. Acta 59, 4029–4056.
Hoppe, P., Lodders, K., Fujiya, W., 2015. Sulfur in presolar silicon carbide grains from asymptotic giant branch stars. Meteorit. Planet. Sci. 50, 1122–1138.
Howard, K.T., Benedix, G.K., Bland, P.A., Cressey, G., 2009. Modal mineralogy of CM2 chondrites by X-ray diffraction (PSD-XRD): Part 1. Total phyllosilicate abundance and the degree of aqueous alteration. Geochim. Cosmochim. Acta 73, 4576–4589.
Hu, J., Sharp, T.G., 2016. High-pressure phases in shock-iniduced melt of the unique highly shocked LL6 chondrite Northwest Africa 757. Meteorit. Planet. Sci. 51, 1353–1369.
Hua, X., Eisenhur, D.D., Buseck, P.R., 1995. Cobalt-rich, nickel-poor metal (wairauite) in the Ningqiang carbonaceous chondrite. Meteoritics 30, 106–109.
Hunt, A.C., Benedix, G.K., Hammond, S., Bland, P.A., 2012. Constraining the precursor composition of the Winonaite parent body using geochemical data. Meteoritical Society meeting, 75, 5238.pdf.
Hurt, S.M., Rubin, A.E., Wasson, J.T., 2012. Fractionated matrix composition in CV3 Vigarano and alteration processes on the CV parent asteroid. Meteorit. Planet. Sci. 47, 1035–1048.
Huss, G.R., 1990. Ubiquitous interstellar diamond and SiC in primitive chondrites: abundances reflect metamorphism. Nature 347, 159–162.
Huss, G.R., Lewis, R.S., 1995. Presolar diamond, SiC, and graphite in primitive chondrites: abundances as a function of meteorite class and petrologic type. Geochim. Cosmochim. Acta 59, 115–160.
Huss, G.R., Keil, K., Taylor, G.J., 1981. The matrices of unequilibrated ordinary chondrites: implications for the origin and history of chondrites. Geochim. Cosmochim. Acta 45, 33–51.
Huss, G.R., Fahey, A.J., Russell, S.S., Wasserburg, G.J., 1995. Oxygen isotopes in refractory oxide minerals from primitve chondrites (abstract). Lunar Planet. Sci. 26, 641–642.
Huss, G.R., Hutcheon, I.D., Wasserburg, G.J., 1997. Isotopic systematics of presolar silicon carbide from the Orgueil (CI) chondrite: implications for solar system formation and stellar nucleosynthesis. Geochim. Cosmochim. Acta 61, 5117–5148.
Huss, G.R., MacPherson, G.J., Wasserburg, G.J., Russell, S.S., Srinivasan, G., 2001. Aluminum-26 in calcium-aluminum-rich inclusions and chondrules from unequilibrated ordinary chondrites. Meteorit. Planet. Sci. 36, 975–997.
Huss, G.R., Meshik, A.P., Smith, J.B., Hohenberg, C.M., 2003. Presolar diamond, silicon carbide, and graphite in carbonaceous chondrites: implications for thermal processing in the solar nebula. Geochim. Cosmochim. Acta 67, 4823–4848.
Huss, G.R., Rubin, A.E., Grossman, J.N., 2006. Thermal metamorphism in chondrites. Meteorit. Early Solar Syst. II, 567–586.
Hutchison, R., 2004. Meteorites: A Petrologic, Chemical and Isotopic Synthesis. Cambridge University Press, 506.
Hutchison, R., Alexander, C.M.O., Barber, D.J., 1987. The Semarkona meteorite; First recorded occurrence of smectite in an ordinary chondrite, and its implication. Geochim. Cosmochim. Acta 51, 1875–1882.
Hwang, S.L., Shen, P., Chu, H.T., Chui, T.F., Varela, M.E., Iizuka, Y., 2014. Kuratite (IMA 2013-109): TheUnknown Fe-Al-Ti Silicate from the Angrite D'Orbigny. Lunar Planet. Sci. 45, abstract#1818.
Hwang, S.-L., Shen, P., Chu, H.-T., Yui, T.-F., Varela, M.E., Iizuka, Y., 2016a. Matyhite, IMA 2015-121. CNMNC Newsletter No. 31, June 2016 page 692. Mineral. Mag. 80, 691–697.
Hwang, S.L., Shen, P., Chu, H.T.Y., Varela, T.F., Iizu, M.E., 2016b. Tsangpoite: the unknown calcium silico phosphate phase in the angrite D'Orbigny. Lunar Planet. Sci. 47, abstract#1466.
Hyman, M., Ledger, E.B., Rowe, M.W., 1985. Magnetite morphologies in the Essebi and Haripura CM chondrites. Lunar Planet. Sci. Conf. 4, C710–C714.
Ikeda, Y., Prinz, M., 1993. Petrologic stidy of the Belgica-7904 carbonaceous chondrite: hydrous alteration and oxygen isotopes, and relationship to CM and CI chondrites. Geochim. Cosmochim. Acta 57, 439–452.
Imae, N., Zolensky, M.E., 2003. Mineralogical description of PRE 95404: a Rumuruti chondrite that includes a large unequilibrated clast. Meteorit. Planet. Sci. 38, abstract#5176.
Ireland, T.R., Wlotzka, F., 1992. The oldest zircons in the solar system. Earth Planet. Sci. Lett. 109, 1–10.
Irving, A.J., Bunch, T.E., Rubin, A.E., Wasson, J.T., 2010. Northwest Africa 2828/Al Haggounia 001 is a weathered, unequilibrated EL chondrite: trace element and petrologic evidence. Meteorit. Planet. Sci. 73, abstract#5378.
Isa, J., Ma, C., Rubin, A.E., 2016. Joegoldsteinite: a new sulfide mineral ($MnCr_2S_4$) from the Social Circle IVA iron meteorite. Am. Mineral. 101, 1217–1221.
Ishii, H.A., Krot, A.N., Bradley, J.P., 2010. Discovery, mineral paragenesis, and origin of wadalite in a meteorite. Am. Mineral. 95, 440–448.
Ivanov, A.V., Zolensky, M.E., Saito, A., Ohsumi, K., Yang, V., Kononkova, N.N., Mikouchi, T.1, 2000. Florenskyite, FeTiP, a new phosphide from the Kaidun meteorite. Am. Mineral. 85, 1082–1086.
Ivanov, A.V., Kononkova, N.N., Zolensky, M.E., Migdisova, L.F., Stroganov, I.A., 2001. The Kaidun meteorite: a large albite crystal-fragment of an alkaline rock. Lunar Planet Sci. 32, abstract#1080.
Ivanova, I.A., Lebedinets, V.N., Maksakov, B.I., Portnyagin, Y.I., 1968. Rate of vaporization of stone meteorites as determined by comparison with the rate of vaporization of iron. Geokhimiya 1968, 239-242. English translation. Geochem. Int. 1968, 190–193.
Ivanova, M.A., Nazarov, M.A., Kononkova, N.N., Brandstaetter, F., 2005. Isheyevo: a new CB chondrite. Meteorit. Planet. Sci. 40 (A74), abstract#5073.
Ivanova, M.A., Kononkova, N.N., Franchi, I.A., Verchovsky, A.B., Korochantseva, E.V., Trieloff, M., Krot, A.N., Brandstaetter, F., 2006. Isheyevo meteorite: genetic link between CH and CB chondrites? Lunar Planet. Sci. 37, abstract#1100.
Ivanova, M.A., Lorenz, C.A., Ma, C., Ivanov, A.V., 2016. The Kaidun breccia material variety: new clasts and updated hypothesis on a space trawl origin (abstract). Meteorit. Planet. Sci. 51, 6100.
Jambon, A., Sautter, V., Barrat, J.-A., Gattacceca, J., Rochette, P., Boudouma, O., Badia, D., Devouard, B., 2016. Northwest Africa 5790: revisiting nakhlite petrogenesis. Geochim. Cosmochim. Acta 190, 191–212.
Jarosewich, E., 1990. Chemical analyses of meteorites: a compilation of stony and iron meteorite analyses. Meteoritics 25, 323–337.
Johnson, C.A., Prinz, M., Weisberg, M.K., Clayton, R.N., Mayeda, T.K., 1990. Dark inclusions in ALlende, Leoville, and Vigarano: evidence for nebular oxidation of CV3 constituents. Geochim. Cosmochim. Acta 54, 819–831.
Johnson, M.C., Rutherford, M.J., Hess, P.C., 1991. Chassigny petrogenesis: melt compositions, intensive parameters, and water contents of martian(?) magmas. Geochim. Cosmochim. Acta 55, 349–366.
Jones, J.H., 1982. The geochemical coherence of Pu and Nd and the $^{244}Pu/^{238}U$ ratio of the early solar system. Geochim. Cosmochim. Acta 46, 1793–1804.
Jones, R.H., 1990. Petrology and mineralogy of type II, FeO-rich chondrules in Semarkona (LL3.0): origin by closed-system fractional crystallization, with evidence for supercooling. Geochim. Cosmochim. Acta 54, 1785–1802.
Jones, R.H., 1996a. FeO-rich, porphyritic pyroxene chondrules in unequilibrated ordinary chondrites. Geochim. Cosmochim. Acta 60, 3115–3138.
Jones, R.H., 1996b. Relict grains in chondrules: evidence for chondrule recycling. In: Hewins, R.H., Jones, R.H., Scott, E.R.D. (Eds.), Chondrules and the Protoplanetary Disk. Cambridge Univ., pp. 163–172.
Jones, R., Grossman, J., Rubin, A., 2005. Chemical, mineralogical and isotopic properties of chondrules: clues to their origin. In: Hewins, R.H., Jones, R.H., Scott, E.R.D. (Eds.), Chondrites and the protoplanetary disk, 251.
Jones, R.H., McCubbin, F.M., Dreeland, L., Guan, Y., Burger, P.V., Shearer, C.K., 2014. Phosphate minerals in LL chondrites: a record of the action of fluids during metamorphism on ordinary chondrite parent bodies. Geochim. Cosmochim. Acta 132, 120–140.
Jurewicz, A.J.G., Mittlefehldt, D.W., Jones, J.H., 1993. Experimental partial melting of the Allende (CV) and Murchison (CM) chondrites and the origin of asteroidal basalts. Geochim. Cosmochim. Acta 57, 2123–2139.
Kallemeyn, G.W., Rubin, A.E., 1995. Coolidge and Loongana 001: a new carbonaceous chondrite grouplet. Meteoritics 30, 20–27.

Kallemeyn, G.W., Wasson, J.W., 1985. The compositional classification of chondrites: IV. Ungrouped chondritic meteorites and clasts. Geochim. Cosmochim. Acta 49, 261–270.
Kallemeyn, G.W., Boynton, W.V., Willis, J., Wasson, J.T., 1978. Formation of the Bencubbin polymict meteorite breccia. Geochim. Cosmochim. Acta 42, 507–515.
Kallemeyn, G.W., Rubin, A.E., Wasson, J.T., 1991. The compositional classification of chondrites: V. The Karoonda (CK) group of carbonaceous chondrites. Geochim. Cosmochim. Acta 55, 881–892.
Kallemeyn, G.W., Rubin, A.E., Wasson, J.T., 1996. The compositional classification of chondrites: VII. The R chondrite group. Geochim. Cosmochim. Acta 60, 2243–2256.
Karwowski, L., Muszynski, A., 2008. Multimineral inclusions in the Morasko coarse octahedrite. Meteorit. Planet. Sci., A71.
Karwowski, Ł., Kusz, J., MuszyŃski, A., Kryza, R., Sitarz, M., Galuskin, E.V., 2015. Moraskoite, $Na_2Mg(PO_4)F$, a new mineral from the Morasko IAB- MG iron meteorite (Poland). Mineralogical Magazine 79, 387–398.
Keil, K., 1968. Mineralogical and chemical relationships among enstatite chondrites. J. Geophys. Res. 73, 6945–6976.
Keil, K., 1989. Enstatite meteorites and their parent bodies. Meteoritics 24, 195–208.
Keil, K., 2007. Occurrence and origin of keilite, $(Fe_{>0.5}, Mg_{<0.5})$ S, in enstatite chondrite impact-melt rocks and impact-melt breccias. Chem. Erde-Geochem. 67, 37–54.
Keil, K., 2010. Enstatite achondrite meteorites (aubrites) and the histories of their asteroidal parent bodies. Chem. Erde 70, 295–317.
Keil, K., 2012. Angrites: a small but diverse suite of ancient, silica-undersaturated volcanic-plutonic mafic meteorites, and the history of their parent asteroid. Chem. Erde-Geochem. 72, 191–218.
Keil, K., 2014. Brachinite meteorites: partial melt residues from an FeO-rich asteroid. Chem. Erde-Geochem. 74, 311–329.
Keil, K., Brett, R., 1974. Heideite, $(Fe,Cr)_{1+x}(Ti,Fe)_2S_4$, A new mineral in the Bustee enstatite achondrite. Am. Miner. 59, 465–470.
Keil, K., Snetsinger, K.G., 1967. Niningerite: a new meteoritic sulfide. Science 155, 451–453.
Keil, K., Berkley, J.L., Fuchs, L.H., 1982. Suessite, Fe_3Si: a new mineral in the North Haig ureilite. Am. Mineral. 67, 126–131.
Keil, K., Ntaflos, Th., Taylor, G.J., Brearley, A.J., Newsom, H.E., Romig, A.D., 1989. The Shallowater aubrite: evidence for origin by planetesimal impacts. Geochim. Cosmochim. Acta 53, 3291–3307.
Keil, K., Haack, H., Scott, E.R.D., 1994. Catastrophic fragmentation of asteroids: evidence from meteorites. Planet. Space Sci. 42, 1109–1122.
Keller, L.P., 1998. A transmission electron microscope study of iron-nickel carbides in the matrix of the Semarkona unequilibrated ordinary chondrite. Meteorit. Planet. Sci. 33, 913–919.
Keller, L.P., Messenger, S.1, 2011. On the origins of GEMS grains. Geochim. Cosmochim. Acta 75, 5336–5365.
Keller, L.P., Thomas, K.L., McKay, D.S., 1996. Mineralogical changes in IDPs resulting from atmospheric entry heating IAU Colloq. 150: Physics, chemistry, and dynamics of interplanetary dust, 295.
Kelly, K.R., Larimer, J.W., 1977. Chemical fractionations in meteorites-VIII. Iron meteorites and the cosmochemical history of the metal phase. Geochim. Cosmochim. Acta 41, 93–111.
Kerridge, J.F., Bunch, T.E., 1979. Aqueous activity on asteroids: Evidence from carbonaceous meteorite. In: Gehrels, T. (Ed.), Asteroids. University of Arizona Press, Tucson, pp. 745–764.
Kerridge, J.F., Matthews, M.S., 1988. Meteorites and the Early Solar System. Univ. Arizona Press, Tucson, Arizona, pp. 1269.
Kerridge, J.F., MacKay, A.L., Boynton, W.V., 1979. Magnetite in CI carbonaceous meteorites: origin by aqueous activity on a planetesimal surface. Science 205, 395–397.
Killgore, K., Killgore, M., 2002. Southwest Meteorite Collection: A Pictorial Catalog. Southwest Meteorite Press, Payson, Arizona, pp. 201.
Kim, H.Y., Choi, B.-G., Rubin, A.E., 2009. Wüstite in the DOM 03238 magnetite-rich CO3.1 chondrite: formation during atmospheric passage. Meteorit. Planet. Sci. 44, A109.
Kimura, M., 1996. Meteorite minerals (in Japanese). Kobutsugaku Zassi 25, 49–60.
Kimura, M., 2015. Introduction to meteorite mineralogy. Ganseki-Kobutsu- Kagaku 44, 1–9.
Kimura, M., El Goresy, A., 1989. Discovery of E-chondrite assemblages, SiC, and silica-bearing objects in ALH85085: link between E- and C-chondrite (abstract). Meteoritics 24, 286.
Kimura, M., Ikeda, Y., 1992. Mineralogy and petrology of an unusual Belgica-7904 carbonaceous chondrite: genetic relationships between the components. Proc. NIPR Symp. Antarct. Meteorit. 5, 72–117.
Kimura, M., Ikeda, Y., 1995. Anhydrous alteration of Allende chondrules in the solar nebula II. Alkali-Ca exchange reactions and formation of nepheline, sodalite and Ca-rich phases in chondrules. Proc. NIPR Symp. Antarct. Meteorit. 8, 123–138.
Kimura, M., Tsuchiyama, A., Fukuoka, T., Iimura, Y., 1992. Antarctic primitive achondrites, Yamato-74025, -75300, and - 75305: their mineralogy, thermal history, and the relevance to winonaite. Proc. NIPR Symp. Antarct. Meteorites 5, 165–190.
Kimura, M., Suzuki, A., Kondo, T., Ohtani, E., El Goresy, A., 2000. The first discovery of high-pressure polymorphs, jadeite, hollandite, wadsleyite and majorite, from an H-chondrite, Y-75100 (abstract). Antarct. Meteorit. 25, 41–42.
Kimura, M., Chen, M., Yoshida, Y., El Goresy, A., Ohtani, E., 2003. Back-transformation of high-pressure phases in a shock melt vein of an H-chondrite during atmospheric passage: implications for the survival of high-pressure phases after decompression. Earth. Planet. Sci. Lett. 217, 141–150.
Kimura, M., Weisberg, M., Lin, Y., Suzuki, A., Ohtani, E., Okazaki, R., 2005. Thermal history of the enstatite chondrites from silica polymorphs. Meteorit. Planet. Sci. 40, 855–868.
Kimura, M., Grossman, J.N., Weisberg, M.K., 2008. Fe-Ni metal in primitive chondrites: indicators of classification and metamorphic conditions for ordinary and CO chondrites. Meteorit. Planet. Sci. 43, 1161–1177.
Kimura, M., Mikouchi, T., Suzuki, A., Miyahara, M., Ohtani, E., Goresy, A.E., 2009. Kushiroite, $CaAlAlSiO_6$: a new mineral of the pyroxene group from the ALH 85085 CH chondrite, and its genetic significance in refractory inclusions. Am. Mineral. 94, 1479–1482.
Kimura, M., Grossman, J.N., Weisberg, M.K., 2011. Fe-Ni metal and sulfide minerals in CM chondrites: an indicator for thermal history. Meteorit. Planet. Sci. 46, 431–442.
Kimura, M., Sugiura, N., Mikouchi, T., Hirajima, T., Hiyagon, H., Takehana, Y., 2013. Eclogitic clasts with omphacite and pyrope-rich garnet in the NWA 801 CR2 chondrite. Am. Mineral. 98, 387–393.
Kimura, M., Yamaguchi, A., Miyahara, M., Pittarello, L., 2014. Shock vein in an enstatite chondrite, Asuka 10164. 77th Annual Meeting of the Meteoritical Society.
Kimura, M., Yamaguchi, A., Miyahara, M., 2016. Shock-induced thermal history of an EH3 chondrite, Asuka 10164. Meteorit. Planet. Sci. 51, in press.
King, E.A., Butler, J.C., Carman, M.F., 1972a. Chondrules in Apollo 14 samples and size analyses of Apollo 14 and 15 fines. Proc. Lunar Sci. Conf. 3, 673–686.
King, E.A., Carman, M.F., Butler, J.C., 1972b. Chondrules in Apollo 14 samples and implications for the origin of chondritic meteorites. Science 175, 59–60.
Kleine, T., Mezger, K., Palme, H., Scherer, E., Münker, C., 2005. Early core formation in asteroids and late accretion of chondrite parent bodies: evidence from ^{182}Hf-^{182}W in CAIs, metal-rich chondrites, and iron meteorites. Geochim. Cosmochim. Acta 69, 5805–5818.
Kobayashi, S., Tonotani, A., Sakamoto, N., Nagashima, K., Krot, A.N., Yurimoto, H., 2005. Presolar silicate grains from primitive carbonaceous chondrites Y-81025, ALHA 77307, Adelaid and Acfer 094. Lunar Planet. Sci. 36, 1931.
Koeberl, C., Reimold, W.U., Horsch, H.E., Merkle, R.K.W., 1990. New mineralogical and chemical data on the Machinga (L6) chondrite. Malawi. Meteorit. 25, 23–26.
Kojima, T., Tomeoka, K., 1996. Indicators of aqueous alteration and thermal metamorphism on the CV parent body: microtextures of a dark inclusion from Allende. Geochim. Cosmochim. Acta 60, 2651–2666.
Kojima, T., Tomeoka, K., Takeda, H., 1993. Unusual dark clasts in the Vigarano CV3 carbonaceous chondrite: record of parent body process. Meteoritics 28, 649–658.
Komatsu, M., Krot, A.N., Petaev, M.I., Ulyanov, A.A., Keil, K., Miyamoto, M., 2001. Mineralogy and petrography of amoeboid olivine aggregates from the reduced CV3 chondrites Efremovka, Leoville and Vigarano: products of nebular condensation, accretion and annealing. Meteorit. Planet. Sci. 36, 629–641.
Kornacki, A.S., Wood, J.A., 1984. Petrography and classification of Ca,Al-rich and olivine-rich inclusions in the Allende CV3 chondrite. Proc. Lunar Planet. Sci. Conf. 14, B573–B587.
Korochantseva, E.V., Trieloff, M., Lorenz, C.A., Buykin, A.I., Ivanova, M.A., Schwarz, W.H., Hopp, J., Jessberger, E.K., 2007. L-chondrite asteroid breakup tied to Ordovician meteorite shower by multiple isochron 40Ar-39 Ar dating. Meteorit. Planet. Sci. 42, 113–130.
Korotev, R.L., 2005. Lunar geochemistry as told by lunar meteorites. Chem. Erde-Geochem. 65, 297–346.
Kracher, A., 1982. Crystallization of a S-saturated Fe, Ni-melt, and the origin of iron meteorite groups IAB and IIICD. Geophys. Res. Lett. 9, 412–415.
Kracher, A., 1985. The evolution of partially differentiated planetesimals: Evidence from iron meteorite groups IAB and IIICD. Proc. Lunar Planet. Sci. Conf. 15, C689–C698.
Kracher, A., Scott, E.R.D., Keil, K., 1984. Relict and other anomalous grains in chondrules: implications for chondrule formation. Proc. Lunar Planet. Sci. Conf. 14, B559–B566.
Krinov, E.L., 1960. Principles of Meteoritics (Osnovy Meteoritiki). Pergamon Press, New York, New York, pp. 535.
Krot, A.N., 2016. Machiite, IMA 2016-067. CNMNC Newsletter No. 34, December 2016, p. 1317. Mineral. Mag. 80, 1315–1321.
Krot, A.N., Rubin, A.E., 1994. Glass-rich chondrules in ordinary chondrites. Meteoritics 29, 697–707.
Krot, A.N., Rubin, A.E., 1996. Microchondrule- bearing chondrule rims: constraints on chondrule formation. In: Hewins, R.H., Jones, R.H., Scott, E.R.D. (Eds.), Chondrules and the Protoplanetary disk. Cambridge University Press, pp. 181–184.
Krot, A.N., Wasson, J.T., 1994. Silica-merrihueite/roedderite-bearing chondrules and clasts in ordinary chondrites: new occurrences and possible origin. Meteoritics 29, 707–718.
Krot, A.N., Wasson, J.T., 1995. Igneous rims on low-FeO and high-FeO chondrules in ordinary chondrites. Geochim. Cosmochim. Acta 59, 4951–4966.
Krot, A., Rubin, A.E., Kononkova, N.N., 1993. First occurence of pyrophanite $(MnTiO_3)$ and baddeleyite (ZrO_2) in an ordinary chondrite. Meteoritics 28, 232–239.

Krot, A.N., Scott, E.R.D., Zolensky, M.E., 1995. Mineralogical and chemical modification of components in CV3 chondrites: nebular or asteroidal processing? Meteoritics 30, 748–775.

Krot, A.N., Rubin, A.E., Keil, K., Wasson, J.T., 1997a. Microchondrules in ordinary chondrites: implications for chondrule formation. Geochim. Cosmochim. Acta 61, 463–473.

Krot, A., Scott, E.R.D., Zolensky, M., 1997b. Origin of fayalitic olivine rims and lath-shaped matrix olivine in the CV3 chondrite Allende and its dark inclusions. Meteorit. Planet. Sci. 32, 31–49.

Krot, A.N., Zolensky, M.E., Wasson, J.T., Scott, E.R.D., Keil, K., Ohsumi, K., 1997c. Carbide-magnetite assemblages in type-3 ordinary chondrites. Geochim. Cosmochim. Acta 61, 219–237.

Krot, A.N., Petaev, M.I., Zolensky, M.E., Keil, K., Scott, E.R.D., Nakamura, K., 1998a. Secondary calcium-iron-rich minerals in the Bali-like and Allende-like oxidized CV3 chondrites and Allende dark inclusions. Meteorit. Planet. Sci. 33, 623–645.

Krot, A.N., Petaev, M.I., Scott, E.R.D., Choi, B.-G., Zolensky, M.E., Keil, K., 1998b. Progressive alteration in CV3 chondrites: More evidence for asteroidal alteration. Meteorit. Planet. Sci. 33, 1065–1085.

Krot, A.N., Brearley, A.J., Ulyanov, A.A., Biryukov, V.V., Swindle, T.D., Keil, K., Mittlefehldt, D.W., Scott, E.R.D., Clayton, R.N., Mayeda, T.K., 1999. Mineralogy, petrography, bulk chemical, iodine-xenon, and oxygen-isotopic compositions of dark inclusions in the reduced CV3 chondrite Efremovka. Meteorit. Planet. Sci. 34, 67–89.

Krot, A.N., Meibom, A., Keil, K., 2000. A clast of Bali-like oxidized CV material in the reduced CV chondrite breccia Vigarano. Meteorit. Planet. Sci. 35, 817–825.

Krot, A.N., McKeegan, K.D., Russell, S.S., Meibom, A., Weisberg, M.K., Zipfel, J., Krot, T.V., Fagan, T.J., Keil, K., 2001. Refractory calcium- aluminum-rich inclusions and aluminum-diopside-rich chondrules in the metal-rich chondrites Hammadah al Hamra 237 and Queen Alexandra Range 94411. Meteorit. Planet. Sci 36, 1189–1216.

Krot, A.N., Meibom, A., Weisberg, M.K., Keil, K., 2002. The CR chondrite clan: implications for early solar system processes. Meteorit. Planet. Sci. 37, 1451–1490.

Krot, A.N., MacPherson, G.J., Ulyanov, A.A., Petaev, M.I., 2004a. Fine-grained, spinel-rich inclusions from the reduced CV chondrites Efremovka and Leoville: I. Mineralogy, petrology, and bulk chemistry. Meteorit. Planet. Sci. 39, 1517–1553.

Krot, A.N., Petaev, M.I., Russell, S.S., Itoh, S., Fagan, T.J., Yurimoto, H., Chizmadia, L., Weisberg, M.K., Komatsu, M., Ulyanov, A.A., 2004b. Amoeboid olivine aggregates and related objects in carbonaceous chondrites: records of nebular and asteroid processes. Chem. Erde-Geochem. 64, 185–239.

Krot, A.N., Fagan, T.J., Keil, K., McKeegan, K.D., Sahupal, S., Hutcheon, I.D., Petaev, M.I., Yurimoto, H., 2004c. Ca,Al-rich inclusions, amoeboid olivine aggregates, and Al- rich chondrules from the unique carbonaceous chondrite Acfer 094: I. Mineralogy and petrology. Geochim. Cosmochim. Acta 68, 2167–2184.

Krot, A.N., Amelin, Y., Cassen, P., Meibom, A., 2005. Young chondrules in CB chondrites from a giant impact in the early Solar System. Nature 436, 989–992.

Krot, A.N., Ulyanov, A.A., Ivanova, M.A., 2006. Refractoryt inclusions and aluminum-rich chondrules in the CB/CH-like carbonaceous chondrite Isheyevo. Lunar Planet. Sci. 37, abstract#1226.

Ksanda, C.J., Henderson, E.P., 1939. Identification of diamond in the Canyon Diablo iron. Am. Mineral. 24, 677–680.

Kuehner, S.M., Irving, A.J., Bunch, T.E., Wittke, J.H., 2006. EL3 chondrite (not aubrite) Northwest Africa 2828: An unusual paleometeorite occurring as cobbles in a terrestrial conglomerate. American Geophysical Union, Fall Meeting 2006.

Kunihiro, T., Rubin, A.E., McKeegan, K.D., Wasson, J.T., 2004. Oxygen-isotope composition of relict and host grains in chondrules in the Yamato 81020 CO3.0 chondrite. Geochim. Cosmochim. Acta 68, 3599–3606.

Kunihiro, T., Rubin, A.E., Wasson, J.T., 2005. Oxygen-isotopic compositions of low-FeO relicts in high-FeO host chondrules in Acfer 094, a type 3.0 carbonaceous chondrite closely related to CM. Geochim. Cosmochim. Acta 69, 3831–3840.

Kunz, G.F., 1890. Gems and Precious Stones of North America. Scientific Publishing Co., New York.

Kurat, G., Brandstatter, H., Palme, H., Michel-Levy, M.C., 1981. Rusty Ornans. Meteoritics 16, 343–344.

Kurat, G., Koeberl, C., Presper, T., Franz, B., Maurette, M., 1994. Petrology and geochemistry of Antarctic micrometeorites. Geochim. Cosmochim. Acta 58, 3879–3904.

Kyte, F.T., 1998. A meteorite from the Cretaceous/Tertiary boundary. Nature 396, 237–239.

Lambert, D.L., Gustafsson, B., Eriksson, K., Hinkle, K.H., 1986. The chemical composition of carbon stars. I-Carbon, nitrogen, and oxygen in 30 cool carbon stars in the Galactic disk. Astrophys. J. Suppl. Ser. 62, 373–425.

Langenhorst, F., Poirier, J.P., 2000. Anatomy of black veins in Zagami: clues to the formation of high-pressure phases. Earth Planet. Sci. Lett. 184, 37–55.

Larimer, J.W., 1967. Chemical fractionations in meteorites—I. Condensation of the elements. Geochim. Cosmochim. Acta 31, 1215–1238.

Lauretta, D.S., Lodders, K., Fegley, B., Kremser, D.T., 1997. The origin of sulfide-rimmed metal grains in ordinary chondrites. Earth Planet. Sci. Lett. 151, 289–301.

Lee, M.R., Chatzitheodoridis, E., 2016. Replacement of glass in the Nakhla meteorite by berthierine: implications for understanding the origins of aluminum-rich phyllosilicates on Mars. Meteorit. Planet. Sci, 1–11.

Lee, M.R., Leroux, H., 2015. Planetary Mineralogy. Mineralogical Society of Great Britain and Ireland, Twickenham, U.K, pp. 314.

Lee, M.R., Russell, S.S., Arden, J.W., Pillinger, C.T., 1995. Nierite (Si_3N_4), a new mineral from ordinary and enstatite chondrites. Meteoritics 30, 387–398.

Lee, M.R., Hutchison, R., Graham, A.L., 1996. Aqueous alteration in the matrix of the Vigarano (CV3) carbonaceous chondrite. Meteorit. Planet. Sci. 31, 477–483.

Lee, M.R., Lindgren, P., Sofe, M.R., 2014. Aragonite, breunnerite, calcite and dolomite in the CM carbonaceous chondrites: High fidelity recorders of progressive parent body aqueous alteration. Geochim. Cosmochim. Acta 144, 126–156.

Lee, M.R., MacLaren, I., Andersson, S.M.L., Kovács, A., Tomkinson, T., Mark, D.F., Smith, C.L., 2015. Opal-A in the Nakhla meteorite: a tracer of ephemeral liquid water in the Amazonian crust of Mars. Meteorit. Planet. Sci. 50, 1362–1377.

Lee, M.S., Rubin, A.E., Wasson, J.T., 1992. Origin of metallic Fe-Ni in Renazzo and related chondrites. Geochim. Cosmochim. Acta 56, 2521–2533.

Lee, T., Papanastassiou, D.A., Wasserburg, G.J., 1976. Demonstration of ^{26}Mg excess in Allende and evidence for ^{26}Al. Geophys. Res. Lett. 3, 109–112.

Lehner, S., Petaev, M., Zolotov, M.Y., Buseck, P., 2013. Formation of niningerite by silicate sulfidation in EH3 enstatite chondrites. Geochim. Cosmochim. Acta 101, 34–56.

Leshin, L.A., Rubin, A.E., McKeegan, K.D., 1997. The oxygen isotopic composition of olivine and pyroxene from CI chondrites. Geochim. Cosmochim. Acta 61, 835–845.

Lewis, J.A., Jones, R.H., 2014. Nephelinization and metasomatism in the ordinary chondrite Parnallee (LL3. 6). Lunar Planet. Sci. 45, abstract#1661.

Lewis, J.A., Jones, R.H., 2015. Microtextural study of feldspar in petrologic type 4 ordinary chondrites: contrasting records of parent body metasomatism. Meteorit. Planet. Sci. 50, abstract#5119.

Lewis, J.A., Jones, R.H., 2016. Phosphate and feldspar mineralogy of equilibrated L chondrites: the record of metasomatism during metamorphism in ordinary chondrite parent bodies. Meteorit. Planet. Sci. 51, 1886–1913.

Lewis, J.A., Jones, R.H., Brearley, A.J., 2016. Alkali feldspar exsolution in ordinary chondrites: Alkali metasomatism, metamorphism, and cooling rates. Lunar Planet. Sci. 47, abstract#2559.

Li, A., Draine, B., 2001. Infrared emission from interstellar dust: II. The diffuse interstellar medium. Astrophys. J. 554, 778.

Lin, Y.T., El Goresy, A.E., 2002. A comparative study of opaque phases in Qingzhen (EH3) and MacAlpine Hills 88136 (EL3): representatives of EH and EL parent bodies. Meteorit. Planet. Sci. 37, 577–599.

Lin, Y.T., Kimura, M., 1996. Discovery of complex titanium oxide associations in a plagioclase-olivine inclusion (POI) in the Ningqiang carbonaceous chondrite (abstract). Lunar Planet. Sci. 27, 755–756.

Lin, Y.T., Nagel, H.-J., Lundberg, L.L., El Goresy, A., 1991. MAC88136 – The first EL3 chondrite (abstract). Lunar Planet. Sci. 22, 811–812.

Lin, Y., El Goresy, A., Boyer, M., Feng, L., Zhang, J., Hao, J., 2011. Earliest solid condensates consisting of the assemblage oldhamite, sinoite, graphite and excess 36S in lawrencite from Almahata Sitta MS-17 EL3 chondrite. Workshop on Formation of the First Solids in the Solar System, abstract#9040.

Lindgren, P., Hanna, R.D., Dobson, K.J., Tomkinson, T., Lee, M.R., 2015. The paradox between low shock-stage and evidence of compaction in CM carbonaceous chondrites explained by mulitple low-intensity impacts. Geochim. Cosmochim. Acta 148, 159–178.

Lindstrom, M.M. (Ed.), 1990. Antarct. Meteorit. Newslett. 13, 9–24.

Lipschutz, M.E., 1964. Origin of diamonds in the ureilites. Science 143, 1431–1434.

Liu, Y., Ma, C., Beckett, J.R., Chen, Y., Guan, Y., 2016. Rare-earth-element minerals in martian breccia meteorites NWA 7034 and 7533: implications for fluid–rock interaction in the martian crust. Earth Planet. Sci. Lett. 451, 251–262.

Lofgren, G.E., 1989. Dynamic crystallization of chondrule melts of porphyritic olivine composition: textures experimental and natural. Geochim. Cosmochim. Acta 53, 461–470.

Lofgren, G.E., 1996. A dynamic crystallization model for chondrule melt. In: Hewins, R.H., Jones, R.H., Scott, E.R.D. (Eds.), Chondrules and the Protoplanetary Disk. Cambridge University Press, Cambridge, pp. 187–196.

Lofgren, G.E., Russell, W.J., 1986. Dynamic crystallization of chondrule melts of porphyritic and radial pyroxene composition. Geochim. Cosmochim. Acta 50, 1715–1726.

Lord, H.C., 1965. Molecular equilibria and condensation in a solar nebula and cool stellar atmospheres. Icarus 4, 279–288.

Lorenz, C.A., Nazarov, M.A., Brandstaetter, F., Ntaflos, T., 2010. Metasomatic alterations of olivine inclusions in the Budulan mesosiderite. Petrology 18, 461–470.

Lovering, J.F., Wark, D.A., Sewell, D.K.B., 1979. Refractory oxide, titanate, niobate and silicate accessory mineralogy of some type B Ca-Al inclusions in the Allende meteorite (abstract). Lunar Planet. Sci. 10, 745–746.

Lunning, N.G., Corrigan, C.M., McSween, H.Y., Tenner, T.J., Kita, N.T., Bodnar, R.J., 2016. CV and CM chondrite impact melts. Geochim. Cosmochim. Acta 189, 338–358.

Ma, C., 2010. Hibonite-(Fe),(Fe, Mg) $Al_{12}O_{19}$, a new alteration mineral from the Allende meteorite. Am. Miner. 95, 188–191.

Ma, C., 2011. Discovery of meteoritic lakargiite ($CaZrO_3$), a new ultra-refractory mineral from the Acer 094 carbonaceous chondrite. Meteorit. Planet. Sci. 46, A144.

Ma, C., 2012. Discovery of meteoritic eringaite, $Ca_3(Sc,Y,Ti)_2Si_3O_{12}$, the first solar garnet? Meteorit. Planet. Sci. 47, A256.

Ma, C., 2015a. Nanomineralogy of meteorites by advanced electron microscopy: discovering new minerals and new materials from the early solar system. Microsc. Microanal. 21, 2353–2354.

Ma, C., 2015b. Discovery of nuwaite, Ni_6GeS_2, a new alteration mineral in Allende. Meteorit. Planet. Sci. 50, abstract#5151.

Ma, C., 2017. Discovery of new mineral butianite, Ni_6SnS_2, an alteration phase from Allende. Meteorit. Planet. Sci., 52, abstract#6032.

Ma, C., Beckett, J.R., 2016a. Burnettite, $CaVAlSiO_6$, and paqueite, $Ca_3TiSi_2(Al_2Ti)O_{14}$, two new minerals from Allende: clues to the evolution of a V-rich Ca-Al-rich inclusion. Lunar Planet. Sci. 47, abstract#1595.

Ma, C., Beckett, J.R., 2016b. Majindeite, $Mg_2Mo_3O_8$, a new mineral from the Allende meteorite and a witness to post-crystallization oxidation of a Ca-Al-rich refractory inclusion. Am. Mineral. 101, 1161–1170.

Ma, C., Krot, A.N., 2014a. Hutcheonite, $Ca_3Ti_2(SiAl_2)O_{12}$, a new garnet mineral from the Allende meteorite: An alteration phase in a Ca-Al-rich inclusion. Am. Mineral. 99, 667–670.

Ma, C., Krot, A.N., 2014b. Discovery of a new Cl-rich silicate mineral, $Ca_{12}(Al_2Mg_3Si_7)O_{32}Cl_6$: an alteration phase in Allende. Meteorit. Planet. Sci. 49, A248.

Ma, C., Krot, A.N., 2015. Addibischoffite, IMA 2015- 006. CNMNC Newsletter No. 25, June 2015, p. 532. Mineral. Mag. 79, 529–535.

Ma, C., Rossman, G.R., 2008. Discovery of tazheranite (cubic zirconia) in the Allende Meteorite. Geochim. Cosmochim. Acta 72, A577.

Ma, C., Rossman, G.R., 2009a. Tistarite, Ti_2O_3, a new refractory mineral from the Allende meteorite. Am. Mineral. 94, 841–844.

Ma, C., Rossman, G.R., 2009b. Davisite, $CaScAlSiO_6$, a new pyroxene from the Allende meteorite. Am. Mineral. 94, 845–848.

Ma, C., Rossman, G.R., 2009c. Grossmanite, $CaTi^{3+}AlSiO_6$, a new pyroxene from the Allende meteorite. Am. Mineral. 94, 1491–1494.

Ma, C., Tschauner, O., 2016. Discovery of tetragonal almandine, $(Fe,Mg,Ca,Na)_3(Al,Si,Mg)_2Si_3O_{12}$, a new high-pressure mineral in Shergotty. Meteorit. Planet. Sci. 51, abstract#6124.

Ma, C., Tschauner, O., 2017. Zagamiite, IMA 2015-022a. CNMNC Newsletter No. 36, April 2017, page 409. Mineral. Mag. 81, 403–409.

Ma, C., Simon, S.B., Rossman, G.R., Grossman, L., 2009. Calcium Tschermak's pyroxene, $CaAlAlSiO_6$, from the Allende and Murray meteorites: EBSD and micro- Raman characterizations. Am. Mineral. 94, 1483–1486.

Ma, C., Beckett, J., Rossman, G., 2010. Grossmanite, davisite, and kushiroite: three newly-approved diopside-group clinopyroxenes in CAIs. Lunar Planet. Sci. 41, abstract#1494.

Ma, C., Beckett, J.R., Rossman, G.R., 2011a. Murchisite, Cr_5S_6, a new mineral from the Murchison meteorite. Am. Mineral. 96, 1905–1908.

Ma, C., Beckett, J.R., Tschauner, O., Rossman, G.R., 2011b. Thortveitite ($Sc_2Si_2O_7$), the first solar silicate? Meteorit. Planet. Sci. 46, A144.

Ma, C., Connolly, H.C., Beckett, J.R., Tschauner, O., Rossman, G.R., Kampf, A.R., Zega, T.J., Smith, S.A.S., Schrader, D.L., 2011c. Brearleyite, $Ca_{12}Al_{14}O_{32}Cl_2$, a new alteration mineral from the NWA 1934 meteorite. Am. Mineral. 96, 1199–1206.

Ma, C., Kampf, A.R., Connolly, H.C., Beckett, J.R., Rossman, G.R., Smith, S.A.S., Schrader, D.L., 2011d. Krotite, $CaAl_2O_4$, a new refractory mineral from the NWA 1934 meteorite. Am. Mineral. 96, 709–715.

Ma, C., Beckett, J.R., Rossman, G.R., 2012a. Browneite, MnS, a new sphalerite-group mineral from the Zakłodzie meteorite. Am. Mineral. 97, 2056–2059.

Ma, C., Beckett, J.R., Rossman, G.R., 2012b. Buseckite, (Fe,Zn,Mn)S, a new mineral from the Zakłodzie meteorite. Am. Mineral. 97, 1226–1233.

Ma, C., Tschauner, O., Beckett, J.R., Rossman, G.R., Liu, W., 2012c. Panguite, $(Ti^{4+}, Sc, Al, Mg, Zr, Ca)_{1.8}O_3$, a new ultra- refractory titania mineral from the Allende meteorite: synchrotron micro- diffraction and EBSD. Am. Miner. 97, 1219–1225.

Ma, C., Beckett, J.R., Connolly, H.C., Rossman, G.R., 2013a. Discovery of meteoritic loveringite, $Ca(Ti,Fe,Cr,Mg)_{21}O_{38}$, in an Allende chondrule: late- stage crystallization in a melt droplet. Lunar Planet. Sci. 44, abstract #1443.

Ma, C., Krot, A.N., Bizzarro, M., 2013b. Discovery of dmisteinbergite (hexagonal $CaAl_2Si_2O_8$) in the Allende meteorite: a new member of refractory silicates formed in the solar nebula. Am. Mineral. 98, 1368–1371.

Ma, C., Tschauner, O., Beckett, J.R., Rossman, G.R., Liu, W., 2013c. Kangite, $(Sc,Ti,Al,Zr,Mg,Ca,\square)_2O_3$, a new ultra-refractory scandia mineral from the Allende meteorite: synchrotron micro-Laue diffraction and electron backscatter diffraction. Am. Mineral. 98, 870–878.

Ma, C., Beckett, J.R., Rossman, G.R., 2014a. Allendeite ($Sc_4Zr_3O_{12}$) and hexamolybdenum (Mo,Ru,Fe), two new minerals from an ultrarefractory inclusion from the Allende meteorite. Am. Mineral. 99, 654–666.

Ma, C., Beckett, J.R., Rossman, G.R., 2014b. Monipite, MoNiP, a new phosphide mineral in a Ca-Al-rich inclusion from the Allende meteorite. Am. Mineral. 99, 198–205.

Ma, C., Krot, A.N., Beckett, J.R., Nagashima, K., Tschauner, O., 2015a. Discovery of warkite, $Ca_2Sc_6Al_6O_{20}$, a new Sc-rich ultra- refractory mineral in Muchison and Vigarano. Meteorit. Planet. Sci. 50, abstract#5025.

Ma, C., Tschauner, O., Beckett, J.R., Liu, Y., Rossman, G.R., Zhuravlev, K., Prakapenka, V., Dera, P., Taylor, L.A., 2015b. Tissintite, $(Ca,Na,\square)AlSi_2O_6$, a highly-defective, shock-induced, high-pressure clinopyroxene in the Tissint martian meteorite. Earth Planet. Sci. Lett. 422, 194–205.

Ma, C., Tschauner, O., Beckett, J.R., Rossman, G.R., 2015c. Liebermannite: A new potassic hollandite ($KAlSi_3O_8$) from the Zagami basaltic shergottite. Lunar Planet. Sci. 46, abstract#1401.

Ma, C., Krot, A.N., Nagashima, K., 2016a. Discovery of a new mineral addibischoffite, $Ca_2Al_6Al_6O_{20}$, in a Ca-Al-rich refractory inclusion from the Acfer 214 CH3 meteorite. Meteorit. Planet. Sci. 51, abstract#6016.

Ma, C., Paque, J.M., Tschauner, O., 2016b. Discovery of beckettite, $Ca_2V_6Al_6O_{20}$, a new alteration mineral in a V-Rich Ca-Al-rich inclusion from Allende. Lunar Planet. Sci. 47, abstract#1704.

Ma, C., Tschauner, O., Beckett, J.R., Liu, Y., Rossman, G.R., Sinogeikin, S.V., Smith, J.S., Taylor, L.A., 2016c. Ahrensite, γ-Fe_2SiO_4, a new shock-metamorphic mineral from the Tissint meteorite: implications for the Tissint shock event on Mars. Geochim. Cosmochim. Acta 184, 240–256.

Ma, C., Yoshizaki, T., Nakamura, T., Muto, J., 2017a. Rubinite, IMA 2016-110. CNMNC Newsletter No. 36, April 2017, page 408. Mineral. Mag. 81, 403–409.

Ma, C., Tschauner, O., Beckett, J.R., 2017b. A new high-pressure calcium aluminosilicate ($CaAl_2Si_{3.5}O_{11}$) in martian meteorites: Another after-life for plagioclase and connections to the CAS phase. Lunar Planet Sci. 48, abstract#1128.

Ma, C., Lin, C., Bindi, L., Steinhardt, P.J., 2017c. Hollisterite (Al_3Fe), kryachkoite $(Al,Cu)_6(Fe,Cu)$, and stolperite $(AlCu)$: three new minerals from the Khatyrka CV3 carbonaceous chondrite. Am. Mineral. 102, 690–693.

Ma, C., Yoshizaki, T., Krot,A, N., Beckett, J.R., Nakamura, T., Nagashima, K., Muto, J., Ivanova, M.A., 2017d. Discovery of rubinite, $Ca_3Ti^{3+}{}_2Si_3O_{12}$, a new garnet mineral in refractory inclusions from carbonaceous chondrites. Meteorit. Planet. Sci., 52, abstract#6023.

MacPherson, G.J., 2005. In: Davis, A.M., Holland, H.D., Turekian, K.K. (Eds.), Calcium- aluminum-rich inclusions in chondritic meteorites. Meteorites, Comets and Planets: Treatise on Geochemistry, Volume 1. Elsevier, Amsterdam, The Netherlands, pp. 201–246.

MacPherson, G.J., Delaney, J.S., 1985. A fassaite-two olivine- pleonaste-bearing refractory inclusion from Karoonda (abstract). Lunar Planet. Sci. 16, 515–516.

MacPherson, G.J., Grossman, L., 1984. Fluffy Type A Ca-, Al-rich inclusions in the Allende meteorite. Geochim. Cosmochim. Acta 48, 29–46.

MacPherson, G.J., Krot, A.N., 2002. Distribution of Ca-Fe-silicates in CV3 chondrites: possible controls by parent-body compaction. Meteorit. Planet. Sci. 37, A91.

MacPherson, G.J., Krot, A.N., 2014. The formation of Ca-, Fe- rich silicates in reduced and oxidized CV chondrites: the roles of impact- modified porosity and permeability, and heterogeneous distribution of water ices. Meteorit. Planet. Sci. 49, 1250–1270.

MacPherson, G.J., Wark, D.A., Armstrong, J.T., 1988. Primitive material surviving in chondrites: refractory inclusions. In: Kerridge, J.F., Matthews, M.S. (Eds.), Meteorites and the Early Solar System. Univ. Arizona, pp. 746–807.

MacPherson, G., Simon, S., Davis, A., Grossman, L., Krot, A., 2005. In: Krot, A.N., Scott, E.R.D., Reipurth, B. (Eds.), Calcium-aluminum-rich inclusions: Major unanswered questions. Chondrites and the protoplanetary disk, 225–250.

MacPherson, G.J., Lin, C., Hollister, L.S., Bindi, L., Andronicos, C.L., Steinhardt, P.J., 2016. The Khatyrka meteorite: a summary of evidence for a natural origin of its remarkable Cu-Al metal alloys. Lunar Planet. Sci. 47, abstract#2655.

Malvin, D.J., Wang, D., Wasson, J.T., 1984. Chemical classification of iron meteorities-X. Multielement studies of 43 irons, resolution of group IIIE from IIIAB, and evaluation of Cu as a taxonomic parameter. Geochim. Cosmochim. Acta 48, 785–804.

Mao, X.-Y., Ward, B.J., Grossman, L., MacPherson, G.J., 1990. Chemical composition of refractory inclusions from the Vigarano and Leoville carbonaceous chondrites. Geochim. Cosmochim. Acta 54, 2121–2132.

Marchi, S., Delbo, M., Morbidelli, A., Paolicchi, P., Lazzarin, M., 2009. Heating of near- Earth objects and meteoroids due to close approaches to the Sun. Mon. Not. R. Astron. Soc. 400, 147–153.

Marrocchi, Y., Gounelle, M., Blanchard, I., Caste, F., Kearsley, A.T., 2014. The Paris CM chondrite: secondary minerals and asteroidal processing. Meteorit. Planet. Sci. 49, 1232–1249.

Marvin, U.B., 1962. Cristobalite in the Carbo iron meteorite. Nature 196, 634–636.

Marvin, U.B., Klein, C., 1964. Meteoritic zircon. Science 146, 919–920.

Mason, B., 1962. Meteorites. John Wiley & Sons, Inc, New York, New York, pp. 274.

Mason, B., 1967. Extraterrestrial mineralogy. Am. Mineral. 52, 307–325.

Mason, B., 1972. The mineralogy of meteorites. Meteoritics 7, 309–326.

Mason, B., Jarosewich, E., 1967. The Winona meteorite. Geochim. Cosmochim. Acta 31, 1097–1099.

Mason, B., Taylor, S.R., 1982. Inclusions in the Allende meteorite. Smithsonian Contribut. Earth Sci. 25, 30.

Mathis, J.S., 1993. Observations and theories of interstellar dust. Rep. Prog. Phys. 56, 605.

McCall, G.J.H., 1966. The petrology of the Mount Padbury mesosiderite and its achondrite enclaves. Mineral. Mag. 35, 1029–1060.

McCall, G.J.H., 1973. Meteorites and Their Origins. David & Charles, Devon, U.K, pp. 352.

McCanta, M.C., Treiman, A.H., Dyar, M.D., Alexander, C.M.O.D., Rumble, D., Essene, E.J., 2008. The LaPaz Icefield 04840 meteorite: mineralogy, metamorphism, and origin of an amphibole-and biotite-bearing R chondrite. Geochim. Cosmochim. Acta 72, 5757–5780.

McConville, P., Kelley, S., Turner, G., 1988. Laser probe 40Ar-39Ar studies of the Peace River shocked L6 chondrite. Geochim. Cosmochim. Acta 52, 2487–2499.

McCord, T.B., Li, J.Y., Combe, J.P., McSween, H.Y., Jaumann, R., Reddy, V., Tosi, F., Williams, D.A., Blewett, D.T., Turrini, D., 2012. Dark material on Vesta from the infall of carbonaceous volatile-rich material. Nature 491, 83–86.

McCoy, T.J., Keil, K., Scott, E.R.D., Haack, H., 1993. Genesis of the IIICD iron meteorites: evidence from silicate-bearing inclusions. Meteoritics 28, 552–560.

McCoy, T.J., Steele, I.M., Keil, K., Leonard, B.F., Endress, M., 1994. Chladniite, $Na_2CaMg_7(PO_4)_6$: a new mineral from the Carlton (IIICD) iron meteorite. Am. Mineral. 79, 375–380.

McCoy, T.J., Keil, K., Clayton, R.N., Mayeda, T.K., Bogard, D.D., Garrison, D.H., Huss, G.R., Hutcheon, I.D., Wieler, R., 1996. A petrologic, chemical, and isotopic study of Monument Draw and comparison with other acapulcoites: evidence for formation by incipient partial melting. Geochim. Cosmochim. Acta 60, 2681–2708.
McCoy, T.J., Keil, K., Muenow, D.W., Wilson, L., 1997. Partial melting and melt migration in the acapulcoite- lodranite parent body. Geochim. Cosmochim. Acta 61, 639–650.
McCubbin, F.M., Tosca, N.J., Smirnov, A., Nekvasil, H., Steele, A., Fries, M., Lindsley, D.H., 2009. Hydrothermal jarosite and hematite in a pyroxene-hosted melt inclusion in martian meteorite Miller Range (MIL) 03346: implications for magmatic-hydrothermal fluids on Mars. Geochim. Cosmochim. Acta 73, 4907–4917.
McKay, D.S., Clanton, U.S., Morrison, D.A., Ladle, G.H., 1972. Vapor phase crystallization in Apollo 14 breccia. Proc. Lunar. Sci. Conf. 3, 739–752.
McKay, G.A., Le, L., Wagstaff, J., Lindstrom, D., 1988. Experimental trace element partitioning for LEW 86010: petrogenesis of a unique achondrite. Meteorit. 23, 289.
McKinley, S.G., Scott, E.R.D., Keil, K., 1984. Composition and origin of enstatite in E chondrites. Proc. Lunar Planet. Sci. Conf. 14, B567–B572.
McSween, H.Y., 1977. Carbonaceous chondrites of the Ornans type: a metamorphic sequence. Geochim. Cosmochim. Acta 41, 477–491.
McSween, H.Y., 1979. Alteration in CM carbonaceous chondrites inferred from modal and chemical variations in matrix. Geochim. Cosmochim. Acta 43, 1761–1770.
McSween, H.Y., 1994. What we have learned about Mars from SNC meteorites. Meteoritics 29, 757–779.
McSween, H.Y., 2006. Water on Mars. Elements 2, 135–137.
McSween, H.Y., 2008. Martian meteorites as crustal samples. In: Jim Bell III (Ed.), The Martian Surface – Composition, Mineralogy, and Physical Properties. Cambridge University Press, p. 383.
McSween, H.Y., Huss, G.R., 2010. Cosmochemistry. Cambridge University Press, pp. 549.
McSween, H.Y., Labotka, T.C., 1993. Oxidation during metamorphism of the ordinary chondrites. Geochim. Cosmochim. Acta 57, 1105–1114.
McSween, H.Y., Treiman, A.H., 1998. Martian meteorites. Rev. Mineral. Geochem. 36 (6), 1–6.53.
McSween, H.Y., Ghosh, S., Grimm, R.E., Wilson, L., Young, E.D., 2002. Thermal Evolution Models of Asteroids. In: WF, Paolicchi, P., Binzel, R.P. (Eds.), Asteroids III. University of Arizona Press, Tucson, pp. 559–571.
Melosh, H.J., 1989. Impact Cratering: A Geologic Process. Oxford University Press, Oxford, U.K, pp. 245.
Messenger, S., Keller, L.P., Stadermann, F.J., Walker, R.M., Zinner, E., 2003. Samples of stars beyond the solar system: silicate grains in interplanetary dust. Science 300, 105–108.
Messenger, S., Speck, A., Volk, K., 2013. Probing the "30μm" feature: lessons from exteme carbon stars. Astrophys. J. 764, 1–15.
Metzler, K., 1985. Gefüge und Zusammensetzung von Gesteinsfragmenten in polymikten achondritischen Breccien. University of Münster.
Metzler, K., Bischoff, A., Stöffler, D., 1992. Accretionary dust mantles in CM chondrites: evidence for solar nebula processes. Geochim. Cosmochim. Acta 56, 2873–2897.
Meyer, C., 1996. Mars Meteorite Compendium – 1996. NASA, Johnson Space Center, Houston, pp. 175.
Mikouchi, T., Miyamoto, M., McKay, G.A., 1995. Mineralogical study of angrite Asuka-881371: its possible relation to angrite LEW87051 (abstract). NIPR Symp. Antarct. Meteor. 20, 159–162.
Mikouchi, T., Yamada, I., Miyamoto, M., 2000. Symplectic exsolution in olivine from the Nakhla martian meteorite. Meteorit. Planet. Sci. 35, 937–942.
Mikouchi, T., Ota, K., Makishima, J., Monkawa, A., Sugiyama, K., 2007. Mineralogy and crystallography of LAP04840: implications for metamorphism at depth in the R chondrite parent body. Lunar Planet. Sci.
Mikouchi, T., Zolensky, M., Ivanova, M., Tachikawa, O., Komatsu, M., Le, L., Gounelle, M., 2009. Dmitryivanovite: a new high-pressure calcium aluminum oxide from the Northwest Africa 470 CH3 chondrite characterized using electron backscatter diffraction analysis. Am. Mineral. 94, 746–750.
Mikouchi, T., Hagiya, K., Sawa, N., Kimura, M., Ohsumi, K., Komatsu, M., Zolensky, M., 2016. Synchrotron radiation XRD analysis of indialite in Yamato- 82094 ungrouped carbonaceous chondrite. Lunar Planet. Sci. 47, abstract#1919.
Mittlefehldt, D.W., Lindstrom, M.M., 1990. Geochemistry and genesis of the angrites. Geochim. Cosmochim. Acta 54, 3209–3218.
Mittlefehldt, D.W., Lindstrom, M.M., 2001. Petrology and geochemistry of Patuxent Range 91501, a clast- poor impact melt from the L-chondrite parent body and Lewis Cliff 88663, an L7 chondrite. Meteorit. Planet. Sci. 36, 439–457.
Mittlefehldt, D.W., Rubin, A.E., Davis, A.M., 1992. Mesosiderite clasts with the most extreme positive Eu anomalies among solar system rocks. Science 257, 1096–1099.
Mittlefehldt, D.W., Lindstrom, M.M., Bogard, D.D., Garrison, D.H., Field, S.W., 1996. Acapulco-and Lodran-like achondrites: Petrology, geochemistry, chronology, and origin. Geochim. Cosmochim. Acta 60, 867–882.
Mittlefehldt, D.W., McCoy, T.J., Goodrich, C.A., Kracher, A., 1998. Non-chondritic meteorites from asteroidal bodies. Rev. Miner. 36 (4), 1–195.
Mittlefehldt, D.W., Killgore, M., Lee, M.T., 2002. Petrology and geochemistry of D'Orbigny, geochemistry of Sahara 99555, and the origin of angrites. Meteorit. Planet. Sci. 37, 345–369.
Miyashiro, A., 1966. Minerals of meteorites (in Japanese). Kobutsugaku Zassi 8, 49–59.
Mori, H., Takeda, H., 1981. Thermal and deformational histories of diogenites as inferred from their microtextures of orthopyroxene. Earth Planet. Sci. Lett. 53, 266–274.
Mostefaoui, S., Hoppe, P., 2004. Discovery of Abundant In Situ Silicate and Spinel Grains from Red Giant Stars in a Primitive Meteorite. Appl. J. Lett., 613.
Mostefaoui, S., Hoppe, P., Marhas, K.K., Gröner, E., 2003. Search for in situ presolar oxygen-rich dust in meteorites. Meteorit. Planet. Sci. 38, 5185.
Nagahara, H., 1981. Evidence for secondary origin of chondrules. Nature 292, 135–136.
Nagahara, H., 1992. Yamato-8002: partial melting residue on the unique chondrite parent body. Proc. NIPR Symp. Antarct. Meteorit. 5, 191–223.
Nagashima, K., Krot, A.N., Yurimoto, H., 2004. Stardust silicates from primitive meteorites. Nature 428, 921–924.
Nagashima, K., Krot, A., Libourel, G., Huss, G., 2013. Magnesian porphyritic chondrules surrounded by ferroan igneous rims from CR chondrite GRA 95229. Lunar Planet. Sci., 1780.
Nakagawa, Y., Sekiya, M., Hayashi, C., 1986. Settling and growth of dust particles in a laminar phase of a low-mass solar nebula. Icarus 67, 375–390.
Nakamura, K., Nogushi, T., Ozono, Y., Osawa, T., Nagao, K., 2005. Mineralogy of ultracarbonaceous large micrometeorites (abstract). Meteorit. Planet. Sci. 40, A110.
Nakamura, T., 2005. Post-hydration thermal metamorphism of carbonaceous chondrites. J. Mineral. Petrol. Sci. 100, 260–272.
Nakamura-Messenger, K., Keller, L.P., Clemett, S.J., Messenger, S., Jones, J.H., Palma, R.L., Pepin, R.O., Klöck, W., Zolensky, M.E., Tatsuoka, H., 2010. Brownleeite: a new manganese silicide mineral in an interplanetary dust particle. Am. Mineral. 95, 221–228.
Nakamura-Messenger, K., Clemett, S.J., Rubin, A.E., Choi, B.-G., Zhang, S., Rahman, Z., Oikawa, K., Keller, L.P., 2012. Wassonite: a new titanium monosulfide mineral in the Yamato 691 enstatite chondrite. Am. Miner. 97, 807–815.
Nakamuta, Y., Aoki, Y., 2000. Mineralogical evidence for the origin of diamond in ureilites. Meteorit. Planet. Sci. 35, 487–493.
Nakato, A., Nakamura, T., Kitajima, F., Nogouchi, T., 2008. Evaluation of dehydration mechanism during heating of hydrous asteroids based on mineralogical and chemical analysis of naturally and experimentally heated CM chondrites. Earth Planets Space 60, 855–864.
Nathues, A., Hoffmann, M., Cloutis, E.A., Schäfer, M., Reddy, V., Christensen, U., Sierks, H., Thangjam, G.S., Le Corre, L., Mengel, K., 2014. Detection of serpentine in exogenic carbonaceous chondrite material on Vesta from Dawn FC data. Icarus 239, 222–237.
Nehru, C.E., Zucker, S.M., Harlow, G.E., Prinz, M., 1980. Olivines and olivine coronas in mesosiderites. Geochim. Cosmochim. Acta 44, 11031109–11071118.
Nehru, C.E., Prinz, M., Delaney, J.S., 1982a. The Tucson iron and its relationship to enstatite meteorites. Proc. Lunar Planet. Sci. Conf. 13, A365–A373.
Nehru, C.E., Prinz, M., Delaney, J.S., 1982b. The Tucson iron and the aubrites. Proc. Lunar Planet. Sci. 13, 586–587.
Nehru, C.E., Prinz, M., Delaney, J.S., Dreibus, G., Palme, H., Spettel, B., Wänke, H., 1983. Brachina: A new type of meteorite, not a chassignite. Proc. Lunar Planet. Sci. Conf. 14 (88), B237–B244.
Nehru, C.E., Prinz, M., Weisberg, M.K., Ebihara, M., Clayton, R.N., Mayeda, T.K., 1992. Brachinites: A new primitive achondrite group (abstract). Meteoritics 27, 267.
Nehru, C.E., Prinz, M., Weisberg, M.K., Ebihara, M.E., Clayton, R.N., Mayeda, T.K., 1996. A new brachinite and petrogenesis of the group (abstract). Lunar Planet. Sci. 27, 943–944.
Nelson, V.E., Rubin, A.E., 2002. Size-frequency distributions of chondrules and chondrule fragments in LL3 chondrites: Implications for parent-body fragmentation of chondrules. Meteorit. Planet. Sci. Lett. 37, 1361–1376.
Nesvorný, D., Vokrouhlický, D., Bottke, W.F., Gladman, B., Häggström, T., 2007. Express delivery of fossil meteorites from the inner asteroid belt to Sweden. Icarus 188, 400–413.
Newsom, H.E., Drake, M.J., 1979. The origin of metal clasts in the Bencubbin meteoritic breccia. Geochim. Cosmochim. Acta 43, 689–707.
Nguyen, A.N., Zinner, E., 2004. Discovery of ancient silicate stardust in a meteorite. Science 303, 1496–1499.
Nickel, E.H., Graham, J., 1987. Paraotwayite: a new nickel hydroxide mineral from Western Australia. Can. Meteorol. 25, 409–411.
Nielsen, H.P., Buchwald, V.F., 1981. Roaldite, a new nitride in iron meteorites. Proc. Lunar Planet. Sci. Conf. 12, 1343–1348.
Nishiizumi, K., Caffee, M.W., Hamajima, Y., Reedy, R.C., Welten, K.C., 2014. Exposure history of the Sutter's Mill carbonaceous chondrite. Meteorit. Planet. Sci. 49, 2056–2063.
Nittler, L.R., Hoppe, P., Alexander, C.M.O.D., Amari, S., Eberhardt, P., Gao, X., Lewis, R.S., Strebel, R., Walker, R.M., Zinner, E., 1995. Silicon nitride from supernovae. Astrophys. J. 453, L25–L28.
Noguchi, T., 1989. Texture and chemical composition of pyroxenes in chondrules in carbonaceous and unequilibrated ordinary chondrites. Proc. NIPR Sympo. Antarctic. Meteorit. 2, 169–199.
Norman, M.D., Keil, K., Griffin, W.L., Ryan, C.G., 1995. Fragments of ancient lunar crust: petrology and geochemistry of ferroan noritic anorthosites from the Descartes region of the Moon. Geochim. Cosmochim. Acta 59, 831–847.
Nuth, J.A., Brearley, A.J., Scott, E.R.D., 2005. Microcrystals and amorphous material in comets and primitive meteorites: Keys to understanding processes in the early solar system. In: Krot, A.N., Scott, E.R.D., Reipurth, B. (Eds.), Chondrites

and the Protoplanetary Disk ASP Conference Series, 341. Astronomical Society of the Pacific, San Francisco, pp. 675–700.
Nyquist, L., Reese, Y., Wiesmann, H., Shih, C.-Y., Takeda, H., 2003. Fossil 26 Al and 53 Mn in the Asuka 881394 eucrite: evidence of the earliest crust on asteroid 4 Vesta. Earth Planet. Sci. Lett. 214, 11–25.
Nystrom, J.O., Wickman, F.E., 1991. The Ordovician chondrite from Brunflo, central Sweden, II. Secondary minerals. Lithos 27, 167–185.
Okada, A., Keil, K., 1982. Caswellsilverite, $NaCrS_2$: a new mineral in the Norton County enstatite achondrite. Am. Mineral. 67, 132–136.
Okada, A., Keil, K., Taylor, G.J., 1981. Unusual weathering products of oldhamite parentage in the Norton County enstatite achondrite. Meteoritics 16, 141–152.
Okada, A., Keil, K., Leonard, B.F., Hutcheon, I.D., 1985. Schollhornite, $Na_{0.3}(H_2O)_1[CrS_2]$, a new mineral in the Norton County enstatite achondrite. Am. Mineral. 70, 638–643.
Okada, A., Keil, K., Taylor, G.J., Newsom, H., 1988. Igneous history of the aubrite parent asteroid: Evidence from the Norton County enstatite achondrite. Meteoritics 23, 59–74.
Olsen, E., 1981a. Meteoritic minerals. In: Frye, K. (Ed.), The Encyclopedia of Mineralogy. Hutchinson Ross Publishing Company, Stroudsburg, Pennsylvania, pp. 240–246.
Olsen, E.J., 1981b. Vugs in ordinary chondrites. Meteoritics 16, 45–59.
Olsen, E.J., Bunch, T.E., 1984. Equilibration temperatures of the ordinary chondrites: a new evaluation. Geochim. Cosmochim. Acta 48, 1363–1365.
Olsen, E., Fredriksson, K., 1966. Phosphates in iron and pallasite meteorites. Geochim. Cosmochim. Acta 30, 459–470.
Olsen, E., Fuchs, L.H., 1968. Krinovite, $NaMg_2CrSi_3O_{10}$: a new meteorite mineral. Science 161, 786–787.
Olsen, E., Jarosewich, E., 1970. The chemical composition of the silicate inclusions in the Weekeroo Station iron meteorite. Earth Planet. Sci. Lett. 8, 261–266.
Olsen, E., Jarosewich, E., 1971. Chondrules: first occurrence in an iron meteorite. Science 174, 583–585.
Olsen, E.J., Steele, I.M., 1997. Galileiite: A new meteoritic phosphate mineral. Meteorit. Planet. Sci 32, A155–A156.
Olsen, E., Huebner, J.S., Douglas, J.A.V., Plant, A.G., 1973. Meteoritic amphiboles. Am. Mineral. 58, 869–872.
Olsen, E., Erlichman, J., Bunch, T.E., Moore, P.B., 1977. Buchwaldite, a new meteoritic phosphate mineral. Am. Mineral. 62, 362–364.
Olsen, E.J., Fredriksson, K., Rajan, S., Noonan, A., 1990. Chondrule-like objects and brown glasses in howardites. Meteoritics 25, 187–195.
Olsen, E.J., Kracher, A., Davis, A.M., Steele, I.M., Hutcheon, I.D., Bunch, T.E., 1999. The phosphates of IIIAB iron meteorites Meteorit. Planet. Sci. 34, 285–300.
Ormö, J., Sturkell, E., Nõlvak, J., Melero-Asensio, I., Frisk, Å., Wikström, T., 2014. The geology of the Målingen structure: A probable doublet to the Lockne marine-target impact crater, central Sweden. Meteorit. Planet. Sci. 49, 313–327.
Ota, K., Mikouchi, T., Sugiyama, K., 2009. Crystallography of hornblende amphibole in LAP04840 R chondrite and implication for its metamorphic history. J. Mineral. Petrol. Sci. 104, 215–225.
Ott, U., 1996. Interstellar grains: Some facts, implications, and ideas (abstract). Meteorit. Planet. Sci. 31, A102–A103.
Overlin, S., 2008. Interplanetary cat's eye peridot. Gems Gemol. 44, 177.
Palme, H., Schultz, L., Spettel, B., Weber, H.W., Wänke, H., Michel-Levy, M.C., Lorin, J.C., 1981. The Acapulco meteorite: chemistry, mineralogy and irradiation effects. Geochim. Cosmochim. Acta 45, 727–752.
Papike, J.J., 1998. Planetary Materials. Reviews in Mineralogy, 36. Mineralogical Society of America, Washington, D.C.
Papike, J., Taylor, L., Simon, S., 1991. Lunar minerals. In: Heiken, G.H., Vaniman, D.T., French, B.M. (Eds.), Lunar Sourcebook: A User's Guide to the Moon. Cambridge University Press, Cambridge, pp. 121–181.
Papike, J.J., Ryder, G., Shearer, C.K., 1998. Lunar samples. Rev. Mineral. Geochem. 36, 5.1–5.234.
Paque, J.M., Beckett, J.R., Barber, D.J., Stolper, E.M., 1994. A new titanium-bearing calcium aluminosilicate phase: I: Meteoritic occurrences and formation in synthetic systems. Meteoritics 29, 673–682.
Patzer, A., Hill, D.H., Boynton, W.V., 2004. Evolution and classification of acapulcoites and lodranites from a chemical point of view. Meteorit. Planet. Sci. 39, 61–85.
Pederson, T.P., 1999. Schwertmannite and awaruite as alteration products in iron meteorites. Meteorit. 62, 5117.
Pekov, I., 1998. Minerals first discovered on the territory of the former Soviet Union. Ocean Pictures Ltd, Moscow, pp. 369.
Pekov, I.V., Perchiazzi, N., Merlino, S., Kalachev, V.N., Merlini, M., Zadov, A.E., 2007. Chukanovite, $Fe_2(CO_3)(OH)_2$, a new mineral from the weathered iron meteorite Dronino. Eur. J. Mineral. 19, 891–898.
Petaev, M.I., Jacobsen, S.B., 2009. Petrologic study of SJ101, a few forsterite-bearing CAI from the Allende CV3 chondrite. Geochim. Cosmochim. Acta 73, 5100–5114.
Petaev, M.I., Wood, J.A., 1998a. The condensation with partial isolation (CWPI) model of condensation in the solar nebula. Meteor. Planet. Sci. 33, 1123–1137.
Petaev, M.I., Wood, J.A., 1998b. The CWPI model of nebular condensation: effects of pressure on the condensation sequence. Meteor. Planet. Sci. 33, A122.
Petaev, M.I., Clarke Jr., R.S., Olsen, E.J., Jarosewich, E., Davis, A.M., Steele, I.M., Lipschutz, M.E., Wang, M.-S., Clayton, R.N., Mayeda, T.K., Wood, J.A., 1993. Chaunskij: the most highly metamorphosed, shock-modified and metal-rich mesosiderite abstract. Lunar Planet. Sci. 24, 1131–1132.
Petrovic, J.J., 2001. Review: Mechanical properties of meteorites and their constituents. J. Material. Sci. 36, 1579–1583.
Pierazzo, E., Melosh, H.J., 2000. Understanding oblique impacts from experiments, observations, and modeling. Annu. Rev. Earth Planet. Sci. 28, 141–167.
Powell, B.N., 1969. Petrology and chemistry of mesosiderites-I. Textures and compositions of nickel-iron. Geochim. Cosmochim. Acta 33, 789–810.
Powell, B.N., 1971. Petrology and chemistry of mesosiderites-II. Silicate textures and compositions and metal- silicate relationships. Geochim. Cosmochim. Acta 35, 5–34.
Pratesi, G., Bindi, L., Moggi- Cecchi, V., 2006. Icosahedral coordination of phosphorus in the crystal structure of melliniite, a new phosphide mineral from the Northwest Africa 1054 acapulcoite. Am. Mineral. 94, 451–454.
Price, G.D., Putnis, A., Agrell, S.O., 1979. Electron petrography of shock-produced veins in the Tenham chondrite. Contrib. Mineral. Petrol. 71, 211–218.
Prinz, M., Nehru, C.E., Delaney, J.S., 1982. Sombrerete: An iron with highly fractionated amphibole- bearing Na-P-rich silicate inclusions (abstract). Lunar Planet. Sci. 13, 634–635.
Prinz, M., Nehru, C.E., Weisberg, M.K., Delaney, J.S., 1984. Type 3 enstatite chondrites: a newly recognized group of unequilibrated enstatite chondrites (UEC's) (abstract). Lunar Planet. Sci. 15, 653–654.
Prinz, M., Weisberg, M.K., Nehru, C.E., 1988. Gunlock: a new type 3 ordinary chondrite with a golfball-sized chondrule (abstract). Meteoritic 23, 297.
Quirico, E., Bourot-Denise, M., Robin, C., Montagnac, G., Beck, P., 2011. A reappraisal of the metamorphic history of EH3 and EL3 enstatite chondrites. Geochim. Cosmochim. Acta 75, 3088–3102.
Rambaldi, E.R., 1981. Relict grains in chondrules. Nature 293, 558–561.
Ramdohr, P., 1963. Opaque minerals in stony meteorites. J. Geophys. Res. 68, 2011–2036.
Ramdohr, P., 1967. Die Schmelzkruste der Meteoriten. Earth Planet. Sci. Lett. 2, 197–209.
Ramdohr, P., 1973. The Opaque Minerals in Stony Meteorites. Elsevier, Amsterdam, pp. 245.
Rancourt, D.G., Scorzelli, R.B., 1995. Low-spin γ-Fe-Ni (γLS) proposed as a new mineral in Fe-Ni-bearing meteorites: epitaxial intergrowth of γLS and tetrataenite as a possible equilibrium state at∼ 20-40 at% Ni. J. Magnet. Magnet. Mater. 150, 30–36.
Reeves, H., Audouze, J., 1968. Early heat generation in meteorites. Earth Planet. Sci. Lett. 4, 135–141.
Reid, A.M., Cohen, A.J., 1967. Some characteristics of enstatite from enstatite achondrites. Geochim. Cosmochim. Acta 31, 661IN13671–13670IN14672.
Rietmeijer, F.J.M., 1996. The ultrafine mineralogy of a molten interplanetary dust particle as an example of the quench regime of atmospheric entry heating. Meteorit. Planet. Sci. 31, 237–242.
Rietmeijer, F.J.M., MacKinnon, I.D.R., 1987. Interstellar titanium oxides in interplanetary dust (abstract). Meteorit. 22, 490–491.
Rietmeijer, F.J.M., MacKinnon, I.D.R., 1990. Titanium oxide magneli phases in four chondritic interplnaetary dust particles. Proc. Lunar Planet. Sci. Conf. 20, 323–333.
Righter, K., Cosca, M.A., Morgan, L.E., 2016. Preservation of ancient impact ages on the R chondrite parent body: $^{40}Ar/^{39}Ar$ age of hornblende-bearing R chondrite LAP 04840. Meteorit. Planet. Sci. 51, 1678–1684.
Rubin, A.E., 1982. Petrology and origin of brecciated chondritic meteorites. In: Ph.D. thesis. The University of New Mexico, Albuquerque, New Mexico, pp. 220.
Rubin, A.E., 1983a. The Adhi-Kot enstatite chondrite breccia and implications for the origin of silica-rich clasts and chondrules. Earth Planet. Sci. Lett. 64, 201–212.
Rubin, A.E., 1983b. The Atlanta enstatite chondrite breccia. Meteoritics 18, 113–121.
Rubin, A.E., 1984a. Coarse-grained chondrule rims in type 3 chondrites. Geochim. Cosmochim. Acta 48, 1779–1789.
Rubin, A.E., 1984b. The Blithfield meteorite and the origin of sulfide-rich, metal-poor clasts and inclusions in brecciated enstatite chondrites. Earth Planet. Sci. Lett. 67, 273–283.
Rubin, A.E., 1985. Impact melt products of chondritic material. Rev. Geophys. 23, 277–300.
Rubin, A.E., 1988. Formation of ureilites by impact-melting of carbonaceous chondritic material. Meteoritics 23, 333–337.
Rubin, A.E., 1990. Kamacite and olivine in ordinary chondrites: Intergroup and intragroup relationships. Geochim. Cosmochim. Acta 54, 1217–1232.
Rubin, A.E., 1991. Euhedral awaruite in the Allende meteorite: Implications for the origin of awaruite- and magnetite-bearing nodules in CV3 chondrites. Am. Mineral. 76, 1356–1362.
Rubin, A.E., 1992. A shock-metamorphic model for silicate darkening and compositionally variable plagioclase in CK and ordinary chondrites. Geochim. Cosmochim. Acta 56, 1705–1714.
Rubin, A.E., 1994a. Metallic copper in ordinary chondrites. Meteoritics 29, 93–98.
Rubin, A.E., 1994b. Euhedral tetrataenite in the Jelica meteorite. Mineral. Mag. 58, 215–221.
Rubin, A.E., 1995a. Petrologic evidence for collisional heating of chondritic asteroids. Icarus 113, 156–167.
Rubin, A.E., 1995b. Fractionation of refractory siderophile elements in metal from the Rose City meteorite. Meteoritics 30, 412–417.
Rubin, A.E., 1997a. Mineralogy of meteorite groups. Meteorit. Planet. Sci. 32, 231–247.
Rubin, A.E., 1997b. Mineralogy of meteorite groups: An update. Meteorit. Planet. Sci. 32, 733–734.

Rubin, A.E., 1997c. The Hadley Rille enstatite chondrite and its agglutinate-like rim: Impact melting during accretion to the Moon. Meteorit. Planet. Sci. 32, 135–141.
Rubin, A.E., 1997d. Igneous graphite in enstatite chondrites. Mineral. Mag. 61, 699–703.
Rubin, A.E., 1997e. Sinoite (Si_2N_2O): Crystallization from EL chondrite impact melts. Am. Mineral. 82, 1001–1006.
Rubin, A.E., 1998. Correlated petrologic and geochemical characteristics of CO3 chondrites. Meteorit. Planet. Sci. 33, 385–391.
Rubin, A.E., 1999. Formation of large metal nodules in ordinary chondrites. J. Geophys. Res. 104, 30799–30804.
Rubin, A.E., 2000. Petrologic, geochemical and experimental constraints on models of chondrule formation. Earth Sci. Rev. 50, 3–27.
Rubin, A.E., 2002a. Post-shock annealing of MIL99301 (LL6): Implications for impact heating of ordinary chondrites. Geochim. Cosmochim. Acta 66, 3327–3337.
Rubin, A.E., 2002b. The Smyer H- chondrite impact-melt breccia and evidence for sulfur vaporization. Geochim. Cosmochim. Acta 66, 683–695.
Rubin, A.E., 2003. Chromite-plagioclase assemblages as a new shock indicator; Implications for the shock and thermal histories of ordinary chondrites. Geochim. Cosmochim. Acta 67, 2695–2709.
Rubin, A.E., 2004. Postshock annealing and postannealing shock in equilibrated ordinary chondrites: implications for the thermal and shock histories of chondritic asteroids. Geochim. Cosmochim. Acta 68, 673–689.
Rubin, A.E., 2005. Relationships among intrinsic properties of ordinary chondrites: oxidation state, bulk chemistry, oxygen-isotopic composition, petrologic type and chondrule size. Geochim. Cosmochim. Acta 69, 4907–4981.
Rubin, A.E., 2006. Shock, post-shock annealing, and post-annealing shock in ureilites. Meteorit. Planet. Sci. 41, 125–133.
Rubin, A.E., 2007. Petrogenesis of acapulcoites and lodranites: A shock-melting model. Geochim. Cosmochim. Acta 71, 2383–2401.
Rubin, A.E., 2008. Explicating the behavior of Mn-bearing phases during shock melting and crystallization of the Abee EH-chondrite impact-melt breccia. Meteorit. Planet. Sci. 43, 1481–1485.
Rubin, A.E., 2010a. Physical properties of chondrules in different chondrite groups: Implications for multiple melting events in dusty environments. Geochim. Cosmochim. Acta 74, 4807–4828.
Rubin, A.E., 2010b. Impact melting in the Cumberland Falls and Mayo Belwa aubrites. Meteorit. Planet. Sci. 45, 265–275.
Rubin, A.E., 2011. Origin of the differences in refractory-lithophile-element abundances among chondrite groups. Icarus 213, 547–558.
Rubin, A.E., 2012a. A new model for the origin of Type-B and Fluffy Type-A CAIs: Analogies to remelted compound chondrules. Meteorit. Planet. Sci. 47, 1062–1074.
Rubin, A.E., 2012b. Collisional facilitation of aqueous alteration of CM and CV carbonaceous chondrites. Geochim. Cosmochim. Acta 90, 181–194.
Rubin, A.E., 2013a. An amoeboid olivine inclusion (AOI) in CK3 NWA 1559, comparison to AOIs in CV3 Allende, and the origin of AOIs in CK and CV chondrites. Meteorit. Planet. Sci. 48, 432–444.
Rubin, A.E., 2013b. Multiple melting in a four-layered barred-olivine chondrule with compositionally heterogeneous glass from LL3. 0 Semarkona. Meteorit. Planet. Sci. 48, 445–456.
Rubin, A.E., 2014. Shock and annealing in the amphibole-and mica-bearing R chondrites. Meteorit. Planet. Sci. 49, 1057–1075.
Rubin, A.E., 2015a. Impact features of enstatite-rich meteorites. Chem. Erde 75, 1–28.
Rubin, A.E., 2015b. Shock and annealing in aubrites: Implications for parent-body history. Meteorit. Planet. Sci. 50, 1217–1227.
Rubin, A.E., 2015c. An American on Paris: extent of aqueous alteration of a CM chondrite and the petrography of its refractory and amoeboid olivine inclusions. Meteorit. Planet. Sci. 50, 1595–1612.
Rubin, A.E., 2015d. Maskelynite in asteroidal, lunar and planetary basaltic meteorites: An indicator of shock pressure during impact ejection from their parent bodies. Icarus 257, 221–229.
Rubin, A.E., 2016. Impact melting of the largest known enstatite meteorite: Al Haggounia 001, a fossil EL chondrite. Meteorit. Planet. Sci. 51, 1576–1587.
Rubin, A.E., Choi, B.-G., 2009. Origin of halogens and nitrogen in enstatite chondrites. Earth Moon Planet. 105, 41–53.
Rubin, A.E., Grossman, J.N., 1985. Phosphate-sulfide assemblages and Al/Ca ratios in type 3 chondrites. Meteoritics 20, 479–489.
Rubin, A.E., Huber, H., 2005. A weathering index for CK and R chondrites. Meteorit. Planet. Sci. 40, 1123–1130.
Rubin, A.E., Kallemeyn, G.W., 1989. Carlisle Lakes and Allan Hills 85151: Members of a new chondrite grouplet. Geochim. Cosmochim. Acta 53, 3035–3044.
Rubin, A.E., Kallemeyn, G.W., 1993. Carlisle Lakes chondrites: Relationship to other chondrite groups. Meteoritics 28, 424–425.
Rubin, A.E., Kallemeyn, G.W., 1994. Pecora Escarpment 91002: A member of the new Rumuruti (R) chondrite group. Meteoritics 29, 255–264.
Rubin, A.E., Keil, K., 1983. Mineralogy and petrology of the Abee enstatite chondrite breccia and its dark inclusions. Earth Planet. Sci. Lett. 62, 118–131.
Rubin, A.E., Mittlefehldt, D.W., 1992. Classification of mafic clasts from mesosiderites: Implications for endogenous igneous processes. Geochim. Cosmochim. Acta 56, 827–840.
Rubin, A.E., Mittlefehldt, D.W., 1993. Evolutionary history of the mesosiderite asteroid: A chronologic and petrologic synthesis. Icarus 101, 232–252.
Rubin, A.E., Moore, W.B., 2011. What's up? Preservation of gravitational direction in the Larkman Nunatak 06299 LL impact melt breccia. Meteorit. Planet. Sci. 46, 737–747.
Rubin, A.E., Scott, E.R.D., 1997. Abee and related EH chondrite impact-melt breccias. Geochim. Cosmochim. Acta 61, 425–435.
Rubin, A.E., Wasson, J.T., 1986. Chondrules in the Murrey CM2 meteorites and compositional differences between CM-CO and ordinary condrite chondrules. Geochim. Cosmochim. Acta 50, 307–315.
Rubin, A.E., Wasson, J.T., 1987. Chondrules, matrix and coarse-grained chondrule rims in the Allende meteorite: Origin, interrelationships and possible precursor components. Geochim. Cosmochim. Acta 51, 1923–1937.
Rubin, A.E., Wasson, J.T., 2005. Non-spherical lobate chondrules in CO3.0 Y-81020: General implications for the formation of low-FeO porphyritic chondrules in CO chondrites. Geochim. Cosmochim. Acta 69, 211–220.
Rubin, A.E., Wasson, J.T., 2011. Shock effects in EH6 enstatite chondrites and implications for collisional heating of the EH and EL parent asteroids. Geochim. Cosmochim. Acta 75, 3757–3780.
Rubin, A.E., Scott, E.R.D., Keil, K., 1982. Microchondrule- beqring clast in the Piancaldoli LL3 meteorite: A new kind of type 3 chondrite and its relevance to the history of chondrules. Geochim. Cosmochim. Acta 46, 1763–1776.
Rubin, A.E., Jerde, E.A., Zong, P., Wasson, J.T., Westcott, J.W., Mayeda, T.K., Clayton, R.N., 1986. Properties of the Guin ungrouped iron meteorite: The origin of Guin and of group-IIE irons. Earth Planet. Sci. Lett. 76, 209–226.
Rubin, A.E., Scott, E.R.D., Keil, K., 1997. Shock metamorphism of enstatite chondrites. Geochim. Cosmochim. Acta 61, 847–858.
Rubin, A.E., Sailer, A.L., Wasson, J.T., 1999. Troilite in the chondrules of type-3 ordinary chondrites: Implications for chondrule formation. Geochim. Cosmochim. Acta 63, 2281–2298.
Rubin, A.E., Ulff-Møller, F., Wasson, J.T., Carlson, W.D., 2001. The Portales Valley meteorite breccia: Evidence for impact- induced melting and metamorphism of an ordinary chondrite. Geochim. Cosmochim. Acta 65, 323–342.
Rubin, A.E., Zolensky, M.E., Bodnar, R.J., 2002. The halite-bearing Zag and Monahans (1998) meteorite breccias: Shock metamorphism, thermal metamorphism, and aqueous alteration on the H-chondrite parent body. Meteorit. Planet. Sci. 37, 125–141.
Rubin, A.E., Griset, C.D., Choi, B.-G., Wasson, J.T., 2009. Clastic matrix in EH3 chondrites. Meteorit. Planet. Sci. 44, 589–601.
Rubin, A.E., Baecker, B., Wasson, J.T., 2015a. Overgrowth Layers on Olivine Phenocrysts in High-FeO Semarkona Chondrules Revealed by P, Fe, and Cr X-Ray Maps: Evidence for Multiple Melting of Chondrules (abstract). In: 78th Annual Meeting of the Meteoritical Society, Lunar and Planetary Institute, Houston, p. 5033.
Rubin, A.E., Breen, J.P., Wasson, J.T., Pitt, D., 2015b. Shock effects in the Willamette ungrouped iron meteorite. Meteorit. Planet. Sci. 50, 1984–1994.
Rubin, A.E., Kallemeyn, G.W., Wasson, J.T., Clayton, R.N., Mayeda, T.K., Grady, M.M., Verchovsky, A.B., Eugster, O., Lorenzetti, S., 2003. Formation of metal and silicate globules in Gujba: A new Bencubbin-like meteorite fall. Geochim. Cosmochim. Acta 67, 3283–3298.
Rubin, A.E., Trigo- Rodríguez, J.M., Huber, H., Wasson, J.T., 2007. Progressive aqueous alteration of CM carbonaceous chondrites. Geochim. Cosmochim. Acta 71, 2361–2382.
Russell, C.T., Raymond, C.A., Coradini, A., McSween, H.Y., Zuber, M.T., Nathues, A., De Sanctis, M.C., Jaumann, R., Konopliv, A.S., Preusker, F., 2012. Dawn at Vesta: Testing the protoplanetary paradigm. Science 336, 684–686.
Russell, C.T., Raymond, C.A., Jaumann, R., McSween, H.Y., Sanctis, M.C., Nathues, A., Prettyman, T.H., Ammannito, E., Reddy, V., Preusker, F., 2013. Dawn completes its mission at 4 Vesta. Meteorit. Planet. Sci. 48, 2076–2089.
Russell, C.T., Raymond, C.A., Ammannito, E., Buczkowski, D.L., De Sanetis, M.C., Hiesinger, H., Jaumann, R., Konopliv, A.S., McSween, H.Y., Nathues, A., Park, R.S., Pieters, C.M., Prettyman, T.H., McCord, T.B., McFadden, L.A., Mottola, S., Combe, J.P., Ermakov, A., Fu, R.R., Hoffmann, M., Jia, Y.D., King, S.D., Lawrence, D.J., Li, J.-Y., Marchi, S., Preusker, F., Roatsch, T., Ruesch, O., Schenk, P., Villarreal, M.N., Yamashita, N., 2016. Dawn arrives at Ceres: Exploration of a small, volatile-rich world. Science 353, 1008–1010.
Russell, S.S., Pillinger, C.T., Arden, J.W., Lee, M.R., Ott, U., 1992. A new type of meteoritic diamond in the enstatite chondrite Abee. Science 256, 206–209.
Russell, S.S., Huss, G.R., Fahey, A.J., Greenwood, R.C., Hutchison, R., Wasserburg, G.J., 1998. An isotopic and petrologic study of calcium-aluminum-rich inclusions from CO3 meteorites. Geochim. Cosmochim. Acta 62, 689–714.
Ruzicka, A., 2014. Silicate-bearing iron meteorites and their implications for the evolution of asteroidal parent bodies. Chem. Erde-Geochem. 74, 3–48.
Ruzicka, A., Boynton, W.V., Ganguly, J.1, 1994. Olivine coronas, metamorphism, and the thermal history of the Morristown and Emery mesosiderites. Geochim. Cosmochim. Acta 58, 2725–2741.
Ruzicka, A., Fowler, G.W., Snyder, G.A., Prinz, M., Papike, J.J., Taylor, L.A., 1999. Petrogenesis of silicate inclusions in the Weekeroo Station IIE iron meteorite: Differentiation, remelting, and dynamic mixing. Geochim. Cosmochim. Acta 63, 2123–2143.
Ruzicka, A., Floss, C., Hutson, M., 2012. Amoeboid olivine aggregates (AOAs) in the Efremovka, Leoville and Vigarano (CV3) chondrites: A record of condensate evolution in the solar nebula. Geochim. Cosmochim. Acta 79, 79–105.
Saini- Eidukat, B., Kucha, H., Keppler, H., 1994. Hibbingite, γ-$Fe_2(OH)_3Cl$, a new mineral from the Duluth Complex, Minnseota, with implications for the oxidation of Fe-bearing compounds and transport of metals. Am. Mineral. 79, 555–561.

Saito, J., Takeda, H., 1990. Information of elemental distributions in heavily shocked ureilites as a guide to deduce the ureilite formation process. Lunar Planet. Sci. Conf.
Satterwhite, C., Mason, B., MacPherson, G.J., 1993. Description of LEW88774. Antarct. Meteor. Newslett. 16 (1), 15.
Schaal, R.B., Hörz, F., Thompson, T.D., Bauer, J.F., 1979. Shock metamorphism of granulated lunar basalt. Proc. Lunar Planet. Sci. Conf. 10, 2547–2571.
Schaudy, R., Wasson, J.T., Buchwald, V.F., 1972. The chemical classification of iron meteorites-VI: A reinvestigation of irons with Ge concentrations lower than 1 ppm. Icarus 17, 174–192.
Schiller, M., Baker, J.A., Bizzarro, M., 2010. ^{26}Al-^{26}Mg dating of asteroidal magmatism in the young Solar System. Geochim. Cosmochim. Acta 74, 4844–4864.
Schmitz, B., Tassinari, M., Peucker- Ehrenbrink, B., 2001. A rain of ordinary chondritic meteorites in the early Ordovician. Earth Planet. Sci. Lett. 194, 1–15.
Schmitz, B., Häggström, T., Tassinari, M., 2003. Sediment-dispersed extraterrestrial chromite traces a major asteroid disruption event. Science 300, 961–964.
Schmitz, B., Yin, Q.Z., Sanborn, M.E., Tassinari, M., Caplan, C.E., Huss, G.R., 2016. A new type of solar-system material recovered from Ordovician marine limestone. Nat. Commun. 7.
Schrader, D.L., McCoy, T.J., Davidson, J., 2016. Widespread evidence for high-temperature formation of pentlandite in chondrites. Geochim. Cosmochim. Acta 189, 359–376.
Schulze, H., Bischoff, A., Palme, H., Spettel, B., Dreibus, G., Otto, J., 1994. Mineralogy and chemistry of Rumuruti: the first meteorite fall of the new R chondrite group. Meteoritics 29, 275–286.
Schwenzer, S.P., Bridges, J.C., Wiens, R.C., Conrad, P.G., Kelley, S.P., Leveille, R., Mangold, N., Martin-Torres, J., McAdam, A., Newsom, H., Zorzano, M.P., Rapin, W., Spray, J., Treiman, A.H., Westall, F., Fairen, A.G., Meslin, P.-Y., 2016. Fluids during diagenesis and sulfate vein formation in sediments at Gale Crater, Mars. Meteorit. Planet. Sci., 1–28.
Scott, E.R.D., 1971. New carbide, $(Fe,Ni)_{23}C_6$, found in iron meteorites. Nature 229, 61–62.
Scott, E.R.D., 1982. Origin of rapidly solidified metal-troilite grains in chondrites and iron meteorites. Geochim. Cosmochim. Acta 46, 813–823.
Scott, E.R.D., Agrell, S.O., 1971. The occurrence of carbides in iron meteorites (abstract). Meteoritics 6, 312–313.
Scott, E.R.D., Jones, R.H., 1990. Disentangling nebular and asteroidal features of CO3 carbonaceous chondrite meteorites. Geochim. Cosmochim. Acta 54, 2485–2502.
Scott, E.R.D., Krot, A.N., 2005. Chondrites and their components. In: Davis, A.M. (Ed.), Meteorites, Comets and Planets. Elsevier, Amsterdam, pp. 143–200.
Scott, E.R.D., Taylor, G.J., 1985. Petrology of types 4-6 carbonaceous chondrites. Proc. Lunar Planet. Sci. Conf. 15, C699–C709.
Scott, E.R.D., Wasson, J.T., 1976. Chemical classification of iron meteorites-VIII. Groups IC, IIE, IIIF and 97 other irons. Geochim. Cosmochim. Acta 40, 103–115.
Scott, E.R.D., Wasson, J.T., Buchwald, V.F., 1973. The chemical classification of iron meteorites—VII: a reinvestigation of irons with Ge concentrations between 25 and 80 ppm. Geochim. Cosmochim. Acta 37, 1957–1983.
Scott, E.R.D., Taylor, G.J., Keil, K., 1986. Accretion, metamorphism, and brecciation of ordinary chondrites: Evidence from petrologic studies of meteorites from Roosevelt County, New Mexico. Proc. Lunar Planet. Sci. Conf. 17, E115–E123.
Scott, E.R.D., Brearley, A.J., Keil, K., Grady, M.M., Pillinger, C.T., Clayton, R.N., Mayeda, T.K., Wieler, R., Signer, P., 1988. Nature and origin of C-rich ordinary chondrites and chondritic clasts. Proc. Lunar Planet. Sci. Conf. 18, 513–523.
Scott, E.R.D., Keil, K., Stöffler, D., 1992. Shock metamorphism of carbonaceous chondrites. Geochim. Cosmochim. Acta 56, 4281–4293.
Scott, E.R.D., Haack, H., McCoy, T., 1996. Core crystallization and silicate-metal mixing in the parent body of the IVA iron and stony-iron meteorites. Geochim. Cosmochim. Acta 60, 1615–1631.
Seab, C.G., 1987. Grain destruction, formation, and evolution. Interstellar Processes, 490–512.
Sears, D.W., 1978. The Nature and Origin of Meteorites. Oxford Univ. Press, New York, New York, pp. 187.
Sears, D.W., Kallemeyn, G.W., Wasson, J.T., 1983. Composition and origin of clasts and inclusions in the Abee enstatite chondrite breccia. Earth Planet. Sci. Lett. 62, 180–192.
Sears, D.W.G., Hasan, E.A., Batchelor, J.D., Lu, J., 1991. Chemical and physical studies of type 3 chondrites – XI. Metamorphism, pairing, and brecciation of ordinary chondrites. Proc. Lunar Planet. Sci. Conf. 21, 493–512.
Sears, D.W.G., Morse, A.D., Hutchison, R., Guimon, R.K., Jie, L., Alexander, C.M.O.D., Benoit, P.H., Wright, I., Pillinger, C.T., Xie, T., Lipschutz, M.E., 1995. Metamorphism and aqueous alteration in low petrographic type ordinary chondrites. Meteorit. Planet. Sci. 30, 169–181.
Sharp, T.G., DeCarli, P.S., 2006. Shock effects in meteorites. In: Lauretta, D.S., McSween, H.Y. (Eds.), Meteorites and the early solar system II, 653–677.
Sharp, T.G., Lingemann, C.M., Dupas, C., Stöffler, D., 1997. Natural occurrence of $MgSiO_3$-ilmenite and evidence for $MgSiO_3$-perovskite in a shocked L chondrite. Science 277, 352–355.
Shearer, C.K., Papike, J.J., Rietmeijer, F.J.M., 1998. The planetary sample suite and environments of origin. In Planetary Materials. In: Papike, J.J. (Ed.), Reviews in Mineralogy, 36. Mineralogical Society of America, Washington, D.C, 1-01–1- 28.
Shearer, C.K., Burger, P.V., Guan, Y., Papike, J.J., Sutton, S.R., Atudorei, N.V., 2012. Origin of sulfide replacement textures in lunar breccias: Implications for vapor element transport in the lunar crust. Geochim. Cosmochim. Acta 83, 138–158.
Shimizu, M., Yoshida, H., Mandarino, J.A., 2002. The new mineral species keilite, (Fe, Mg) S, the iron-dominant analogue of niningerite. Can. Mineral. 40, 1687–1692.
Shimoyama, A., Harada, K., 1984. Amino-acid depleted carbonaceous chondrites (C2) from Antarctica. Geochem. J. 18, 281–286.
Shoemaker, E.N., Wolfe, R.F., Shoemaker, C.S., 1990. Asteroid and comet flux in the neighborhood of the Earth. In: Sharpton, V.L., Ward, P.D. (Eds.), Special Paper 247: Global Catastrophes in Earth History: An Interdisciplinary Conference on Impacts, Volcanism, and Mass Mortality. Geological Society of America, Boulder, CO, pp. 155–170.
Simon, S.B., Grossman, L., 1992. Low-temperature exsolution in refractory siderophile element-rich opaque assemblages from the Leoville carbonaceous chondrite. Earth Planet. Sci. Lett. 110, 67–75.
Simon, S., Davis, A., Grossman, L., 1999. Origin of compact type A refractory inclusions from CV3 carbonaceous chondrites. Geochim. Cosmochim. Acta 63, 1233–1248.
Simonetti, A., Shore, M., Bell, K., 1996. Diopside phenocrysts in nephelinite lavas, Napak Volcano, eastern Uganda: Evidence for magma mixing. Can. Mineral. 34, 411–421.
Simpson, E.S., 1938. Some new and little-known meteorites found in western Australia (Dalgaranga, Dowerin, Gundaring, Kumerina, Landor, Mellenbye, Milly Milly, Premier Downs III, Thangoo?, Tieraco Creek, Wonyulgunna, Yalgoo, Youanmi, Youndegin III and Mooranoppin II). Mineral. Mag. 25, 157–171, 154 plates.
Sinkankas, J., Koivula, J.I., Becker, G., 1992. Peridot as an interplanetary gemstone. Gems Gemol. 28, 43–51.
Skála, R., Drábek, M., 2003. Nickelphosphide from the Vicenice octahedrite: Rietveld crystal structure refinement of a synthetic analogue. Mineral. Mag. 67, 783–792.
Skirius, C., Steele, I.M., Smith, J.V., 1986. Belgica-7904: A new carbonaceous chondrite from Antarctica; Minor-element chemistry of olivine. Mem. NIPR Spec. Issue 41, 243–258.
Smith, J.V., 1979. Mineralogy of the planets: a voyage in space and time. Mineral. Mag. 43, 1–89.
Snellenburg, J.W., 1978. A chemical and petrographic study of the chondrules, in the unequilibrated ordinary chondrites. Semarkona and Krymka.
Snetsinger, K.G., Keil, K., 1969. Ilmenite in ordinary chondrites. Am. Mineral. 54, 780–786.
Squyres, S.W., Grotzinger, J.P., Arvidson, R.E., Bell, J.F., Calvin, W., Christensen, P.R., Clark, B.C., Crisp, J.A., Farrand, W.H., Kerkenhoff, K.E., Johnson, J.R., Klingelhöfer, G., Knoll, A.H., McLennen, S.M., McSween, H.Y., Morris, R.V., Rice, J.W., Rieder, R., Soderblom, L.A., 2004. In situ evidence for an ancient aqueous environment at Meridiani Planum. Mars. Sci. 306, 1709–1714.
Steele, A., Westall, F., T, G.D., Stapleton, D., Toporski, J.K.W., McKay, D.S., McKay, D.S., 1999. Imaging of the biological contamination of meteorites: a practical assessment. Lunar Planet. Sci. 30, 1321.
Steele, I.M., Smith, J.V., 1982. Petrography and mineralogy of two basalts and olivine- pyroxene-spinel fragments in achondrite EETA79001. Proc. Lunar Planet. Sci. Conf. 13, A375–A384.
Stinchcomb, B.L., 2011. Meteorites. Schiffer, Atglen, PA, USA, pp. 160.
Stöffler, D., Ostertag, R., Jammes, C., Pfannschmidt, G., Gupta, P.R.S., Simon, S.B., Papike, J.J., Beauchamp, R.H., 1986. Shock metamorphism and petrography of the Shergotty achondrite. Geochim. Cosmochim. Acta 50, 889–903.
Stöffler, D., Bischoff, A., Buchwald, V., Rubin, A.E., 1988. Shock effects in meteorites. In: Kerridge, J.F., Matthews, M.S. (Eds.), Meteorites and the Early Solar System. Univ. Arizona Press, Tucson, pp. 165–202.
Stöffler, D., Keil, K., Scott, E.R.D., 1991. Shock metamorphism of ordinary chondrites. Geochim. Cosmochim. Acta 55, 3845–3867.
Stolper, E., 1977. Experimental petrology of eucritic meteorites. Geochim. Cosmochim. Acta 41, 587–611.
Sugiura, N., Petaev, M.I., Kimura, M., Miyazaki, A., Hiyagon, H., 2009. Nebular history of amoeboid olivine aggregates. Meteorit. Planet. Sci. 44, 559–572.
Swindle, T.D., Kring, D.A., Weirich, J.R., 2013. 40Ar/39Ar ages of impacts involving ordinary chondrite meteorites. Geol. Soc. Lon. Special Publ. 378, 333–347.
Symes, S.J.K., Sears, D.W.G., Akridge, D., Huang, S., Benoit, P.H., 1998. The crystalline lunar spherules: Their formation and implications for the origin of meteoritic chondrules. Meteorit. Planet. Sci. 33, 13–29.
Tait, K.T., Barkley, M.C., Thompson, R.M., Origlieri, M.J., Evans, S.H., Prewitt, C.T., Yang, H., 2011. Bobdownsite, a new mineral species from Big Fish River, Yukon, Canada, and its structural relationship with whitlockite-type compounds. Can. Meteorol. 49, 1065–1078.
Takeda, H., Graham, A.L., 1991. Degree of equilibration of eucritic pyroxenes and thermal metamorphism of the earliest planetary crust. Meteoritics 26, 129–134.
Takeda, H., Mori, H., 1985. The eucrite-diogenite links and the crystallization history of a crust of their parent body. J. Geophys. Res. 90 (Supplement, PLPSC), C636–C648.
Takeda, H., Huston, T.J., Lipschutz, M.E., 1984. On the chondrite-achondrite transition: mineralogy and chemistry of Yamato 74160 (LL7). Earth Planet. Sci. Lett. 71, 329–339.
Takeda, H., Baba, T., Mori, H., Saito, J., 1992. Mineralogy of a new orthopyroxene-bearing ureilite LEW 88201 and the relationship between magnesian ureilities and lodranites. Lunar Planet. Sci. Conf., 1403.
Takeda, H., Bogard, D.D., Mittlefehldt, D.W., Garrison, D.H., 2000. Mineralogy, petrology, chemistry, and 39Ar-40Ar and exposure ages of the Caddo County

IAB iron: Evidence for early partial melt segregation of a gabbro area rich in plagioclase-diopside. Geochim. Cosmochim. Acta 64, 1311–1327.
Taylor, G.J., Okada, A., Scott, E.R.D., Rubin, A.E., Huss, G.R., Keil, K., 1981. The occurrence and implications of carbide-magnetite assemblages in unequilibrated ordinary chondrites (abstract). Lunar Planet. Sci. 12, 1076–1078.
Taylor, G.J., Warren, P., Ryder, G., Delano, J., Pieters, C., Lofgren, G., 1991. Lunar Rock. In: Heiken, G., Vaniman, D., French, B.M. (Eds.), Lunar Sourcebook – A User's Guide to the Moon. Cambridge University Press, New York, pp. 183–284.
Taylor, L.A., Nazarov, M.A., Demidova, S.I., Patchen, A.D., 2001. Dhofar 287: A new lunar mare basalt from Oman. Meteorit. Planet. Sci. 36, 204.
Taylor, S., Messenger, S., Folco, L., 2016. Cosmic dust: Finding a needle in a haystack. Elements 12, 171–176.
Thorslund, P., Wickman, F.E., 1981. Middle Ordovician chondrite in fossiliferous limestone from Brunflo, central Sweden. Nature 289, 285–286.
Thorslund, P., Wickman, F.E., Nystrom, J.O., 1984. The Ordovician chondrite from Brunflo, central Sweden, I. General description and primary minerals. Lithos 17, 87–100.
Tomeoka, K., 1990. Mineralogy and petrology of Belgica-7904: A new kind of carbonaceous chondrite from Antarctica. Proc. NIPR Symp. Antarct. Meteorit. 3, 40–54.
Tomeoka, K., Buseck, P.R., 1988. Matrix mineralogy of the Orgueil CI carbonaceous chondrite. Geochim. Cosmochim. Acta 52, 1627–1640.
Tomeoka, K., Tanimura, I., 2000. Phyllosilicate-rich chondrule rims in the Vigarano CV3 chondrite: Evidence for parent-body processes. Geochim. Cosmochim. Acta 64, 1971–1988.
Tomeoka, K., Kojima, H., Yanai, K., 1989. Yamato-86720: A CM carbonaceous chondrite having experienced extreme aqueous alteration and thermal metamorphism. Proc. NIPR Symp. Antarct. Meteorit. 2, 55–74.
Tomioka, N., Fujino, K., 1999. Akimotoite,(Mg, Fe) SiO_3, a new silicate mineral of the ilmenite group in the Tenham chondrite. Am. Mineral. 84, 267–271.
Tomioka, N., Miyahara, M., Ito, M., 2016. Discovery of natural $MgSiO_3$ tetragonal garnet in a shocked chondritic meteorite. Sci. Adv. 2, e1501725.
Tomkins, A.G., 2009. What metal- troilite textures can tell us about post-impact metamorphism in chondrite meteorites. Meteorit. Planet. Sci. 44, 1133–1149.
Tonui, E., Zolensky, M., Lipschutz, M.E., 2002. Petrography, mineralogy and trace element chemistry of Yamato-86029, Yamato-793321 and Lewis Cliff 85332: Aqueous alteration and heating events. Anatart. Meteorit. Res. 15, 38–58.
Tonui, E., Zolensky, M., Hiroi, T., Nakamura, T., Lipschutz, M.E., Wang, M.-S., Okudaira, K., 2014. Petrographic, chemical and spectroscopic evidence for thermal metamorphism in carbonaceous chondrites I: CI and CM chondrites. Geochim. Cosmochim. Acta 126, 284–306.
Treiman, A.H., 1985. Amphibole and hercynite spinel in Shergotty and Zagami: Magmatic water, depth of crystallization, and metasomatism. Meteoritics 20, 229–243.
Treiman, A.H., 2005. The nakhlite meteorites: Augite-rich igneous rocks from Mars. Chem. Erde-Geochem. 65, 203–270.
Treiman, A.H., Barrett, R.A., Gooding, J.L., 1993. Preterrestrial aqueous alteration of the Lafayette (SNC) meteorite. Meteoritics 28, 86–97.
Treiman, A.H., Boyce, J.W., Gross, J., Guan, Y., Eiler, J.M., Stolper, E.M., 2014. Phosphate-halogen metasomatism of lunar granulite 79215: Impact-induced fractionation of volatiles and incompatible elements. Am. Mineral. 99, 1860–1870.
Tschauner, O., Ma, C., Beckett, J.R., Prescher, C., Prakapenka, V.B., Rossman, G.R., 2014. Discovery of bridgmanite, the most abundant mineral in Earth, in a shocked meteorite. Science 346, 1100–1102.
Turner, G., 1988. Dating of secondary events. In: Kerridge, M. (Ed.), Meteorites and the early solar system, 276–288.
Ulff-Møller, F., Rasmussen, K., Prinz, M., Palme, H., Spettel, B., Kallemeyn, G., 1995. Magmatic activity on the IVA parent body: Evidence from silicate-bearing iron meteorites. Geochim. Cosmochim. Acta 59, 4713–4728.
Ulff-Møller, F., Choi, B.-G., Rubin, A.E., Tran, J., Wasson, J.T., 1998. Paucity of sulfide in a large slab of Esquel: New perspectives on pallasite formation. Meteorit. Planet. Sci. 33, 227–331.
Ulyanov, A.A., 1991. The meteorite minerals. 14th Brown-Vernadsky Microsymposium on Comparative Planetology.
Urey, H.C., 1955. The cosmic abundances of potassium, uranium and thorium and the heat balances of the earth, the Moon and Mars. Proc. Natl. Acad. Sci. 41, 127–144.
Van Schmus, W.R., Wood, J.A., 1967. A chemical-petrologic classification for the chondritic meteorites. Geochim. Cosmochim. Acta 31, 747–765.
Vdovykin, G.P., 1969. New hexagonal modification of carbon in meteorites. Geochem. Int. 6, 915–918.
Vdovykin, G.P., 1972. Forms of carbon in the new Havero ureilite of Finland. Meteoritics 7, 547–552.
Velbel, M.A., 1988. The distribution and significance of evaporitic weathering products on Antarctic meteorites. Meteoritics 23, 151–159.
Velbel, M.A., 2012. Aqueous alteration in Martian meteorites: Comparing mineral relations in igneous-rock weathering of Martian meteorites and in the sedimentary cycle of Mars. Sediment. Geol. Mars 102, 97–117.
Vilas, F., Gaffey, M.J., 1989. Phyllosilicate absorption features in main-belt and outer- belt asteroid reflectance spectra. Bull. Am. Astronom. Soc., 966.
Vilas, F., Larson, S.M., Hatch, E.C., Jarvis, K.S., 1993. CCD reflectance spectra of selected asteroids. II. Low-albedo asteroid spectra and data extraction techniques. Icarus 105, 67–78.
Vilas, F., Jarvis, K.S., Gaffey, M.J., 1994. Iron alteration minerals in the visible and near-infrared spectra of low-albedo asteroids. Icarus 109, 274–283.
Vogel, N., Renne, P.R., 2008. ^{40}Ar-^{39}Ar dating of plagioclase grain size separates from silicate inclusions in IAB iron meteorites and implications for the thermochronological evolution of the IAB parent body. Geochim. Cosmochim. Acta, 72.
Volk, K., Kwok, S., Langill, P.P., 1992. Candidates for extreme carbon stars. Astrophys. J. 391, 285–294.
Wadhwa, M., Crozaz, G., 1995. Trace and minor elements in minerals of nakhlites and Chassigny: Clues to their petrogenesis. Geochim. Cosmochim. Acta 59, 3629–3645.
Wang, K., 1986. Zhanghengite- a new mineral. Acta Mineral. Sin. 6, 220–223.
Wark, D., 1987. Plagioclase-rich inclusions in carbonaceous chondrite meteorites: Liquid condensates? Geochim. Cosmochim. Acta 51, 221–242.
Wark, D., Boynton, W.V., 2001. The formation of rims on calcium-aluminum-rich inclusions: Step I—Flash heating. Meteorit. Planet. Sci. 36, 1135–1166.
Wark, D.A., Lovering, J.F., 1977. Marker events in the early evolution of the solar system: evidence from rims on Ca-Al-rich inclusions in carbonaceous chondrites. Proc. Lunar Sci. Conf. 8, 95–112.
Wark, D.A., Lovering, J.F., 1978. Refractory/platinum metals and other opaque phases in Allende Ca-Al-rich inclusions (CAI's) (abstract). Lunar Planet. Sci. 9, 1214–1216.
Wark, D.A., Lovering, J.F., 1982. The nature and origin of type B1 and B2 Ca·Al-rich inclusions in the Allende meteorite. Geochim. Cosmochim. Acta 46, 2581–2594.
Wark, D., Boynton, W.V., Keays, R., Palme, H., 1987. Trace element and petrologic clues to the formation of forsterite-bearing Ca-Al-rich inclusions in the Allende meteorite. Geochim. Cosmochim. Acta 51, 607–622.
Warner, J.L., 1972. Metamorphism of Apollo 14 breccias. Proc. Lunar Sci. Conf. 3, 623–643.
Warren, P.H., Jerde, E.A., 1987. Composition and origin of Nuevo Laredo trend eucrites. Geochim. Cosmochim. Acta 51, 713–725.
Warren, P.H., Kallemeyn, G.W., 1988. A new model for ureilite origin: incomplete impact-disruption of partially molten asteroids (abstract). Lunar Planet. Sci. 19, 1238–1239.
Warren, P.H., Kallemeyn, G.W., 1989. Allan Hills 84025: The second brachinite, far more differentiated than Brachina, and an ultramafic achondritic clast from L chondrite Yamato 75097. Proc. Lunar Planet. Sci. Conf. 19, 475–486.
Warren, P.H., Kallemeyn, G.W., 1994. Petrology of LEW88774: an extremely Cr-rich ureilite (abstract). Lunar Planet. Sci. 25, 1465–1466.
Warren, P.H., Rubin, A.E., 2010. Pyroxene-selective impact smelting in ureilites. Geochim. Cosmochim. Acta 74, 5109–5133.
Warren, P.H., Rubin, A.E., Isa, J., Gessler, N., Ahn, I., Choi, B.-G., 2014. Northwest Africa 5738: multistage fluid-driven secondary alteration in an extraordinarily evolved eucrite. Geochim. Cosmochim. Acta 141, 199–227.
Wasserburg, G., Papanastassiou, D., 1982. Some short-lived nuclides in the early solar system – A connection with the placental ISM. In: Barnes, C.A., Clayton, D.D., Schramm, D.N. (Eds.), Essays in Nuclear Astrophysics, 8201. Cambridge University Press, Cambridge, pp. 77–140.
Wasson, J.T., 1985. Meteorites: Their Record of Early Solar-system History. W.H Freeman, New York, pp. 26.
Wasson, J.T., 2008. Evaporation of nebular fines during chondrule formation. Icarus 195, 895–907.
Wasson, J.T., 2016. Evidence that ^{26}Al decay did not melt asteroids. Meteorit. Soc. 79, 6530.
Wasson, J.T., Kallemeyn, G.W., 2002. The IAB iron-meteorite complex: a group, five subgroups, numerous grouplets, closely related, mainly formed by crystal segregation in rapidly cooling melts. Geochim. Cosmochim. Acta 66, 2445–2473.
Wasson, J.T., Rubin, A.E., 2003. Ubiquitous low-FeO relict grains in type II chondrules and limited overgrowths on phenocrysts following the final melting event. Geochim. Cosmochim. Acta 67, 2239–2250.
Wasson, J.T., Wai, C.M., 1970. Composition of the metal, schreibersite and perryite of enstatite achondrites and the origin of enstatite chondrites and achondrites. Geochim. Cosmochim. Acta 34, 169–184.
Wasson, J.T., Chou, C.L., Bird, R.W., Baedecker, P.A., 1976. Classification of and elemental fractionation among ureilites. Geochim. Cosmochim. Acta 40, 1449–1458.
Wasson, J.T., Willis, J., Wai, C.M., 1980. Origin of iron meteorite groups IAB and IIICD. Zeits. Naturforsch. 35a, 781–795.
Wasson, J.T., Rubin, A.E., Kallemeyn, G.W., 1993. Reduction during metamorphism of four ordinary chondrites. Geochim. Cosmochim. Acta 57, 1867–1878.
Wasson, J.T., Kallemeyn, G.W., Rubin, A.E., 1994. Equilibration temperatures of EL chondrules: a major downward revision in the ferrosilite contents of enstatite. Meteoritics 29, 658–662.
Wasson, J.T., Krot, A.N., Lee, M.S., Rubin, A.E., 1995. Compound chondrules. Geochim. Cosmochim. Acta 59, 1847–1869.
Wasson, J.T., Lange, D.E., Francis, C.A., Ulff-Møller, F., 1999. Massive chromite in the Brenham pallasite and the fractionation of Cr during the crystallization of asteroidal cores. Geochim. Cosmochim. Acta 63, 1219–1232.
Wasson, J.T., Yurimoto, H., Russell, S.S., 2001. ^{16}O-rich melilite in CO3.0 chondrites: Possible formation of common, 16O-poor melilite by aqueous alteration. Geochim. Cosmochim. Acta 65, 4539–4549.
Wasson, J.T., Matsunami, Y., Rubin, A.E., 2006. Silica and pyroxene in IVA irons; possible formation of the IVA magma by impact melting and reduction of L-LL-chondrite materials followed by crystallization and cooling. Geochim. Cosmochim. Acta 70, 3149–3172.

Wasson, J.T., Isa, J., Rubin, A.E., 2013. Compositional and petrographic similarities of CV and CK chondrites: a single group with variations in textures and volatile concentrations attributable to impact heating, crushing and oxidation. Geochim. Cosmochim. Acta 108, 45–62.
Wasson, J.T., Baecker, B., Rubin, A.E., 2014. Multiple, hierarchical heating of chondrules and implications for cooling rates (abstract). Lunar Planet. Sci. 45, 2883.
Watanabe, S., Kitamura, M., Morimoto, M., 1986. Oscillatory zoning of proxenes in ALH-77214 (L3) (abstract). Pap. Eleventh Symp. Antarctic Meteor., 74–75.
Watson, L.L., Hutcheon, I.D., Epstein, S., Stolper, E.M., 1994. Water on Mars: Clues from deuterium/hydrogen and water contents of hydrous phases in SNC meteorites. Science 265, 86–90.
Watters, T.R., Prinz, M., 1979. Aubrites: Their origin and relationship to chondrites. Proc. Lunar Planet. Sci. Conf. 10, 1073–1093.
Weber, D., Bischoff, A., 1994a. Grossite ($CaAl_4O_7$)- a rare phase in terrestrial rocks and meteorites. Eur. J. Mineral. 6, 591–594.
Weber, D., Bischoff, A., 1994b. The occurrence of grossite ($CaAl_4O_7$) in chonrdites. Geochim. Cosmochim. Acta 58, 3855–3877.
Weber, D., Bischoff, A., 1997. Refractory inclusions in the CR chondrite Acfer 059 El Djouf 001: petrology, chemical composition, and relationship to inclusion populations in other types of carbonaceous chondrites. Chem. Erde-Geochem. 57, 1–24.
Weidenschilling, S., 1977. Aerodynamics of solid bodies in the solar nebula. Monthly Not. R. Astronom. Soc. 180, 57–70.
Weinbruch, S., Müller, W.F., Hewins, R.H., 2001. A transmission electron microscope study of exsolution and coarsening in iron-bearing clinopyroxene from synthetic analogues of chondrules. Meteorit. Planet. Sci. 36, 1237–1248.
Weisberg, M.K., 1987. Barred olivine chondrules in ordinary chondrites. Proc. Lunar Planet. Sci. Conf. 17, E663–E678.
Weisberg, M.K., Huber, H., 2007. The GRO 95577 CR1 chondrite and hydration of the CR parent body. Meteorit. Planet. Sci. 42, 1495–1503.
Weisberg, M.K., Kimura, M., 2010. Petrology and Raman spectroscopy of high pressure phases in the Gujba CB chondrite and the shock history of the CB parent body. Meteorit. Planet. Sci. 45, 873–884.
Weisberg, M.K., Kimura, M., 2012. The unequilibrated enstatite chondrites. Chem. Erde-Geochem. 72, 101–115.
Weisberg, M.K., Prinz, M., Nehru, C.E., 1988. Petrology of ALH85085: a chondrite with unique characteristics. Earth Planet. Sci. Lett. 91, 19–32.
Weisberg, M.K., Prinz, M., Nehru, C.E., 1990. The Bencubbin chondrite breccia and its relationship to CR chondrites and the ALH85085 chondrite. Meteoritics 25, 269–279.
Weisberg, M.K., Prinz, M., Clayton, R.N., Mayeda, T.K., 1993. The CR (Renazzo-type) carbonaceous chondrite group and its implications. Geochim. Cosmochim. Acta 57, 1567–1586.
Weisberg, M.K., Prinz, M., Clayton, R.N., Mayeda, T.K., 1997. CV3 chondrites: three subgroups, not two (abstract). Meteorit. Planet. Sci. 32, A138–A139.
Weisberg, M.K., Connolly, H.C., Ebel, D.S., 2004. Petrology and origin of amoeboid olivine aggregates in CR chondrites. Meteorit. Planet. Sci. 39, 1741–1753.
Weisberg, M.K., Connolly, H., Zolensky, M., BNland, P., Bradley, J., Brearley, A., Bridges, J., Brownlee, D., Butterworth, A., Dai, Z., Ebel, D., Genge, M., Gounelle, M., Graham, G., Grossman, J., Grossman, L., Harvey, R., Ishii, H., Kearsley, A., Keller, L., Krot, A., Langenhorst, F., Lanzirotti, A., Leroux, H., Matraijt, G., Messenger, K., Mikouchi, T., Nakamura, T., Ohsumi, K., Okudaira, K., Perronnet, M., Simon, S., Stephan, T., Stroud, R., Taheri, M., Tomeoka, K., Toppani, A., Tsou, P., Tsuchiyama, A., Velbel, M., Weber, I., Westphal, A., Yano, H., Zega, T., 2006. Stardust (comet) samples and the meteorite record. American Geophysical Uniton, Fall meeting 2006, abstract#P51E–1243.
Weisberg, M.K., Bunch, T.E., Wittke, J.H., Rumble, D., Ebel, D.S., 2012. Petrology and oxygen isotopes of NWA 5492, a new metal-rich chondrite. Meteorit. Planet. Sci. 47, 363–373.
Wentworth, S.J., Gooding, J.L., 1993. Weathering features and secondary minerals in Antarctic shergottites ALHA77005 and LEW88516. Lunar Planet. Sci. 24, 1507–1508.
Wentworth, S.J., Gooding, J.L., 1994. Carbonates and sulfates in the Chassigny meteorite: further evidence for aqueous chemistry on the SNC parent planet. Meteoritics 29, 860–863.
White, J.S., Henderson, E.P., Mason, B., 1967. Secondary minerals produced by weathering of the Wolf Creek meteorite. Am. Mineral. 52, 1190–1197.
Widom, E., Rubin, A.E., Wasson, J.T., 1986. Composition and formation of metal nodules and veins in ordinary chondrites. Geochim. Cosmochim. Acta 50, 1989–1995.
Wilson, W.E., 1972. The Bondoc mesosiderite: Mineralogy and petrology of the metal nodules. Arizona State Univ., Tempe, pp. 74.
Wlotzka, F., 1993. A weathering scale for the ordinary chondrites (abstract). Meteoritic 28, 460.
Wojnarowska, A., Dziel, T., Gałązka-Friedman, J., 2008. New mineralogical phases identified by Mössbauer measurements in Morasko meteorite. Hyperf. Interact. 186, 167–171.
Wood, J.A., 1963. On the origin of chondrules and chondrites. Icarus 2, 152–180.
Wood, J.A., Hashimoto, A., 1993. Mineral equilibrium in fractionated nebular systems. Geochim. Cosmochim. Acta 57, 2377–2388.
Wopenka, B., Swan, P.D., 1985. Identification of micron-sized phases in meteorites by lasar Raman microprobe spectroscopy (abstract). Meteoritics 20, 788–789.
Wright, E.L., 1987. Long-wavelength absorption by fractal dust grains. Astrophys. J. 320, 818–824.
Xie, X., Minitti, M.E., Chen, M., Mao, H.K., Wang, D., Shu, J., Fei, Y., 2002. Natural high-pressure polymorph of merrillite in the shock veins of the Suizhou meteorite. Geochim. Cosmochim. Acta 66, 2439–2444.
Xie, X., Minitti, M.E., Chen, M., Mao, H.K., Wang, D., Shu, J., Fei, Y., 2003. Tuite, γ-Ca3(PO4)2: A new mineral from the Suizhou L6 chondrite. Eur. J. Mineral. 15, 1001–1005.
Xie, X., Gu, X., Yang, H., Chen, M., Li, K., 2016. Wangdaodeite, IMA 2016 -007 CNMNC Newsletter No. 31. June 2016, page 695. Mineral. Mag. 80, 691–697.
Yagi, K., Lovering, J.F., Shima, M., Okada, A., 1978. Petrology of the Yamato meteorites (j), (k), (l), and (m) from Antarctica. Meteoritics 13, 23–45.
Yamada, I., Mikouchi, T., Miyamoto, M., 1997a. Symplectic Exsolution in Olivine from Nakhla Martian. Meteorite. Meteorit. Planet. Sci., 32.
Yamada, I., Mikouchi, T., Miyamoto, M., Murakami, T., 1997b. Lamellar inclusion in olivine from Nakhla (SNC) meteorite. Lunar Planet. Sci. 28, 1597–1598.
Yamaguchi, A., Mori, H., Takeda, H., 1993. Mineralogy and shock textures in the Padvarninkai eucrite (abstract). Meteoritics 28, 462–463.
Yamaguchi, A., Taylor, G.J., Keil, K., 1996. Global crustal metamorphism of the eucrite parent body. Icarus 124, 97–112.
Yamaguchi, A., Taylor, G.J., Keil, K., Floss, C., Crozaz, G., Nyquist, L.E., Bogard, D.D., Garrison, D.H., Reese, Y.D., Wiesmann, H., 2001. Post- crystallization reheating and partial melting of eucrite EET90020 by impact into the hot crust of asteroid 4Vesta~4. 50 Ga ago. Geochim. Cosmochim. Acta 65, 3577–3599.
Yanai, K., 1981. Photographic Catalog of the Selected Antarctic Meteorites. National Inst. Polar Res., Tokyo, pp. 104.
Yanai, K., Kojima, H., 1987. Photographic Catalog of the Selected Antarctic Meteorites. National Inst. Polar Res., Tokyo, pp. 298.
Yanai, K., Kojima, H., 1991. Yamato -74063: Chondritic meteorite classified between E and H chondrite groups. Proc. NIPR Sympos. Antarct. Meteorit., 118–130.
Yang, C.-W., Williams, D.B., Goldstein, J.I., 1997a. A new empirical cooling rate indicator for meteorites based on the size of the cloudy zone of the metallic phases. Meteorit. Planet. Sci. 32, 423–429.
Yang, C.W., Williams, D.B., Goldstein, J.I., 1997b. Low-temperature phase decomposition in metal from iron, stony-iron, and stony meteorites. Geochim. Cosmochim. Acta 61, 2943–2956.
Yin, Q.-Z., Sanborn, M.E., Ziegler, K., 2017. Testing the common source hypothesis for CV and CK chondrite parent body using $\Delta^{17}O$-$\varepsilon^{54}Cr$ isotope systematics. Lunar Planet. Sci. 48, abstract#1771.
Yoneda, S., Grossman, L., 1995. Condensation of CaO-MgO-Al_2O_3-SiO_2 liquids from cosmic gases. Geochim. Cosmochim. Acta 59, 3413–3444.
Yu, Z., 1984. Two new minerals gupeiite and xifengite in cosmic dusts from Yanshan. Acta Petrol. Mineral. Anal. 3, 230–237.
Yudin, I.A., Kolomenskiy, V.D., 1987. Mineralogy of Meteorites (in Russian). Academy of Sciences, Sverdlovsk, Russia, pp. 200.
Yugami, K., Takeda, H., Kojima, H., Miyamoto, M., 1997. Modal abundances of minerals of primitive achondrites and the endmember mineral assemblage of the differentiation trend. Antarct. Meteorit. XXII, 220–222.
Zanda, B., Bourot-Denise, M., Perron, C., Hewins, R.H., 1994. Origin and metamorphic redistribution of silicon, chromium and phosphorus in the metal of chondrites. Science 265, 1846–1849.
Zhang, A.C., Ma, C., Sakamoto, N., Wang, R.C., Hsu, W.B., Yurimoto, H., 2015. Mineralogical anatomy and implications of a Ti–Sc-rich ultrarefractory inclusion from Sayh al Uhaymir 290 CH3 chondrite. Geochim. Cosmochim. Acta 163, 27–39.
Zinner, E.K., 2005. Presolar grains. In: Davis, A.M. (Ed.), Meteorites, Comets, and Planets. Elsevier, Oxford, pp. 17–39.
Zinner, E., Ming, T., Anders, E., 1989. Interstellar SiC in the Murchison and Murray meteorites: isotopic composition of Ne, Xe, Si, C, and N. Geochim. Cosmochim. Acta 53, 3276–3290.
Zipfel, J., Palme, H., Kennedy, A.K., Hutcheon, I.D., 1995. Chemical composition and origin of the Acapulco meteorite. Geochim. Cosmochim. Acta 59, 3607–3627.
Zolensky, M.E., 1999. Identical origin for halide and sulfate efflorescences on meteorite finds annd suflate veins in Orgueil. In Workshop on Extraterrestrial Materials from Cold and Hot Deserts. In: L. Schultz, Franchi, I.A., Reid, A.M., Zolensky, M.E. (Eds.), LPI Contribution 997, 95. Lunar and Planetary Institute, Houston, Texas, USA.
Zolensky, M.E., Gooding, J.L., 1986. Aqueous alteration on carbonaceous-chondrite parent bodies as inferred from weathering of meteorites in Antarctica (abstract). Meteoritics 21, 548–549.
Zolensky, M., Ivanov, A.V., 2003. The Kaidun microbreccia meteorite: a harvest from the inner and outer asteroid belt. Chem. Erde 63, 185–246.
Zolensky, M.E., Krot, A.N., 1996. Mineralogical and compositional study of an Allende dark inclusion (abstract). Lunar Planet. Sci. 27, 1503–1504.
Zolensky, M.E., McSween, H.Y., 1988. Aqueous alteration. In: Kerridge, J.F., Matthews, M.S. (Eds.), Meteorites and the Early Solar System. Univ. Arizona Press, pp. 114–143.
Zolensky, M.E., Pun, A., Thomas, K.L., 1989. Titanium carbide and titania phases in Antarctica ice particles of probable extraterrestrial origin. Proc. Lunar Planet. Sci. Conf. 19, 505–511.
Zolensky, M.E., Hewins, R.H., Mittlefehldt, D.W., Lindstrom, M.M., Xiao, X., Lipschutz, M.E., 1992. Mineralogy, petrology and geochemistry of carbonaceous chondritic clasts in the LEW 85300 polymict eucrite. Meteoritics 27, 596–604.
Zolensky, M.E., Weisberg, M.K., Buchanan, P.C., Mittlefehldt, D.W., 1996. Mineralogy of carbonaceous chondrite clasts in HED achondrites and the Moon. Meteorit. Planet. Sci. 31, 518–537.

Zolensky, M.E., Mittlefehldt, D.W., Lipschutz, M.E., Wang, M.-S., Clayton, R.N., Mayeda, T.K., Grady, M.M., Pillinger, C.T., Barber, D., 1997. CM chondrites exhibit the complete petrologic range from type 2 to 1. Geochim. Cosmochim Acta 61, 5099–5115.

Zolensky, M.E., Bodnar, R.J., Gibson, E.K., Nyquist, L.E., Reese, Y., Shih, C.-Y., Wiesmann, H., 1999. Asteroidal water within fluid inclusion-bearing halite in an H5 chondrite, Monahans. Science 285, 1377–1379.

Zolensky, M., Nakamura, K., Weisberg, M.K., Prinz, M., Nakamura, T., Ohsumi, K., Saitow, A., Mukai, M., Gounelle, M., 2003. A primitive dark inclusion with radiation-damaged silicates in the Ningqiang carbonaceous chondrite. Meteorit. Planet. Sci. 38, 305–322.

Zolensky, M., Gounelle, M.u., Mikouchi, T., Ohsumi, K., Le, L., Hagiya, K., Tachikawa, O., 2008. Andreyivanovite: a second new phosphide from the Kaidun meteorite. Am. Mineral. 93, 1295–1299.

Zolensky, M.E., Mikouchi, T., Hagiya, K., Ohsumi, K., Komatsu, M., Jenniskens, P., Le, L., Yin, Q.Z., Kebukawa, Y., Fries, M.D., 2013. The Nature of C asteroid regolith from meteorite observations. Lunar Planet. Sci. 44, abstract #2179.

Zolensky, M.E., Ziegler, K., Weisberg, M.K., Gounelle, M., Berger, E.L., Le, L., Ivanov, A., 2014a. Aqueous alteration of enstatite chondrites. Lunar Planet. Sci. 45, abstract#2116.

Zolensky, M., Mikouchi, T., Fries, M., Bodnar, R., Jenniskens, P., Yin, Q.-Z., Hagiya, K., Ohsumi, K., Konatsu, M., Colbert, M., Hanna, R., Maisano, J., Ketcham, R., Kebukawa, Y., Nakamura, T., Matsuoka, M., Sasaki, S., Tsuchiyama, A., Gounelle, M., Le, L., Martinez, J., Ross, K., Rahman, Z., 2014b. Mineralogy and petrography of C asteroid regolith: The Sutter's Mill CM meteorite. Meteorit. Planet. Sci. 49, 1997–2016.

Zolensky, M.E., Fries, M.D., Chan, Q.H.-S., Kebukawa, Y., Bodnar, R., Burton, A., Callahan, M., Steele, A., Sandford, S., 2015. Survival of organic materials in ancient cryovolcanically-produced halite crystals Workshop on the Potential for Finding Life in a Europa Plume , Mofft Field, CA.

Zolensky, M., Mikouchi, T., Hagiya, K., Ohsumi, K., Komatsu, M., Chan, Q.H.S., Le, L., Kring, D., Cato, M., Fagan, A.L., Gross, J., Tanaka, A., Takegawa, D., Hoshikawa, T., Yoshida, T., Sawa, N., 2016. Unique view of C asteroid regolith from the Jbilet Winselwan CM chondrite. Lunar Planet. Sci. 47, abstract#2148.

Zubkova, N.V., Pekov, I.V., Chukanov, N.V., Pushcharovsky, D.Y., Kazantsev, S.S., 2008. Nickelhexahydrite from the weathered meteorite Dronino: variations of chemical composition, crystal structure, and genesis. Doklady Earth Sci. 422, 1109–1112.

Zurfluh, F.J., Hofmann, B.A., Gnos, E., Eggenberger, U., Jull, A.J., 2016. Weathering of ordinary chondrites from Oman: correlation of weathering parameters with ^{14}C terrestrial ages and a refined weathering scale. Meteorit. Planet. Sci., 1–16.